Daniel Khede Dourado Villa

LOAD TRANSPORTATION BY INDIVIDUAL AND COOPERATIVE QUADROTORS USING ADAPTIVE AND SLIDING MODE CONTROL

Vitória, Espírito Santo
2022

Daniel Khede Dourado Villa

LOAD TRANSPORTATION BY INDIVIDUAL AND COOPERATIVE QUADROTORS USING ADAPTIVE AND SLIDING MODE CONTROL

Tese de Doutorado apresentada ao Programa de Pós-Graduação em Engenharia Elétrica do Centro Tecnológico da Universidade Federal do Espírito Santo, como requisito parcial para obtenção do Grau de Doutor em Engenharia Elétrica, na linha de pesquisa Robótica, Controle e Automação.

Universidade Federal do Espírito Santo – UFES
Centro Tecnológico
Programa de Pós-Graduação em Engenharia Elétrica

Supervisor: Prof. Dr. Mário Sarcinelli Filho
Co-supervisor: Prof. Dr. Alexandre Santos Brandão

Vitória, Espírito Santo
2022

Ficha catalográfica disponibilizada pelo Sistema Integrado de Bibliotecas - SIBI/UFES e elaborada pelo autor

---

Villa, Daniel Khede Dourado, 1986-
V712l Load transportation by individual and cooperative quadrotors using adaptive and sliding mode control / Daniel Khede Dourado Villa. - 2022.
174 f. : il.

Orientador: Mário Sarcinelli Filho.
Coorientador: Alexandre Santos Brandão.
Tese (Doutorado em Engenharia Elétrica) - Universidade Federal do Espírito Santo, Centro Tecnológico.

1. Robôs - Sistemas de controle. 2. Controle automático. 3. Equações diferenciais não-lineares. 4. Dinâmica dos corpos rígidos. I. Sarcinelli Filho, Mário. II. Brandão, Alexandre Santos. III. Universidade Federal do Espírito Santo. Centro Tecnológico. IV. Título.

CDU: 621.3

DANIEL KHEDE DOURADO VILLA

LOAD TRANSPORTATION BY INDIVIDUAL AND COOPERATIVE QUADROTORS USING ADAPTIVE AND SLIDING MODE CONTROL

Tese de Doutorado apresentada ao Programa de Pós-Graduação em Engenharia Elétrica da Universidade Federal do Espírito Santo, como requisito parcial para obtenção do Grau de Doutor em Engenharia Elétrica, na linha de pesquisa Robótica, Controle e Automação.

Aprovada em 06 de abril de 2022.

COMISSÃO EXAMINADORA

Prof. Dr. Mário Sarcinelli Filho
Universidade Federal do Espírito Santo - Orientador

Prof. Dr. Alexandre Santos Brandão
Universidade Federal de Viçosa - Coorientador

Prof. Dr. Rogelio Lozano
Université de Technologie de Compiègne, França

Prof. Dr. Ricardo Carelli
Universidad Nacional de San Juan, Argentina

Prof. Dr. Ignacio Agustin Mas
Instituto Tecnologico de Buenos Aires y CONICET, Argentina

Prof. Dr. José Leandro Félix Salles
Universidade Federal do Espírito Santo

A minha namorada Vanessa.

Aos meus pais Stella e José Carlos, e aos meus irmãos Glauber, Aline, Júlia e Luisa.

Acknowledgements

Primeiramente, agradeço a minha namorada Vanessa pelo apoio incondicional durante toda essa jornada, e muitas outras que virão.

Agradeço aos meus pais Stella e José Carlos, por me entregarem amor, esforço, e exemplo de vida, valências tão importantes para que eu tivesse forças de seguir em frente.

Agradeço aos meus irmãos, Glauber, Aline, Júlia e Luisa. Mas o que dizer sem que eles fiquem se achando demais? São ótimas pessoas.

Agradeço ao PPGEE-UFES e seus professores, por todo conhecimento que me foi passado e pela oportunidade de pesquisa.

Um agradecimento em especial para o "Proféssor" Dr. Mário Sarcinelli-Filho. Academicamente, tudo o que eu esperava de um orientador. Um pouco exagerado nas cobranças, mas algo que a gente perdoa por ser um monstro nas correções dos trabalhos e sugestões. Um verdadeiro privilégio trabalhar com você. Pessoalmente, fico feliz que nossos caminhos tenham se cruzado. Abraço proféssor!

Um agradecimento em especial também para o meu orientador *default*, Prof. Dr. Alexandre Santos Brandão. Já perdi a conta de quantos anos estamos trabalhando juntos, e nunca nos cansamos um do outro (ao menos não eu dele). A cada parada para o café saem idéias de trabalhos para duas gerações de estudantes.

Agradeço também ao Prof. Dr. Ricardo Carelli, que conheci durante minha breve estadia na UNSJ. Apesar dos poucos meses de convívio com o Prof. Carelli, o aprendizado e amadurecimento foram tremendos, me fazendo retornar ao Brasil cheio de novas ideias para trabalhos.

Agradeço também aos professores Dr. Rogelio Lozano, Dr. Ricardo Carelli, Dr. Ignacio Agustin Mas, e Dr. José Leandro Félix Salles por aceitarem avaliar esta tese.

Agradeço também aos colegas de laboratório, pessoas com as quais passei mais tempo nos últimos anos do que com minha família. Em especial, um abraço para a galera da "maratona do ICUAS" de onde saem as melhores ideias e os melhores resultados – em especial o transporte de latas utilizando quadrimotores. Um abraço Kevin, Valentim, Caldeira, Baju, Pacheco e Mauro.

Por fim, agradeço aos meus amigos da vida. Em especial, para a galera do RPG no Espírito Santo, e galera da Masmorra em Viçosa. Sem vocês a parada não ia ter a mesma graça.

Também agradeço ao CNPq - Conselho Nacional de Desenvolvimento Científico e Tecnológico, e à FAPES - Fundação de Amparo à Pesquisa e Inovação do Espírito Santo, pelo apoio financeiro que disponibilizou os equipamentos e materiais usados nesta pesquisa. Em

particular também agradeço à CAPES, pela bolsa de estudos que me foi outorgada, a qual me permitiu dedicar-me exclusivamente ao Doutorado.

Daniel Khede Dourado Villa

"All models are wrong, but some are useful."
George Box

Resumo

Esta tese apresenta um estudo prático sobre o tema do transporte de cargas utilizando quadrimotores. Em específico, ao longo dos trabalhos apresentados, tratamos a carga transportada como um distúrbio não modelado, e diferentes abordagens foram testadas para lidar com este tipo de sistema. As dificuldades presentes em transportar individualmente ou cooperativamente uma carga também foram analisadas, bem como o controle da orientação da carga transportada para o caso de transporte cooperativo. Para contribuir no entendimento geral acerca do tema, primeiramente é apresentada uma revisão abrangente do estado da arte em transporte de cargas por drones. A seguir, propomos diferentes estratégias para lidar com as incertezas de modelo e distúrbios causados pela carga transportada, ou pelos efeitos dinâmicos causados por um veículo sobre o outro, no caso de transporte cooperativo. Propusemos essas estratégias considerando dois dos ramos principais da engenharia para aumentar a robustez de um sistema: controle adaptativo por modelo de referência e controle por modos deslizantes. Para validar as propostas, testamos nossos algoritmos em condições adversas, sob perturbações do tipo vento e ao ar livre, por exemplo, e em missões de transporte com altas acelerações, longe de movimento quase-estático. Como resultado, o desempenho obtido nos experimentos demonstraram a efetividade na rejeição de distúrbios com o uso do controlador adaptativo robusto e dos controladores por modos deslizantes aqui propostos. Para pôr tudo dentro de um contexto, é também apresentada uma análise qualitativa dos resultados práticos obtidos, ressaltando a relevância deste trabalho diante ao estado da arte.

Palavras-Chave: Controle adaptativo robusto; rejeição de distúrbios; distúrbios por vento; controle não linear; transporte de carga; VANT; robótica móvel

Abstract

This thesis presents a practical study on the topic of load transportation using quadrotors. In specific, along the present works we treat the transported payload as an unmodeled disturbance, and different approaches are tested to deal with this kind of system. The difficulties involving individual and cooperative load transportation are analyzed, as well as payload orientation, in the case of cooperative transportation. For a broad understanding of the subject, a comprehensive state-of-the-art review is firstly presented. In the following, we proposed different frameworks to deal with the model uncertainties and disturbances caused by the payload, or by the dynamic effects caused by one vehicle on the other, in the case of cooperative transportation. We proposed these frameworks considering two major branches in engineering to improve robustness: model reference adaptive control and sliding mode control. To validate the proposals, we tested our algorithms in adverse conditions, under wind-like disturbances and outdoors, for instance, and in transportation missions far from quasi-static motion. As a result, the performance during the experiments demonstrated the effectiveness in disturbance rejection for the here proposed robust adaptive controller and adaptive sliding mode controllers, allowing safe and agile transportation when considering a single quadrotor or a team of two quadrotors for the task. For the sake of completeness, a qualitative analysis of the practical results obtained is also provided, emphasizing the relevance of this work in face of the state-of-the-art.

Keywords: Robust adaptive control; disturbance rejection; wind disturbances; nonlinear control; load transportation; UAV; mobile robotics

Contents

List of Figures

List of Tables

1 Introduction

This thesis presents control algorithms focused on the problem of transporting payloads using quadrotors. Load transportation using quadrotors is advantageous because these vehicles are low-cost, offer exceptional agility, with high thrust-to-weight ratio, and high potential to generate angular accelerations due to the outward mounting of the motors and propellers [1]. These features allow the quadrotors to perform complex and highly dynamic demanding tasks, such as navigation in narrow, tight, and cluttered urban environments, for instance.

The possibility of fast and safe transportation of payloads by using quadrotors is one of the most anticipated trends in the logistics industry, also finding great appeal in civil society. Instead of carrying the load attached to the aerial vehicle, which turns the quadrotor sluggish due to the increased inertia, manipulating the payload via a cable suspension retains the beneficial agility of the quadrotors.

This problem is not new and has been studied for a variety of system configurations and control paradigms. However, most of the past work has focused on payload stabilization, load swing elimination, and quasi-static motion with very low accelerations [2]. Although safe, these strategies are overconservative and do not use the full potential of these aerial platforms [3].

We can divide the works that consider fast and agile transportation as an objective into two families. The first one treats coupled dynamics as a whole, which considers modeling all the dynamic effects involved in such systems. For control, this family of works close the loop on the payload and explicitly plan for feasible, smooth, and safe trajectories for the payload. It also uses flatness property and coordinate-free dynamic modeling to generate the quadrotor control inputs such that the tracking of these payload trajectories is possible. Examples of works of the first family can be found in [4; 5; 6] and references within. The other family treats the problem as a decoupled one, closing the loop in the quadrotor, considering, in some cases, payload measurements or observations only to model the dynamic effects to be feed-forwarded in inverse dynamics fashion. As a result, the second family of agile transportation exchanges precision for implementation simplicity. Once the payload is not directly controlled in closed-loop, works of this family can only predict the payload behavior (examples [7; 8; 2]).

Aiming at proposing a control framework that is simple and readily implementable in off-the-shelf quadrotors, without the need for any additional sensor other than the ones needed to measure the quadrotor state, we opt to close the loop on the quadrotor and treat the dynamic effects caused by the transported payload as a disturbance. Therefore, for simplicity,

the approaches of the first family were avoided in this thesis.

1.1 Objectives

The main objective of this thesis is to present algorithms readily applicable to commercial off-the-shelf quadrotors, allowing these vehicles to transport payloads, individually or cooperatively, at high-speed. This goal was achieved by fulfilling the following specific objectives:

- Understand the challenges and limitations of using small aerial vehicles such as quadrotors to deliver payloads. Also, to understand the strengths and weaknesses of the strategies already presented in the literature;
- Proposition of control algorithms that only rely on sensors commonly found in commercial off-the-shelf quadrotors.
- Proposition of control algorithms that are efficient from a practical perspective.
- Proposition of adaptive and robust control algorithms that reject the disturbances caused by the payload and by the interaction between the vehicles when dealing with cooperative transportation.
- Proposition of a control framework that rejects disturbances using a continuous control signal, and allows two quadrotors to cooperatively carry a bar-shaped payload at high-speeds, even in the presence of wind-like disturbances.
- Proposition of a control framework that rejects disturbances by using a discontinuous control signal, and allows a quadrotor to transport payloads even if they are subject to wind-like disturbances.

1.2 Thesis Structure

This thesis is organized according to the following structure:

Chapter 1: Introduction

This chapter introduces the main engineering problem related to this thesis, as well as the motivation and objectives for this work, also highlighting the main contributions achieved.

Chapter 2: Paper P1 - A survey on load transportation using multirotor UAVs

This chapter presents an already published work by this author, providing a comprehensive state-of-the-art review on the main subject of this thesis, namely load transportation using quadrotors. This paper was published in *Journal of Intelligent & Robotic Systems*.

Chapter 3: Paper P2 - Cooperative load transportation with two quadrotors using adaptive control

This chapter corresponds to another already published work by this author, presenting a simple framework that allows two quadrotors to work cooperatively to carry a suspended rod-shaped payload. The system kinematics is treated as a robot formation problem, and an adaptive dynamic compensator was used to obtain good performance in trajectory tracking under far from quasi-static motion. The paper was published in *IEEE Access*.

Chapter 4: Paper P3 - Cooperative load transportation with quadrotors using robust adaptive control

This chapter contains a novel approach bringing together the advantages of adaptive control and robust control. The proposal merges a model reference adaptive (MRAC) controller with a robust integral of the sign of error (RISE) controller, guaranteeing asymptotic stability for the quadrotors even under unknown disturbances. Exhaustive experiments were run, validating the proposed method and showing its strengths.

Chapter 5: Paper P4 - Adaptive sliding mode control applied to quadrotors – a practical comparative study

This chapter presents a comparative study, evaluating the advantages and disadvantages of the three most common methods to implement adaptive sliding mode controllers. Aiming at testing the compared methods in realistic and harsh conditions, the three controllers are tested far from quasi-static motion and under severe disturbances. The quadrotors were subjected to disturbances such as unmodeled payload dynamics, wind-gusts, payloads hanged in one of the robot arms, thus out of the center of mass, and trajectory tracking with a damaged propeller.

Chapter 6: Paper P5 - Outdoor load transportation using two quadrotors and adaptive sliding mode control

In this chapter, a step is given towards the application of robust control techniques to quadrotors flying in outdoor environments. Two quadrotors perform a load transportation task in an outdoor environment, the load is treated as an unmodeled disturbance, and its effects on the quadrotor, as well as, the effects of the quadrotors on each other, are treated by a traditional first-order adaptive sliding mode controller.

Chapter 7: Conclusion and Future works

This chapter outlines the main conclusions and highlights of the present work. Also, this chapter discusses the challenges faced in our practical experimentation using quadrotors to transport payloads. A guideline for future works is traced, aiming at solutions for the difficulties found.

1.3 Thesis Contributions

Here we summarize the scientific contributions for each one of the papers that constitute this thesis. In total, two journal papers yet published, besides three still unpublished papers are discussed.

[P1] Villa, Daniel K. D.; Brandão, Alexandre S. ; Sarcinelli-Filho, Mário . **A Survey On Load Transportation Using Multirotor Uavs**. Journal Of Intelligent & Robotic Systems, V. 98, P. 267-296, 2020.

Contribution: This survey presents a state-of-the-art review on load transportation using quadrotors, accounting for the following aspects: cable-suspended or grasped load carrying, individual or cooperative schemes, and smooth or aggressive maneuvers. These aspects were used to classify the approaches adopted in each referenced work. Moreover, all analyzed works present experimental results, with online videos showing their achievements.

[P2] Villa, Daniel Khede Dourado; Brandao, Alexandre Santos ; Carelli, Ricardo ; Sarcinelli-Filho, Mario . C**ooperative Load Transportation With Two Quadrotors Using Adaptive Control**. IEEE Access, V. 9, P. 129148-129160, 2021.

Contribution: The main contributions of this paper can be summarized as follows: (i) a simple method for planning the transportation missions is provided, allowing the operator to directly plan the navigation of center-of-mass of the payload and the payload orientation using the virtual structure formation paradigm; (ii) the proposal of a model reference adaptive controller, thus allowing real-time compensation for thrust-related uncertainties and drag-related disturbances; (iii) no use of additional sensor to obtain the states of the payload; and (iv) the presentation of a comparative survey relating the main features found in the recent works regarding load transportation with quadrotors, which also highlights two experimental contributions of this work: transportation far from quasi-static motion, tracking 3D desired trajectories in accelerations up to 1.6 m/s^2, and transportation with payload-to-quadrotor weight ratio up to 0.575, far from the weight ratio usually found in other works of the literature.

[P3] Villa, Daniel K. D.; Brandao, Alexandre S. ; Sarcinelli-Filho, Mario. **Cooperative load transportation with quadrotors using robust adaptive control**. To be submitted for publication.

Contribution: (i) a novel RISE feedback controller that uses no prior knowledge of the disturbance derivative bounds and achieves asymptotic stability of the tracking errors for systems subjected to smooth disturbances; (ii) an improvement over the formation control paradigm proposed in paper [P2], substituting the velocity mapping between the formation and quadrotor variables by an acceleration mapping; (iii) the proposition of a control framework that is readily applicable in commercial off-the-shelf quadrotors, such as the *Parrot Bebop 2* used in the experiments that validate this work; (iv) once the load swing motion during the transportation tasks is not suppressed, this proposal allows agile maneuvers; (v) numerous high performance experiments, demonstrating the stability and performance of the proposed controller in different scenarios, and (vi) the performance comparison against common used controllers to improve robustness, such as MRAC and industrial standard PID controller.

[P4] Villa, Daniel K. D.; Brandao, Alexandre S. ; Sarcinelli-Filho, Mario. **Adaptive sliding mode control applied to quadrotors – a practical comparative study**. To be submitted for publication.

Contribution: (i) experimental implementation of the most common approaches for first-order adaptive sliding mode control in quadrotors; (ii) evaluation of the robust behavior and performance of these controllers in adverse situations and strong disturbances – such as stabilization under intermittent wind, landing precisely subject to wind-gusts, high-speed trajectory tracking while carrying an unmodeled suspended payload with a CoM offset, and trajectory tracking with a damaged propeller –; and (iii) the presentation of an experimental survey comparing the main features of each adaptive sliding mode control scheme when applied to quadrotors, also comparing these controllers to the industrial standard PID controller.

[P5] Villa, Daniel K. D.; Brandao, Alexandre S. ; Sarcinelli-Filho, Mario. **Outdoor load transportation using two quadrotors and adaptive sliding mode control**. To be submitted for publication.

Contribution: The main objective of this research work is the robust transportation of a cable-suspended payload by a quadrotor formation in an outdoor scenario. For getting robustness against the disturbances frequently present in outdoor scenarios, an adaptive sliding mode controller is used. In specific, the approach here proposed does not rely on: (i) an expensive motion capture (e.g., VICON) or high-precision global position system

(e.g., RTK-GPS) to fulfill the mission, (ii) mathematical model or knowledge about the time-behavior of the disturbances (just the actuators feasibility should be addressed), and (iii) communication links between the aerial vehicles.

Finally, it is worth mentioning that this thesis research generated the followings papers, already published:

1. Villa, Daniel Khede Dourado; Brandao, Alexandre Santos ; Carelli, Ricardo ; Sarcinelli-Filho, Mario . C**ooperative Load Transportation With Two Quadrotors Using Adaptive Control**. IEEE Access, V. 9, P. 129148-129160, 2021.

2. Villa, Daniel K. D.; Brandão, Alexandre S. ; Sarcinelli-Filho, Mário . **A Survey On Load Transportation Using Multirotor Uavs**. Journal Of Intelligent & Robotic Systems, V. 98, P. 267-296, 2020.

3. Villa, Daniel K. D.; Brandao, Alexandre S. ; Sarcinelli-Filho, Mario . **Outdoor Navigation Using Two Quadrotors And Adaptive Sliding Mode Control**. In: 2020 International Conference On Unmanned Aircraft Systems (ICUAS), 2020, Athens.

4. Villa, Daniel Khede Dourado; Brandao, Alexandre Santos ; Sarcinelli-Filho, Mario . **Rod-Shaped Payload Transportation Using Multiple Quadrotors**. In: 2019 International Conference On Unmanned Aircraft Systems (ICUAS), 2019, Atlanta.

5. Villa, Daniel Khede Dourado; Brandao, Alexandre Santos ; Sarcinelli-Filho, Mario . **Path-Following And Attitude Control Of A Payload Using Multiple Quadrotors**. In: 2019 19th International Conference On Advanced Robotics (ICAR), 2019, Belo Horizonte.

6. Villa, Daniel K. D.; Brandao, Alexandre S. ; Sarcinelli-Filho, Mario . **Load Transportation Using Quadrotors: A Survey Of Experimental Results**. In: 2018 International Conference On Unmanned Aircraft Systems (ICUAS), 2018, Dallas.

7. De Carvalho, Kevin Braathen ; Villa, Daniel Khede Dourado ; Sarcinelli-Filho, Mário ; Brandão, Alexandre Santos . **Gestures-Teleoperation Of A Heterogeneous Multi-Robot System**. International Journal Of Advanced Manufacturing Technology (Internet), V. 118, P. 1999–2015, 2022.

8. Vasconcelos, Joao Vitor R. ; Villa, Daniel K. D. ; Caldeira, Alexandre G. ; Sarcinelli-Filho, Mario ; Brandao, Alexandre S. . **Agent Fault-Tolerant Strategy In A Heterogeneous Triangular Formation**. In: 2020 International Conference On Unmanned Aircraft Systems (ICUAS), 2020, Athens.

1.4 References

[1] HEHN, M.; D'ANDREA, R. Quadrocopter trajectory generation and control. *IFAC proceedings Volumes*, Elsevier, v. 44, n. 1, p. 1485–1491, 2011.

[2] VILLA, D. K. D. et al. Cooperative load transportation with two quadrotors using adaptive control. *IEEE Access*, IEEE, v. 9, p. 129148–129160, 2021.

[3] TANG, S.; KUMAR, V. Mixed integer quadratic program trajectory generation for a quadrotor with a cable-suspended payload. In: IEEE. *2015 IEEE international conference on robotics and automation (ICRA)*. [S.l.], 2015. p. 2216–2222.

[4] SREENATH, K.; LEE, T.; KUMAR, V. Geometric control and differential flatness of a quadrotor uav with a cable-suspended load. In: IEEE. *52nd IEEE Conference on Decision and Control*. [S.l.], 2013. p. 2269–2274.

[5] SREENATH, K.; MICHAEL, N.; KUMAR, V. Trajectory generation and control of a quadrotor with a cable-suspended load-a differentially-flat hybrid system. In: IEEE. *Robotics and Automation (ICRA), 2013 IEEE International Conference on*. [S.l.], 2013. p. 4888–4895.

[6] TANG, S.; WüEST, V.; KUMAR, V. Aggressive flight with suspended payloads using vision-based control. *IEEE Robotics and Automation Letters*, v. 3, n. 2, p. 1152–1159, 2018.

[7] FOEHN, P. et al. Fast trajectory optimization for agile quadrotor maneuvers with a cable-suspended payload. Robotics: Science and Systems Foundation, 2017.

[8] HANOVER, D. et al. Performance, precision, and payloads: Adaptive nonlinear mpc for quadrotors. *IEEE Robotics and Automation Letters*, IEEE, v. 7, n. 2, p. 690–697, 2021.

2 [P1] - A survey on load transportation using multirotor uavs

Load transportation by quadrotors and similar aircrafts is a topic of great interest to the robotics community nowadays, most likely due to logistic gains for deliveries of commercial cargo. Aiming at being the first reading for novice researchers and graduate students, this survey highlights meaningful research works of several groups worldwide, considering two basic approaches, namely grasped and cable-suspended load transportation. Different control techniques and maneuver strategies are analyzed, and their benefits and drawbacks are discussed. Moreover, experimental validation was a key aspect to the highlighted works, thus, links to the videos showing the experimental results are provided for each work.

2.1 Introduction

Researchers who work with unmanned aerial vehicles (UAVs) are nowadays witnessing progressive advances in the field, which includes using quadrotors to grasp, manipulate and transport objects. Besides the increase of their application in load transportation, the quadrotors themselves have been designed with better vision systems and sensing capabilities, increased thrust-to-weight ratio, improved battery efficiency and onboard processing. These advances turn feasible the design of controllers to perform aggressive maneuvers [1], to navigate in cluttered scenarios [2], and the online planning of paths on dynamic environments [3]. However, the small size of those UAVs limits their payload capacity, which motivated some research groups to work with a team of agents to overcome such a limitation. Moreover, a UAV platoon can also guarantee the accomplishment of a transportation mission even if one or more quadrotors suffer a structural, power or electronic malfunction.

There are several applications in which UAV load transportation is beneficial, such as package delivery in urban areas [4]; plantation monitoring and application of pesticides in precision agriculture [5]; providing supplies in conflict zones [6], among others. As a matter of fact, load transportation using quadrotors attend commercial, militarian, and civilian interests.

Despite the wide range of UAV applications, work with them is still quite challenging, once these machines are inherently unstable and have complex and strongly coupled dynamics, besides being a nonlinear and multi-variable system [7]. Talking specifically about load transportation, it has been accomplished using two major carrying strategies, which are either

the suspension of the load through cables or the attachment of the cargo to the quadrotor body [4]. For the former, the cable-suspended load increases the number of under-actuated degrees of freedom, thus modifying the system dynamics. For the latter, the load attached to the quadrotor body increases its inertia, making it unfit for fast attitude responses and agile maneuvers. In both cases, notice that the controller in charge of guiding the vehicle should be quite different from a controller designed to guide the UAV when navigating without a load. Therefore, load transportation by quadrotors opens a large number of possibilities in terms of controller design.

In such a context, this survey presents a state-of-the-art review on load transportation using quadrotors, accounting for the following aspects: cable-suspended or grasped load carrying, individual or cooperative schemes, and smooth or aggressive maneuvers. These aspects were used to classify the approaches adopted in each referenced work. Moreover, all analyzed works present experimental results, with online videos showing their achievements. The classification framework can be seen in Figure 2.1, and, to the best of our knowledge, this is the first survey on this subject.

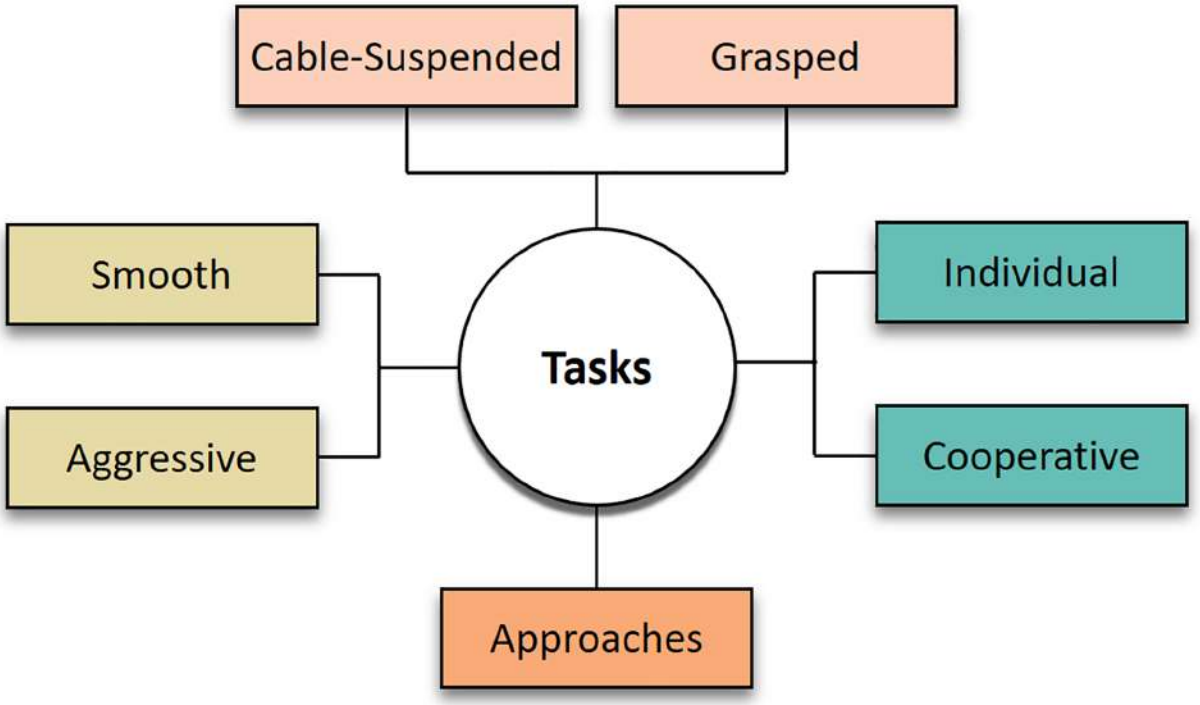

Figure 2.1 – Main aspects of load transportation tasks considered in this work.

The development of this survey is divided as follows: Section 2.2 explains the criteria and the way the survey was conducted. In Section 2.3, the main load transportation aspects receive a broader analysis. Section 2.4 briefly discusses the general tasks present on load transportation applications. In the sequel, Section 2.5 highlights the relevant works that adopt the cable-suspended load carrying strategy, and, likewise, Section 2.6 highlights works

adopting the grasped load carrying strategy. In Section 2.7 we briefly discuss the importance of other types of multirotors and the differences over quadrotors. Section 2.8 brings important remarks, trends, major achievements, and potential challenges that we found about our research. Finally, 2.9 summarizes the concluding remarks.

2.2 The Search Method

The search method for original articles or reviews on the subject "load transportation using quadrotors" follows the criteria presented in Table 2.1. An important aspect of this survey is that unpublished dissertations and thesis were not included in this review, as well as published manuscripts that only present numerical and simulation results. This premise is considered because quadrotors are highly complex nonlinear systems, requiring accurate mathematical methods to describe their dynamics and to design their controllers. Modeling and control demands further increase when a payload is added to the system. Thus, practical experiments to validate the simulations and the adopted control techniques were mandatory for a work to be included in this survey.

Table 2.1 – Search criteria.

Criteria	Data
Scientific Database	IEEEXplore OR Google Scholar, Science Direct OR Engineering Village
Publication Period	FROM 2008 TO July/2019
Keywords	("quadrotor" OR "unmanned aerial vehicle" OR "UAV" OR "quad-copter" OR "multi-rotor") AND ("transport" OR "transportation" OR "delivery" OR "load" OR "payload" OR "slung-load" OR "suspended load" OR "cargo")

Finally, a manual search across the reference lists of the selected articles was also performed, looking for relevant studies on the subject. Therefore, works with results that we consider most interesting using the criteria of relevance to the field, technical quality, and originality, are here presented and critically analyzed.

2.3 Load Transportation Aspects

2.3.1 Cable-suspended or grasped load carrying

A UAV can carry a cargo attaching it on its rigid body or suspending it through cables. The dynamic model changes in both cases, because the system becomes UAV plus the additional load, and the flight controller should be capable of dealing with this new condition.

For the cable-suspended load approach, the control problem is similar to a pendulum stabilization problem. Commonly, the cargo adds passive degrees of freedom to the UAV, affecting directly its dynamic characteristics and generating swinging during flight. Thus, the controller should handle such weight fluctuations and their consequences. The most traditional way is to stabilize and minimize the load swings by counteracting these unwanted motions. Alternatively, some works handle this issue using feedback control to track the desired load trajectories or trajectory planning algorithms for the quadrotor-with-load multi-body system [8].

Moreover, it is harder to obtain an accurate mathematical model for the UAV-cargo system, once the lifting, transporting and delivering stages have distinct characteristics. For instance, during the transport stage, the payload transfer forces through the cable, whereas in the very beginning of the lifting stage there is no force transferred through the cable. Indeed, such force transfer depends only whether the cable is taut or not, which can occur in any of the three stages.

Some researchers treat the cable conditions as different subsystems in a hybrid dynamic model, in which each aforementioned stage has its specific and specialized controller, and a supervisory system is responsible for switching among such simpler controllers. In contrast, other groups work on the search for a general solution to the problem of suspended cable transport, no matter what stage the mission is in.

Another way to transport a load is by attaching it to the rigid body of the UAV through mechanical or electromagnetic grippers, robotics claws, or robotic hands. Although this option provides simpler ways to attach or detach a load, this method reduces the rotorcraft agility.

Even assuming that the attached load does not unbalance the UAV, for the grasped load approach more thrust is required, increasing energy consumption. Moreover, the center of gravity commonly changes, introducing control disturbances. Another meaningful aspect is that the moments of inertia increase, thus affecting the pitch and roll maneuvers and, consequently, making the UAV slower in terms of attitude response, and less robust to perturbations.

2.3.2 Smooth or aggressive maneuvers

Concerning cable-suspended load transportation, the traditional swing suppression approach is not energetically optimal once energy is expended to counteract the load motions and the controllers should be tuned to achieve smooth and non-agile movement. Unfortunately, this goes in the opposite direction of task automation, where agility, fast movement, and aggressive maneuvers are wanted.

The navigation is considered under aggressive maneuvers when it is purposely planned to

use the vehicle's entire range of motions, e.g., navigation under large load swings, in-flight load pick-ups and releases, and periods under variable cable tautness condition [9]. These maneuvers allow a broader spectrum of trajectory planning solutions, such as traversing through passages with a height shorter than the cable length or performing a load throwing when the vehicle is not directly above the payload release location.

Moreover, enhanced trajectories and aggressive maneuvers can be exploited to produce more agile solutions in almost every load transportation application, guaranteeing better navigation and maneuverability for the quadrotor-with-load system even in cluttered scenarios or 3D navigation. Although theoretically optimal, it should be noted that aggressive maneuvers elevates the complexity of an already complex system. As a consequence, current researches in load transportation under aggressive maneuvers often do not go beyond the design of control algorithms and simulation results. Even when experiments are presented, they may be limited in some way, such as considering only 2D movement or an obstacle-free scenario, for instance.

2.3.3 Individual or Cooperative Scheme

Load transportation using quadrotors can be done by a single agent or by a squad of agents. Although the use of a single robot is simpler and straightforward, there are transportation tasks that can only be performed by multi-agent systems, such as carrying a load heavier than the payload capacity of the single quadrotor or successfully deliver an object under a robot failure. For the latter example, if a team executes the task, the remaining agents may be able to cooperate and accomplish the mission without significant damage, showing that a multi-agent approach can lead to redundant solutions with greater fault tolerance and flexibility.

Cooperative load carrying tasks can be grouped either as multiple robots collaborating to carry and manipulate a single load (e.g., for transporting a heavier load), or multiple robots cooperating while carrying individual payloads (e.g. for faster delivery of multiple loads in a disaster scenario).

Multiple quadrotors carrying a single load result in a challenging dynamic analysis, as each UAV heavily affects the motion of the other. Therefore, when a quadrotor team is carrying a single load, the interactions required are not only associated with information sharing between agents, but also to the physical coupling between them. For slung-load carrying, those physical connections impose complex dynamics on the system, and there is not a trivial solution to describe the pose of the payload, the deformation and displacement of the cables, and the maneuvering of the aerial vehicles [10]. However, most of the existing works for cooperative single load transportation neglects these coupled events and treats the dynamics of the cable and payload as arbitrary external disturbances acting on the quadrotor.

Therefore, the maneuverability of those systems is severely compromised, not allowing agile transportation or aggressive maneuvers. Conversely, the dynamic coupling in grasped solutions is more easily addressed, once the payload is rigidly held underneath the vehicle and do not require to be modeled as a separate body.

For multiple robots cooperating while carrying individual payloads, the control signals should guarantee synchronization among the UAVs to achieve cooperation and to avoid collisions. To manage the navigation complexity of a multi-robot platoon composed by quadrotor-with-load agents, normally an optimization motion planning problem is proposed to generate the collision-free trajectories for the vehicles. For the cooperative execution of a task, some degree of coupling is imposed among the units. Hence, the cooperative behavior of agents is intrinsically related to this degree, and the bigger the coupling-degree is, the bigger the challenge to formulate effective cooperative solutions is [11].

Another valuable option in cooperative schemes is the squads composed by heterogeneous robots. Thereby, teams with different sensing and actuation capabilities can work cooperatively. For instance, in a heterogeneous multi-robot setting, those robots in the boundary may be guidance-specialized UAVs, responsible for mapping and guiding the team during its navigation, while the others may be larger and better-suited agents for the transport of a single heavy load. The opportunity to distribute different capabilities among the robot-team members allows a deeper degree of specialization for the mission, also allowing a mission execution prowess unreachable for a single type of robot. Therefore, these systems present a paradigm shift and the challenge goes from how to build and deploy the best technologies into a single agent, to how to design the more specialized and efficient multi-robot heterogeneous systems so that the resulting performance is optimized.

Ultimately, cooperative systems can overcome the limited load controllability and heading positioning of the individual schemes, guaranteeing higher load carrying capacity and the ability to perform tasks where the load should be oriented, such as the deployment of sensor nodes or firefighting.

2.4 Common Tasks

2.4.1 Transport of loads with varied weights

Since the applications on load transportation using quadrotors are diverse, the carried objects may have different shapes and weights, and, consequently, produce different effects on the dynamics of the quadrotors. For simple transportation, the influence of the shape of the load can be standardized (e.g., by using some type of container) and the versatility of an approach now lies in its ability to handle loads of different weights.

This versatility is represented as the interaction of three main aspects associated with the quadrotor: payload capacity, energy source and flight time. Even with the recent technological advancements, it is still a hard struggle for quadrotors manufacturers to balance these aspects, which is nowadays the main barrier to be overcome for broader integration of UAVs in society. The relevance of this subject is such that researches in energy-efficient algorithms and aircraft design are constantly being conducted by the scientific and industrial community. As an example, the US Government has recently proposed *The Unmanned Aerial Systems Flight and Payload Government Challenge* [12], which consists in a competition, with US$432,000 in prizes for the team who manages to keep a UAV and its payload in the air for more time.

Although those three aspects compose the main challenge for this task, there are also other difficulties in handling heavy or weight-varying loads. Considering cable-suspended load transportation, while the heavy load is suspended, excessive load swings will increase the underactuation level, which may cause a degradation in the quadrotor performance or even in its stability. As for the grasped load case, a heavier load impacts, even more, the inertia of the aircraft, also requiring a more complex grasping mechanism. Due to this, the use of simpler mechanisms, such as electromagnets or ingressive grippers, may not be an option. Ultimately, for both cases, to build a system model able to handle the disturbances caused by the dynamic fluctuations of a heavy load is a painful and burdensome job, being almost mandatory to implement some sort of adaptive module in the control loop, which further increases the complexity of the controller.

Another option for carrying heavy loads is to use a team of UAVs, rather than a larger or a highly specialized one. As discussed in Section 2.3.3, cooperative transport brings more versatility to the task accomplishment and increases the overall load capacity, at a price of increasing the system complexity.

2.4.2 Load manipulation

Aerial manipulation can provide several advantages for load transportation using quadrotors. In simple terms, an aerial manipulator combines the maneuverability of the quadrotor with the versatility of a grasp/hand manipulator. This powerful combination is essential for the awaited transition from the passive usage of UAVs in tasks of surveillance, monitoring, and remote sensing, to their active usage in tasks such as capture of a moving target, handling of hazardous material, perching to conserve power, removal of obstacles that are blocking the viewpoint of a transportation task, and so on.

This scheme also creates the possibility of manipulating objects without landing, which decreases the time and energy to complete the tasks and allows the robots to operate in terrain not suitable for landing, such as the tops of power lines, radio masts, or near water surfaces

[13]. To accomplish the manipulation maneuvers in the air the robot should be equipped with the proper tools, and, according to [14], the usual solutions can be divided into a UAV equipped with a flying hand (e.g., a mounted gripper, a multi-fingered robotic hand) or an unmanned aerial manipulator (e.g., one or more multi-link robotic arms).

The flying hand (FH) approach is adopted as a simpler option, of lower-cost and lower energy consumption. However, it lacks dexterity, so that it is mainly used for pick-and-place operations. Its end-effector gripper falls within two design concepts: the impactive and the ingressive gripper [15]. Impactive grippers use fingers or solid jaws to grasp the object. These systems normally adopt a highly compliant grasper that enables the FH to grab a variety of target objects, also enhancing the robustness against small disturbances. In turn, ingressive grippers use some sort of claws or oppositive hooks to penetrate in the surface of the object and attach it to the load, being applicable even for objects without a well-defined attachment point, at a cost of being restricted to materials that admit this kind of deformation. The necessary grasping force in both design concepts is generated by a combination of servomechanisms, solenoids, and springs. Furthermore, impactive and ingressive grippers are not mutually exclusive and paired with adjusts and modifications they can be used for a wide range of objects. Prototypes containing the grippers and the grasping mechanisms can be seen in Figure 2.2.

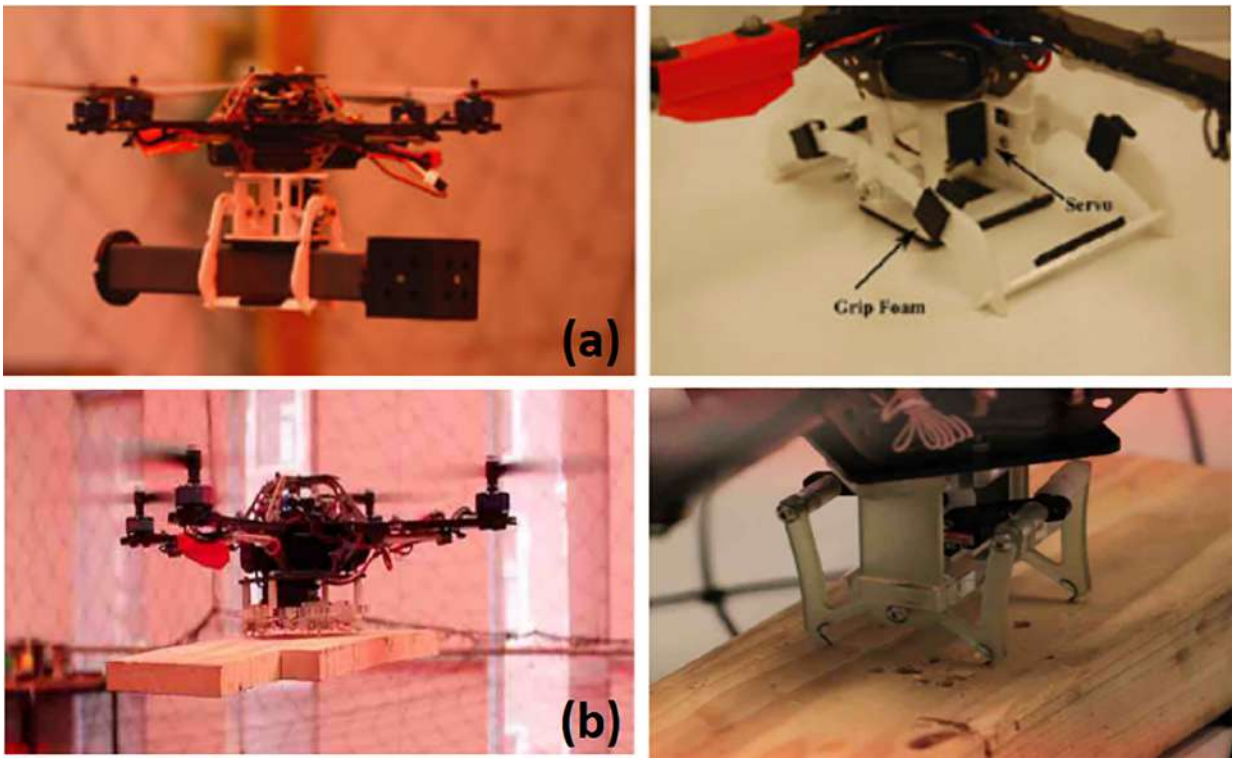

Figure 2.2 – The two more common grippers: (a) impactive grippers, (b) ingressive grippers [16].

A quite attractive solution to accomplish the desired transition from passive to active UAV usage are the unmanned aerial manipulators (UAM). Aerial robots equipped with one or more multi-link robotic arms have increased manipulation capacities and dexterity, being better-suited to perform more advanced applications such as door/drawer opening, hose transportation, peg-in-hole insertion missions, structure assembly, or infrastructure maintenance (e.g., painting, washing, repairing). Moreover, UAM robots can benefit from the arms hyper redundancy to realize secondary tasks with them (e.g., obstacle-avoidance, minimization of torques in the joints), and to compensate the unavoidable perturbations that occur when the robot is near or manipulating an object, assuring greater reliability. Examples of UAM systems can be seen in Figure 2.3. Two approaches are used for planning trajectories and controlling these systems: a centralized approach, which models the system and treats the dynamics and forces involved as a whole, and a decentralized approach, in which UAV and UAM are treated individually according to their poses, kinematics, and dynamics, handling the coupled bodies as external disturbances. Furthermore, the use of adaptive controllers heightens the performance and brings finesse to these systems, once this technique seeks to mimic the way humans handle an unknown object. Sensing and adapting in the absence of accurate knowledge of the kinematics and dynamics of the object provides the flexibility to handle the unforeseen uncertainties of a real-world scenario [17].

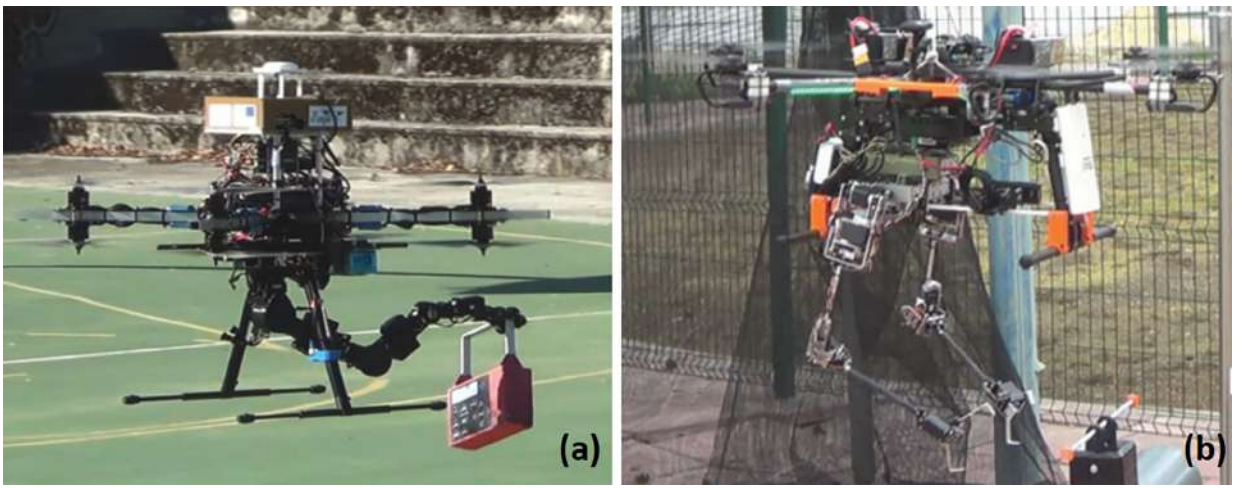

Figure 2.3 – (a) 7-DoF UAM developed at the University of Seville within the ARCAS project [18] (more details are available in [19], (b) dual-arm UAM system also developed at the University of Seville within AEROARMS project [20] (more details are available in [21].

Despite the advantages, the difficulties of aerial manipulation are numerous. UAVs do not have a stable base and, consequently, suffers the direct influence of forces and torques generated by the payload and manipulation mechanisms. Since the most common approach for aerial manipulation is to approximate and hover perpendicularly to the plane of the target,

the quadrotor should overcome these dynamic disturbances and provide adequate hover positioning even for basic manipulation, guaranteeing that the load stays in the manipulator workspace during its operation [22]. Moreover, for applications in which the target object is moving, the positioning task is changed to a trajectory tracking task, which increases something more the challenges due to disturbances and more noticeable dynamic effects. Likewise, the highly dexterous UAM systems impose many difficulties to aerial manipulation, such as inferior robustness, once the dynamics of the mounted robotic arm depends on its actual configuration, and increased mechanical and control complexity. Additionally, the substantial weight of the arm degrades the already critical load limitation of the UAVs.

To handle the mentioned difficulties, measures and analyzes are concentrated into few aspects that describe the quality of the aerial manipulation: arrival at the target and relative alignment, grasping performance, aircraft stability during contact, and flight stability while carrying the load [23]. Although the scientific community is far from a satisfactory fulfillment of these aspects, several papers already showed the potential of the aerial manipulation systems in experiments. To mention a few examples, in the following works quadrotors cooperate in harmony to play musical instruments [24], to construct simple structures made of intertwined rope [25] or cuboid nodes [16], to grab and release an object over a shelf [26], to use hyper redundancy and execute hierarchically multiple tasks [27] (watch the videos available at `https://goo.gl/MyP1VK` and `https://goo.gl/6mfYpn`), and tracking and grasp a moving target [22] (watch the video available at `https://goo.gl/QvmSRH`). Furthermore, some experiments also show UAM executing tasks involving to exert force/torque against the environment, such as valve turning [28] and door/drawer opening [29] (watch the video available at `https://goo.gl/HvyBU7`). As a last example, in [30], instead of using a low-speed approximation and hovering to grab a target, the researchers emulate the strategy used by raptors to catch a moving and elusive prey, moving the leg-like grasping mechanism backward to obtain a close to zero relative speed and execute the capture (watch the video available in `https://goo.gl/8PNFFs`).

In such a context, UAV systems capable of load carrying and endowed with manipulation skills can be considered the natural evolution of mobile robotics, being well-suited to be employed as workers, human co-workers, inspectors, and logistic robots, able to grasp, transport, position, and assembly/disassembly various mechanisms or devices [14].

2.4.3 Fragile and dangerous load

Some load transportation applications demand special care, such as the case of transporting a fragile or dangerous load. Obstacle-avoidance policies are mandatory in such situations, preventing the load to crash against an obstacle during the flight, hurt humans or damage

structures.

Safety considerations should be taken into account regarding both cable-suspended and grasped load carrying systems. However, the problem is more noticeable in cable-suspended load transportation, since the load swings and oscillations may cause damage to the load itself or people around as well. In general, three strategies are used to obtain swing-free cable-suspended load transportation using quadrotors (i) close the control loop on the load and generate swing-free feasible trajectories for the load, also taking into account the quadrotor maneuverability and stability during navigation, (ii) counteract the load swings actively using the quadrotor thrusts, or (iii) carry the load in a cooperative formation that suppress the oscillations (e.g., using two quadrotors in a line, one behind the load and the other ahead, which naturally suppresses the oscillation in the direction of movement).

Exploiting redundant UAV systems are also an interesting approach to this subject. UAVs with more than four propellers, such as hexacopters or octocopters, have increased autonomy, because even if one of the propellers fails the vehicle can still sustain a stable flight (in the case of hexa or octocopters, even more than one blade can fail). Moreover, due to the additional propellers, these vehicles have a more stable flight and more robustness against adverse environments (e.g., wind gusts), also being faster, which can be of great benefit in the case of transporting a dangerous load. Furthermore, as pointed out in 2.3.3, multi-agent systems can reconfigure themselves under a robot failure and still accomplish the transportation mission, assuring more autonomy.

2.5 Works Considering Cable-Suspended Load

2.5.1 Optimal Trajectories

We start the highlights on the relevant works regarding cable-suspended load transportation, presenting results that use a trajectory planner to obtain optimal trajectories and execute the slung-load transportation mission.

In [31] an open-loop method is introduced, which aims at an optimal swing-free trajectory for a quadrotor carrying a suspended load. This approach expects to minimize the load displacement angles, through minimizing the forces and torques acting on the quadrotor and the dynamical changes caused by the swinging load. The swing-free trajectory was obtained employing dynamic programming on a discrete-time linearized model of the system.

An adaptive feedback linearization controller was proposed to stabilize the rotorcraft, without taking into account the suspended load. In such a case, the cargo disturbances are minimized (or suppressed) by the adaptive part of the controller. According to the authors, the proposed controller overcomes the lack of robustness against the model uncertainties.

The experiments were run at (Multi-Agent, Robotics, and Heterogeneous Systems) MARHES lab, University of New Mexico. The testbed is composed by AscTec Hummingbird quadrotors and a Vicon motion capture system. A centralized station is responsible for getting the pose of the UAVs, compute and sent their control signals at a 100 Hz sampling rate, using XBee modules. The videos of the experiments are available at https://goo.gl/AsLBa4. Notice that the desired heading angles of the quadrotors were set to zero.

Some applications demand swing-free maneuvers. Fragile or dangerous load transportation and deployment in cluttered scenarios are some examples. However, to fulfill this requirement a recise model describing the UAV and the cargo is essential. Thereby, assuming the existence of modeling inaccuracies, the same research group proposed a new approach to the swing-free trajectory optimization task, using reinforcement learning (RL) technique [32]. Since the RL does not need information about the mathematical model, then detailed knowledge of the system dynamics is not necessary. Thus, cumulative errors are reduced and model uncertainties are avoided. Another advantage of RL is its possibility to generate multiple paths, once trained. In such a work, the best path is found by a greedy algorithm, that evaluates the residual oscillations for the quadrotor-with-load system and searches for the minimal one. In addition, to accomplish the collision-free path-following task, the working environment is structured, and the quadrotor and load are modeled as a cylinder-cone volume.

The new experiments were performed in the same test-bed at MARHES lab and their videos are available in https://goo.gl/R7bnyj. To demonstrate the reliability of the proposed methods, the task accomplished is the delivery of a glass of water to one of the researchers.

In contrast to [31; 32], where structured scenarios are considered, in [3] a Model Predictive Control (MPC) with Sequential Linear Quadratic (SLQ) solver is employed to obtain real-time path planning. The vehicle is able to operate in dynamic environments, where obstacles can appear abruptly or move unexpectedly. The proposed collision-avoidance algorithm considers not only the quadrotor but also the suspended load and the cable.

In general, when an MPC approach is used for UAV navigation in cluttered scenarios the choice is to treat it as a constrained MPC problem [33; 34], and a trade-off between time horizon and delay should be established, due to the computational complexity of the MPC algorithms. To reduce the computation time, the authors considered an unconstrained MPC problem, shifting all constraints to a cost function with soft constraints. This leveraged approach contemplates in a cost function the desired positions and the distance to obstacles as a potential field, aiming at finding the trajectories and control inputs that minimize the cost for load transportation and obstacle avoidance. The adopted SLQ solver was previously demonstrated performing agile flight experiments in [35], and its main role is to evaluate the optimal control problem and provide the desired trajectories for the quadrotor-with-load

system, using a geometric controller whose stability is verified. This SLQ-MPC approach satisfies both the feasibility and optimality in trajectory generation.

The presented approach was validated by experiments, and two obstacles in the shape of a building compose the cluttered scenario in which the quadrotor carrying a load should navigate. Experiments were conducted at the Intelligent Control Systems Laboratory, Seoul National University, using a DJI Flame Wheel F450 quadrotor. The multi-rotor and suspended load states were measured by a Vicon motion capture system, operating at 100 Hz. A ground station running ROS process the optimal control problem and sends the desired control signals via Wi-Fi to a Pixhawk Mini, which runs the low-level controller. To handle the reduced magnitudes of the control inputs, as the vehicle was reaching the final desired state, an adaptive time horizon (1.6-2.0 s) was implemented, maintaining the appropriate magnitudes by decreasing the time horizon proportionally to the error with respect to the final position. In the experiment thus conducted, the final desired state was changed six times during one minute, with the purpose of showing the real-time trajectory generation and obstacle avoidance when navigating close to obstacles or passing through the narrow gap formed by the building-like structures. The performance of the quadrotor-with-load system can be checked in the video available in https://goo.gl/WtuiXQ. It should be noted that it is out of the scope of such work to damp the load swing.

2.5.2 Smooth maneuvers applied to cooperative load transportation

The need to deal with large and bulky loads has given rise to the idea of using a team of robots to manipulate and transport them. In fact, for many researchers and enthusiasts, aerial robotic squads are the future for many applications, such as package delivery, urban safety, search and rescue missions, personal assistance, and agriculture, just to name a few.

As mentioned in Section 2.3.3, connections between agents introduce additional dynamics, reduce maneuverability, and bring up disturbance and stability issues. The trajectory generation should also guarantee that the UAVs will not collide during flight, taking into consideration load distributions and swing control. Furthermore, all those difficulties further increase in a scenario of communication delay and/or packet loss.

In such a context, in [36] the authors propose a method to manipulate and transport a payload in a 3D environment via cable. Since only limited controllability can be obtained with a single point of attachment, this study discusses the general conditions to achieve the system equilibrium at a desired pose using an arbitrary number of robots. In general, the case for $n > 2$ robots is analyzed, once $n = 2$ limits the ability to achieve desired angle rotations about the line connecting the two robots.

The problem was modeled in a way similar to cable-actuated parallel manipulators in

3D environments, as can be seen in Figure 2.4, with the number of unconstrained degrees of freedom for the load being equal to six minus the number of robots. To obtain the direct relationship between the positions of the robots, q_i, and the desired payload position and orientation, a numerical formulation that seeks to minimize the potential energy of the payload for a given robot configuration is proposed.

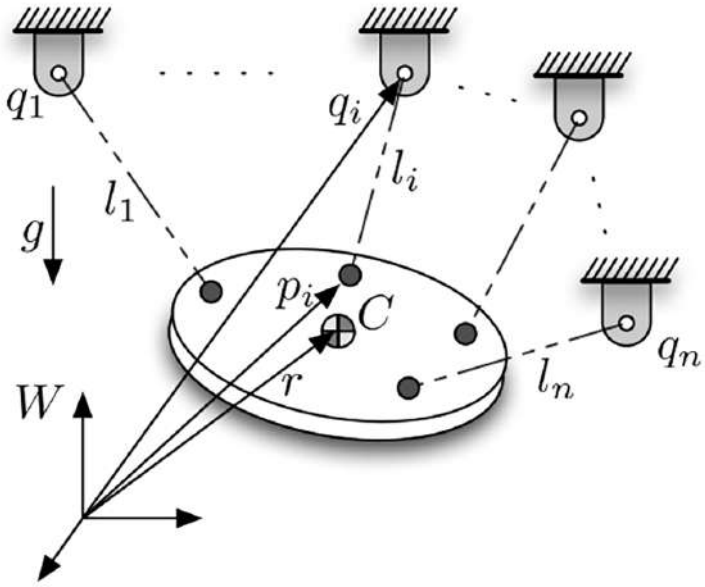

Figure 2.4 – A rigid body suspended by n cables with world-frame points q_i. Analysis techniques for cable-actuated parallel manipulators assume that q_i is fixed while l_i varies in magnitude, while for cooperative aerial manipulation l_i is fixed and q_i varies by changing the positions of the aerial robots. [36].

A dynamic model was proposed, considering the agents as point robots and assigning the transformation from the desired applied forces to the control inputs required for task fulfillment. In the sequel, these control inputs are delivered to a PID feedback controller with feedforward compensation. Also, a potential-field collision-avoidance controller was implemented, with each robot being modeled as a sphere of radius R, guaranteeing that $\|q_i - q_j\| > 2R$ for all pairs of robots. A limitation on the proposed controller is that it has coupled control terms, and for any desired input there is a thrust in f_z direction. Another issue related to the method lies in the inability to damp the oscillations generated by the cable-suspended load and perturbations in the robot positions, limiting the system to transport the load using smooth and slow motions.

To validate the proposals, real-world experiments were conducted at General Robotics, Automation, Sensing and Perception (GRASP) laboratory, University of Pennsylvania. Three AscTec Hummingbird quadrotors are used to transport a triangular rigid body weighing 0.25 kg, with cable lengths of $l_i = 1\ m$. The algorithms are implemented using Player/Gazebo,

with the commands being sent to each robot via Zigbee at 20 Hz, and localization information is provided by a Vicon motion capture system at 100 Hz. Two tasks are assigned to the squad of robots: the first one is cooperatively lifting the rigid body load, and the second one is to manipulate and transport the object through given waypoints. During the experiment run, one robot suffered a momentary actuator failure, losing power and dropping, providing useful information about the system's ability to recover and resume the desired configuration. The experimental results can be seen in the video available at https://goo.gl/NCFSPb.

In a follow-up work by the same authors [37], the cooperative aerial manipulation using the underlying mechanical similarities of cable-actuated parallel manipulators was further investigated. A limitation present in the previous study is that the problem admitted multiple solutions for any desired payload equilibrium pose. To address this issue, a Linear Complementary Problem (LCP) formulation was proposed, introducing complementary constraints for squad configuration and guaranteeing the existence of a unique payload pose.

When the constraints are added, a new form to determine the solutions that minimize the potential energy of the payload was obtained, transforming the static equilibrium equations into inequalities, which also transformed the non-convex problem in a convex one, allowing convergence to a global minimum (unique solution). In fact, the chosen constraints alleviate and relax the equalities, ensuring that the tension on a cable is non-zero only when the distance between two end-points is equal to the free lengths. This formulation allows the equilibrium pose of the payload, given by the positions of robots, to be solved as a second-order cone program (SOCP) [38].

Control laws similar to those in the former paper were proposed in this approach, being only slightly modified to deal with the convergence error while enforcing the SOCP constraints. A path planning for the payload was also developed in the paper, taking into account feasible robot configurations to each pose of the payload along the trajectory, and the possibility of exploiting the configurations redundancy for the realization of secondary tasks, such as minimization of the traveled distance or disturbances attenuation.

To validate the proposals, experiments were conducted using the same testbed and hardware of the former article. The first test consisted in manipulating the payload through a circular trajectory while varying its row and pitch, and the results showed an RMS error on robot control of about 9 cm and for the center of mass of the payload 7 cm and 3° for the orientation. To test the system ability to execute secondary tasks, additional experiments were made in which an external disturbance was applied during aerial manipulation, verifying the robustness of the system in a metric quality measure and a frequency-based quality measure. Although the perturbation was significant to influence the poses of the robots and the payload, for both tests the robots were still able to maintain the cone constraints. These results can be watched in the video available at https://goo.gl/P3r7dL.

Using the concept of distance mismatches in a rigid formation to generate desired accelerations, presented in [39], and the Incremental Nonlinear Dynamic Inversion (INDI) controller to track desired accelerations, presented in [40], the authors of [41] proposed a robust formation control system for a team of quadrotors transporting heavy objects. The authors claim that the system robustness comes from the fact that the INDI controller reacts very quickly to compensate strong disturbances and because the algorithms only demand local measurements from the robots, i.e., the relative positions of members with respect to their neighbors, making it suitable to transportation missions in GPS-denied or adverse environments.

The employed distance mismatch algorithm works as a gradient-descent strategy that aims at minimizing error distances between formation members to form the desired formation shape, modeling the energy/cost of the system as if the robots were connected by springs. To also provoke formation movement, mismatches are introduced toward the desired distances, once sets of disagreements can generate translational and rotational accelerations signals without compromising the formation shape [39]. Thereafter, those signals are delivered to the INDI controller to track the error in linear and angular accelerations. One advantage of this control strategy is that the desired thrust of the actuators are not obtained directly from the vehicle's model, but according to the difference between the vehicle's accelerometer measurements and the desired accelerations. In short, this controller works as simple as the integration part of a PID controller, but instead of blindly adding input, the INDI controller takes into account the actuator effectiveness, actuator dynamics, and acceleration filtering, being able to better estimate the size of the input increments required to track the desired acceleration signals. As said, this treatment also allows faster reactions to disturbances, which is especially interesting for aerial vehicles performing transportation missions, once these systems suffer from dynamic disturbances caused by dynamic objects and varying cable tension, and also to wind disturbances due to wind gusts in outdoor missions or propellers backwash in indoor missions. To test the algorithms, experiments were conducted at Cyberzoo Lab, Delft University of Technology, using a team of four Parrot Bebop 1 quadrotors to lift, transport and manipulate a heavy load suspended by cables. To run the mismatched formation control and INDI controller, the Paparazzi open source autopilot was used, and the code was left available as open access at [42]. A joystick is used to choose the desired formation shape and position, and a ground station takes this information and calculates the desired acceleration signals that are sent to the quadrotors. The position information was given by a motion capture system that runs at 4 Hz and with an accuracy of the order of centimeters, suggesting that this approach can be applied in a fully distributed scheme without any external localization system. The experimental results can be watched in the video available at `https://goo.gl/8emmUF`. Moreover, just to increase insight on the INDI controller, its performance controlling a quadrotor flying in and out of a 10 m/s wind tunnel

is described in [40], and can be watched in the video available at https://goo.gl/NqKSFu.

2.5.3 Hybrid modeling

Cable-suspended load transportation is a hard mission due to dynamics changes during lift and flight. Indeed, a mathematical model of the UAV-cargo system at all flight stages is still an open problem. By glimpsing the possibility of taking advantage of large swings of the load to give agility to the UAV displacement, a hybrid load trajectory generation is introduced in [43]. According to the authors, two situations are stated: (a) the suspended load is not restricted to swing minimally if the active feedback control is enabled, and (b) the controller should track trajectories even when the tension in the cable goes to zero.

The UAV-cargo system is modeled employing the Lagrange-d'Alembert principle, with eight degrees of freedom, being four of them under-actuated. In short, the system evaluates taut or not taut cable conditions, so that the quadrotor with a cable-suspended load can be dealt with as a hybrid differential-flat system.

The flatness property was utilized to plan trajectories, and an optimization problem was then modeled to find the coefficients of the sixth-derivative of the load position. The paper also presents the design of a feedback controller that can track either the quadrotor attitude, the load attitude or the load position. It is worth mentioning that the quadrotor attitude and the load posture are completely decoupled, according to the proposed modeling. A video that illustrates the experiments to validate the method is available at https://goo.gl/oG9CZ2.

A critical maneuver in cable-suspended load transportation tasks is lifting the cargo from the ground. In [44], a hybrid approach splits the lifting process into three discrete states: Setup, Pull and Raise (see Figure 2.5). All these transitions have their own mathematical model, and consequently, its dynamical particularities. In summary, at setup mode, the load is on the ground and the cable is not taut. At pull mode, the cable goes from slack to taut at some instant during this maneuver, so that the cable tension on the quadrotor goes from zero to some non-zero value, and the total thrust should be increased to lift the load. Finally, another state change occurs when the load leaves the ground, configuring the raise mode.

A differential-flat hybrid system was proposed to describe the system's states, and dynamic inversion combined with a PD controller was responsible to guide the quadrotor-with-load through a series of waypoints, containing the setup, pull, and raise situations.

The video available at https://goo.gl/v715hd compares three load lift experiments: the full proposed approach, lifting without switching control and lifting without considering waypoints. The tests were conducted at MARHES laboratory [32] and pointed out the better performance of the proposed approach in comparison to the other two cases.

To manage the switching dynamics under different cable's tautness conditions, the authors

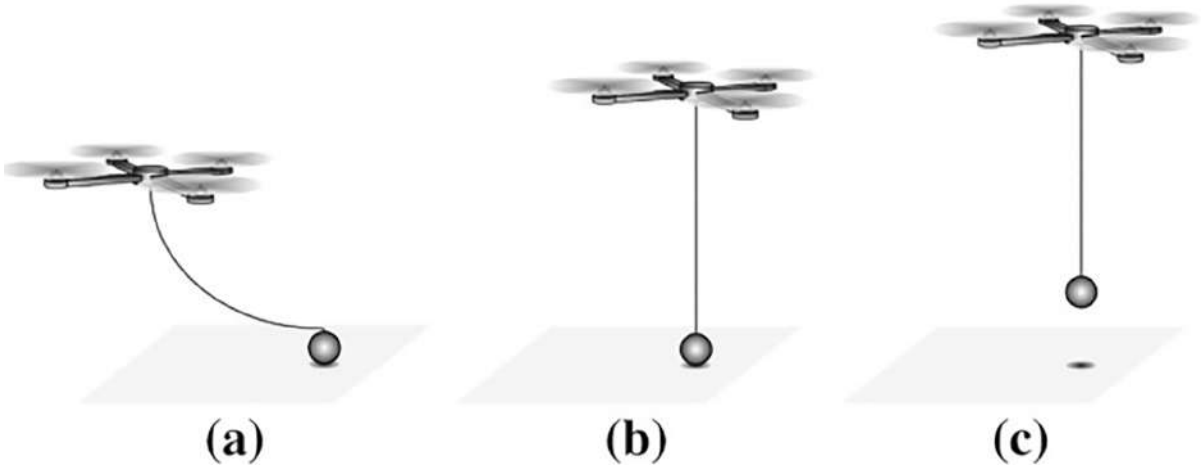

Figure 2.5 – The lift states in [44]: (a) Setup, (b) Pull, (c) Raise.

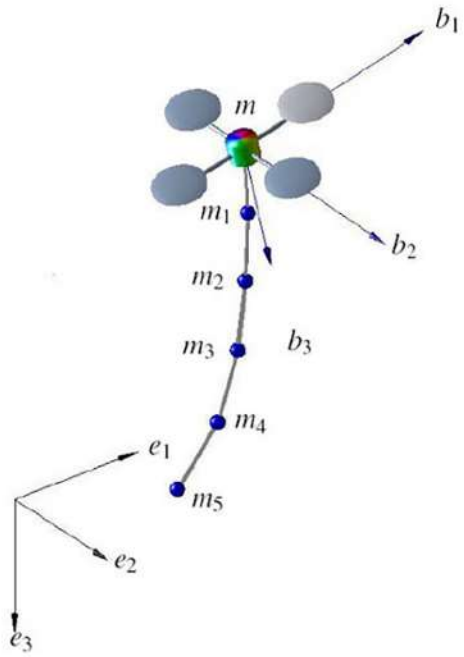

Figure 2.6 – Cable modeled as a serial connection of arbitrary number of links [45].

in [45] does not use the premise of a massless and always taut cable, modeling it instead as a series of links connected by spherical joints (see Figure 2.6). This approach allows the analysis of the effects of a deformed cable in many situations, such as when the mass of the load and the cable are comparable, in cases where the load is distributed along the cable, or in situations where the tension in the cable is minimal. Lagrange formulation is applied to describe the motion of an arbitrary number of links, with different sizes and masses.

To navigate, a geometric nonlinear controller was designed to get the hanging configuration asymptotically, and its stability was proven considering the theory of Lyapunov. The controller was implemented in a UAV using a Gumstix Overo onboard CPU, which is connected to

a ground station via Wi-Fi. The tests occurred in the facilities of The George Washington University, at Motion Capture and Analyses (MOCA) laboratory. This lab is equipped with a Vicon motion capture system that transferred the motion coordinates to the onboard CPU via an XBee module. A video correspondent to such experiment can be found in https://goo.gl/TQhVVg.

The authors extend the previous work to a rigid body payload in [46], presenting a complete dynamic model and geometric nonlinear controller for the payload and flexible cables, in a scenario with an arbitrary number of quadrotors. The coupling effects between the agents and the payload attitude and stability are also considered in this analysis.

To demonstrate the desirable properties of the proposed system, two quadrotors are designed to stabilize a rod weighing 0.52 kg, with a length of 2.05 m. This rigid body payload is connected to the quadrotors by wires of 1.3 m of length. Initially, the rod is pulled by 30° and released as a disturbance, and two tests are made to compare the influence of considering the dynamics of the payload and cables in the controller. The same testbed and experimental apparatus were used to perform this comparison. The results showed a reduction in the undesired oscillations, as one can see watching the video available in https://goo.gl/W3EscE.

To deal with the limitation on trajectory tracking that the above-mentioned controllers present, another expansion for the flexible cable approach is presented in [4]. This paper uses a finite-horizon linear quadratic regulator to track the desired trajectory with a large region of attraction. Optimal results were obtained through numerical simulations in different transportation systems: (a) single quadrotor with a point-mass load suspended through flexible cables, (b) multiple quadrotors with a point-mass load suspended through flexible cables, and (c) multiple quadrotors carrying a rigid-body load suspended through flexible cables. However, due to the increased number of states in this system, the experimental implementation of the controller was harder to achieve. Nevertheless, the authors hope that they can present that soon.

2.5.4 Aggressive maneuvers for load transportation

Regarding suspended load transportation, some researchers have worked to allow large swings in aggressive maneuvers under feedback control. In contrast to conservative strategies that aim minimal swing to payload motions, an optimal strategy exploiting the entire range of motion is proposed in [47], allowing large load swings, load pick-up and release with the vehicle not directly above the load, and periods of zero cable tension under trajectory control. To achieve it, two hybrid stages are considered: quadrotor with and without load. In the first case, the cable is taut and the UAV is controlling the load motion. In the second one, the UAV

is under control while the load is described as a free-fall system. Using hybrid modeling for the vehicle-with-load and a mixed integer quadratic programming (MIQP) for trajectories, the authors accomplish a collision-free trajectory planning considering a set of known obstacles.

Experiments were conducted at GRASP laboratory, at the University of Pennsylvania, with a Hummingbird quadrotor and using a Vicon motion capture system. The first experiment was to make a quadrotor with a suspended load pass through a window whose opening is too small for the quadrotor plus suspended load to pass through. To accomplish this maneuver, the load is swung into the opening and, while it undergoes free-fall motion, the quadrotor should change its attitude and pass through the window. It was verified that the load had to be swung at an angle greater than 40° in this maneuver. A second experiment was to pick-up and release a load while performing an elliptical trajectory. The load was not below the quadrotor, so the pickup and release maneuvers were realized at an angle of 20° from the vertical. An electromagnet was used to attach and detach the load. In this test, the hybrid switching allowed the pickup and release of the load without a meaningful increase in the trajectory-tracking error, even at the transition points. The accomplishment of these tasks can be watched at the video available in https://goo.gl/no8WWm.

Whenever a suspended load system does not need to counterbalance the cargo motions, and consequently does not require a direct swing suppression, aggressive maneuvers can be performed in an optimal way. Although the previously presented methods treat well the cable tautness variations, the solutions involve optimization task. Therefore, the challenge becomes to design simple and easy-to-implement controllers capable of performing those agile motions.

A further step in this direction is presented in [8], where a novel parametrization is proposed to represent the cable-suspended load transportation system. The employed modeling departs from state-of-art by describing the payload behavior based on the displacement of three passive joints, two of which are revolute joints whereas the other one is a prismatic one.

To create safe and optimal trajectories for the agents, the trajectory planning problem was formulated as a Mathematical Program with Complementary Constraints (MPCC), and a solution inspired in [48; 49] was implemented using Sequential Quadratic Programming (SQP). This approach allowed many constraints to be considered during the trajectory optimization, such as propellers' thrust profile, cable's length, joint's limit displacement (due to physical limits or to avoid collision of the cable and the UAV), obstacles in the environment, and so on.

According to the authors, the proposed methods (i) outperform the state of the art in terms of speed without restricting the trajectory complexity, (ii) provides a way of parameterizing different tasks, (iii) and guarantees the feasibility of the trajectory with respect to the system dynamics and control input bounds.

To validate these bold assumptions, experiments were made showing a quadrotor performing

various tasks, namely to throw the payload towards a target, to fly through waypoints at different speeds, and to avoid both vertical and horizontal obstacles. The experiments were conducted at the University of Zurich, using a custom-made quadrotor equipped with an Odroid-XU4 onboard computer. An Optitrack motion capture system provides posture information at 200 Hz. The trajectories were generated in a ground station and then sent to the CPU onboard the quadrotor via ROS. The 3D agile maneuvers can be seen at the video available in https://goo.gl/pZYvjy.

2.5.5 Aggressive maneuvers applied to cooperative load transportation

Some works, such as [36], [50], [51], [52] and [53], avoid some complexities of a multi-robot cooperative task using non-agile, sub-optimal motions or simplified models. Aiming at performing agile maneuvers even in a cooperative transportation environment, [54] presents a trajectory generation algorithm for a multi-agent team of aerial robots carrying suspended payloads. The main goal achieved was to propose feasible trajectories in an obstacle-free 3D workspace. The problem was modeled as a labeled multi-robot planning problem, in which the robots should transport the payloads from a start position to a fixed goal position.

Up to nine robots were used to validate the proposed trajectories. To avoid inter-agent collisions, each quadrotor with its payload was modeled as a kinematic cylinder, and algorithms were proposed for path planning and trajectory tracking. The motion planning problem was solved using iterative geometric motion planning algorithm. This algorithm is an extension of the HOOP algorithm [55] proposed by the same research group. Figure 2.7 shows an overview of the proposed path planning method. Payloads should navigate into lines of the same color, from circles to stars. At first, the algorithm allows each quadrotor to move in a straight line towards the goal. Once the first collision is identified, it is avoided in a roundabout-like manner, using circular holding patterns. Each load stays in this holding pattern until a safe set of trajectories is found. Every path generated by the path planner keeps the distance between any pair of quadrotors above two times the cylinder radius.

Since the path planner guarantees that the agents are separated by at least $2r_Q$, where r_Q is the radius of the quadrotor, it is possible to discover a safe corridor, allowing the trajectory planner to propose feasible trajectories inside those safe corridors. The quadrotors dynamics are modeled as coordinate free, and multi-body geometric controllers were proposed to control the agents under agile motions. To validate the algorithms, experiments were performed at GRASP laboratory, University of Pennsylvania. The proposed algorithms and control modules are implemented in C++/ROS in a ground station, and the Gurobi Optimizer was used to solve the trajectory optimization.

According to the authors, the loop was closed on the quadrotor instead of on the payload,

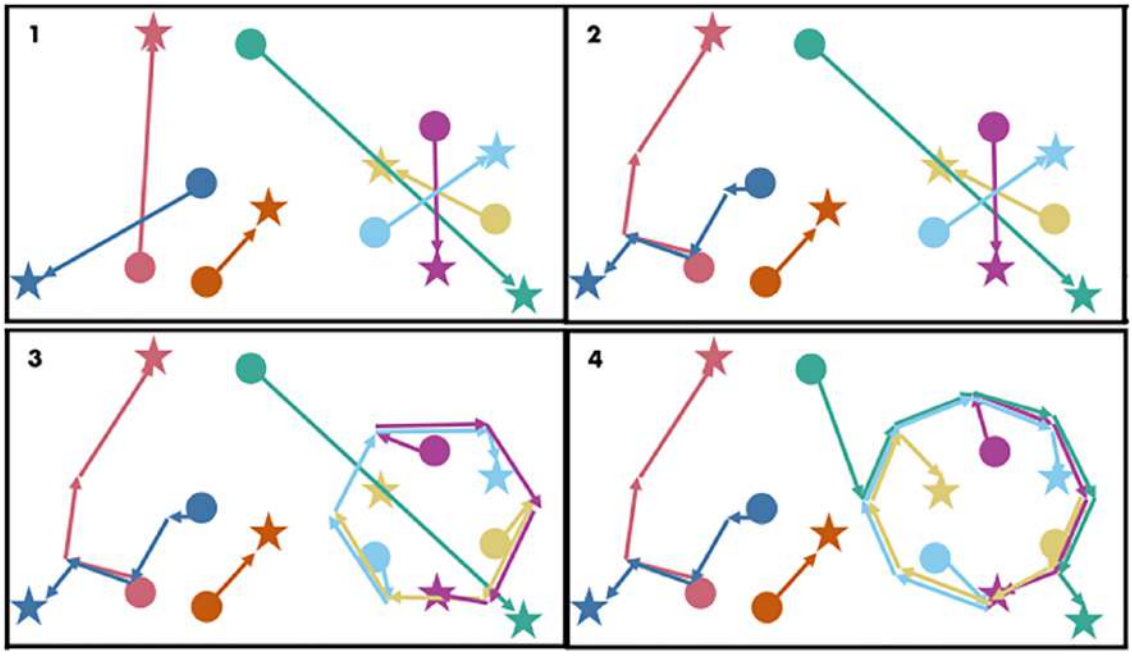

Figure 2.7 – Summary of the proposed algorithm. 1. Payloads start moving to their goals. 2. The first collision between the red and blue loads is resolved using a Circular Holding Pattern. 3. The next collision between the purple, light blue, and yellow loads is resolved using a separate Circular Holding Pattern. 4. The existing Circular Holding Pattern is refined to accommodate the teal payload. The algorithm ends, as a collision-free motion plan is found [54].

because the motivation is to validate the dynamic feasibility of the obtained trajectories. After the desired thrust and orientation were obtained by the algorithms running in the ground station, they were sent to the quadrotors via XBee modules, and an onboard attitude controller tracks the desired orientation. A Vicon motion capture was used, transferring the coordinates at a 100 Hz rate.

Experiments were performed with two, six and nine robots. As expected, as the size of the team and holding patterns increase, the identified safe trajectories become increasingly longer than the straight-line distances. However, the payload was still able to swing, reaching angles of about 40°. The experiment was recorded in a video that can be watched by accessing https://goo.gl/i8AqzP.

A similar cooperative multi-body system is introduced in [56]. Once more, the differential flatness concept is used to find dynamically feasible trajectories for a system composed of a quadrotor with a suspended load. However, in this study, it was shown that this mathematical approach could also be applied to a team of robots carrying a point-mass or a rigid-body payload. Moreover, it is shown that for a multiple-quadrotor cable-suspended point-mass load the system can be considered differentially-flat if the number of quadrotors is more than one. As for the case of a rigid-body load, the minimum number of agents to achieve differential

flatness is four.

Three hummingbird quadrotors were used to validate the hybrid models proposed, transporting a rigid-mass load along an elliptical trajectory with smoothly increasing frequency. A Vicon motion capture system was used to obtain the posture of the quadrotor. Similar to the previously analyzed paper, to achieve aggressive and agile maneuvers for a squad of UAVs, the geometric controller closes the loop on the quadrotor and not on the load. The experimental results can be checked in the video available at https://goo.gl/1ciFeT.

2.5.6 Vision-based load transportation

In order to enable autonomous flight, vehicle's state estimation and some kind of environment mapping, it is necessary to plan safe trajectories and perform accordingly. Inside the laboratories, these requirements are normally achieved using motion capture systems, while, in outdoors, GPS systems can be used to obtain a similar effect. However, both systems show remarkable drawbacks. For the former, to enable safe autonomous flight, the environment should be well structured and every dynamical agent should carry reflective markers. Additionally, motion capture systems are very expensive. For the latter, since quadrotors are small and highly maneuverable, it is hard to maintain a reliable GPS information, lacking state accuracy and performing poorly near large obstacles.

In such a context, it is encouraged to equip the aerial vehicles with sensors, allowing the robot to localize itself. The most common onboard sensors are the Inertial Measurement Unit (IMU), GPS, monocular cameras, and ultrasonic or laser scanners. Once those sensors present inherent flaws (e.g., accumulated drift errors in IMU, lack of precision in GPS, range limitation in scanners), to obtain a reliable state estimation, a common approach is to fuse the sensorial data using Kalman filters or information filters.

Until some years ago, cameras were not viable sensing devices onboard quadrotors, due to the high demand for power and processing that a vision algorithm requires. However, the recent advances in processing capacities, combined to the light weight and small size of modern cameras, permitted monocular visual-inertial system (VINS) composed only by a monocular camera and an IMU to become widely used. The basic vision technique used in those visual-inertial systems is the feature-based method, in which a camera detects features and determine its position relative to those features using some triangulation method. The most common technique is the so-called Simultaneous Localization and Mapping (SLAM). Furthermore, features captured by the camera and other sensors could be assembled into a map, allowing the robot to map and understand its surroundings, allowing collision-free navigation.

Pursuing solutions that do not use motion capture systems to estimate the coordinates

of the quadrotor and load, [5] proposes an agile system capable of controlling the payload's position and evaluate the load state by using a downward-facing camera and an onboard IMU. Although some previously analyzed works, such as [54] and [8], have also performed large load swings, both of them closed the loop on the quadrotor and not on the load.

Differential flatness was used to obtain safe trajectories, being the sixth-derivative problem formulated as a piecewise polynomial quadratic program, that was solved using commercially available optimization software. The payload estimation was conducted using a fisheye lens camera facing downwards combined with an Extended Kalman Filter (EKF). To detect the payload in the images captured by the camera, a black and white circular tag was attached to the load, and the tag position was obtained by a light-robust image processing algorithm.

A hierarchical geometric controller was proposed, using the desired load trajectory to control the load and quadrotor's positions and attitudes. To estimate the load position, data provided by the camera, IMU and Vicon motion capture system were fused, whereas for estimating the position of the quadrotor, data provided by just the IMU and the Vicon motion capture were fused. In both cases, an EKF was adopted as the fusion engine.

To validate the proposed algorithms, experiments were conducted at the testbed of the GRASP laboratory, University of Pennsylvania. AscTec Hummingbird quadrotors with onboard ODROID CPU were used. For position and attitude estimates, a Vicon system operating at a 100 Hz rate broadcasts the information over a Wi-Fi channel to the onboard CPU. The payload was observed by an MLC200w Matrix-Vision camera, and the images were received by the CPU via USB at a rate of 50 Hz. The IMU orientation information was delivered via a serial connection at a rate of 100 Hz. The quadrotor attitude control was run on an onboard low-level micro-controller, and all other algorithms were implemented in C++/ROS on the onboard ODROID.

The experiments consisted of three circular trajectories being tracked at three different period times. Each trajectory was tracked with a different cable length. Although the circuits and dynamical systems were different, the proposed control algorithms achieved stable navigation control without re-tuning the controller gains. Moreover, the proposed methods allow optimal and agile trajectories even through a slalom course. Experiments on slalom traverse were performed at three different speeds, reaching stable control even for the fastest speed, where swings up to 53° from the vertical were detected. A video containing the experiments can be watched at the link `https://goo.gl/Jen79E`.

A different approach to the modeling and control for a swing-free vision-based load transportation is presented in [6]. There, the integrated dynamics of the quadrotor, cable, and payload is considered using a mathematical model based on Euler-Lagrange formulation and described by Hamiltonian mechanics.

In order to achieve precise and fast payload positioning with minimum swing, an Inter-

connection and Damping Assignment-Passivity Based Control (IDA-PBC) was implemented to asymptotically stabilize the load angle oscillations. This methodology is novel, regarding cable-suspended load transportation, treating the inherent underactuated behavior of the system as an energy minimization problem in the control loop, resulting in increased robustness against non-modeled dynamics. Furthermore, such treatment pursuits to avoid undesired swing oscillations of the load without any expensive motion capture system or external reference instrument for positioning.

To validate the technique, experiments were conducted at the testbed of the Heudiasyc Laboratory, at the University of Technology of Compiègne (UTC). A Parrot AR.Drone was connected to a load of 0.05 kg by a rigid rod with one degree-of-freedom. Data provided by an onboard kit containing three gyroscopes and three accelerometers, an ultrasound altimeter, an air pressure sensor, and a magnetic compass were fused by an EK Filter with two onboard cameras to achieve load and quadrotor positioning. One of the cameras faced downwards, at a rate of 60 fps, to estimate the horizontal velocities through an optic flow algorithm. The other camera faced forward, capturing images at 30 fps for monocular vision-based navigation.

This vision-based navigation uses monocular SLAM and Parallel Tracking and Mapping (PTAM) techniques to split tracking and mapping into two different tasks processed in parallel, achieving camera pose estimation, and, by consequence, the UAV pose, in a totally new and unknown scene. The algorithms are computed at a ground station using ROS, and all sensors communicate with the ground station at a frequency of 200 Hz. For the sake of performance analysis, an Optitrack motion capture system was used to estimate the swing angle of the payload. The motion capture was not included in the control closed loop.

In order to simplify the control design, the model was reduced to a 2D transverse plane scenario, and a feedback linearization control was used to control the *x-position* and *pitch* states, while a proportional derivative controller was employed for *yaw* regulation. The experiments exhibited good results for this IDA-PBC method, performing fast load displacements with RMS load oscillations of 2.6°. The results can be watched in the video available at `https://goo.gl/vAgpFP`.

Another novel vision-based collaborative transportation scheme is introduced in [57], in which two quadrotors transport a cable-suspended load without explicit communication, making it robust to communication failures or delays. The system comprises two quadrotors, in a leader-follower configuration, carrying a suspended payload. Each agent was modeled as a decoupled quadrotor-with-suspended-load system, allowing the design of a control scheme that relies solely on the cable gripper state estimate and the quadrotor state estimate.

A Linear Quadratic Regulator (LQR) was employed for quadrotor and load control. The control algorithm was designed to keep the follower quadrotor exactly above its load gripper, ensuring minimum force on the load during the transportation. A PD controller is used for

this load tracking, and the follower final control signal, composed by the PD and the LQR control signals, is delivered to an onboard attitude controller.

Furthermore, the authors proposed a trajectory planner to produce the piecewise polynomial trajectories that were used to describe the temporal evolution of the leader's load gripper states, and the leader's position could be directly derived from its gripper position. A proportional controller was also deployed to align the follower's yaw angle and height with those of the leader, preventing movement of the payload along the axis of the follower's yaw and the cable from hitting the rotors of one of the quadrotors.

For validation, the system relied only on onboard sensing, using a camera and IMU for state estimation and control of the quadrotors. The experiments were conducted at the University of Zurich, using quadrotors equipped with an ODROID XU4 CPU to run the algorithms and a Pixhawk PX4 for low-level control. Magnetic grippers were used to attach the load to the cables, containing markers for visual tracking. A standard USB fisheye lens camera was used for visual odometry, state estimation, and to track the grippers. An AprilTag was attached to the back of the team leader, and a dedicated pinhole camera was installed on the follower to track the tag attached to the leader.

In eleven out of thirteen runs of the experiment, the system was able to safely transport the payload along a linear trajectory at moderate speed. It was noticed that the two failures were caused by perception errors due to bad tag detection or visual-tracking losses by the visual odometry, due to rapid motions. Moreover, it was showed that the follower could track the leader's yaw angle and height, and execute the proposed transportation methods with few centimeters of deviation. A video illustrating such experiments can be accessed at the link https://goo.gl/fwfoNx.

2.6 Works Considering Grasped Load

In grasped transportation, the load gets rigidly connected underneath the vehicle and, differently from cable-suspended transportation, it is neither necessary to model it as a separated body nor to consider changes in the system dynamics during flight. Furthermore, once the load is not tied or hanging in a flexible cable, this approach provides easier design options to capture and deliver the load. Most likely because of this, in the early years of load transportation using quadrotors, most works adopted the grasped load approach.

A proposal to accomplish grasped load transportation is presented in [53], considering individual and cooperative schemes. The quadrotors are equipped with light-weight, low-complexity grippers (similar to Figure 2.2b), which allow grasping and releasing the load quite simply. Since a cooperative approach is adopted, objects that are heavier than the maximum payload of a single quadrotor can also be transported. A set of linear control laws are

defined around a near-hover position, allowing payload stabilization along three-dimensional trajectories. Additionally, an estimation of the inertia parameters of the grasped load is made and used to adapt the controller and improve the performance during flight. Such a solution also adopts a motion capture system to provide an accurate position of both the UAV and payload, using this information to feedback the controller.

Experiments were run with teams of quadrotors cooperatively grasping, manipulating, and transporting payloads along 3D trajectories. Two experimental trials were designed. One consists in a team of four quadrotors rigidly attached to wooden payloads of different configurations (line, L, T and cross, as shown in 2.8), whereas the other consists of a team of two quadrotors whose task is to pick up and transport a bar which is $0.8m$ long, weighing $320g$. The experiments were conducted at GRASP laboratory, University of Pennsylvania. The position and orientation of the quadrotor are gotten by a Vicon motion capture system, and the angular velocities are sensed by the IMU onboard the quadrotor. The communication of the quadrotor with the ground station is made via Zigbee, at the same 100 Hz rate of the Vicon system. Such information is computed in Matlab through a ROS-Matlab bridge. The velocity of the quadrotor is obtained by numerical differentiation. The experimental validations achieved speeds up to 0.5 m/s during navigation, as one can see in the video available in `https://goo.gl/SnfUBu`, which illustrates the performance of the quadrotors in the accomplishment of the two proposed tasks.

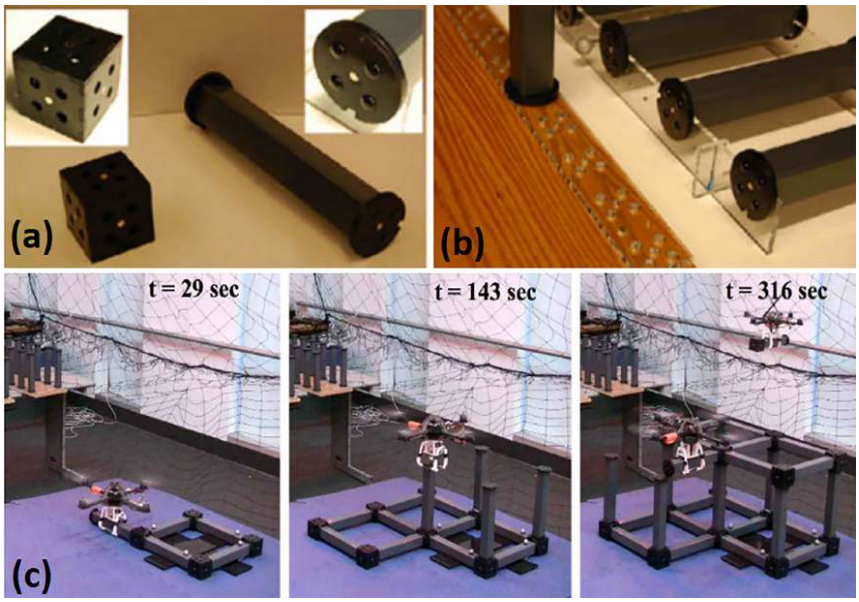

Figure 2.8 – Graphical depictions of the four configurations addressed in [53].

A similar approach is adopted in [50], now considering an elastic load, rather than a rigid one. This is a particularly interesting analysis since even if the vehicles are rigidly attached, the load may suffer not only oscillations but also deformations.

In this work the system is also linearized around a near-hover condition, now using a quaternion-based attitude representation, to avoid singularities. The dynamic models of the vehicles and the flexible load were obtained analytically, and a hybrid Kalman filter estimator was designed to observe the pose of the bodies and deliver their full state information, including the current magnitude of the load deformations. An infinite-horizon LQR controller determines the desired positions for the quadrotors and load, also controlling the deformations, in order to eliminate them. Furthermore, the estimated deviations obtained by the filter are inserted in the quadratic cost function, helping the controller to handle noises and incomplete state information.

To validate the proposal, experiments were carried out in the Flying Machine Arena, at ETH Zurich [58]. Six modified AscTec Hummingbird quadrotors [59] were used to carry a flexible aluminum ring with 1 m of radius weighing 0.54 kg. The vehicles were uniformly attached around the ring circumference, at a tilt angle that allows their thrusts to have a horizontal component, to perform horizontal accelerations. Information sharing was implemented by a low-latency radio link at 50 Hz, and the absolute position and attitude were measured by a motion capture system at 200 Hz. For comparison, two transportation experiments were run, firstly considering the flexible load treatment, and secondly not considering it. The results showed that the controller, when treating the load deformations, was able to manage the deformations and accomplish the transportation task in opposition to the experiment without such a treatment, in which the ring went to a crash. These results can be seen in the video available in `https://goo.gl/BPGhta`.

2.6.1 Cooperative load transportation applied to robotic construction

Construction automation is an interesting field that pursues to apply computer-controlled processes, mechanization, and the latest automation technologies directly to activities related to building subdivisions (e.g., civil engineering, fabrication of building components) [60]. Traditionally, only ground robots are employed in construction-related tasks (such as industrial robots or CNC machines), restraining the robot actions to a predefined working space and limiting the type and size of the job it can execute [61]. Conversely, aerial robots are not limited by the same constraints of ground-based ones, and rotorcrafts are already being used in construction applications, accomplishing aerial lifting or load transportation in hard-to-reach locations. However, those aerial vehicles are manually operated and, therefore, are limited by the pilot skills and safety policies imposed by the operator [62].

Driven by the early results regarding load transportation using quadrotors, as depicted in [36], [50], and [53], the concept of aerial robotic construction (ARC), which refers to the use of aerial robots in construction-related tasks performed by unmanned quadrotors, gained

prominence and importance among robotic researchers. Since aerial robots can move and operate dynamically in 3D space, their use opens up a new set of possibilities to the field of construction, and brings several advantages such as (i) they are capable of freely move in the 3D space and do not need any kind of rails or scaffolding to operate, being more versatile and efficient from bottom-to-top in the construction task, (ii) they can connect to data blueprints, building directly from the digital architectonic design, (iii) they can use cooperative schemes that are very scalable, fault tolerant, and able to accomplish complex tasks unattainable by a single robot, and (iv) they bring the possibility of building structures without human intervention, assuring construction quality, efficiency, safety, and flexibility in architectural designs [60].

The success of this kind of mission is strictly related to the development of two competencies for the aerial vehicles, namely the ability to reach a precise position/orientation in complicated and unstructured environments, and their capacity to grab, transport and manipulate a payload. In such a context, some works took the first steps to investigate and address the challenges related to building tasks. In [51] a work developed in ETH Zurich employed four quadrotors to raise a 6 m tall tower made of 1500 polyurethane foam bricks. The construction demanded 18 hours and was made during a four-day-long live exhibition at Regional Contemporary Art Fund in Orléans, France.

The quadrotor's framework that was used in the exhibition is similar to the ETH Flying Machine Arena platform previously mentioned, comprising customized Hummingbirds quadrotors, a motion capture system, wireless communication channels, and the necessary software libraries. In a short description, glued bricks were manually placed into a pickup station and, after the authorization from a human operator, a quadrotor hovers over the brick, actuates the ingressive gripper for picking it up, and flew to the desired placing position in the structure to release the brick. The placement instructions and sequence order are given by a blueprint, executing the construction straightforwardly from the digital design. The process is conducted as a pick and place state machine, for which a general scheme can be seen in Figure 2.9.

To perform the navigation, a trajectory planner was implemented, subdividing the allowable fly region into waypoints, and using a waypoint reservation system to coordinate the vehicles. The working principle of the reservation system is such that while a vehicle is navigating into a segment between two waypoints, it tries to reserve the next segment. If the reservation is successful, the vehicle continues. Otherwise, it stops and hovers at the end of the current navigational segment, waiting for the availability. To handle the hours of flight required for continuous operation a battery-charging station was built, charging the batteries of the quadrotors upon contact. A video exhibiting this accomplishment can be seen at the link `https://goo.gl/zrC7rP`.

Another use of quadrotors for ARC was conducted at the GRASP Lab, University of

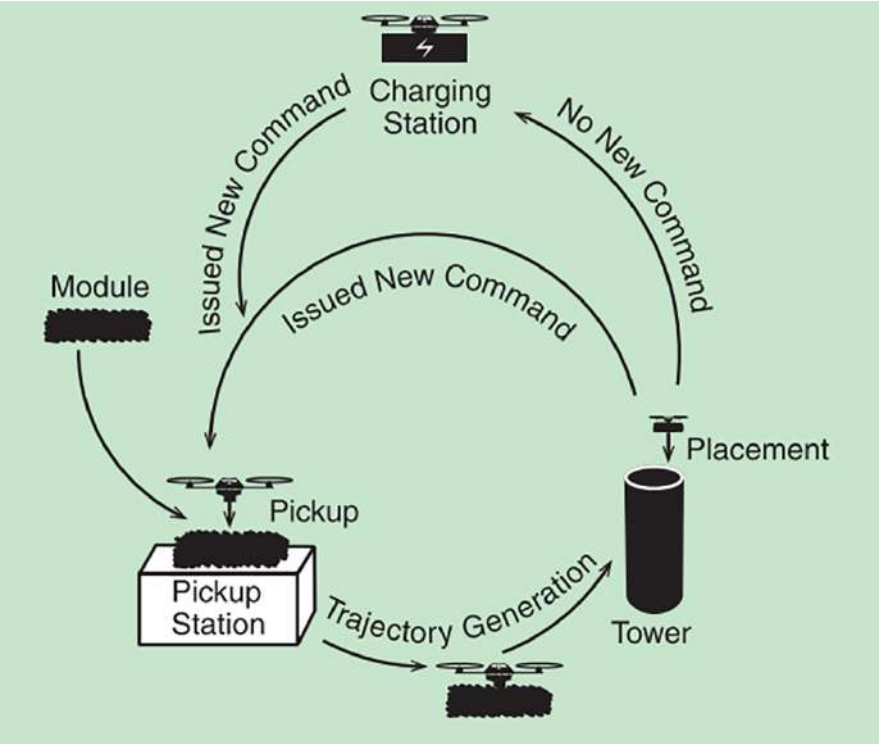

Figure 2.9 – The pick-and-place state machine used to assembly the tower-like structure in [51].

Pennsylvania. It investigated the usage of a quadrotor team to autonomously build tower-like cubic structures using modular parts [52]. A special cubic structure algorithm was implemented to elaborate the construction blueprint, and a pick and place state machine, similar to the one illustrated in Figure 2.9, was adopted to assemble the parts.

The modular parts used in this work were nodes and members, as shown in Figure 2.10a. In such a case, a module is a single node attached to a single member, as illustrated in Figure 2.2a. The attachment is made by magnets present at the face of each piece, also aided by complementary protrusions that allow a snap-fit connection. The constructive parts are stored in bins, as it is shown in Figure 2.10b, with each node weighing 60 g, each member weighing 119 g, and each module (a node attached to a member) weighing 179 g. Members that are used as columns of the cubic structure are stored vertically in a bin, and impactive grippers were used to manipulate the load.

To control the AscTec Hummingbird quadrotors adopted to accomplish such a task, linear controllers similar to those presented in [53] were employed, and the state estimation was provided by a Vicon motion capture system. Since the vehicles had to pick up members or modules in the horizontal or vertical directions to construct the cubic structures (Figure 2.10c), two control approaches were used. To pick up columns, the quadrotor gets closer to the piece flying at an altitude greater than the height of it, hovers over it and close the gripper,

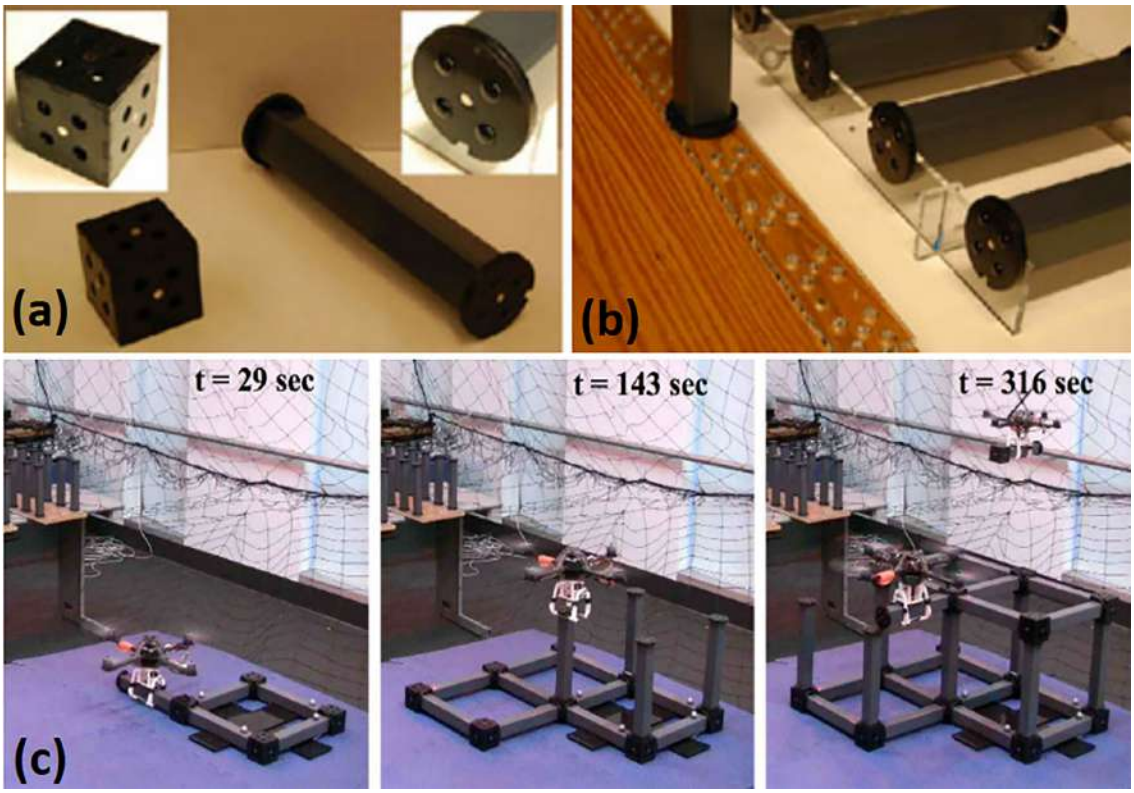

Figure 2.10 – (a) a node (left) and a member (right), (b) bins containing the members, and (c) cubic structures used in [16].

thus picking up the piece. An integral term in the control loop is responsible to adapt to the load, and the thrust required to control the quadrotor is verified to determine if the quadrotor has grasped the column successfully. If it exceeds the nominal thrust, it is understood that this additional thrust is a compensation for the load weight, and the quadrotor continues to assembly the piece into the structure. Otherwise, the robot tries again or change to the next available column. To pick up the horizontal modules, the quadrotor hovers over it, descends and "lands"on the member, and then closes the grippers. Again, the adaptation through the integral control and the required thrust allows the determination of a successful picking up.

To validate the proposal, a team of quadrotors was employed to construct tower-like cubic structures directly from the digital blueprint provided by the special cubic structure algorithm. The experiments showed that the system is robust and can operate with very small errors. The results obtained can be accessed in the video available in `https://goo.gl/R6iAxG`.

As the last ARC application example, a research was conducted in ETH Zurich using quadrotors to build tensile structures with flying machines [25]. This construction application is particularly interesting in emergency response, constructing, for example, bridges and pathways in hazardous areas after a disaster, or placing points of support to climbers and mountaineers, either to improve safety or to accomplish rescue missions.

Such authors investigated the building elements required to assembly load-bearing tensile structures and translated them to rope knotting principles and feasible trajectories for quadrotors equipped with a passive roller responsible to deploy the rope. Using an algorithm similar to the one presented in [63], collision-free trajectories were obtained for multiple quadrotors flying simultaneously. To guarantee the trajectory tracking by the UAVs while applying constant force along the rope direction, a requirement to build the tensile elements, an admittance controller was implemented, in cascade with a position and attitude controller. This hybrid force-position control was employed to build a linear and a surface tensile structure. The experiments were conducted in the ETH Zurich Flying Machine Arena, and the performance of the quadrotors to build a tensile structure can be seen in the video available at https://goo.gl/oaEXXz.

It is secure to say that aerial robotic construction research is still in its childhood and there is still much work to do. As pointed out in the literature, several important issues should be investigated, such as development of modular components that are suitable to construction and contributes positively when taking into account dynamic considerations related to the vehicle, design of optimal ARC blueprints, accounting for the connection of complex architectural pieces by individual or cooperative squads of aerial robots, developments in aerial robotic manipulation and aerial towing controllers, and mechanical improvements in the end-effector actuators (e.g., mechanical grippers, dexterous hands, robotic arms). Furthermore, to achieve the flight precision necessary for construction, quadrotors still relies on external motion capture systems, and improvements in environment perception (depth cameras, stereo cameras, LIDARs) and onboard processing are awaited to change this perspective. Also, as discussed in Section 2.4.1, the central bottleneck in quadrotor technology nowadays is the balance between payload capacity, energy source and flight time, limiting their lift capabilities and making difficult their applicability to construction tasks. Despite these critical outlines, the drastic improvements achieved in UAV technology in recent years raises the optimism about what we will achieve soon.

2.6.2 Vision-based cooperative grasped load transportation

Taking into account the relevance of cooperative load transportation and vision-based algorithms, the authors of [64] propose a cooperative control strategy to move structures that are too heavy or too big for a single quadrotor. They introduce a new approach to coordinated control that allows independent control of each vehicle, ensuring system stability and a new cooperative scheme that allows each vehicle to benefit from measurements acquired by other vehicles.

The system composed by two quadrotors and a cargo is modeled as a whole and a

constrained quadratic optimization problem is formulated to find motor speeds required to achieve the attitude of each UAV during a load transportation and delivery task. To achieve it, extended and unscented Kalman filters get data from the onboard camera and IMU to estimate the pose of each UAV independently. Then, a motion refinement algorithm improves the pose information, combining these estimations with the physical constraint imposed by the shape of the carried object. This optimization helps to preserve the integrity of the object by reducing the forces acting on it, allowing also better energy profiles by reducing the counterbalance of undesired forces between the robots.

To validate the proposed methods, experiments were run at the University of Pennsylvania, this time at Penn Engineering Research and Collaboration Hub (PERCH) laboratory. Both quadrotors are equipped with a Qualcomm SnapDragon board and an electromagnet to attach the load to their body. All developed tasks and algorithms are run onboard, in a ROS environment. Experiments were performed with and without the refinement algorithm, and, as expected, increased performance was observed in the first case. During the flight maneuvers, speeds up to 4.2 m/s and accelerations up to 5 m/s^2 were achieved. Such experiments can be seen in the video available at the link https://goo.gl/nwi4QL.

2.6.3 UAV-UGV cooperative load transportation

Surveillance, mapping, and load transportation are real-world applications for which cooperative working brings more benefits when compared to a single specialized agent. Moreover, these tasks can be better accomplished when heterogeneous robotic agents with different capabilities and types of sensors are used. Despite the numerous advantages that the UAV possesses, an unmanned ground vehicle (UGV) can carry additional payload and sensors, far beyond the weight and power limits of the UAV. Working together, UAV and UGVs can collaborate amongst themselves to accomplish a given task more efficiently, exploring their particular characteristics [65].

A cooperative load carrying task is presented in [66] for a heterogeneous formation, where a UAV equipped with a pair of manipulation arms should either to pick up or deliver a load over a UGV. In such a problem, all robots have information about the initial and final position of the load, as well as a 3D occupancy map of the environment. Then, a task decomposition method coordinates their displacements, while a Generalized Partial Global Planning controls them.

To evaluate the proposal, two Pioneer P3-DX ground robots and one 3D Robotics quadrotor equipped with a dual-arm manipulator were used. The UGVs are equipped with their basic sensors (encoders and sonar), and the UAV with an ArduPilot Mega and an ODROID U3, for stabilization and attitude control. All robots run an Ubuntu distribution plus ROS to

execute the high-level mission planner, and the required posture information is acquired by an Optitrack Motion Capture System and streamed to them via Wi-Fi. The experiments were performed at the Laboratory for Robotics and Intelligent Control Systems (LARICS) Lab, University of Zagreb, and the video demonstrating the mission accomplishment is available at https://goo.gl/A2WftY.

2.6.4 Aerial load manipulation

Aerial manipulation, as discussed in Subsection 2.4.2, is an area that has aroused much research interest due to its direct relation to real-world robotic applications. For being small flying units equipped with onboard sensors for guidance and navigation, and able to manipulate objects, UAVs have become a very attractive choice to perform manipulation tasks.

In such a context, a research developed in the LARICS Lab, University of Zagreb, which deals with aerial load manipulation [67] deserves mention. The authors proposed a controller for a quadrotor with a multi-DOF dexterous arm system, and benchmark its manipulation capabilities while performing classical manipulation missions. The missions were analyzed with respect to its environmental coupling, being broken into missions involving momentary coupling (interactions with objects of finite mass, not attached to the environment, as picking and manipulating in the air), loose coupling (interacting with objects attached to environment without perching, such as assembling, inserting), and strong coupling (when the UAV becomes firmly attached to the environment, such as perching onto fixed objects).

According to the authors, the critical gap in aerial manipulation continues being the need to characterize, measure, or estimate reactionary forces and torques, as well as the impact of these reactions into the flying robot body. This study of coupling forces was performed by reflecting, all the way back to the frame of the quadrotor, the end-effector forces and external forces acting on it. In such a way it was possible to model the manipulator forces and the torques in the quadrotor body. To test this proposal, conventional PID controllers were adopted and stability analyses were performed for three missions: pick and place (momentary), peg-in-hole (loose), and valve turning (strong coupling). Since the accuracy and robustness are worse for quadrotor pose control than for manipulator pose control, redundancy was utilized in such a way that the manipulator moves to compensate for errors in quadrotor control. The execution of these missions leads to changes in the system dynamics, between contact and contactless situations, requiring stability criteria to be addressed for both cases. However, that still does not guarantee stability during the switching, which may lead the system to instability, and further studies on this subject are recommended. In the scope of this article, the switching stability was addressed by assuring a reasonable dwell-time constraint, as detailed in [68].

The testbed utilized in LARICS lab to test the algorithm and vehicles performances was the same described when discussing the work in [65]. The first experiment was a pick-and-place mission (momentary coupling), where the vehicle was commanded to fly to the target, descend until a pre-assigned threshold, actuate the manipulators to grab the object and fly towards the drop-off point to finally release the load. From a total of 10 runs, the success rate was of 90%. During navigation, adjusts in required thrust are achieved by calculating changes in mass or inertia in advance, or by estimating it, as it was done in [15], if the load is an unknown object. The second experiment was to carry a preloaded plastic peg (20 mm of outer diameter) towards an insertion point and use the manipulator to insert the peg in the hole (a case of loose coupling). To execute the insertion, once the vehicle reaches the target, it performs a dithering motion until getting contact, and then the peg is inserted. The algorithm was tested for different hole diameters, achieving a 100% success rate for $D = 5$ cm and 91.6% for $D = 3$ cm. The third and last test consisted of the quadrotor and UAM system perching onto a valve to open/close it (a case of strong coupling). The quadrotor starts at a distance from the valve and is commanded to navigate towards it. Upon arriving, the manipulation arms are deployed and, if this operation is successful, the vehicle lands on the valve to turn it. Ten experiments were conducted with a success rate beyond 80%. A video showing these accomplishments can be accessed in `https://goo.gl/pMDE3w`.

As stated, aerial manipulation missions are prone to significant disturbance when the quadrotor and UAM interact with the environment. To handle the intrinsical system nonlinearity and the influence of external disturbances and model uncertainties, several control techniques were adopted, as it can be perceived searching the literature (e.g., visual servoing [69], nested PID [70], cartesian impedance control [71], gain scheduling plus model reference [72], hierarchical [27], hybrid-MPC [73], backstepping [74], and behavioral [75]). In the work reported in [26], for instance, an adaptive sliding mode control was employed to control an aerial manipulation system composed by a quadrotor with a 2-DOF manipulator while executing the momentary coupling mission of pick an object and place it inside a shelf. An adaptive controller was chosen due to its ability to handle problems such as battery drains, miscalculated mechanical properties, non-modeled mechanics, measurement bias, and noise. The stability of the controller was proved in the sense of Lyapunov. As in [67], the proposed kinematic and dynamic models consider the quadrotor and the UAM as a single system.

Experiments were run at the Intelligent Control Systems Laboratory, Seoul National University. The testbed was composed by a Smart Xcopter quadrotor with a customized arm of 0.32 m when fully stretched and weighing 0.37 kg. Spectrum DX7 transmitters connect the vehicle and the ground station and the estimations of a Vicon and an indoor GPS were used for getting the position and attitude of the quadrotor. The pick-and-place mission consisted of taking off the quadrotor, moving it towards a wooden block of (7.5 x 5 x 1.5)cm, grabbing it

with an impactive gripper and moving to a point close to the releasing point, then actuating the robotic arm to release the block inside a shelf that only a two or higher DOF robotic arm can reach. Even though no information about the mass and the moment of inertia of the block was given, the manipulation was successful due to the robustness of the sliding mode controller. The results demonstrated a small RMS error ($\approx$2.3 cm) during the switching dynamic phases (pick and release). The experiments can be seen in the video available in https://goo.gl/BjeHsa.

2.6.5 Cooperative aerial load manipulation

Quadrotors are essentially underactuated systems unable to change the thrust direction without tilting the platform itself. This limitation represents a fundamental challenge in aerial load manipulation since it cannot push sideways or resist to lateral forces/wrenches without tilting its body, which adds more difficulty to manipulation and stability during contact, also restraining the use of torque-controlled robot arms, since the dynamic interaction may lead to instability [76].

To overcome this limitation and guarantee full actuation, some works consider multirotors with propellers that can themselves be tilted [77; 78]. Such multirotor platforms are referred to as tilting multirotor platforms [79; 80], in which the tilt angles of the rotors are actively controlled by extra actuators. Into this direction, a novel aerial platform, the so-called SmQ (Spherically-connected multi-Quadrotor), is presented in [81], providing a full actuation in 3D without the drawbacks of the approaches using tilted propellers (e.g., inter-rotor flow interference, complex mechanisms and increased energy consumption due to extra actuators). This platform consists of multiple quadrotors connected to a rigid frame via passive spherical joints. An example of an S3Q (an SmQ actuated by 3 quadrotors, so $m = 3$) can be seen in Figure 2.11.

The SmQ approach considers that each quadrotor is an actuator for the frame. Therefore, the thrust force of each vehicle is controlled under the constraints of the spherical joints (typically $\pm 35°$ in the pitch and roll directions, causing the cone constraints as seen in Figure 2.12 to arise). Moreover, depending on the number of quadrotors, the underactuation problem can be completely ($m > 3$) or partially ($m = 2$) overcome by this platform, also guaranteeing a larger payload capacity or force generation, compared to a single quadrotor.

To perform the manipulation missions, the paper provides the design and dynamical model for an SmQ platform system with m ($m = 1, 2, ..., n$) quadrotors attached to the frame, in addition to a position and attitude controller for two proposed configurations: a S3Q (as in Figure 2.11) and a S2Q (as in Figure 2.12).

An analysis of control feasibility and actuation capacity was performed for both confi-

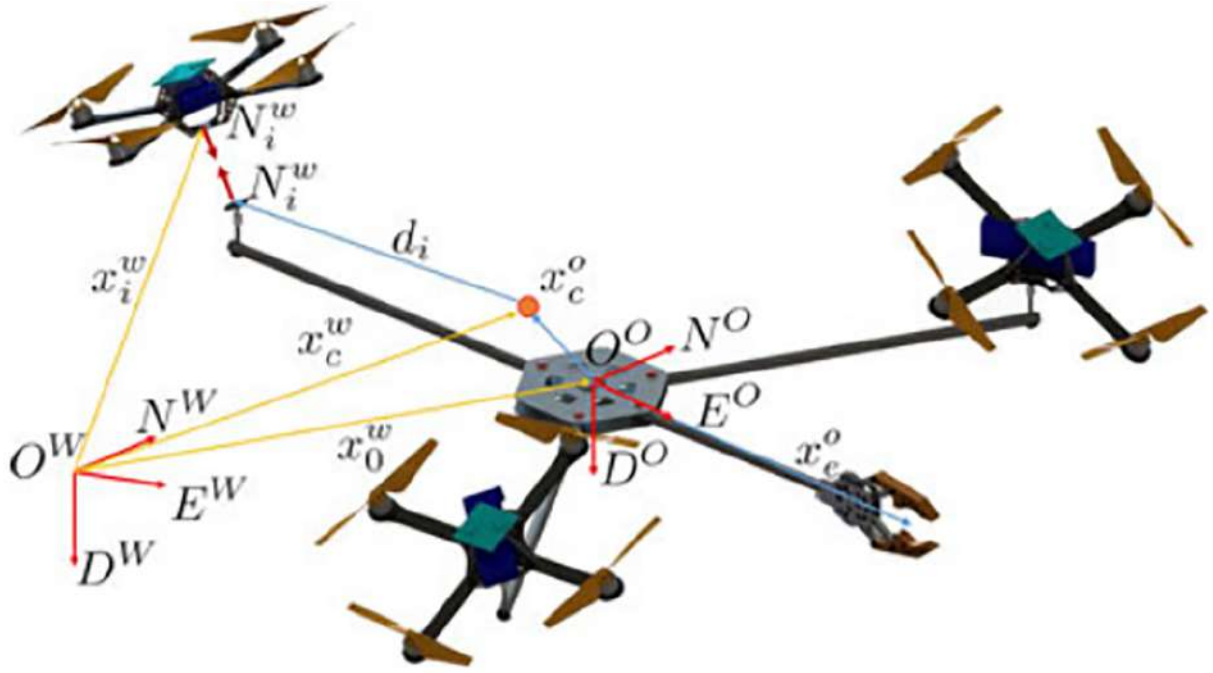

Figure 2.11 – Example of an S3Q platform, as proposed in [81], where north-east-down convention are used to each frame. The sub-notations w, c, and O represent world frame, the center of mass of the system, and the center of mass of the SmQ frame, respectively, while i represent the i-th quadrotor.

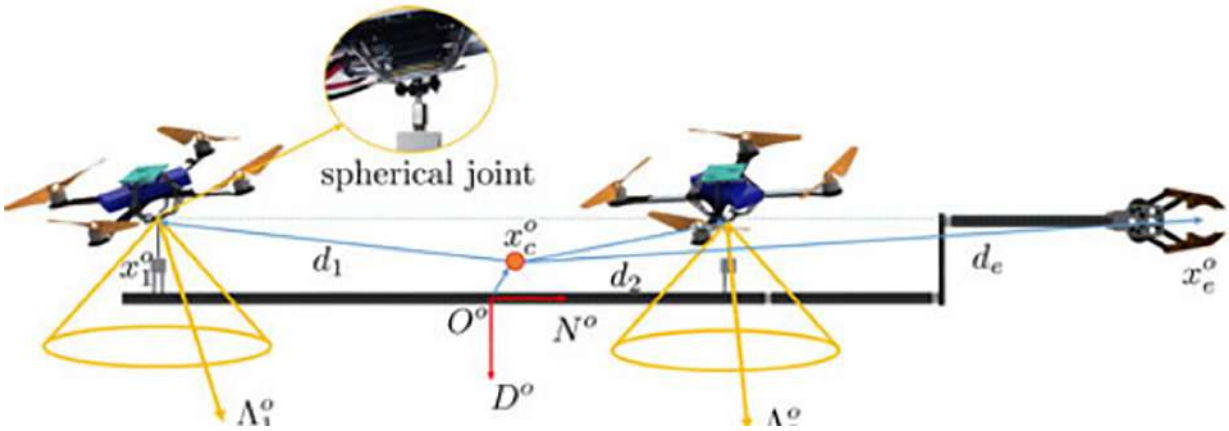

Figure 2.12 – Example of an S2Q platform with a manipulation tool [81].

gurations, based on Lyapunov stability theory. The results showed that the S3Q platform can freely perform 3D trajectory tracking and control the position and orientation of a mechanical tool rigidly attached to the platform (such as a drill or a grasping hand). As for the control feasibility of the S2Q configuration, it is bounded regarding a task-design approach proposed in the paper (based on the analogy of forces on a multifingered grasping hand under a friction-cone constraint [82]). In addition, a low-level constrained optimization controller was implemented, taking into account the range constraint of the spherical joints and the

thrust saturation of the propellers of the quadrotors, also prioritizing the elimination of any internally dissipated thrust actuation.

To test the algorithms and system performance, experiments were run for both configurations at the Interactive and Networked Robotics Laboratory, Seoul National University. The prototypes of the S3Q and S2Q platforms were built using lightweight carbon fiber, connecting AscTec Hummingbird quadrotors to the frame using passive spherical joints (angle of motion of 32°). A ground station sent the computed input commands to the quadrotors via Xbee communication, and a Vicon motion capture was responsible to measure the pose of the quadrotors and the frame. Several tests were made: hovering with human force interaction (compliant/backdrivable interaction), motion tracking around geometric shapes, row-pitch-yaw motions, telemanipulation and interaction with the environment via a haptic device (push a box, close a drawer, transport a cup of coke). The system performance can be checked in the videos available in https://goo.gl/iWZvPy, for the S3Q case, and in https://goo.gl/kQck34, for the S2Q case. However, since this is a novel aerial manipulation platform, further researches are necessary to get more insight into the feasibility of such a proposal for aerial manipulation tasks. Moreover, aspects such as motion planning are only briefly addressed in the paper.

An alternative approach to aerial manipulation is presented in [83], where it is proposed a new class of quadrotor systems that have the 3D navigation and maneuverability of a single quadrotor combined with surface adhesion and the ability of forcefully tugging up to 40 times the vehicle's mass. The strategy basically exploits controllable bio-inspired adhesion or the use of tiny metal hooks, called micro-spines, to firmly adhere to the ground and uses a winch to pull heavy objects. The strategy is similar to the one adopted for μTugs ground robot [84], now applied to aerial systems. The robot, called FlyCroTug, and its basic procedure are illustrated in Figures 2.13 and 2.14. For general manipulation, the robot flies towards an object and activates the end-effectors to attach the cable to it. Then it flies a certain distance while dropping a tether, and lands with the desired orientation, anchoring the system to the surface before starting pulling the tether with a large force.

To adhere into smooth surfaces, the FlyCroTugs uses a square 25-by-25 mm^2 pad of directional gecko-like dry adhesives [85], capable of generating shear forces up to $45N$ in that surfaces. For rough surfaces, the robot is also equipped with a set of 32 microspines, capable to hold 2 to 3 kg in shear when attached on exposed concrete faces in a debris-ridden disaster zone. An energetic analysis was also performed in the paper, showing that for objects exceeding the FlyCroTug mass, tugging is superior, while for lighter objects, simple carrying as a common cable-suspended system is more energy-efficient. Moreover, a scalability study was also performed, pointing that the adhesion and tugging concept is most beneficial at smaller sizes, although the proposed approach is feasible and useful at larger sizes, as depicted in [86],

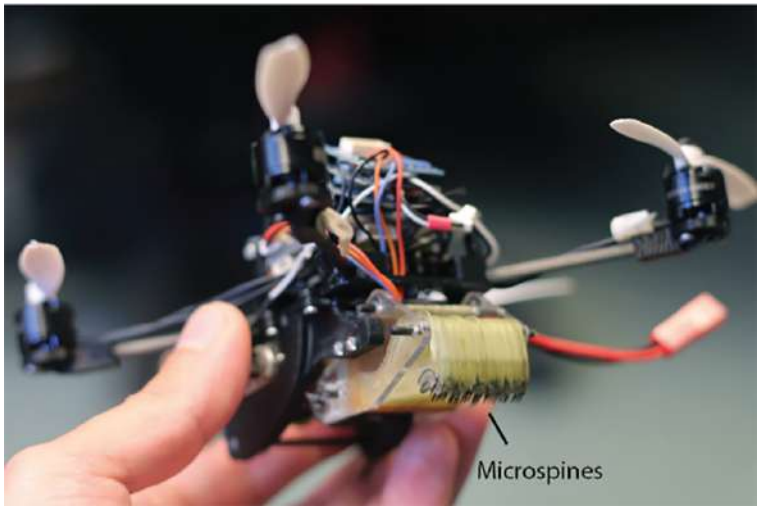

Figure 2.13 – A FlyCroTug with gecko-like microspines for anchoring [83].

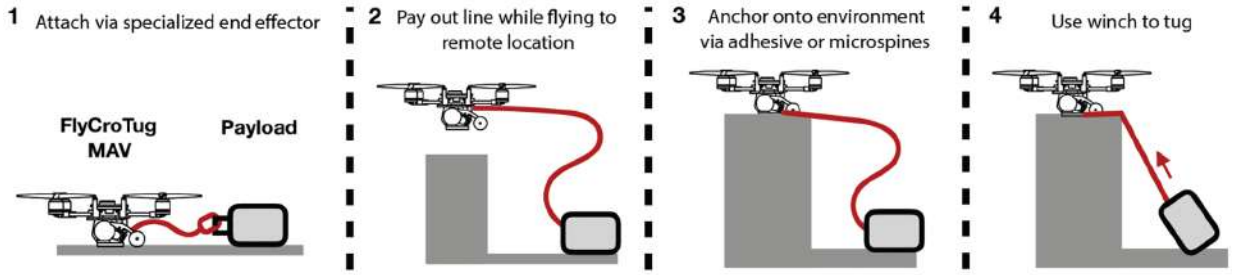

Figure 2.14 – Principle of operation: (1) the FlyCroTug flies towards an object and attaches the end-effector to it, (2) then it flies to a determined location while dropping out a cable, and (3) lands and anchors to a surface using the microspines. Finally, in (4) it pulls on the cable using a winch. Wheeled locomotion can be added in steps (1) and (3), for more precise positioning [83].

where a 120-by-100 mm^2 microspines pad was able to support $710N$ in shear, equivalent to the force exerted by a typical human being.

To validate the proposals, experiments were conducted at the Laboratory of Intelligent System, École Polytechnique Fédérale de Lausanne. Each FlyCroTug robot is a custom-built quadrotor based on the TayLabs Sparky 2.0 and weighs about $100g$. Two experiments are used to demonstrate the robot capabilities, one using the FlyCroTug to anchor atop a partially collapsed building, using mounted up sensors to find small openings in the rubble and reorienting for better anchoring, and then pulling a load that weighs twice the robot weight. The other experiment consisted of cooperation between two FlyCroTugs to open a door, using one to adhere to the door and pull the door handle downwards while the other pulls the door anchored in the ground. To perform the tasks, each vehicle was manually operated, using a FrSky Taranis radio controller to move the quadrotor and a TinyDuino microcontroller communicating with the Sparty 2.0 autopilot to control the actuation. The

obtained results can be watched in the video available at https://goo.gl/hx8LBw.

Continuing to explore the subject of cooperative manipulation, expected progress is the use of squads of aerial manipulators to cooperatively execute complex tasks. In [87], the authors presented the methods and algorithms used by a team of quadrotors in tasks of picking and transporting objects in an outdoor environment. They were employed at the Mohamed Bin Zayed International Robotics Challenge (MBZIRC) [88], which consists in a treasure hunt competition where the agents should collaboratively pick colored ferromagnetic disks on the ground of an outdoor arena and drop them into a predefined drop zone. To check the performance of the team of agents during the MBZIRC competition, the reader should access the video available in the links https://goo.gl/R2yodx and https://goo.gl/87ydWd.

This aforementioned competition attracted worldwide interest of the robotics community (143 teams registered for such a challenge), serving as a motivational standard for the multi-robot manipulation systems. Furthermore, other scientific papers describing the routines and results obtained in this competition enhance the load transportation literature, such as [89], [90], and [91].

2.7 Brief discussion about other multirotor UAVs

In recent years other multirotor configurations have appeared (e.g., hexarotors, octorotors, coaxial multirotors), and some applications using these new UAVs have been reported. Among these vehicles, the hexarotors gained much attention due to increased reliability obtained through a little cost increase. Such configuration comprises six propellers (motor plus blade), which are equally distributed along a circle, so that two adjacent propellers are 60° apart, and rotates in opposition, just like in the case of a quadrotor (see Figure 2.15).

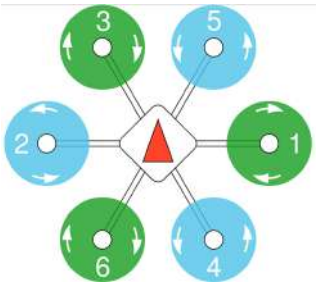

Figure 2.15 – A basic configuration (cross) of a hexarotor UAV [92].

When comparing the use of a hexarotor to the broadly used quadrotor, two important aspects should be highlighted. First, the use of more propellers allows a single UAV to carry a heavier payload and travel faster, therefore, bringing important assets to aerial vehicles in load transportation missions. The second aspect is that using six rotors instead of four

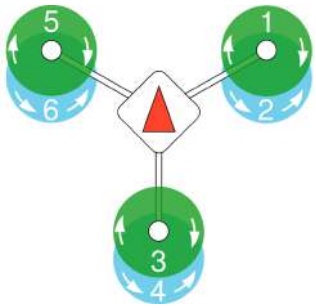

Figure 2.16 – A configuration with six propellers in three arms (coaxial hexarotor) [92].

produces the benefit that if one motor fails, it is still possible for the controller to adapt and use the remaining rotors to address all the DoF.

Although these aspects show that hexarotors are potentially safer and more reliable, the additional propellers bring some issues to the table. This new frame demands longer arms to allow the propellers to be put conveniently apart from each other and avoid interference, which difficult the flight in cluttered or tight scenarios and increases the mass of the frame, also demanding more energy to fly and requiring bigger, heavier and more costly batteries. Furthermore, the additional propellers surround a wider span around the vehicle, assuring stability at a price of more conservative angles of attack and flight maneuverability.

A second possibility of using six propellers is shown in Figure 2.16, in which two propellers are installed into a single arm in a coaxial manner, composing a three-arms UAV frame. This coaxial setup maintains the commented benefits of hexacopters (e.g., redundancy, increased lift capacity), with an equivalent energy consumption profile once the lighter weight due to having only three arms are counterbalanced by the less effective use of the thrust produced by the propellers. The advantages of this framework are the reduced vehicle's size and the capacity of better handling windy environments [93; 94].

Using the same principle of increasing the number of propellers, another usual configuration present on market and literature are the UAVs with eight propellers, the octorotors. The eight equally spaced arms with rotors guarantee even more robustness to failures (more motors can fail without obliging the vehicle to stop navigating), stability, and navigation height and speed. However, these powerful advantages come with issues in vehicle's size and energy consumption, at an even deeper degree than in the case of hexarotors.

2.7.1 Works considering hexarotors in transportation missions

Several interesting results were obtained in recent years with hexarotors in load transportation tasks. Although these vehicles are not the main subject of this paper, we briefly discuss here some of these experimentally validated achievements, taking in mind that many of the

below-described techniques are applicable to quadrotor load transportation systems with few or none adaptations.

In [95], a collaborative transport system is presented, using two hexarotors to carry a bulky payload without relying on a communication network. The proposed approach is based on the master-slave paradigm, in which the master simply lift and carry the load to the desired direction, and the slave, that is also attached to the load, actively guarantees compliance to the actions of the master by making use of an admittance controller, while external forces are estimated using an Unscented Kalman Filter (UKF) via position, velocity, attitude and angular velocity information. The state information is obtained by an onboard visual inertial navigation system. To validate the approach, two experiments were run at the Autonomous Systems Lab, ETH Zurich. In the first setup, a human operator carries the UAV using a string attached to the bottom of the hexarotor, and in the second setup, a 1.2 m carton tube weighing 370 g was attached to two hexarotors by a nylon wire. In this last setup, the master UAV was controlled remotely by a human operator while the slave UAV trajectory was obtained by the admittance controller. The results obtained can be watched in the video available at https://goo.gl/8FaKk8.

The previously described strategy was extended in [96], considering larger and heavier payloads being carried by a master and multiple slave agents. The aerial robots still transport without any communication between them, relying only on onboard sensors present in each vehicle to detect the force applied by the master and behave accordingly, also by using an admittance controller and force estimates provided by a UKF. The main difference between this study and the previous one is the treatment to uncertainties and unmodeled dynamics using robust control techniques to guarantee stability even in bad scenarios (e.g., under state estimator imperfections, communication failure, in the absence of precise knowledge of the payload shape/parameters, or due to grasp arbitrary points on the load). This can be considered a major improvement over the former paper, qualifying a system that uses only onboard sensors to indoor and outdoor aerial load transportation experiments. The proposal was validated in real-world experiments at the Autonomous Systems Lab, ETH Zurich, considering also outdoor flight under wind gusts and varying light conditions. One experiment used two hexarotors to carry a payload 1.5 m long, weighing 1.8 kg, whereas another experiment used three hexarotors to transport a hexagonal structure made of wood with 0.7 m of side length and 2.46 kg of mass. The results can be seen in the video available at https://goo.gl/sh78J9.

In [89], the authors used a team of hexarotors to identify, grasp, and deliver ferrous objects in a challenging desert-like environment. The proposed planning and estimation algorithms guarantee inter-robot collision-free paths and plan safe trajectories to the UAVs during the pick-and-place manipulation. Additionally, a map for the environment and objects is created

cooperatively. To generate the trajectories, a Zamboni or lawn mover pattern was used, treating the path planning as a Coverage Path Planning (CPP) [97], with the assignment of an independent zone for each UAV to localize and collect the objects. To estimate the vehicle's states, a linear Kalman Filter fuses the data coming from a GPS, a downward-facing height sensor, and an object detector. A geometric nonlinear PID controller was proposed to track the desired trajectories, exploiting the integral term to handle the tough operating conditions and uncertainties (e.g., strong or inconsistent wind around dunes in the desert). The algorithms are validated in an area of $70x45\ m^2$ in the Abu Dhabi desert, United Arab Emirates. This harsh and challenging scenario tested the algorithms to handle inconsistent wind and light, uneven terrain, and sandy conditions. While executing the trajectory, each UAV tries to detect the ferrous object, then, when detected, stop to follow the trajectory and tries to grasp it. After delivering or after a number of unsuccessful grasp attempts, the UAV continues the search from the last point on the trajectory. The experiments demonstrated a success rate of 90% when grasping and 95% when dropping objects, flying at wind speeds up to 10 m/s. Furthermore, during the mission each robot traveled an average path of 250 m in an average height of 10 m (Figure 2.17 illustrates the paths traveled by the vehicles during the grasping task). Such impressive results can be watched at the video available at https://goo.gl/znsBcw.

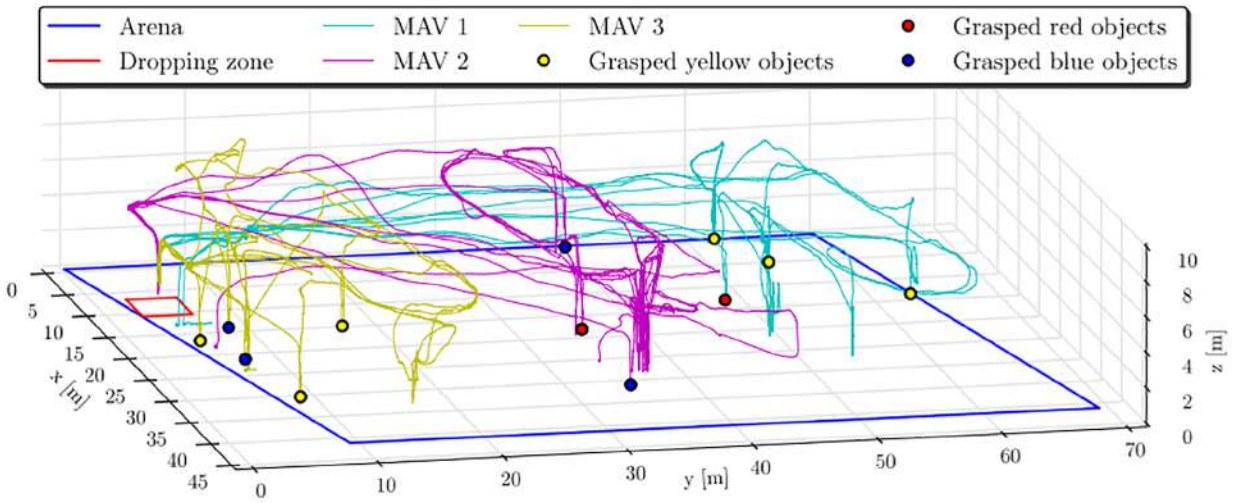

Figure 2.17 – Paths traveled by the vehicles during the pick-and-place transportation missions [89].

On the subject of aerial manipulation with dexterous robotic arms, [98] proposes a cooperative aerial manipulation system with two aerial manipulators with three-DoF controlling the pose of a rod-shaped object. A robust motion controller is designed using the extended high-gain observer concept [99], and a disturbance observer approach is used to estimate and treat the external disturbances caused by the reaction forces associated to an object [100]. To

obtain desired velocities while taking into account safe cooperation, not only the convergence of the object pose or velocity were considered, but also a null-space behavior approach. By hierarchically organizing the tasks, this null-space approach guarantees internal force estimation and regulation to small values via observed disturbance, and collision avoidance between the rod and aerial vehicle. The algorithms were validated using two hexarotors and a 2.5 m rod weighing 500 g. To monitor if the internal forces are properly regulated, a load cell was installed between the rod and end-effector, showing less than 0.5 N of internal forces during the mission. The experiments consisted in tracking a circular trajectory at 2 m/s while the robotic arm is moving and cooperatively manipulate the object into desired positions. The experiments were run at Intelligent Control System Lab at Seoul National University, and the obtained results can be watched in the video available at https://goo.gl/WHkELN.

Still considering cooperative aerial manipulation, the authors of [101] propose an extension to the RRT*-PDMP motion planning framework presented in [102]. This motion planning combines Rapidly-exploring Random Tree star (RRT*) [103] and Parametric Dynamic Movement Primitives (PDMP) [104] algorithms for an optimal motion, obtaining safe and efficient travel into environments with unknown obstacles. When compared to conventional planning approaches, such as optimization-based (e.g., nonlinear programming, model predictive control) or sampling-based, the proposed online replanning algorithm handles better the tradeoff between motion optimality and computational time. As the main contributions over the former RRT*-PDMP article, this study presents an adaptive sliding mode controller to track the desired joint velocities in the manipulator and handle the manipulator uncertainties (e.g., miscalculated mechanical properties, varying battery characteristics, ground effects, and downwash from other manipulators). In addition, a low-level robust controller that uses a disturbance observer approach, as discussed in [98], was implemented to track the velocity error in the aerial vehicles. The validating experiments were run at Intelligent Control Systems Laboratory, Seoul National University, and were composed by two scenarios: one with two hexarotors cooperatively transporting a load and advancing forward while avoiding obstacles, and another with the same squad transporting a load in a roundabout manner, while avoiding two obstacles. The experimental results can be watched in the video available at https://goo.gl/HioV6u.

2.8 Results

In this section, the performance of the control systems discussed so far is analyzed, and some important remarks regarding our research are pointed.

2.8.1 Trends and Major Achievements

Revisiting the videos from experiments and verifying the range of applications that have been achieved, it can be said that there has been tremendous progress in autonomous load transportation using quadrotors in recent years. The main reasons for this were advances in modeling and trajectory planning algorithms, which, in combination with nonlinear controllers, allowed aerial vehicles to exploit its full range of motions, generating the so-called aggressive maneuvers. In specific, the use of hybrid modeling to handle model variations and geometric representation of the environment combined with differential flatness to achieve safe and feasible trajectories, even outside of near-hover equilibrium, led to the control robustness that was lacking when considering quadrotor-with-load systems. In addition, the analyzed works proved that the use of attitude controllers in some form of hierarchical control (position + attitude) are mandatory, manipulating pitch, roll, and motor speeds, to handle the disturbances generated by the interaction of the vehicles and the load while they are moving.

The above-mentioned advances also covered cooperative robotic schemes, turning possible the accomplishment of tasks that a single robot can not. Challenging tasks like collaborative transport of a heavy load, collaborative orientation of a large load, or multiple robots cooperating while carrying individual loads in a high-dynamical environment are now achievable. Cable-suspended and grasped transportation were here used for different purposes, trading agility for simplicity. Integration between heterogeneous agents was also realized, showing the different tasks in which those systems can be adopted.

Regarding the way autonomous UAV technology will impact our daily lives, the major achievements found in this research were efficient computer vision and filtering techniques, permitting online onboard mapping and state estimation. This is a real game changer, once it allows the transition from robots performing under motion capture systems in laboratories, to robots executing tasks in real-world scenarios.

2.8.2 Potential Challenges and Future

Once the generation of dynamically feasible trajectories demonstrated to be the best approach for reliable load transportation using quadrotors, future studies should look over the open challenges in this subject. Although fast methods for trajectory computation have been used for navigation in practical experiments, not often optimality criteria are taken into account, making nonlinear and hybrid optimization of trajectories an open challenge. Also, these optimization problems increase in complexity when dealing with unknown/unstructured dynamic environments and cooperative multi-robot systems.

As for cooperative transportation, most of the works here presented use centralized architecture, which causes the lack of robustness against a central agent or control station

failure, being also sensible to bottlenecks and channel-unreliability associated to centralized communication. A cooperative system that is safe, scalable, able to perform agile, and at high speeds, using only robotic vision and local communication between neighbors, are yet to be found.

As stated, the success of individual or cooperative robot systems in daily tasks is closely related to advances in robotic vision and sensor fusion. Many open questions remain in this area and the solutions are particularly not trivial. The faster an aerial vehicle flies, the longer will be its stopping distance. Therefore, to move in an agile and fast manner, it is necessary to detect obstacles far away. However, the longer the range of such sensors, the heavier they are used to be, which increase the weight of the vehicle and reduce its agility due to a decrease in its thrust/weight ratio. As pointed out before, one way to avoid this dilemma is to rely solely on monocular cameras and IMU. However, visual-inertial odometry has its own challenges yet to be solved. A major drawback of monocular camera configurations is the need for an initialization phase before key parameters can be estimated, which become an even bigger problem when visual tracking is lost midflight [105]. Additionally, to navigate or perform exploration missions in an unknown environment, while also assigning autonomously new steps during space exploration, it is necessary the construction of an onboard map, which is computationally heavy. Therefore, many questions still demand feasible solutions.

Throughout this survey, we discussed how much transportation-related tasks are close to social and commercial applications. This opens up many areas for improvements and new ideas on how these devices can interact with our society. Robots still depend on humans to provide task specifications and goals, so that the addition of social integration algorithms and routines should be encouraged. Artificial intelligence and machine learning algorithms applied to social robotics already achieved relative success in establishing communication. However, to translate this communication to safe and reliable actions (e.g., quadrotors helping in construction sites, delivering packages, being easily integrated to a precision agriculture process) there is plenty of room to be explored.

Ultimately, to guide the reader among the various topics discussed in this survey, Table 2.2 has been compiled, which contains our opinion on which approaches are more promising to fulfill the wide diversity of tasks that quadrotors transportation systems can perform.

2.9 Concluding Remarks

This survey shows, through the cited and discussed works, that we are experiencing remarkable advances in both cable-suspended and grasped load transportation, pointing out that the nature of the missions will determine which configuration is better suited to fulfill the specific needs, considering each particular scenario.

Table 2.2 – Eligibility on tasks according to the authors. CS - Cable-suspended, GR - Grasped, R - Recommended, NR - Not Recommended, C - Challenging.

		Maneuverability		**Load Weight**		**Environment**	
		Medium	High	Light	Heavy	Free	Cluttered
Individual	**CS**	R	R	R	NR	R	C
	GR	R	C	R	NR	R	R
Cooperative	**CS**	R	C	NR	R	R	NR
	GR	R	NR	NR	R	R	C

Indeed, several solutions to a vast collection of problems have been reported, which have been pointed and discussed in their essence, although not exhaustively, what would demand much more analyzes, a deeper study and, consequently a lot of additional description pages. Therefore, as the main trends in terms of load transportation were identified and presented, we claim that the main objective of being an entry point for novice researchers and graduate students was achieved.

Finally, to avoid problems with the expiration of the *goo.gl* shortened links for such videos, a Google sites page was created [106], which contains the original links to access the videos illustrating all experiments here discussed.

2.10 References

[1] MELLINGER, D.; MICHAEL, N.; KUMAR, V. Trajectory generation and control for precise aggressive maneuvers with quadrotors. *The International Journal of Robotics Research*, SAGE Publications Sage UK: London, England, v. 31, n. 5, p. 664–674, 2012.

[2] RICHTER, C.; BRY, A.; ROY, N. Polynomial trajectory planning for aggressive quadrotor flight in dense indoor environments. In: *Robotics Research*. [S.l.]: Springer, 2016. p. 649–666.

[3] SON, C. Y. et al. Model predictive control of a multi-rotor with a suspended load for avoiding obstacles. In: IEEE. *2018 IEEE International Conference on Robotics and Automation (ICRA)*. [S.l.], 2018. p. 1–6.

[4] KOTARU, P.; WU, G.; SREENATH, K. Differential-flatness and control of quadrotor (s) with a payload suspended through flexible cable (s). *arXiv preprint arXiv:1711.04895*, 2017.

[5] TANG, S.; WüEST, V.; KUMAR, V. Aggressive flight with suspended payloads using vision-based control. *IEEE Robotics and Automation Letters*, v. 3, n. 2, p. 1152–1159, 2018.

[6] GUERRERO, M. et al. Passivity based control for a quadrotor uav transporting a cable-suspended payload with minimum swing. In: IEEE. *Decision and Control (CDC), 2015 IEEE 54th Annual Conference on*. [S.l.], 2015. p. 6718–6723.

[7] PIZETTA, I. H. B.; BRANDÃO, A. S.; SARCINELLI-FILHO, M. Modelling and control of a pvtol quadrotor carrying a suspended load. In: IEEE. *Unmanned Aircraft Systems (ICUAS), 2015 International Conference on*. [S.l.], 2015. p. 444–450.

[8] FOEHN, P. et al. Fast trajectory optimization for agile quadrotor maneuvers with a cable-suspended payload. In: *Robotics: Science and Systems*. [S.l.: s.n.], 2017. p. 1–10.

[9] TANG, S.; SREENATH, K.; KUMAR, V. Aggressive maneuvering of a quadrotor with a cable-suspended payload. In: CITESEER. *Robotics: Science and Systems, Workshop on Women in Robotics*. [S.l.], 2014.

[10] LEE, T. Collision avoidance for quadrotor uavs transporting a payload via voronoi tessellation. In: IEEE. *American Control Conference (ACC), 2015*. [S.l.], 2015. p. 1842–1848.

[11] BEARD, R. et al. Decentralized cooperative aerial surveillance using fixed-wing miniature uavs. 2006.

[12] NUNEZ, E. Unmanned aerial systems flight and payload challenge. 2018.

[13] POUNDS, P. E.; DOLLAR, A. Hovering stability of helicopters with elastic constraints. In: AMERICAN SOCIETY OF MECHANICAL ENGINEERS. *ASME 2010 Dynamic Systems and Control Conference*. [S.l.], 2010. p. 781–788.

[14] RUGGIERO, F.; LIPPIELLO, V.; OLLERO, A. Aerial manipulation: A literature review. *IEEE Robotics and Automation Letters*, IEEE, v. 3, n. 3, p. 1957–1964, 2018.

[15] MELLINGER, D. et al. Design, modeling, estimation and control for aerial grasping and manipulation. In: IEEE. *Intelligent Robots and Systems (IROS), 2011 IEEE/RSJ International Conference on*. [S.l.], 2011. p. 2668–2673.

[16] LINDSEY, Q.; MELLINGER, D.; KUMAR, V. Construction of cubic structures with quadrotor teams. *Proc. Robotics: Science & Systems VII*, 2011.

[17] CHEAH, C.-C.; LIU, C.; SLOTINE, J.-J. E. Adaptive tracking control for robots with unknown kinematic and dynamic properties. *The International Journal of Robotics Research*, SAGE Publications, v. 25, n. 3, p. 283–296, 2006.

[18] ARCAS. *ARCAS Project*. 2011. URL http://www.arcas-project.eu.

[19] HEREDIA, G. et al. Control of a multirotor outdoor aerial manipulator. In: IEEE. *Intelligent Robots and Systems (IROS 2014), 2014 IEEE/RSJ International Conference on*. [S.l.], 2014. p. 3417–3422.

[20] AEROARMS. *Aeroarms Project*. 2015. URL https://aeroarms-project.eu.

[21] SUAREZ, A. et al. Anthropomorphic, compliant and lightweight dual arm system for aerial manipulation. In: IEEE. *Intelligent Robots and Systems (IROS), 2017 IEEE/RSJ International Conference on*. [S.l.], 2017. p. 992–997.

[22] ZHANG, G. et al. Grasp a moving target from the air: System & control of an aerial manipulator. In: IEEE. *2018 IEEE International Conference on Robotics and Automation (ICRA)*. [S.l.], 2018. p. 1681–1687.

[23] POUNDS, P. E.; BERSAK, D. R.; DOLLAR, A. M. Grasping from the air: Hovering capture and load stability. In: IEEE. *Robotics and Automation (ICRA), 2011 IEEE International Conference on*. [S.l.], 2011. p. 2491–2498.

[24] KUMAR, V. *Robot quadrotors perform James Bond theme, University of Pennsylvania, General Robotics, Automation, Sensing and Perception (GRASP) Lab, Feb 2012*.

[25] AUGUGLIARO, F. et al. Building tensile structures with flying machines. In: IEEE. *Intelligent Robots and Systems (IROS), 2013 IEEE/RSJ International Conference on*. [S.l.], 2013. p. 3487–3492.

[26] KIM, S.; CHOI, S.; KIM, H. J. Aerial manipulation using a quadrotor with a two dof robotic arm. In: IEEE. *Intelligent Robots and Systems (IROS), 2013 IEEE/RSJ International Conference on*. [S.l.], 2013. p. 4990–4995.

[27] LIPPIELLO, V. et al. Hybrid visual servoing with hierarchical task composition for aerial manipulation. *IEEE Robotics and Automation Letters*, IEEE, v. 1, n. 1, p. 259–266, 2016.

[28] KORPELA, C.; ORSAG, M.; OH, P. Towards valve turning using a dual-arm aerial manipulator. In: IEEE. *Intelligent Robots and Systems (IROS 2014), 2014 IEEE/RSJ International Conference on*. [S.l.], 2014. p. 3411–3416.

[29] KIM, S.; SEO, H.; KIM, H. J. Operating an unknown drawer using an aerial manipulator. In: IEEE. *Robotics and Automation (ICRA), 2015 IEEE International Conference on*. [S.l.], 2015. p. 5503–5508.

[30] THOMAS, J. et al. Toward autonomous avian-inspired grasping for micro aerial vehicles. *Bioinspiration & biomimetics*, IOP Publishing, v. 9, n. 2, p. 025010, 2014.

[31] PALUNKO, I.; CRUZ, P.; FIERRO, R. Agile load transportation: Safe and efficient load manipulation with aerial robots. *IEEE robotics & automation magazine*, IEEE, v. 19, n. 3, p. 69–79, 2012.

[32] FAUST, A. et al. Automated aerial suspended cargo delivery through reinforcement learning. *Artificial Intelligence*, Elsevier, v. 247, p. 381–398, 2017.

[33] KAMEL, M. et al. Fast nonlinear model predictive control for multicopter attitude tracking on so (3). In: IEEE. *Control Applications (CCA), 2015 IEEE Conference on*. [S.l.], 2015. p. 1160–1166.

[34] DAI, L. et al. Distributed mpc for formation of multi-agent systems with collision avoidance and obstacle avoidance. *Journal of the Franklin Institute*, Elsevier, v. 354, n. 4, p. 2068–2085, 2017.

[35] NEUNERT, M. et al. Fast nonlinear model predictive control for unified trajectory optimization and tracking. In: IEEE. *Robotics and Automation (ICRA), 2016 IEEE International Conference on*. [S.l.], 2016. p. 1398–1404.

[36] MICHAEL, N.; FINK, J.; KUMAR, V. Cooperative manipulation and transportation with aerial robots. *Autonomous Robots*, Springer, v. 30, n. 1, p. 73–86, 2011.

[37] FINK, J. et al. Planning and control for cooperative manipulation and transportation with aerial robots. *The International Journal of Robotics Research*, SAGE Publications Sage UK: London, England, v. 30, n. 3, p. 324–334, 2011.

[38] LOBO, M. S. et al. Applications of second-order cone programming. *Linear algebra and its applications*, Elsevier, v. 284, n. 1-3, p. 193–228, 1998.

[39] MARINA, H. G. D.; JAYAWARDHANA, B.; CAO, M. Taming mismatches in inter-agent distances for the formation-motion control of second-order agents. *IEEE Transactions on Automatic Control*, IEEE, v. 63, n. 2, p. 449–462, 2018.

[40] SMEUR, E. J.; CROON, G. de; CHU, Q. Cascaded incremental nonlinear dynamic inversion for mav disturbance rejection. *Control Engineering Practice*, PERGAMON-ELSEVIER SCIENCE LTD THE BOULEVARD, LANGFORD LANE, KIDLINGTON, OXFORD OX5 1GB, ENGLAND, v. 73, p. 79–90, 2018.

[41] MARINA, H. G. de; SMEUR, E. Flexible collaborative transportation by a team of rotorcraft. *arXiv preprint arXiv:1902.00279*, 2019.

[42] PAPARAZZI. *Uav open-source project.* 2018. URL http://wiki.paparazziuav.org.

[43] SREENATH, K.; MICHAEL, N.; KUMAR, V. Trajectory generation and control of a quadrotor with a cable-suspended load-a differentially-flat hybrid system. In: IEEE. *Robotics and Automation (ICRA), 2013 IEEE International Conference on*. [S.l.], 2013. p. 4888–4895.

[44] CRUZ, P. J.; FIERRO, R. Cable-suspended load lifting by a quadrotor uav: hybrid model, trajectory generation, and control. *Autonomous Robots*, Springer, v. 41, n. 8, p. 1629–1643, 2017.

[45] GOODARZI, F. A.; LEE, D.; LEE, T. Geometric control of a quadrotor uav transporting a payload connected via flexible cable. *International Journal of Control, Automation and Systems*, Springer, v. 13, n. 6, p. 1486–1498, 2015.

[46] GOODARZI, F. A.; LEE, T. Stabilization of a rigid body payload with multiple cooperative quadrotors. *Journal of Dynamic Systems, Measurement, and Control*, American Society of Mechanical Engineers, v. 138, n. 12, p. 121001, 2016.

[47] TANG, S.; KUMAR, V. Mixed integer quadratic program trajectory generation for a quadrotor with a cable-suspended payload. In: IEEE. *Robotics and Automation (ICRA), 2015 IEEE International Conference on*. [S.l.], 2015. p. 2216–2222.

[48] POSA, M.; TEDRAKE, R. Direct trajectory optimization of rigid body dynamical systems through contact. In: *Algorithmic foundations of robotics X*. [S.l.]: Springer, 2013. p. 527–542.

[49] POSA, M.; KUINDERSMA, S.; TEDRAKE, R. Optimization and stabilization of trajectories for constrained dynamical systems. In: IEEE. *2016 IEEE International Conference on Robotics and Automation (ICRA)*. [S.l.], 2016. p. 1366–1373.

[50] RITZ, R.; D'ANDREA, R. Carrying a flexible payload with multiple flying vehicles. In: IEEE. *Intelligent Robots and Systems (IROS), 2013 IEEE/RSJ International Conference on*. [S.l.], 2013. p. 3465–3471.

[51] AUGUGLIARO, F. et al. The flight assembled architecture installation: Cooperative construction with flying machines. *IEEE Control Systems*, IEEE, v. 34, n. 4, p. 46–64, 2014.

[52] LINDSEY, Q.; MELLINGER, D.; KUMAR, V. Construction with quadrotor teams. *Autonomous Robots*, Springer, v. 33, n. 3, p. 323–336, 2012.

[53] MELLINGER, D. et al. Cooperative grasping and transport using multiple quadrotors. In: *Distributed autonomous robotic systems*. [S.l.]: Springer, 2013. p. 545–558.

[54] TANG, S.; SREENATH, K.; KUMAR, V. Multi-robot trajectory generation for an aerial payload transport system. In: *Proc. Int. Symp. Robot. Res.* [S.l.: s.n.], 2017.

[55] TANG, S.; THOMAS, J.; KUMAR, V. Hold or take optimal plan (hoop): A quadratic programming approach to multi-robot trajectory generation. *The International Journal of Robotics Research*, v. 37, n. 9, p. 1062–1084, 2018.

[56] SREENATH, K.; KUMAR, V. Dynamics, control and planning for cooperative manipulation of payloads suspended by cables from multiple quadrotor robots. In: *Proceedings of Robotics: Science and Systems*. Berlin, Germany: [s.n.], 2013.

[57] GASSNER, M.; CIESLEWSKI, T.; SCARAMUZZA, D. Dynamic collaboration without communication: Vision-based cable-suspended load transport with two quadrotors. In: IEEE. *Robotics and Automation (ICRA), 2017 IEEE International Conference on*. [S.l.], 2017. p. 5196–5202.

[58] LUPASHIN, S. et al. A platform for aerial robotics research and demonstration: The flying machine arena. *Mechatronics*, Elsevier, v. 24, n. 1, p. 41–54, 2014.

[59] GURDAN, D. et al. Energy-efficient autonomous four-rotor flying robot controlled at 1 khz. In: IEEE. *Robotics and Automation, 2007 IEEE International Conference on*. [S.l.], 2007. p. 361–366.

[60] ARDINY, H.; WITWICKI, S.; MONDADA, F. Construction automation with autonomous mobile robots: A review. In: IEEE. *Robotics and Mechatronics (ICROM), 2015 3rd RSI International Conference on*. [S.l.], 2015. p. 418–424.

[61] BRANKO, K. Architecture in the digital age. design and manufacturing. *New York and London, Taylor & Francis*, 2003.

[62] WILLMANN, J. et al. Aerial robotic construction towards a new field of architectural research. *International journal of architectural computing*, SAGE Publications Sage UK: London, England, v. 10, n. 3, p. 439–459, 2012.

[63] AUGUGLIARO, F.; SCHOELLIG, A. P.; D'ANDREA, R. Generation of collision-free trajectories for a quadrocopter fleet: A sequential convex programming approach. In: IEEE. *Intelligent Robots and Systems (IROS), 2012 IEEE/RSJ International Conference on*. [S.l.], 2012. p. 1917–1922.

[64] LOIANNO, G.; KUMAR, V. Cooperative transportation using small quadrotors using monocular vision and inertial sensing. *IEEE Robotics and Automation Letters*, IEEE, 2017.

[65] PIPPIN, C. Integrated hardware/software architectures to enable uavs for autonomous flight. In: *Handbook of Unmanned Aerial Vehicles*. [S.l.]: Springer, 2015. p. 1725–1747.

[66] ARBANAS, B. et al. Aerial-ground robotic system for autonomous delivery tasks. In: IEEE. *Robotics and Automation (ICRA), 2016 IEEE International Conference on*. [S.l.], 2016. p. 5463–5468.

[67] ORSAG, M. et al. Dexterous aerial robots—mobile manipulation using unmanned aerial systems. *IEEE Transactions on Robotics*, IEEE, v. 33, n. 6, p. 1453–1466, 2017.

[68] HESPANHA, J. P.; MORSE, A. S. Stability of switched systems with average dwell-time. In: IEEE. *Decision and Control, 1999. Proceedings of the 38th IEEE Conference on*. [S.l.], 1999. v. 3, p. 2655–2660.

[69] SEO, H.; KIM, S.; KIM, H. J. Aerial grasping of cylindrical object using visual servoing based on stochastic model predictive control. In: IEEE. *Robotics and Automation (ICRA), 2017 IEEE International Conference on*. [S.l.], 2017. p. 6362–6368.

[70] GHADIOK, V.; GOLDIN, J.; REN, W. On the design and development of attitude stabilization, vision-based navigation, and aerial gripping for a low-cost quadrotor. *Autonomous Robots*, Springer, v. 33, n. 1-2, p. 41–68, 2012.

[71] LIPPIELLO, V.; RUGGIERO, F. Exploiting redundancy in cartesian impedance control of uavs equipped with a robotic arm. In: IEEE. *Intelligent Robots and Systems (IROS), 2012 IEEE/RSJ International Conference on*. [S.l.], 2012. p. 3768–3773.

[72] ORSAG, M. et al. Hybrid adaptive control for aerial manipulation. *Journal of intelligent & robotic systems*, Springer, v. 73, n. 1-4, p. 693–707, 2014.

[73] ALEXIS, K. et al. Aerial robotic contact-based inspection: planning and control. *Autonomous Robots*, Springer, v. 40, n. 4, p. 631–655, 2016.

[74] MEBARKI, R.; LIPPIELLO, V.; SICILIANO, B. Image-based control for dynamically cross-coupled aerial manipulation. In: IEEE. *Intelligent Robots and Systems (IROS 2014), 2014 IEEE/RSJ International Conference on*. [S.l.], 2014. p. 4827–4833.

[75] BAIZID, K. et al. Experiments on behavioral coordinated control of an unmanned aerial vehicle manipulator system. In: IEEE. *Robotics and Automation (ICRA), 2015 IEEE International Conference on*. [S.l.], 2015. p. 4680–4685.

[76] BARTELDS, T. J. et al. Compliant aerial manipulators: Toward a new generation of aerial robotic workers. *IEEE Robotics and Automation Letters*, v. 1, n. 1, p. 477–483, 2016.

[77] ŞENKUL, A. F.; ALTUĞ, E. System design of a novel tilt-roll rotor quadrotor uav. *Journal of Intelligent & Robotic Systems*, Springer, v. 84, n. 1-4, p. 575–599, 2016.

[78] BRESCIANINI, D.; D'ANDREA, R. Design, modeling and control of an omni-directional aerial vehicle. In: IEEE. *Robotics and Automation (ICRA), 2016 IEEE International Conference on*. [S.l.], 2016. p. 3261–3266.

[79] RYLL, M.; BÜLTHOFF, H. H.; GIORDANO, P. R. A novel overactuated quadrotor unmanned aerial vehicle: Modeling, control, and experimental validation. *IEEE Transactions on Control Systems Technology*, IEEE, v. 23, n. 2, p. 540–556, 2015.

[80] OOSEDO, A. et al. Flight control systems of a quad tilt rotor unmanned aerial vehicle for a large attitude change. In: IEEE. *Robotics and Automation (ICRA), 2015 IEEE International Conference on*. [S.l.], 2015. p. 2326–2331.

[81] NGUYEN, H.-N. et al. A novel robotic platform for aerial manipulation using quadrotors as rotating thrust generators. *IEEE Transactions on Robotics*, IEEE, v. 34, n. 2, p. 353–369, 2018.

[82] LI, J.-W.; LIU, H.; CAI, H.-G. On computing three-finger force-closure grasps of 2-d and 3-d objects. *IEEE Transactions on Robotics and Automation*, IEEE, v. 19, n. 1, p. 155–161, 2003.

[83] ESTRADA, M. A. et al. Forceful manipulation with micro air vehicles. *Science Robotics*, Science Robotics, v. 3, n. 23, p. eaau6903, 2018.

[84] CHRISTENSEN, D. L. et al. μtugs: Enabling microrobots to deliver macro forces with controllable adhesives. In: IEEE. *Robotics and Automation (ICRA), 2015 IEEE International Conference on*. [S.l.], 2015. p. 4048–4055.

[85] DAY, P. et al. Microwedge machining for the manufacture of directional dry adhesives. *Journal of Micro and Nano-Manufacturing*, American Society of Mechanical Engineers, v. 1, n. 1, p. 011001, 2013.

[86] WANG, S.; JIANG, H.; CUTKOSKY, M. R. A palm for a rock climbing robot based on dense arrays of micro-spines. In: IEEE. *Intelligent Robots and Systems (IROS), 2016 IEEE/RSJ International Conference on*. [S.l.], 2016. p. 52–59.

[87] BEUL, M. et al. Team nimbro at mbzirc 2017: Fast landing on a moving target and treasure hunting with a team of micro aerial vehicles. *Journal of Field Robotics*, Wiley Online Library.

[88] MBZIRC. *Mohamed Bin Zayed International Robotics Challenge.* 2017. URL https://www.mbzirc.com.

[89] LOIANNO, G. et al. Localization, grasping, and transportation of magnetic objects by a team of mavs in challenging desert like environments. *IEEE Robotics and Automation Letters*, IEEE, 2018.

[90] BÄHNEMANN, R. et al. A decentralized multi-agent unmanned aerial system to search, pick up, and relocate objects. *arXiv preprint arXiv:1707.03734*, 2017.

[91] GAWEL, A. et al. Aerial picking and delivery of magnetic objects with mavs. In: IEEE. *Robotics and Automation (ICRA), 2017 IEEE International Conference on.* [S.l.], 2017. p. 5746–5752.

[92] PX4. *PX4 Development Guide.* 2018. URL https://dev.px4.io/en/airframes/.

[93] SAIED, M. et al. Fault diagnosis and fault-tolerant control strategy for rotor failure in an octorotor. In: IEEE. *Robotics and Automation (ICRA), 2015 IEEE International Conference on.* [S.l.], 2015. p. 5266–5271.

[94] YOO, D.-W. et al. Dynamic modeling and stabilization techniques for tri-rotor unmanned aerial vehicles. *International Journal of Aeronautical and Space Sciences*, The Korean Society for Aeronautical & Space Sciences, v. 11, n. 3, p. 167–174, 2010.

[95] TAGLIABUE, A. et al. Collaborative transportation using mavs via passive force control. In: IEEE. *Robotics and Automation (ICRA), 2017 IEEE International Conference on.* [S.l.], 2017. p. 5766–5773.

[96] TAGLIABUE, A. et al. Robust collaborative object transportation using multiple mavs. *arXiv preprint arXiv:1711.08753*, 2017.

[97] GALCERAN, E.; CARRERAS, M. A survey on coverage path planning for robotics. *Robotics and Autonomous systems*, Elsevier, v. 61, n. 12, p. 1258–1276, 2013.

[98] KIM, S. et al. Cooperative aerial manipulation using multirotors with multi-dof robotic arms. *IEEE/ASME Transactions on Mechatronics*, IEEE, v. 23, n. 2, p. 702–713, 2018.

[99] KHALIL, H. K.; PRALY, L. High-gain observers in nonlinear feedback control. *International Journal of Robust and Nonlinear Control*, Wiley Online Library, v. 24, n. 6, p. 993–1015, 2014.

[100] BACK, J.; SHIM, H. An inner-loop controller guaranteeing robust transient performance for uncertain mimo nonlinear systems. *IEEE Transactions on Automatic Control*, IEEE, v. 54, n. 7, p. 1601–1607, 2009.

[101] KIM, H. et al. Cooperation in the air: A learning-based approach for efficient motion planning of aerial manipulators. *IEEE Robotics & Automation Magazine*, IEEE, 2018.

[102] KIM, H. et al. Motion planning with movement primitives for cooperative aerial transportation in obstacle environment. In: IEEE. *Robotics and Automation (ICRA), 2017 IEEE International Conference on*. [S.l.], 2017. p. 2328–2334.

[103] KARAMAN, S.; FRAZZOLI, E. Sampling-based algorithms for optimal motion planning. *The international journal of robotics research*, Sage Publications Sage UK: London, England, v. 30, n. 7, p. 846–894, 2011.

[104] MATSUBARA, T.; HYON, S.-H.; MORIMOTO, J. Learning parametric dynamic movement primitives from multiple demonstrations. *Neural networks*, Elsevier, v. 24, n. 5, p. 493–500, 2011.

[105] TANG, S.; KUMAR, V. Autonomous flight. *Annual Review of Control, Robotics, and Autonomous Systems*, Annual Reviews, v. 1, p. 29–52, 2018.

[106] VILLA, D. K. D. *Load Transportation Using Quadrotors: A Survey of Experimental Results. ICUAS'18 – The 2018 International Conference on Unmanned Aircraft Systems*. URL https://sites.google.com/view/loadtransportationsurvey/home.

3 [P2] - Cooperative load transportation with two quadrotors using adaptive control

The problem of carrying a bar-shaped payload suspended by flexible cables attached to two quadrotors is analyzed in this work. The aerial vehicles and the load are dealt with as a single system, whose kinematics is described as a multi-robot formation using the virtual structure approach. The dynamic effects caused by the tethered load over the quadrotors, as well as those caused by each quadrotor over the other, are treated by an adaptive dynamic compensator. To validate the proposal, experiments were run testing the system in adverse conditions: transportation far from quasi-static motion, high payload-to-quadrotor weight ratio, 20% of error in the robot model parameters, transportation under wind disturbances, and payload weight changes during flight. The good performance of the proposed control system in all these tests allows concluding that the proposed system is able to accomplish payload positioning, orientation, and trajectory tracking under adverse conditions, with accelerations up to 1.6 m/s^2.

3.1 Introduction

An emerging application of unmanned aerial vehicles (UAVs) is the use of quadrotors to grasp, manipulate, and transport payloads [1; 2; 3; 4]. Commonly, this can be achieved using one out of two strategies: by tethering the payload to the vehicle body, characterizing a cable-suspended load transportation, or by attaching the load directly on the body of the vehicle, characterizing a grasped load transportation. In the first case, the number of underactuated degrees of freedom increases, but the agility of the vehicle to maneuver is preserved. As for the second case, it is easier to obtain the mathematical model of the system, but the inertia of the vehicle is increased, thus decreasing its agility to maneuver. There are successful works considering both strategies, using a single agent [5; 6; 7] or even a team of agents [8; 9; 10] carrying payloads. Specifically talking about a team of quadrotors carrying a payload, the focus of this work, the main advantages are the viability of carrying a load that is too heavy for the thrust capability of a single quadrotor, and the possibility of increasing redundancy and safety.

As discussed in the survey presented in [4], in spite of the feasibility, there are many open challenges regarding the transportation of slung loads by quadrotors. Carrying a cable-suspended payload demands that the controllers deal with a pendulum stabilization problem

while flying. In addition, it is hard to obtain a generic mathematical model for this task, once it can be divided into three flight modes: (i) lifting, (ii) transportation, and (iii) delivery, which have distinct dynamic characteristics and are affected by the weight and shape of the load. Moreover, for a squad of agents, the controllers should be robust enough to keep tracking a desired trajectory under load swings and to deal with the forces each agent exerts on the others.

3.1.1 Related Work

Recent publications proposed control solutions for the manipulation and transportation of suspended payloads using quadrotors working cooperatively. In [11; 12; 13], for instance, the position and attitude of the payload are controlled in a cable-driven parallel robot fashion, whereas an approach without communication is presented in [14; 15], using force feedback to control the pose of the payload. In [16; 17; 18; 19; 20], by its turn, the manipulation task is performed by a quadrotor formation, which allows easy configuration and trajectory/task planning for the robots. With regard to [21], a force-based consensus algorithm ensures an equal share of the payload mass among the quadrotors in the formation. Despite their impressive contributions, to be able to handle the different transportation flight modes and perform trajectory tracking and path following at velocities suitable for real-world applications, the robustness of these techniques still needs to be improved.

Accordingly, a control algorithm that provides robustness in the presence of model uncertainties and external disturbances is certainly a reasonable option for load transportation. Different strategies have been used to achieve this for quadrotors carrying suspended payloads. As an example, in [22] reinforcement learning was used to achieve end-to-end (i.e., from load pick-up to delivery) payload transportation, where a meta-learning method updates the dynamic model of the system whenever variations of the payload occur. Reinforcement learning was also used in [23] to transport payloads by a team of three quadrotors, in which learning was used for planning smooth and swing-free trajectories. In [24; 25; 26], by their turn, adaptive control was used to counteracts the model parameter uncertainties by adjusting them in real-time, also allowing quick adaptation to new dynamics in pick-up or delivery tasks. Moreover, many authors achieved impressive results in terms of robustness using energy-based and passivity-based approaches for load transportation, as in [27; 28; 29; 30], where damping is injected to dissipate undesired energy and achieve stability. Another common approach employed to obtain robustness is the use of sliding mode controllers. This technique turns the system not susceptible to uncertainties by driving its states to a switching surface in the state space. The authors of [31] and [26] demonstrated that for applications considering a single vehicle and cooperative transportation.

Nevertheless, these controllers have some drawbacks with respect to their practical application. Learning algorithms suffer to deliver generalized solutions, requiring exhaustive real-world training under diverse environmental conditions, whereas normally the training data are obtained indoor or running a system simulation using traditional dynamic models. Regarding adaptive controllers, as they adapt themselves online for optimal model parameters, a solid prior knowledge of the structure of the system model is essential. With regard to passivity-based approaches, despite their success on disturbance rejection for load stabilization, they still lack experimental validation at velocities/accelerations suitable for real-world applications, once they have been tested only in quasi-static motion. As for sliding mode controllers, although being quite robust they are inherently flawed to deliver smooth solutions due to the chattering effect, which may cause vibration and load oscillation.

3.1.2 Contributions

In such a context, the main objective of this work is to propose a robust and simple control system for two quadrotors working cooperatively to carry a suspended rod-shaped payload, as depicted in Figure 3.1. The kinematics of the quadrotors are managed as a robot formation problem, and a virtual structure formation in combination with a kinematic controller handles the desired position and velocity for the vehicles, to which the load is attached through cables.

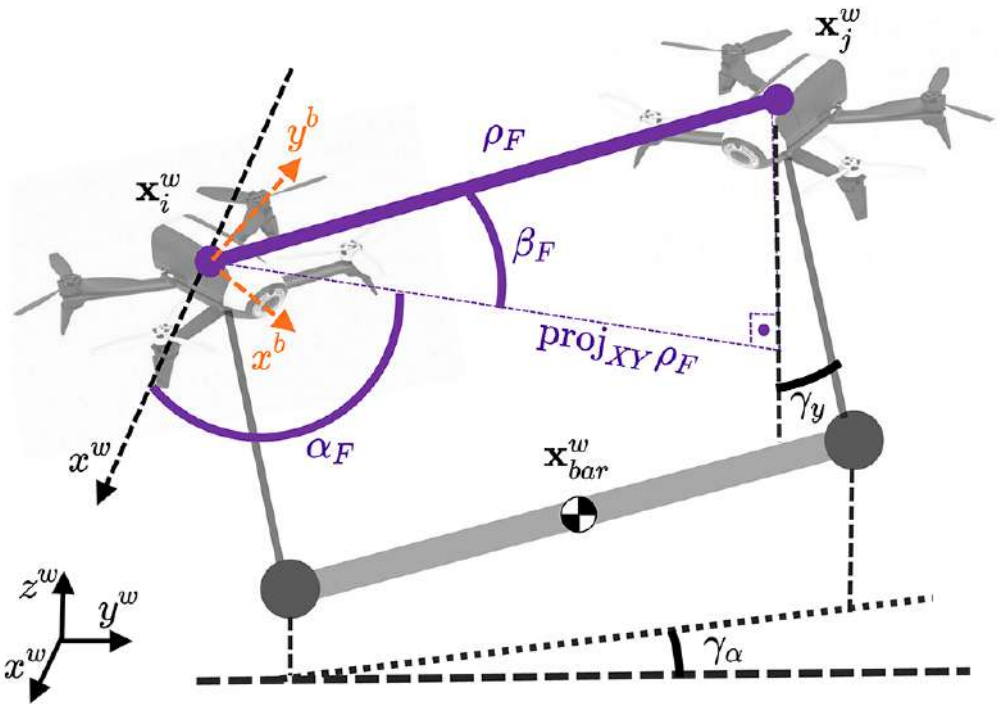

Figure 3.1 – Virtual structure formation for two UAVs carrying a payload. The virtual structure is depicted in purple.

Among the robust controller drawbacks discussed in Subsection 3.1.1, those associated with adaptive controllers seem to us to be the more amendable from a practical viewpoint, once the model structure for a variety of tasks using quadrotors is a well-discussed subject in the literature (such as the dynamic models found in the references of this paper). Thus, to improve the tracking of the velocity references given by the kinematic controller responsible to guide the formation, an adaptive dynamic compensator is proposed for each UAV in the formation to deal with the model uncertainties.

The main contributions of this paper can be summarized as follows: (i) we provide a simple method for planning the transportation missions, allowing the operator to directly plan the navigation of center-of-mass of the payload and the payload orientation using the virtual structure formation paradigm (see Figure 3.2). In addition, the virtual structure configuration is easily interchangeable for different loads being carried and cable lengths; (ii) the adaptation law is updated online, thus allowing real-time compensation for thrust-related uncertainties and drag-related disturbances; (iii) our controller requires no sensory data related to the payload; and (iv) we provide a comparative survey relating the main features found in the recent works regarding load transportation with quadrotors, which also highlights two experimental contributions of this work: transportation far from quasi-static motion, tracking 3D desired trajectories in accelerations up to 1.6 m/s^2, and transportation with payload-to-quadrotor weight ratio up to 0.575, far from the weight ratio usually found in other works of the literature.

To discuss such topics the paper is hereinafter split in a few sections, starting with Section 3.2, which characterizes the formation adopted. Following, Section 3.3 describes the kinematic controller in charge of dealing with how the formation as a whole should behave, whereas Section 3.4 discusses the system dynamics and Section 3.5 presents the adaptive dynamic compensation module associated to each quadrotor in the formation. In the sequel, Section 3.6 discusses the setup adopted for running the validating experiments, whereas Section 3.7 shows and discusses the results of the experiments run. Finally, Section 3.8 highlights the main conclusions of the work.

3.2 Multiple robot formation

As our system considers two UAVs cooperatively carrying a bar-shaped payload, we choose to formulate this problem as a robot formation problem, rather than individually plan desired trajectories that synchronizes the robots for the task. Therefore, we just need to obtain the formation navigation references from the task planner whereas the references for the robots are generated by a formation kinematic controller, whose stability is demonstrated. The proposed formation framework is based on the virtual structure paradigm [32], for which the virtual

structure is a line in the 3D space, the line linking the two UAVs. Such a line is characterized by the so-called formation variables, which are here referred to as

$$\boldsymbol{q} = [\boldsymbol{q}_p^\top \quad \boldsymbol{q}_c^\top]^\top \in \mathbb{R}^6, \tag{3.1}$$

where $\boldsymbol{q}_p = [x_F \ y_F \ z_F]^\top \in \mathbb{R}^3$ represents the position coordinates of the virtual structure in the world frame, here given by the position of one of the UAVs in the formation extremities, whereas $\boldsymbol{q}_c = [\alpha_F \ \beta_F \ \rho_F]^\top \in \mathbb{R}^3$ are the formation configuration that defines the other extremity, as it can be seen in Figure 3.1. As for the formation configuration components, α_F is the angle between the X-axis and the projection of the virtual structure on the XY-plane, β_F is the angle between the XY-plane and the virtual structure, and ρ_F is the length of the virtual structure (the distance between the two UAVs).

In summary, the position of a UAV with respect to the other is given by a set of spherical variables, and the payload is considered hanging below the virtual structure formation at a distance $-\ell\hat{\boldsymbol{z}}^w$, defined by the length of the cables. Considering that the system is in internal equilibrium, the payload orientations in yaw and pitch are given by α_F and β_F. Also, the positions of the two attachment points in the payload coincide with the horizontal positions of the vehicles, and, if a homogeneous payload is symmetrically attached by the cables, its center-of-mass (CoM) is collinear with the centroid of the virtual structure, which is given by

$$\boldsymbol{x}_{bar} = \boldsymbol{q}_p + \boldsymbol{x}_{bar/q} \ , \ \text{with} \ \boldsymbol{x}_{bar/q} = \begin{bmatrix} \frac{1}{2}\rho_F c_{\alpha_F} c_{\beta_F} \\ \frac{1}{2}\rho_F s_{\alpha_F} c_{\beta_F} \\ \frac{1}{2}\rho_F s_{\beta_F} - \ell \end{bmatrix}, \tag{3.2}$$

where $s_{\alpha_F} = \text{sen}\alpha_F$ and $c_{\alpha_F} = \cos\alpha_F$, with $\boldsymbol{x}_{bar/q}$ being the vector that maps the formation position coordinates into the payload center-of-mass.

Defining the desired state for the formation as $\boldsymbol{q}_{des} = [\boldsymbol{q}_{p,des}^\top \ \boldsymbol{q}_{c,des}^\top]^\top \in \mathbb{R}^6$, and the commanded reference state as $\dot{\boldsymbol{q}}_{ref} \in \mathbb{R}^6$, two task-planning approaches can be used to deal with the transportation task here addressed. One of them consists in dealing with the formation states directly, what means to deal with $\boldsymbol{q}_{des}$, knowing that, after stabilization, the payload will be hanging below the formation, whereas the other consists in controlling a point in the payload (its center-of-mass, for instance), from which the desired formation states can be obtained in a way similar to the one that generated (3.2). This setup allows the UAV formation and payload to be used for complex transportation, capable of tracking desired trajectories and paths, and allowing transportation in limited spaces, where it is necessary to tilt and turn the load to avoid collisions. Some examples for the system configuration $\boldsymbol{q}_c$ are provided in Figure 3.2.

To control the formation and vehicles, an inner-outer loop control scheme is adopted, which is illustrated in Figure 3.3. The outer loop corresponds to a kinematic controller, which

generates the formation reference velocities $\dot{\boldsymbol{q}}_{ref}$, based on the desired formation position and configuration and their time derivatives. In the sequel, an inverse Jacobian matrix maps these formation reference signals into velocity references for the two vehicles. Then, the references thus obtained for the vehicles are treated by an adaptive dynamic compensation module, responsible for considering the dynamics of the vehicles and counteracting the dynamic effects caused by the payload and by one vehicle on the other.

3.3 Formation kinematic control

Defining the error between the desired formation state and the current formation state as $\tilde{\boldsymbol{q}} = \boldsymbol{q}_{des} - \boldsymbol{q}$, the control law

$$\dot{\boldsymbol{q}}_{ref} = \dot{\boldsymbol{q}}_{des} + \boldsymbol{\kappa}_1 \tanh(\boldsymbol{\kappa}_2 \tilde{\boldsymbol{q}}) \tag{3.3}$$

is proposed for the kinematic formation controller, where $\boldsymbol{\kappa}_1$ and $\boldsymbol{\kappa}_2$ are positive definite diagonal matrices, and $\tanh(\cdot)$ is used as a smooth saturation function. During robot navigation, a feedback loop updates the formation entries at each control cycle, thus changing the current state of the formation. To compute the formation control feedback, the relationship between the robots space and formation space should be known. Such a relationship is characterized

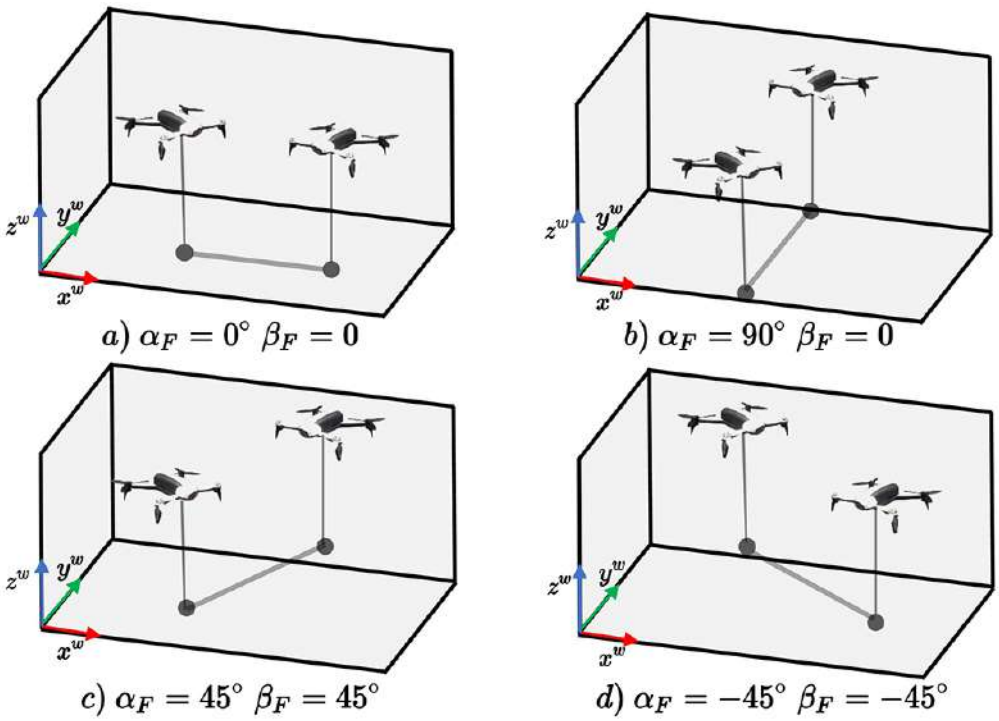

Figure 3.2 – Virtual structure formation at different configurations for two UAVs carrying a payload.

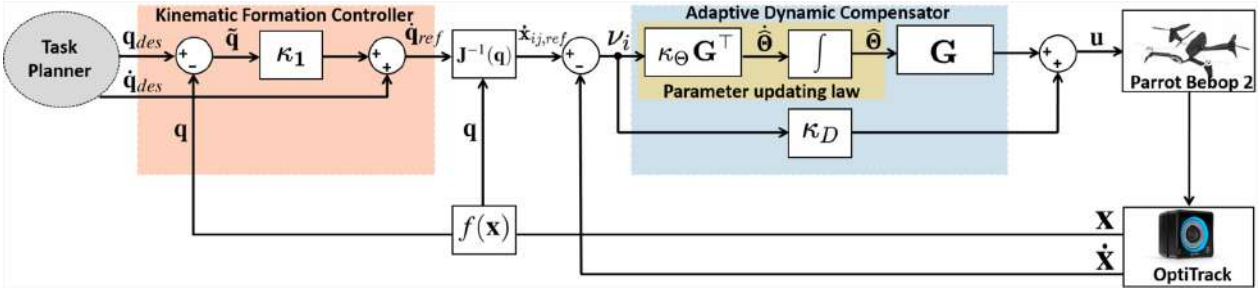

Figure 3.3 – Inner-outer loop control system for the virtual structure formation and the quadrotors. The outer loop kinematic controller generates the velocity reference $\dot{\boldsymbol{q}}_{ref} \in \mathbb{R}^6$ using the payload desired pose and velocity (defined by the user). Thus, a Jacobian matrix maps these references into velocity references for the vehicles, $\dot{\boldsymbol{x}}_{ref} \in \mathbb{R}^6$, where the first three elements are inputs for the quadrotor 1, and the last three for the quadrotor 2. Finally, these velocity references become acceleration references for a dynamic compensator, using the control scheme presented in Section 3.5.1.

by $\boldsymbol{q} = f(\boldsymbol{x}_{ij})$, with

$$\boldsymbol{q} = f(\boldsymbol{x}_{ij}) = \begin{bmatrix} x_i \\ y_i \\ z_i \\ \text{atan2}\left(\frac{y_j - y_i}{x_j - x_i}\right) \\ \text{atan2}\left(\frac{z_j - z_i}{\sqrt{(x_j - x_i)^2 + (y_j - y_i)^2}}\right) \\ ||\boldsymbol{x}_j - \boldsymbol{x}_i||_2 \end{bmatrix}, \tag{3.4}$$

where $\boldsymbol{q}$ is a vector containing the formation variables (characterizing the the formation space) and $\boldsymbol{x}_{ij} = [\boldsymbol{x}_i^\top \ \boldsymbol{x}_j^\top]^\top \in \mathbb{R}^6$ is a vector containing the positions of the robots (characterizing the robots space), with i, j representing the quadrotors, and with $\boldsymbol{x}_i = [x_i \ y_i \ z_i]^\top \in \mathbb{R}^3$ representing the position coordinates of the i-th quadrotor in the world frame.

To map the formation references, $\dot{\boldsymbol{q}}_{ref}$, to the velocity references for the vehicles, $\dot{\boldsymbol{x}}_{ij,ref}$, it is necessary to know the inverse of the Jacobian matrix associated to (3.4), so that $\dot{\boldsymbol{x}}_{ij,ref} = \boldsymbol{J}^{-1}(\boldsymbol{q})\dot{\boldsymbol{q}}_{ref}$ can be obtained. Such a relationship is obtained writing the reverse mapping correspondent to (3.4) and differentiating it to obtain

$$\boldsymbol{J}^{-1}(\boldsymbol{q}) = \begin{bmatrix} \boldsymbol{I}_{3\times3} & \boldsymbol{0}_{3\times3} \\ \boldsymbol{I}_{3\times3} & \boldsymbol{J}_c^{-1} \end{bmatrix}, \tag{3.5}$$

with

$$\boldsymbol{J}_c^{-1} = \begin{bmatrix} -\rho_F s_{\alpha_F} c_{\beta_F} & -\rho_F c_{\alpha_F} s_{\beta_F} & c_{\alpha_F} c_{\beta_F} \\ \rho_F c_{\alpha_F} c_{\beta_F} & -\rho_F s_{\alpha_F} s_{\beta_F} & s_{\alpha_F} c_{\beta_F} \\ 0 & \rho_F c_{\beta_F} & s_{\beta_F} \end{bmatrix}. \tag{3.6}$$

The stability analysis for the control law of (3.3) is provided, based on the theory of Lyapunov. Assuming a perfect tracking of the reference velocity by the robots, i.e., $\boldsymbol{\nu}_{\boldsymbol{q}=\dot{\boldsymbol{q}}_{ref}-\dot{\boldsymbol{q}}=\mathbf{0}}$, the closed-loop kinematic equation can be written as

$$\dot{\boldsymbol{q}}_{des} + \boldsymbol{\kappa}_1 \tanh(\boldsymbol{\kappa}_2 \tilde{\boldsymbol{q}}) = \dot{\boldsymbol{q}}, \tag{3.7}$$

or

$$\dot{\tilde{\boldsymbol{q}}} + \boldsymbol{\kappa}_1 \tanh(\boldsymbol{\kappa}_2 \tilde{\boldsymbol{q}}) = 0. \tag{3.8}$$

To check the stability of the system thus described, the radial-basis function $V(\tilde{\boldsymbol{q}}) = \frac{1}{2}\tilde{\boldsymbol{q}}^\top \tilde{\boldsymbol{q}}$ will be used as the Lyapunov candidate function. Notice that $V(\tilde{\boldsymbol{q}}) > 0$ for all $\tilde{\boldsymbol{q}} \neq \mathbf{0}$ and $V(\tilde{\boldsymbol{q}}) = 0$ only for $\tilde{\boldsymbol{q}} = 0$, as demanded from a Lyapunov candidate function. As for the first time derivative of such a function, it is

$$\dot{V} = \tilde{\boldsymbol{q}}^\top \dot{\tilde{\boldsymbol{q}}}. \tag{3.9}$$

Looking for asymptotic stability, $\dot{V}$ should be negative for all $\tilde{\boldsymbol{q}} \neq \mathbf{0}$. In fact, introducing (3.8) in (3.9) it comes

$$\dot{V} = -\tilde{\boldsymbol{q}}^\top \boldsymbol{\kappa_1} \tanh(\boldsymbol{\kappa_2} \tilde{\boldsymbol{q}}), \tag{3.10}$$

allowing checking that $\dot{V} < 0,\ \forall\ \tilde{\boldsymbol{q}} \neq \mathbf{0}$, and $\dot{V} = 0$ for $\tilde{\boldsymbol{q}} = 0$, since $\tanh(\cdot)$ is an odd function. As a result, $\tilde{\boldsymbol{q}} \to \mathbf{0}$ when $t \to \infty$, allowing concluding that the proposed control law makes the system asymptotically stable.

An important detail in the development of such stability proof is that the tracking error for the reference velocities is assumed to be zero ($\boldsymbol{\nu}_{\boldsymbol{q}=\mathbf{0}}$). This assumption can be made because the formation is a virtual structure, thus not having inertia or dynamics associated to it. In Section 3.5.1, however, where real quadrotors are considered, the dynamic effects will be considered and such assumption will be relaxed, expanding the stability proof to consider the dynamics of the vehicles and the payload.

3.4 System dynamics

The position of the i-th quadrotor in the three-dimensional space is $\boldsymbol{x}_i = [x_i\ y_i\ z_i]^\top$, indicating the longitudinal, lateral and normal displacements with respect to the world referential system $\langle w \rangle$. By its turn, $\boldsymbol{\eta}_i = [\phi_i\ \theta_i\ \psi_i]^\top$ is a vector that contains the roll, pitch and yaw angles correspondent to the vehicle, also in $\langle w \rangle$. In other words, $\boldsymbol{x}_i$ and $\boldsymbol{\eta}_i$ represent, respectively, the translational and attitude variables associated to each UAV. The mathematical model for quadrotors is well covered in the literature, and, for the 6-DoF body in the three-dimensional space, can be given by [33]

$$m\ddot{x} = (c_\psi s_\theta + s_\psi c_\theta s_\phi) u_1 - d_1 \dot{x}, \tag{3.11a}$$

$$m\ddot{y} = (s_\psi s_\theta - c_\psi c_\theta s_\phi)u_1 - d_2\dot{y}, \tag{3.11b}$$

$$m\ddot{z} = (c_\phi c_\theta)u_1 - mg - d_3\dot{z}, \tag{3.11c}$$

$$I_{xx}\ddot{\phi} \approx u_{2,\phi} + (I_{zz} - I_{yy})\dot{\theta}\dot{\psi} - d_4\dot{\phi}, \tag{3.11d}$$

$$I_{yy}\ddot{\theta} \approx u_{2,\theta} + (I_{xx} - I_{zz})\dot{\phi}\dot{\psi} - d_5\dot{\theta}, \tag{3.11e}$$

$$I_{zz}\ddot{\psi} \approx u_{2,\psi} + (I_{yy} - I_{xx})\dot{\phi}\dot{\theta} - d_6\dot{\psi}, \tag{3.11f}$$

where g is the gravity acceleration, m is the mass of the quadrotor, $\boldsymbol{I} = \text{diag}[I_{xx}\ I_{yy}\ I_{zz}]$ is the matrix of moments of inertia of the vehicle, $\boldsymbol{d} = [d_1, ..., d_6]^\top$ are the air drag coefficients, and u_1, $u_{2,\phi}$, $u_{2,\theta}$ and $u_{2,\psi}$ are the thrust and torque commands generated by the low level controllers responsible to stabilize the attitude of the vehicle.

An important remark is that to use the built-in low-level attitude controllers available in most off-the-shelf quadrotors, the payload should not affect the pitch and roll internal control loops, i.e., the payload dynamics should be decoupled from the attitude dynamics of the quadrotor. This is obtained by attaching the cable connecting the load to the quadrotor at its center-of-mass. Although being quite difficult to access the CoM in real quadrotors – it is likely to lie inside the vehicle body or components – we can adjust the attaching point at the base of the vehicle in such a way that any offset is just in the $\hat{\boldsymbol{z}}^b$ direction. Considering that this is done, and that the desired attitude angles are small, the payload dynamics and the quadrotor dynamics can be considered decoupled [34].

Therefore, from (3.11), only equations (3.11a)-(3.11c) need to be modified to include the payload dynamic effects. Considering that the payload is in equilibrium relative to the aerial vehicles, i.e., without swinging, the forces applied by the quadrotors on the load are vertical. Under such conditions internal forces are null, and each vehicle needs to adjust its thrust to carry the same additional weight, which is half of the mass of the bar ($\frac{1}{2}m_{bar}$).

Out of internal equilibrium state, the payload may swing at longitudinal and lateral planes, and twist around horizontal plane, with swing angles γ_x, γ_y, and γ_α, respectively (see Figure 3.1 for examples of γ_y and γ_α). Considering the payload dynamic effects as $\boldsymbol{\Delta}(\cdot)$, the motion equations for a quadrotor, considering a point-mass approximation for the payload, are, then,

$$\ddot{x} = \frac{(c_\psi s_\theta + s_\psi c_\theta s_\phi)}{M}u_1 - \frac{d_1}{M}\dot{x} + \Delta(\gamma_{x,\ddot{x}}), \tag{3.12a}$$

$$\ddot{y} = \frac{(s_\psi s_\theta - c_\psi c_\theta s_\phi)}{M} u_1 - \frac{d_2}{M}\dot{y} + \Delta(\gamma_{y,\ddot{y}}), \tag{3.12b}$$

$$\ddot{z} = \frac{(c_\phi c_\theta)}{M} u_1 - g - \frac{d_3}{M}\dot{z} + \Delta(\gamma_{x,\ddot{z}}) + \Delta(\gamma_{y,\ddot{z}}), \tag{3.12c}$$

$$\Delta(\gamma_{x,\ddot{x}}) \approx \frac{1}{2}(-\frac{m_{bar}}{M}\ell c_{\gamma_x}\ddot{\gamma_x} + \frac{m_{bar}}{M}\ell s_{\gamma_x}\dot{\gamma_x}^2), \tag{3.12d}$$

$$\Delta(\gamma_{x,\ddot{z}}) \approx \frac{1}{2}(-\frac{m_{bar}}{M}\ell s_{\gamma_x}\ddot{\gamma_x} - \frac{m_{bar}}{M}\ell c_{\gamma_x}\dot{\gamma_x}^2), \tag{3.12e}$$

$$\ddot{\gamma_x} \approx \frac{-c_{\gamma_x}}{\ell}\ddot{x} - \frac{s_{\gamma_x}}{\ell}g, \tag{3.12f}$$

$$\ddot{\gamma_y} \approx \frac{-c_{\gamma_y}}{\ell}\ddot{y} - \frac{s_{\gamma_y}}{\ell}g, \tag{3.12g}$$

where $M \approx (m + \frac{1}{2}m_{bar})$. The effects of $\Delta\gamma_y$ are given by equations similar to (3.12d)-(3.12e), and the effects of γ_α can be interpreted as a superposition of γ_x and γ_y swinging.

3.5 Dynamic compensator

As illustrated in Figure 3.3, velocity references from the kinematic formation controller, $\dot{\boldsymbol{x}}_{ij,ref} = \boldsymbol{J}^{-1}(\boldsymbol{q})\dot{\boldsymbol{q}}_{ref}$, are used to guide the aerial robots in the load transportation task, and an error in the reference tracking for each quadrotor occurs due to system dynamics. This means that

$$\boldsymbol{\nu}_i = \dot{\boldsymbol{x}}_{i,ref} - \dot{\boldsymbol{x}}_i \neq 0, \quad \boldsymbol{\nu}_j = \dot{\boldsymbol{x}}_{j,ref} - \dot{\boldsymbol{x}}_j \neq 0. \tag{3.13}$$

To reduce such velocity-tracking error an adaptive dynamic compensator is here proposed for each quadrotor, aiming at improving the performance of the whole control system. Since the same adaptive dynamic compensation module is used for both quadrotors, the i, j notations are dropped, for convenience.

Aiming at safety and accuracy, usually low or moderate velocities are used to transport payloads. Thus, a small-angle linearization can be applied to the quadrotor attitude in (3.12), with minor performance losses. To ensure the validity of the small-angle linearization, limits are established for the desired pitch and roll angles θ_{des} and ϕ_{des}, which are both $\leq 15°$. These limitations are equivalent to translational accelerations up to 2.5 m/s^2.

Exploiting the built-in low-level attitude controllers of the vehicles, the high-level translational inputs are the roll command u_ϕ, the pitch command u_θ, and the altitude rate command $u_{\dot{z}}$. These commands are grouped in a vector defined as $\boldsymbol{u} = \begin{bmatrix} u_\theta & u_\phi & u_{\dot{z}} \end{bmatrix}^\top =$

$\begin{bmatrix} K_{u,\theta}\theta_{des} & K_{u,\phi}\phi_{des} & K_{u,\dot{z}}\dot{z}_{des} \end{bmatrix}^\top$, whose entries are all in the interval $[-1.0, +1.0]$, representing the normalized limits for the desired high-level commands, with K_u being the proportionality constants associating the normalized control commands to the embedded controller limit parameters.

Thus, (3.12a)-(3.12c) can be written as

$$\begin{aligned} \ddot{x} &= \frac{(c_\psi\theta_{des} + s_\psi\phi_{des})}{M}u_1 - \frac{d_1}{M}\dot{x} + \Delta(\gamma_{x,\ddot{x}}), \\ \ddot{y} &= \frac{(s_\psi\theta_{des} - c_\psi\phi_{des})}{M}u_1 - \frac{d_2}{M}\dot{y} + \Delta(\gamma_{y,\ddot{y}}), \\ \ddot{z} &= \frac{1}{\tau_{\dot{z}}}\left(u_{\dot{z}} - \dot{z}\right) - \frac{d_3}{M}\dot{z} + \Delta(\gamma_{x,\ddot{z}}) + \Delta(\gamma_{y,\ddot{z}}), \end{aligned} \tag{3.14}$$

where $\tau_{\dot{z}}$ is the time constant for the altitude rate.

Finally, the model (3.14) for the quadrotor can be written in the linear form as

$$\boldsymbol{u} = R_\psi^{-1}(\boldsymbol{A}\ddot{\boldsymbol{x}} + \boldsymbol{B}\dot{\boldsymbol{x}} + \boldsymbol{\Delta}), \tag{3.15}$$

and the control law

$$\boldsymbol{u} = R_\psi^{-1}(\hat{\boldsymbol{A}}\ddot{\boldsymbol{x}}_{ref} + \hat{\boldsymbol{B}}\dot{\boldsymbol{x}} + \boldsymbol{\kappa}_D\boldsymbol{\nu} + \boldsymbol{\Delta}) \tag{3.16}$$

can be adopted, where R_ψ^{-1} is a rotation matrix relating $\langle w \rangle$ to $\langle b \rangle$, only dependent of ψ, $\boldsymbol{A} = diag(a_1, a_2, a_3)$ and $\boldsymbol{B} = diag(b_1, b_2, b_3)$ are diagonal positive definite matrices containing the thrust-related dynamic parameters for the vehicle, $\boldsymbol{\nu}$ is the tracking error between the reference velocity given by the formation kinematic controller and the velocity of the vehicle (as given in (3.13)), $\ddot{\boldsymbol{x}}_{ref}$ is the acceleration reference obtained by differentiating the reference velocity given by the formation controller ($\dot{\boldsymbol{x}}_{ref}$), and $\boldsymbol{\kappa}_D$ is a diagonal positive definite matrix. To execute the control law, the thrust-related dynamic parameters ($\hat{\boldsymbol{A}}$, $\hat{\boldsymbol{B}}$) can be estimated using a series of samples from experimental trials and least square identification, as in [35] and [36]. The yaw commands for each vehicle are not covered here, and can be selected arbitrarily, since the quadrotor is an omnidirectional vehicle.

3.5.1 Adaptive dynamic compensator

From equations (3.14)-(3.16), the dynamics lumped in matrices $\boldsymbol{A}$ and $\boldsymbol{B}$ depends of u_1, g, M and the air drag coefficients. Thus, it depends on the thrust of the vehicles, and the mass and shape of the vehicles and payload. Therefore, for every different payload being carried, and for every flight mode that the system is executing, the parameters of $\boldsymbol{A}$ and $\boldsymbol{B}$ will be different (e.g., transporting a payload with different mass, or delivering the load and switching between flying with load to flying without load). Instead of using a complex hybrid model to attend the in-flight changes in the dynamics of the vehicles, we exploit the fact

that the dynamics of every flight mode discussed in Section 3.1 can be obtained by changing the parameters of $\boldsymbol{A}$ and $\boldsymbol{B}$ accordingly. To change the dynamic parameters in real-time by feedback, an adaptive action is added to the proposed dynamic compensator.

Also, as shown in (3.12f)-(3.12g), the disturbances caused by the payload swinging angles, $\boldsymbol{\Delta}$, have their origin in the translational accelerations of the vehicles. Thus, to get good performance with the framework here proposed the user should choose desired trajectories with low/moderate accelerations and transportation under constant velocities. In addition, smooth accelerations are advised, with initial and final accelerations equal to zero. Following these considerations, we can assume $\boldsymbol{\Delta} \approx \mathbf{0}$ during constant velocities, with minor deviations occurring when accelerating, which should be addressed by the adaptive PD feedback. These restrictions on the desired trajectories are the giveback for simplifying the proposal, allowing the control of the payload position in open-loop, thus, allowing the use of off-the-shelf quadrotors without any additional sensors. Notice that to control the payload position in open-loop, in this case, means that the closed-loop control is applied to the positions of the two quadrotors, and getting control of such positions one gets control of the load position as a consequence.

As the control law (3.16) depends on constant or slowly-varying terms multiplied by time-varying states, one can write the translational control law in compact form as

$$\boldsymbol{u} = \boldsymbol{G}(\ddot{\boldsymbol{x}}_{\boldsymbol{ref}}, \dot{\boldsymbol{x}})\hat{\boldsymbol{\Theta}} + \boldsymbol{\kappa}_D\boldsymbol{\nu}, \tag{3.17}$$

with

$$\begin{bmatrix} u_\theta \\ u_\phi \\ u_{\dot{z}} \end{bmatrix} = \begin{bmatrix} \ddot{x}_{ref} & \dot{x} & 0 & 0 & 0 & 0 \\ 0 & 0 & \ddot{y}_{ref} & \dot{y} & 0 & 0 \\ 0 & 0 & 0 & 0 & \ddot{z}_{ref} & \dot{z} \end{bmatrix} \begin{bmatrix} a_1 \\ b_1 \\ a_2 \\ b_2 \\ a_3 \\ b_3 \end{bmatrix}, \tag{3.18}$$

and thus the parameter update rule can be selected as

$$\dot{\hat{\boldsymbol{\Theta}}} = \boldsymbol{\kappa}_\Theta \boldsymbol{G}^\top \boldsymbol{\nu}, \tag{3.19}$$

where $\boldsymbol{\kappa}_\Theta \in \mathbb{R}^{3\times3}$ is a symmetric positive definite matrix, $\boldsymbol{G} \in \mathbb{R}^{3\times6}$ is a regression matrix which considers the velocities and accelerations, $\boldsymbol{\Theta} \in \mathbb{R}^6$ is a vector containing the constant or slowly-varying model dynamic parameters, and $\hat{\boldsymbol{\Theta}}$ represents the vector of estimated dynamic parameters (characterized through $\tilde{\boldsymbol{\Theta}} = \hat{\boldsymbol{\Theta}} - \boldsymbol{\Theta}$).

3.5.2 Stability analysis

In this analysis, the assumption of perfect tracking of reference velocity is relaxed, which means that the dynamics of the vehicles affect the closed-loop equations.

Taking the Lyapunov candidate function as the radial-basis function

$$V(\boldsymbol{\nu}, \tilde{\boldsymbol{\Theta}}) = \frac{1}{2}\boldsymbol{\nu}^\top \boldsymbol{A}\boldsymbol{\nu} + \frac{1}{2}\tilde{\boldsymbol{\Theta}}^\top \boldsymbol{\kappa}_\Theta^{-1}\tilde{\boldsymbol{\Theta}}, \tag{3.20}$$

which is positive for all $\boldsymbol{\nu}, \tilde{\boldsymbol{\Theta}} \neq \mathbf{0}$ and null for $\boldsymbol{\nu} = \mathbf{0}$ and $\tilde{\boldsymbol{\Theta}} = \mathbf{0}$, the first time derivative is

$$\dot{V} = \boldsymbol{\nu}^\top \boldsymbol{A}\dot{\boldsymbol{\nu}} + \dot{\tilde{\boldsymbol{\Theta}}}^\top \boldsymbol{\kappa}_\Theta^{-1}\tilde{\boldsymbol{\Theta}}. \tag{3.21}$$

Considering $\dot{\boldsymbol{\nu}} = \ddot{\boldsymbol{x}}_{ref} - \ddot{\boldsymbol{x}}$, and using (3.15) one gets

$$\begin{aligned} \boldsymbol{A}\dot{\boldsymbol{\nu}} &= \boldsymbol{A}\ddot{\boldsymbol{x}}_{ref} - \boldsymbol{A}\ddot{\boldsymbol{x}} \\ &= \boldsymbol{A}\ddot{\boldsymbol{x}}_{ref} + \boldsymbol{B}\dot{\boldsymbol{x}} - \boldsymbol{u} \\ &= \boldsymbol{G}\boldsymbol{\Theta} - \boldsymbol{u} \end{aligned} \tag{3.22}$$

Introducing (3.22) in (3.21) and using the control law of (3.17), one gets, for the closed-loop system,

$$\dot{V} = \boldsymbol{\nu}^\top \left(\boldsymbol{G}\boldsymbol{\Theta} - \boldsymbol{G}\hat{\boldsymbol{\Theta}} - \boldsymbol{\kappa}_D\boldsymbol{\nu}\right) + \dot{\tilde{\boldsymbol{\Theta}}}^\top \boldsymbol{\kappa}_\Theta^{-1}\tilde{\boldsymbol{\Theta}}. \tag{3.23}$$

which simplifies to

$$\dot{V} = -\boldsymbol{\nu}^\top \boldsymbol{\kappa}_D\boldsymbol{\nu} + \left(-\boldsymbol{\nu}^\top \boldsymbol{G} + \dot{\tilde{\boldsymbol{\Theta}}}^\top \boldsymbol{\kappa}_\Theta^{-1}\right)\tilde{\boldsymbol{\Theta}} \tag{3.24}$$

Now, considering $\dot{\tilde{\boldsymbol{\Theta}}} = \dot{\hat{\boldsymbol{\Theta}}}$, since the vector of real parameters $\boldsymbol{\Theta}$ can be considered constant or slowly-varying for a given flight mode or configuration ($\dot{\boldsymbol{\Theta}} = 0$), and inserting the adaptive law (3.19) in (3.24), one finally gets

$$\begin{aligned} \dot{V} &= -\boldsymbol{\nu}^\top \boldsymbol{\kappa}_D\boldsymbol{\nu} + \left(-\boldsymbol{\nu}^\top \boldsymbol{G} + \boldsymbol{\nu}^\top \boldsymbol{G}\right)\tilde{\boldsymbol{\Theta}} \\ \dot{V} &= -\boldsymbol{\nu}^\top \boldsymbol{\kappa}_D\boldsymbol{\nu} \leq 0. \end{aligned} \tag{3.25}$$

Using the Barbalat's lemma [37], the result in (3.25) implies that for bounded desired trajectories, and, as a consequence, considering that the input for the quadrotors $\boldsymbol{u}$ is bounded, $\ddot{V}$ is bounded, and, therefore, $\dot{V}$ is uniformly continuous, which implies in asymptotically stable velocity tracking. In other words, $\boldsymbol{\nu} \to 0$, which also implies that $\dot{\tilde{\boldsymbol{x}}}, \tilde{\boldsymbol{x}} \to 0$ asymptotically. Therefore, the proposed adaptive dynamic controller guarantees the asymptotic convergence of the real velocities to the reference velocities given by the kinematic formation controller and the positions of the vehicles to the desired positions.

3.6 Experimental setup

To validate the proposed algorithms, extensive real-world experiments were run using two *Parrot Bebop 2* quadrotors to carry an aluminum bar measuring $L = 1.45$ m and weighing 155 g. Each robot weighs 500 g, and the load is attached to the robots through flexible cables.

The algorithms run in an offboard station, at a rate of 30 Hz, acquiring the poses of the vehicles and the payload through an *OptiTrack* motion capture system configured with eight cameras, and computing the reference control signals that are sent to the robots via ROS.

As stated in Section 3.3, the formation controller is responsible for receiving the desired navigation references and evaluate the reference velocities that each robot should attain to accomplish the mission. According to Subsection 3.5.1, uncertainties from the model and payload are handled by the adaptive dynamic compensation module, as well as the ability to fly in different flight modes. The initial dynamic parameters for $\hat{\boldsymbol{A}}$ and $\hat{\boldsymbol{B}}$ were obtained according to the method presented in Section 3.5, considering a single quadrotor flying without a payload, and are given by $\boldsymbol{A} = diag(0.39,\ 0.4,\ 0.25)$ and $\boldsymbol{B} = diag(0.21,\ 0.20,\ 1.01)$. It is worthy mentioning, however, that due to the adaptive action of the dynamic compensator, such an identification process can be completely skipped. Indeed, the dynamic parameter matrices $\hat{\boldsymbol{A}}$ and $\hat{\boldsymbol{B}}$ could be both initialized as the unit matrix $\boldsymbol{I}_{3\times3}$. Then, low acceleration trajectories should be performed for a few seconds, thus allowing the algorithm to stabilize and online adapt the parameters to the optimal values.

With regard to the validating experiments, five transportation tasks were executed to test the proposed algorithms. In every experiment, the control of the payload position, $\boldsymbol{x}_{bar}$, and orientation, $\boldsymbol{\eta}_{bar}$, is the main concern. Hence, following the control structure presented in Figure 3.3, the desired payload state is the task planner input, from which $\boldsymbol{q}_{p,des}$ and $\dot{\boldsymbol{q}}_{p,des}$ are obtained using (3.2), and $\boldsymbol{q}_{c,des} = [\psi_{bar,des} \quad \theta_{bar,des} \quad L]^\top$. The payload roll angle, ϕ_{bar}, is not possible to be controlled using our proposal. Also, the yaw angle for the vehicles are not considered, because the quadrotor is an omnidirectional vehicle, as mentioned in Section 3.4.

As for the gains adopted for the controller of each quadrotor in the experiments discussed ahead, they are the diagonal matrices $\boldsymbol{\kappa}_1 = diag(2.5, 2.5, 3.0, 2.0, 2.0, 2.0)$, $\boldsymbol{\kappa}_2 = diag(1.0, 1.0, 1.0, 1.0, 1.0, 1.0)$, $\boldsymbol{\kappa}_D = diag(2.7, 2.7, 3.0)$, and $\boldsymbol{\kappa}_\Theta = 10^{-3} diag(1, 0.1, 1, 0.1, 2, 5)$.

3.7 Results

In this section, the results that validate the proposals here reported are presented. Considering that a successful transportation is one that is precise and safe, the aimed performance in the following trials, so-called a good tracking performance, are position errors around 15 cm (or error norm around $||\boldsymbol{x}_{bar}||_2 = 15\sqrt{3} \approx 26$ cm) and orientation errors around 10°. All

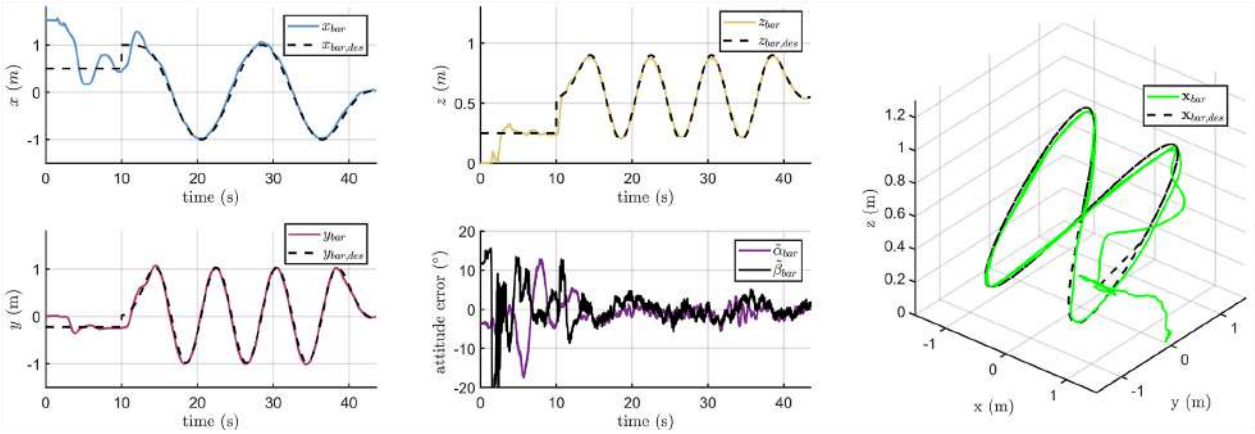

Figure 3.4 – The tracking error for the payload center-of-mass using the proposed adaptive controller during transportation task #1.

error metrics presented in the following were measured considering the center of mass of the transported bar. As our objective is to propose a robust and simple controller for load transportation, simplicity and robustness were preferred, over higher precision.

To test the robustness of our system, we impose the following challenges in the transportation experiments: high payload-to-quadrotor weight ratio, 20% of error in the model parameters of the vehicles, transport under wind-like disturbances, manipulation of the payload orientation during transport, and changes of the payload weight during transportation. We also tested our system using moderate velocities and accelerations, aiming at practical applications, where a robust but not sluggish system is preferred. A video showcasing our system under these challenges can be watched at https://youtu.be/eDFRapPJQ18.

In the following subsections, we further analyze the results obtained in each experiment. Although this proposal does not demand payload information to feedback the controllers, in the experiments run the *OptiTrack* system was also used to measure the position of the center of mass of the payload, just to produce the graphics shown.

3.7.1 Task #1: Transportation at high accelerations and payload weight - Comparison with PID

In task #1 the bar is transported through a tilted lemniscate-shape trajectory parameterized as

$$\boldsymbol{x}_{bar,des} = \begin{bmatrix} r_x \cos\dfrac{2\pi t}{T} & r_y \operatorname{sen}\dfrac{4\pi t}{T} & z_0 + r_z \operatorname{sen}\dfrac{4\pi t}{T} \end{bmatrix}^\top, \tag{3.26}$$

where $r_x = r_y = 1$ m, $r_z = 0.35$ m, $z_0 = 0.55$ m, and $T = 16$ s. The length of the cable attached to the payload is $\ell = 0.8$ m. Further, we attached an additional payload, weighing 180 g, nearby the CoM of the bar. Therefore, for this experiment, the total payload mass is 335 g and the payload-to-quadrotors weight ratio is 0.335, once our vehicles weights 1000 g

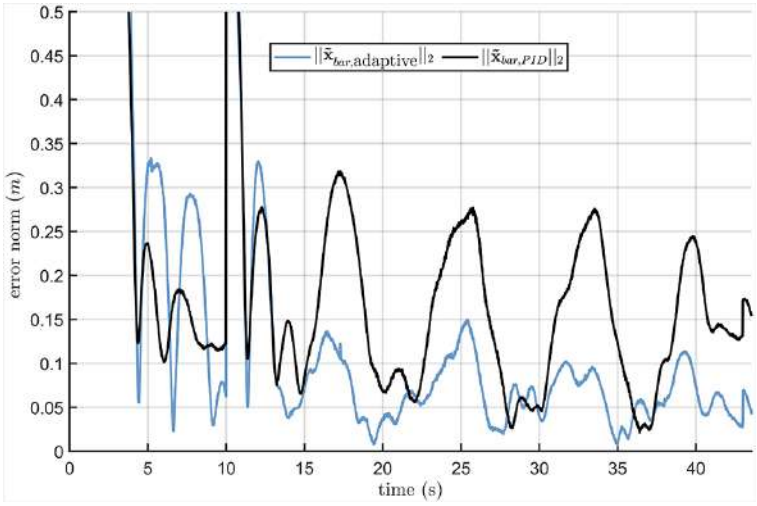

Figure 3.5 – Norm of the error for the adaptive and PID controllers during transportation task #1.

combined. To avoid excessive oscillations, acceleration and deceleration phases were used, to smoothly increase and decrease the trajectory frequency, whose duration was 10 s and 5 s, respectively.

To compare our approach to commonly used robust methods, we benchmark our controller with a well-tuned PID controller. The performance of our approach is presented in Figure 3.4. For the PID controller, several runs were performed with different parameters, and the PID gains which generated the best performance were adopted. For the sake of comparison, the norm of the error is presented in Figure 3.5, considering the controller here proposed and the PID one. As one can see from such a figure, our adaptive controller overperforms the PID controller after having its parameters adapted.

In another test, we further increased the desired acceleration in (3.26) by decreasing the period to $T = 10$ s, which is equivalent to maximum desired acceleration of 1.6 m/s^2. In Figure 3.6 it is possible to see the performance obtained using our approach. We also tried to use a PID controller in this case, for comparison, but the PID controller was not able to accomplish the task, leading to crashes or tracking errors above 50 cm.

3.7.2 Task #2: Transportation with parameter uncertainties

In this task, the desired trajectory in (3.26) was used once again, but here we purposely introduced an error in the identified values of the dynamic parameters, presented in Section 3.6, of around 20%. This test was motivated by a commonly found scenario in real-world applications, where the identified parameters are far from the real ones due to adverse conditions of the vehicle (e.g., component wearing) and environment. In this kind of scenario, adaptive systems are superior due to their parameter adjustment nature, in opposition to PID

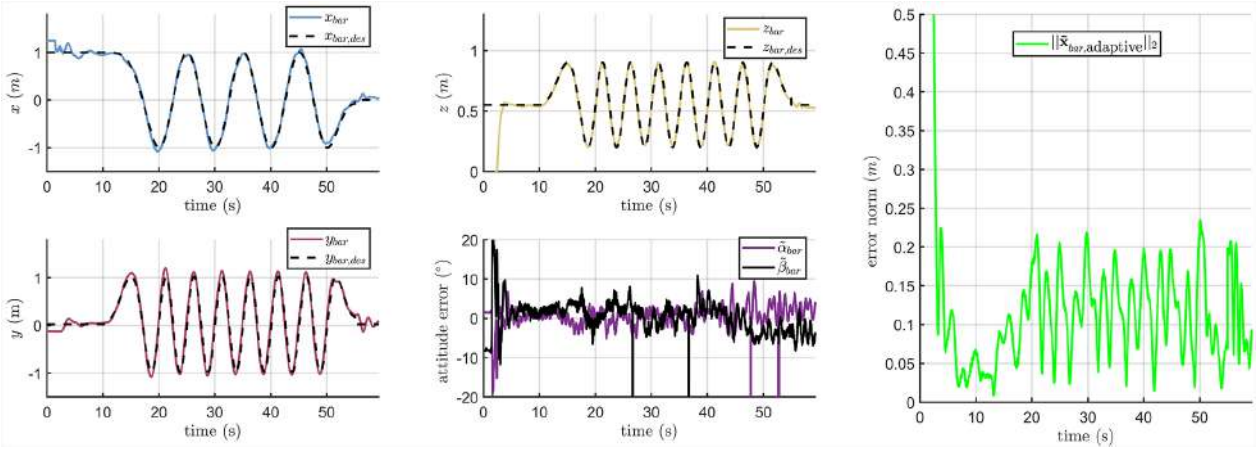

Figure 3.6 – The tracking error for the payload center-of-mass using the adaptive controller under accelerations up to 1.6 m/s^2 for task #1.

systems, which are very restricted when regarding the kind of uncertainty that the system undergoes.

The performance comparison between the proposed adaptive controller and the PID controller can be seen in Figure 3.7, where just the norm of the error is presented, due to the similarity of the component-wise performance to already presented graphs (as the one in Figure 3.4). As expected, the adaptation of the thrust-related dynamic parameters is able to greatly improve the tracking performance under parameter uncertainties in comparison to integral offset correction. In short, the robustness obtained by PID controllers is restricted, at best, to slowly-varying time-varying states or disturbances, not being well-suited to address the errors caused by misidentification of $\hat{\boldsymbol{A}}$ or $\hat{\boldsymbol{B}}$.

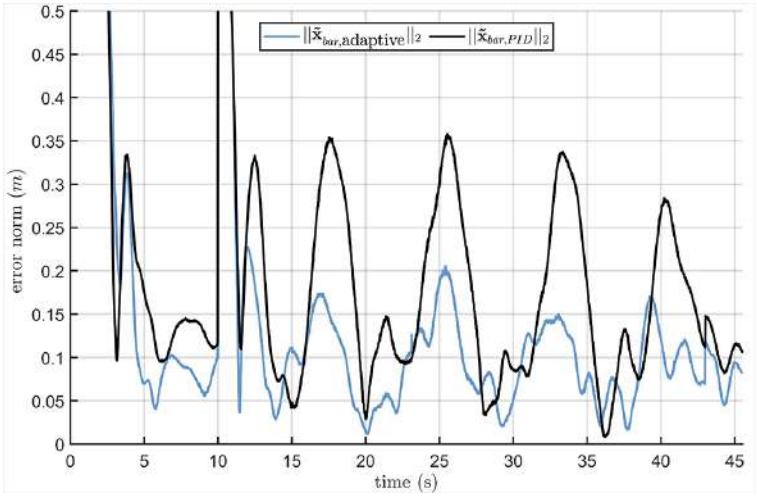

Figure 3.7 – Norm of the payload CoM error for the adaptive and PID controllers during transportation task #2.

3.7.3 Task #3: Transportation under wind-like disturbances

To validate our algorithms for transportation under windy environments, we emulate the dynamical forces caused by opposing wind in quadrotors, attaching to the top of the vehicles a foam plate of $25x25$ cm^2, as shown in Figure 3.8. These foam plates generate opposing drag forces when the quadrotors try to track the trajectories and when they accelerate to compensate for the disturbances. To demonstrate the effects caused solely by those plates, we guided one of the quadrotors through a lemniscate trajectory in two runs, one with and one without the foam plate, and the results of this experiment are shown in Figure 3.9.

As one can perceive in Figure 3.9, the foam plate directly impacts in the tracking performance, but, as our approach adapts for drag in the parameter $\hat{\boldsymbol{B}}$ in (3.16), we expect that the opposing drag forces are counteracted by the proposed controller. To verify it, we maneuver the payload in a cooperative transportation through a circular-shaped trajectory parameterized as

$$\boldsymbol{x}_{bar,des} = \begin{bmatrix} r_x \operatorname{sen}\dfrac{2\pi t}{T} & r_y \cos\dfrac{2\pi t}{T} & z_0 \end{bmatrix}^\top, \tag{3.27}$$

where $r_x = r_y = 1$ m, $z_0 = 0.55$ m, and $T = 5$ s, which corresponds to translational accelerations up to 1.6 m/s^2. The combined load of the two foam plates and the bar-shaped payload during this transportation was 275 g, corresponding to a weight ratio of 0.275. The trajectory tracking results for such experiment are shown in Figure 3.10. As one can see, the impact of opposed drag forces is counteracted by adapting the dynamic parameters involved in

Figure 3.8 – Experimental setup containing the used quadrotors, bar-shaped payload, and drag foam plates.

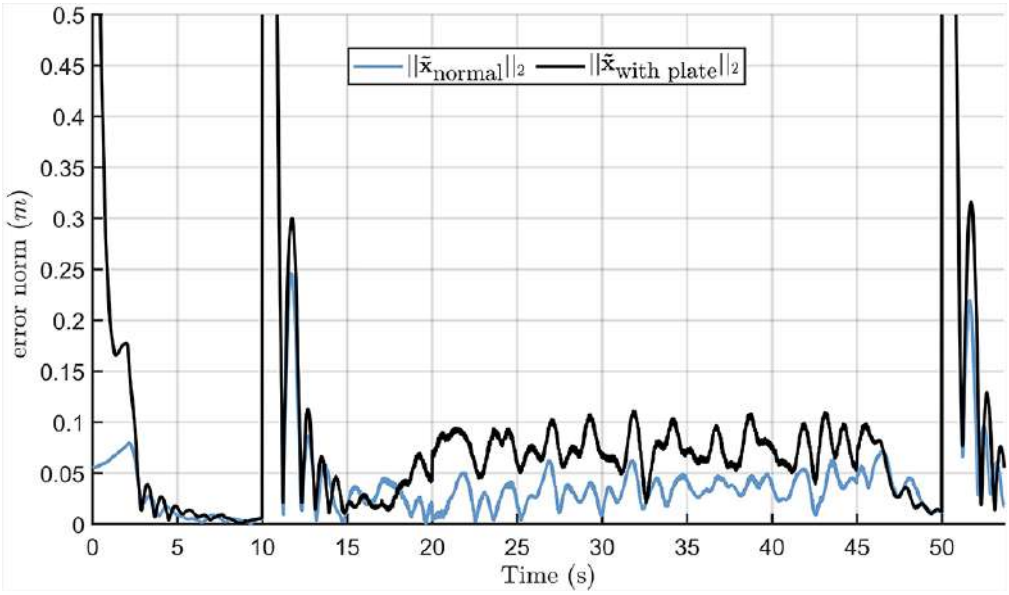

Figure 3.9 – The norm of the translational error for a quadrotor without the foam plate (blue), and with the foam plate (black). Test used for transportation task #3.

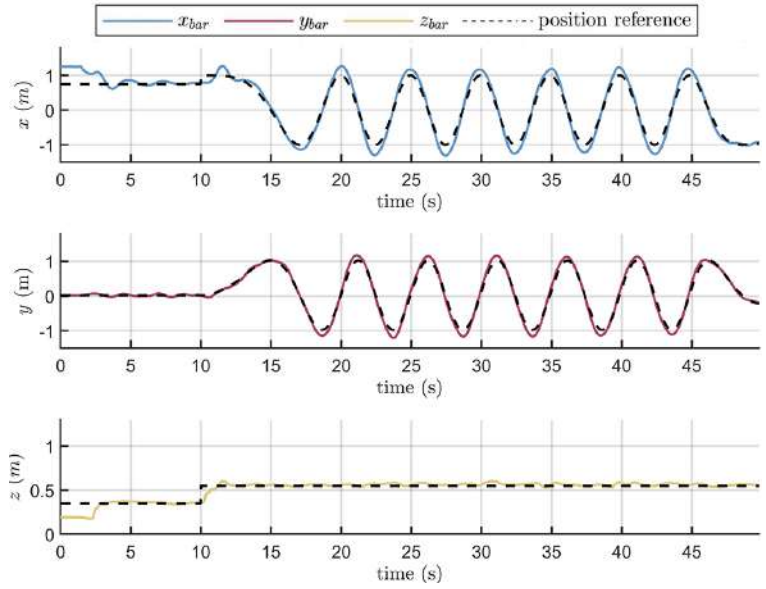

Figure 3.10 – Trajectory tracking for the payload center-of-mass considering additional drag forces under accelerations up to 1.6 m/s^2 during transportation task #3.

the controller. We also tried to compare the results obtained using our approach to standard PID controller, but it resulted in crashes in all of our tries. The conclusion is that PID-based systems are not able to deal with this kind of disturbance.

3.7.4 Task #4: Maneuvering the payload to avoid obstacles

The approach here proposed allows the manipulation of the payload translational positions and attitude angles, except for roll angle. Therefore, it is possible to propose desired trajectories and paths including maneuvers allowing the payload to avoid obstacles.

In this fourth task, the payload should contour obstacles in the center of the testing area, emulating the necessary manipulation used in narrow corridors, for instance, where the payload should be turned to go on in corners. This maneuver is represented by a circular-shaped trajectory parameterized as in , with $r_x = r_y = 1$ m, $z_0 = 0.55$ m, and $T = 9$ s. The cable lengths are $\ell = 0.8$ m.

To contour the circular trajectory, the payload desired orientation is given by the tangent of the trajectory, such that $\alpha_{bar,des} = \text{atan2}\,(y_{bar}, x_{bar}) - 180°$, where $-180°$ was used for quadrotor $\boldsymbol{x}_1$ to lead the formation. We also tilted the payload with $\beta_{bar,des} = 20°$, emulating a tilt that might be necessary to transport the payload in stairs or inclined surfaces, such as access ramps.

The obtained performance is presented in Figure 3.11. It is possible to see that the desired performance was achieved in the accomplishment of this task.

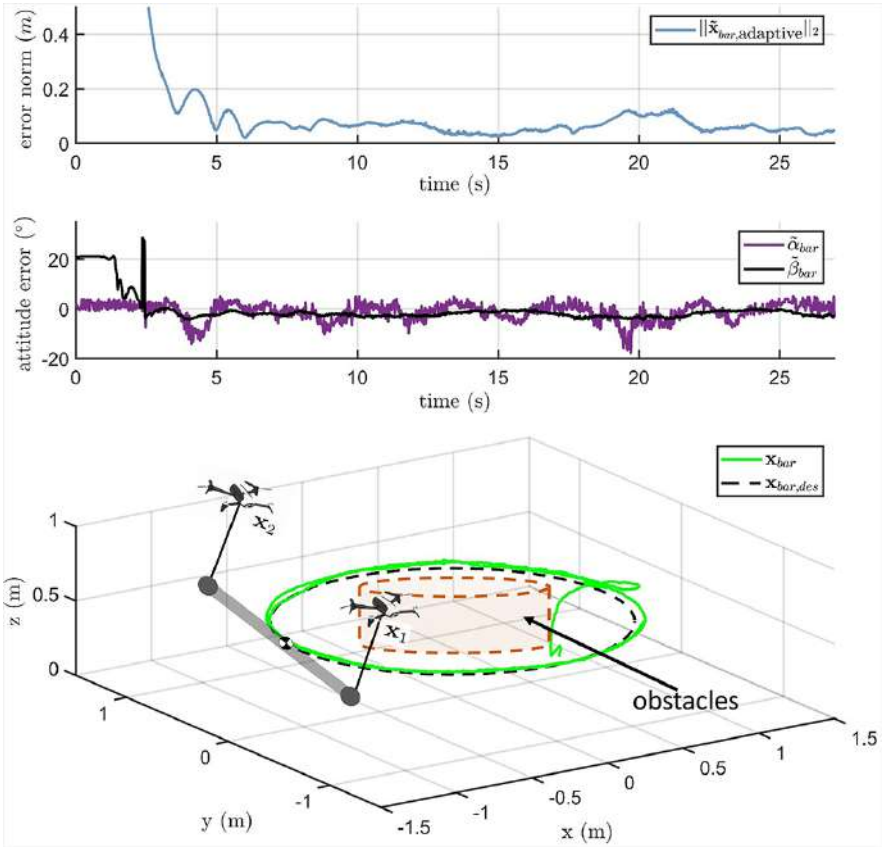

Figure 3.11 – The tracking error norm, attitude error, and 3D view for task #4.

3.7.5 Task #5: Unbalanced load transportation

This last transportation task consists of carrying the bar through a tilted lemniscate-shape trajectory parameterized as

$$\boldsymbol{x}_{bar,des} = \begin{bmatrix} r_x \operatorname{sen}\dfrac{4\pi t}{T} & r_y \cos\dfrac{2\pi t}{T} & z_0 + r_z \operatorname{sen}\dfrac{4\pi t}{T} \end{bmatrix}^\top, \tag{3.28}$$

where $r_x = r_y = 1$ m, $r_z = 0.35$ m, $z_0 = 0.45$ m, and $T = 30$ s. The cable lengths are $\ell = 1.15$ m. Once again we chose a trajectory that excites the system dynamics in three dimensions, with smooth sinusoidal acceleration. Also, during the transportation the payload should be oriented so that $\psi_{bar,des} = 90°$ and $\theta_{bar,des} = 0°$.

During the transportation, additional loads were attached to the extremities of the bar, to unbalance it. After one lemniscate cycle, in $t = 30$ s, a load weighing 180 g was added to one extremity of the bar, and after an additional cycle, in $t = 60$ s, a load weighing 240 g was added to the other extremity. The intent of this experiment is to verify if the proposed control system is able to deal with load fluctuations or loads that do not have uniform mass distribution. The final payload-to-quadrotors weight ratio was 0.575.

Figure 3.12 shows the graphics correspondent to the payload desired and current positions, and Figure 3.13 shows the graphics correspondent to the position and orientation tracking errors. In both figures, enumerated timestamps indicate the instants during the experiment in which a transition occurs (e.g., an additional payload is added to the bar, the system goes to a halt).

Analyzing such figures, one can see that the control system here proposed is able to handle the disturbances corresponding to the load oscillations and the load fluctuations due to the uneven addition of extra loads at the extremities of the bar being transported. As exhibited in Figure 3.13, the position tracking errors are around the expected performance after stabilization. The timestamps ① and ② indicate the time instants where the 180 g and 240 g additional payloads were inserted, respectively. It is important to notice the quick response of the proposed system during these instants, where an increase in the tracking error can be easily noticed in Figure 3.13, which is quickly damped by the control action. Moreover, these instants are critical not only due to the need for online adaptation of the thrust of the vehicles, but also due to the external disturbances caused by the operator manipulation of the aluminum bar payload to attach the additional weight. These external perturbations cause oscillations and swings of the payload, as well as moments in which the payload exerts less force on the vehicles because the bar is held by the operator.

A 3D view of the path followed by the vehicles and the load is shown in Figure 3.14, in which one can check the performance of the whole system in the task accomplishment.

Another important time interval to be checked in this experiment is the acceleration phase from rest to the timestamp ①, where we decided not to use a smooth increase in the desired

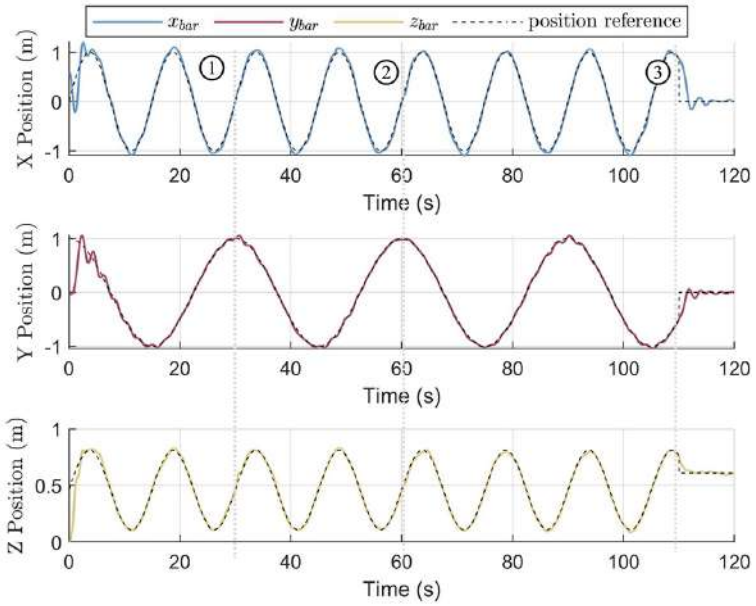

Figure 3.12 – The current and desired positions for the payload center-of-mass during transportation task #5.

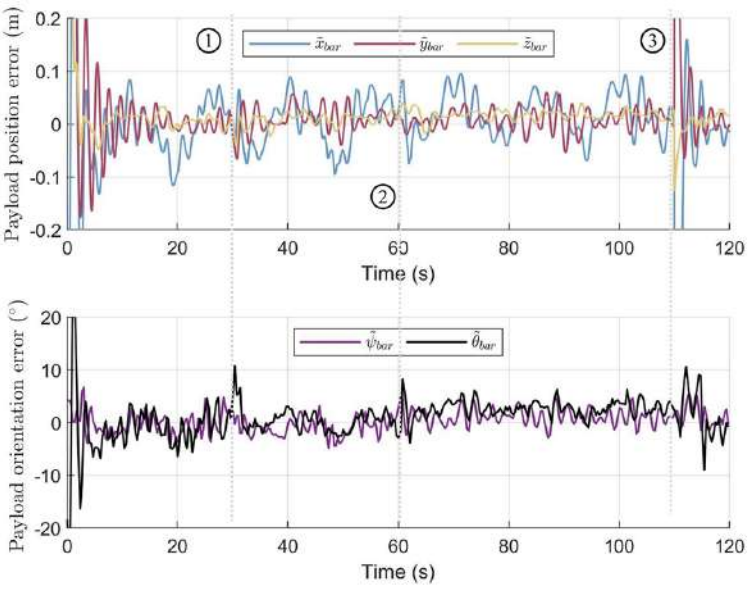

Figure 3.13 – Tracking error for the position of the payload center-of-mass and for the payload orientation during transportation task #5.

trajectory frequency, which induce oscillations due to three initial conditions: (*i*) as pointed in Figure 3.14, the payload starting point is not on the trajectory to be tracked, making initial $\tilde{\boldsymbol{q}}$ big; (*ii*) as one can see in the video, the payload lifting and transportation modes occur simultaneously; and (*iii*) the desired acceleration in the $\hat{\boldsymbol{y}}^w$ direction depends on $cos(t)$, thus starting at its maximum value. Despite these adverse initial conditions, one can check that the oscillations are quickly damped and the transportation becomes smooth in just a few

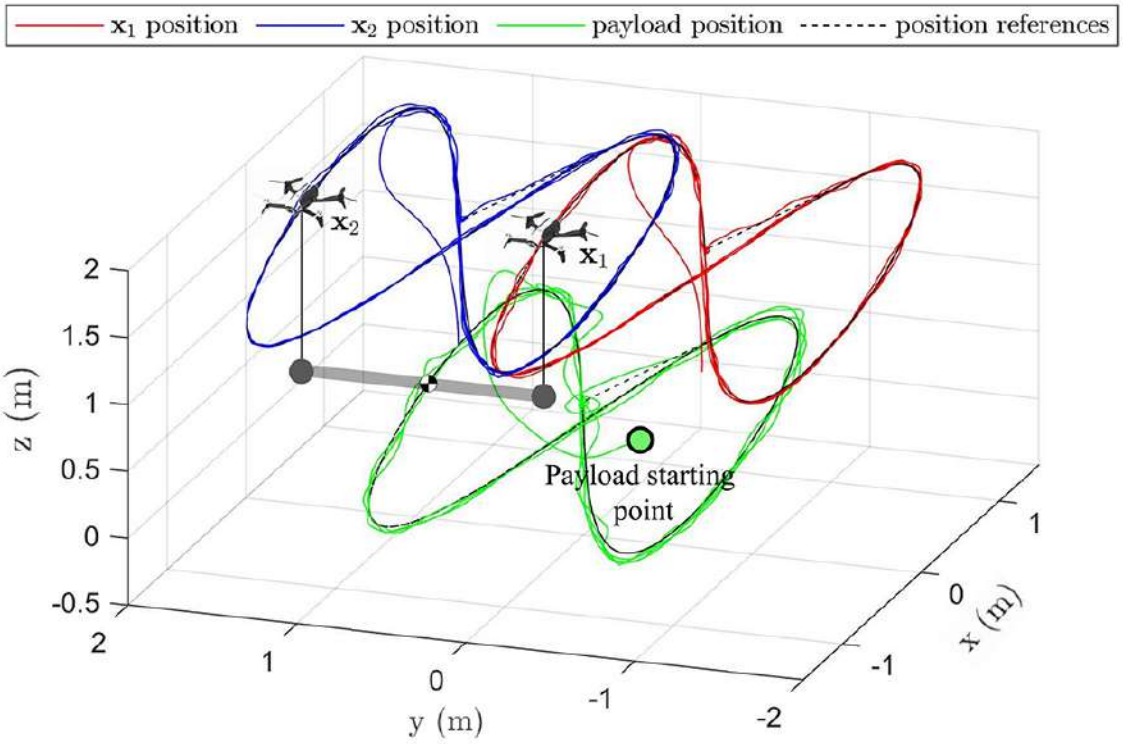

Figure 3.14 – Three dimensional tracking performance for the whole system, payload and quadrotors, during transportation task #5.

seconds.

Finally, in the timestamp ③, the trajectory tracking is halted by the operator, and a positioning task is commanded, with desired state for the payload $\boldsymbol{x}_{bar,des} = [0 \quad 0 \quad 0.6]^\top$ m. As discussed through this manuscript, this discontinuity induces oscillations on the payload and should be avoided. However, here it is was introduced with the purpose of performance analysis. As shown in Figure 3.12, the proposed algorithms can counteract the disturbances and accomplish the positioning task. As a result, the same system here proposed to track a trajectory can be used to perform positioning tasks, which only demands to define constant values of the variables corresponding to the desired formation position and shape.

Despite the recommendations on Subsection 3.5.1 of using smooth desired trajectories with initial and final accelerations equal to zero and transportation under constant velocities, the experiments presented in Subsection 3.7.5 did not follow any of these restrictions, showing the good performance of the proposed approach even when these ideal situations are not completely fulfilled.

	This paper	[11]	[17]	[22]	[24]	[27]	[29]	[30]	[31]
Control technique	Adaptive	$\mathcal{H}_\infty$	Optimal	RL	Adaptive	PB	EB	ESO	SMC
Single or cooperative transportation	Coop.	Coop.	Coop.	Single	Single	Coop.	Single	Coop.	Single
Experiments with 3D trajectories	Yes	No	No	No	No	No	No	No	Yes
Maximum acceleration (m/s^2)	1.6	QS	QS	QS	QS	QS	QS	QS	QS
Payload to quadrotor-weight ratio	0.33 to 0.57	0.11	0.16	0.18	0.20	0.20	0.06	0.09	0.11
Payload tracking precision	Low	High	High	High	High	Low	High	Low	High
Payload orientation	2 DoF	3 DoF	3 DoF	No	No	No	No	No	no
Tested against uncertainties	Yes	Yes	Yes	Yes	Yes	Yes	Yes	Yes	Yes
Tested against wind	Yes	No	Yes	No	No	Yes	No	Yes	Yes
Tested in outdoors	No	No	Yes	No	No	No	No	Yes	No
Robust against disturbances	No	No	No	No	Yes	Yes	No	Yes	Yes
Implementation complexity	Low	Med.	High	High	Med.	Low	Low	Med.	Low

Table 3.1 – Comparison among recent publications on load transportation. QS – Quasi-Static; RL – Reinforcement Learning; PB – Passivity-Based; EB – Energy-based; ESO – Extended State Observer; SMC – Sliding Mode Control; DoF – Degree of Freedom;

3.7.6 Results Overview

To highlight the results of our proposal in contrast with the related works presented in Section 3.1.1, we build a comparative board that compiles the most important features, in our opinion, for load transportation with quadrotors. Further, due to the dynamic complexity of transporting payloads using quadrotors, it is difficult to provide a reliable simulation for this task, which leads us to only compare works whose algorithms were tested in experimental trials. The comparative board thus generated is shown in Table 3.1.

As one can see in Table 3.1, the results presented in this paper bring advantages and drawbacks compared to the most recent works on the subject of load transportation using quadrotors. As main advantages, our proposal manipulate and transport the payload in velocities and accelerations far from quasi-static motion, which is important considering real-world applications. In addition, we also consider heavier payloads than the rest of the compared works. Another advantage is the simplicity of implementation and the ability to suppress drag-related uncertainties (like wind). As a drawback, since we do not use measurements from the payload, our proposal lacks precision in comparison with some of the other works. In our approach, the payload is attached to the vehicles by the flexible cables, so that it is only restricted to be near of the vehicles during transportation. Aiming at getting an approach that is safe and readily applicable to off-the-shelf quadrotors, we gave more emphasis to simplicity over precision. Another important drawback is the lack of outdoor tests, which is our main objective for future works.

3.8 Concluding remarks

The control system here proposed deals with a formation of two quadrotors transporting a rod-shaped load. Adverse conditions for the transporting were tested in real experiments, and the system presented good performance in all of them. In most of these tests, we compared our control paradigm with the PID controller, a industrial standard, and the results demonstrated the superiority of our approach. As a result, we claim that the proposed control system is able to guide the formation in the accomplishment of trajectory tracking tasks, positioning, and load-orientation tasks when transporting a rod-shaped payload.

As future works, we plan to completely get rid of the motion capture system, moving one step further towards a system applicable to real-world scenarios. Solutions for an increased number of vehicles are also being pursued, aiming at the possibility of transporting heavier payloads.

3.9 References

[1] OLLERO, A. et al. Past, present, and future of aerial robotic manipulators. *IEEE Transactions on Robotics*, IEEE, Early Access, p. 1–20, 2021.

[2] TANG, S.; KUMAR, V. Autonomous flight. *Annual Review of Control, Robotics, and Autonomous Systems*, Annual Reviews, v. 1, p. 29–52, 2018.

[3] MOHIUDDIN, A. et al. A survey of single and multi-uav aerial manipulation. *Unmanned Systems*, World Scientific, v. 8, n. 02, p. 119–147, 2020.

[4] VILLA, D. K.; BRANDAO, A. S.; SARCINELLI-FILHO, M. A survey on load transportation using multirotor uavs. *Journal of Intelligent & Robotic Systems*, Springer, v. 98, n. 2, p. 267–296, 2020.

[5] GUERRERO-SÁNCHEZ, M. E. et al. Nonlinear control strategies for a uav carrying a load with swing attenuation. *Applied Mathematical Modelling*, Elsevier, v. 91, p. 709–722, 2021.

[6] FOEHN, P. et al. Fast trajectory optimization for agile quadrotor maneuvers with a cable-suspended payload. In: *Proceedings of Robotics: Science and Systems*. Cambridge, Massachusetts: [s.n.], 2017. p. 1–10.

[7] LOIANNO, G. et al. Localization, grasping, and transportation of magnetic objects by a team of mavs in challenging desert-like environments. *IEEE Robotics and Automation Letters*, IEEE, v. 3, n. 3, p. 1576–1583, 2018.

[8] TANG, S.; SREENATH, K.; KUMAR, V. Multi-robot trajectory generation for an aerial payload transport system. In: *Robotics Research*. Berlin, Germany: Springer, 2020. p. 1055–1071.

[9] KLAUSEN, K. et al. Cooperative control for multirotors transporting an unknown suspended load under environmental disturbances. *IEEE Transactions on Control Systems Technology*, IEEE, v. 28, n. 2, p. 653–660, 2018.

[10] HORYNA, J.; BACA, T.; SASKA, M. Autonomous collaborative transport of a beam-type payload by a pair of multi-rotor helicopters. In: IEEE. *2021 International Conference on Unmanned Aircraft Systems (ICUAS)*. [S.l.], 2021. p. 1139–1147.

[11] SANALITRO, D. et al. Full-pose manipulation control of a cable-suspended load with multiple uavs under uncertainties. *IEEE Robotics and Automation Letters*, IEEE, v. 5, n. 2, p. 2185–2191, 2020.

[12] ERSKINE, J.; CHRIETTE, A.; CARO, S. Wrench analysis of cable-suspended parallel robots actuated by quadrotor unmanned aerial vehicles. *Journal of Mechanisms and Robotics*, American Society of Mechanical Engineers, v. 11, n. 2, p. 020909, 2019.

[13] LI, Z. et al. Design and control of a variable aerial cable towed system. *IEEE Robotics and Automation Letters*, IEEE, v. 5, n. 2, p. 636–643, 2020.

[14] TAGLIABUE, A. et al. Robust collaborative object transportation using multiple mavs. *The International Journal of Robotics Research*, SAGE Publications Sage UK: London, England, v. 38, n. 9, p. 1020–1044, 2019.

[15] GABELLIERI, C. et al. A study on force-based collaboration in swarms. *Swarm Intelligence*, Springer, v. 14, n. 1, p. 57–82, 2020.

[16] GENG, J.; SINGLA, P.; LANGELAAN, J. W. Trajectory planning and control for a multilift system based on load distribution. In: *AIAA Scitech 2021 Forum*. [S.l.: s.n.], 2021. p. 0980.

[17] GENG, J.; LANGELAAN, J. W. Cooperative transport of a slung load using load-leading control. *Journal of Guidance, Control, and Dynamics*, American Institute of Aeronautics and Astronautics, v. 43, n. 7, p. 1313–1331, 2020.

[18] CHEN, T.; SHAN, J.; LIU, H. H. Cooperative transportation of a flexible payload using two quadrotors. *Journal of Guidance, Control, and Dynamics*, American Institute of Aeronautics and Astronautics, p. 1–9, 2021.

[19] GKOUNTAS, K.; TZES, A. Leader/follower force control of aerial manipulators. *IEEE Access*, IEEE, v. 9, p. 17584–17595, 2021.

[20] ROSSI, E. et al. Cooperative aerial load transportation via sampled communication. *IEEE Control Systems Letters*, IEEE, v. 4, n. 2, p. 277–282, 2019.

[21] THAPA, S.; BAI, H.; ACOSTA, J. Á. Cooperative aerial manipulation with decentralized adaptive force-consensus control. *Journal of Intelligent & Robotic Systems*, Springer, v. 97, n. 1, p. 171–183, 2020.

[22] BELKHALE, S. et al. Model-based meta-reinforcement learning for flight with suspended payloads. *IEEE Robotics and Automation Letters*, IEEE, v. 6, n. 2, p. 1471–1478, 2021.

[23] LI, X.; ZHANG, J.; HAN, J. Trajectory planning of load transportation with multi-quadrotors based on reinforcement learning algorithm. *Aerospace Science and Technology*, Elsevier, p. 106887, 2021.

[24] TRAN, V. P. et al. Neural network-based self-learning of an adaptive strictly negative imaginary tracking controller for a quadrotor transporting a cable-suspended payload with minimum swing. *IEEE Transactions on Industrial Electronics*, IEEE, 2020.

[25] TRAN, V. P.; SANTOSO, F.; GARRATT, M. A. Adaptive trajectory tracking for quadrotor systems in unknown wind environments using particle swarm optimization-based strictly negative imaginary controllers. *IEEE Transactions on Aerospace and Electronic Systems*, IEEE, 2021.

[26] ROSSOMANDO, F. et al. Aerial load transportation with multiple quadrotors based on a kinematic controller and a neural smc dynamic compensation. *Journal of Intelligent & Robotic Systems*, Springer, v. 100, n. 2, p. 519–530, 2020.

[27] MOHAMMADI, K.; SIROUSPOUR, S.; GRIVANI, A. Passivity-based control of multiple quad-rotors carrying a cable-suspended payload. *IEEE/ASME Transactions on Mechatronics*, IEEE, 2021.

[28] MOHAMMADI, K.; SIROUSPOUR, S.; GRIVANI, A. Control of multiple quad-copters with a cable-suspended payload subject to disturbances. *IEEE/ASME Transactions on Mechatronics*, IEEE, v. 25, n. 4, p. 1709–1718, 2020.

[29] YANG, S.; XIAN, B. Energy-based nonlinear adaptive control design for the quadrotor uav system with a suspended payload. *IEEE Transactions on Industrial Electronics*, IEEE, v. 67, n. 3, p. 2054–2064, 2019.

[30] LIU, Y. et al. Analysis, planning and control for cooperative transportation of tethered multi-rotor uavs. *Aerospace Science and Technology*, Elsevier, v. 113, p. 106673, 2021.

[31] FALCÓN, R.; RÍOS, H.; DZUL, A. Comparative analysis of continuous sliding-modes control strategies for quad-rotor robust tracking. *Control Engineering Practice*, Elsevier, v. 90, p. 241–256, 2019.

[32] LEWIS, M. A.; TAN, K.-H. High precision formation control of mobile robots using virtual structures. *Autonomous Robots*, v. 4, n. 4, p. 387–403, October 1997. ISSN 1573-7527.

[33] SANTANA, L. V.; BRANDÃO, A. S.; SARCINELLI-FILHO, M. Navigation and cooperative control using the ar.drone quadrotor. *Journal of Intelligent & Robotic Systems*, v. 84, n. 1, p. 327–350, December 2016. ISSN 1573-0409.

[34] ZENG, J.; SREENATH, K. Geometric control of a quadrotor with a load suspended from an offset. In: IEEE. *2019 American Control Conference (ACC)*. [S.l.], 2019. p. 3044–3050.

[35] Santos, M. C. P. et al. A novel null-space-based uav trajectory tracking controller with collision avoidance. *IEEE/ASME Transactions on Mechatronics*, v. 22, n. 6, p. 2543–2553, December 2017.

[36] PINTO, A. O. et al. High-level modeling and control of the *Bebop 2* micro aerial vehicle. In: *To appear in the Proceedings of the 2020 International Conference on Unmanned Aircraft Systems*. Athens, Greece: IEEE, 2020. p. 939–947.

[37] SLOTINE, J.-J.; LI, W. *Applied Nonlinear Control*. [S.l.]: Prentice-Hall, Inc, 1991. ISBN 0-13-040890-5.

4 [P3] - Cooperative load transportation with quadrotors using robust adaptive control

The problem of transport cable-suspended payloads using two quadrotors is analyzed in this work. The system kinematics are treated using a virtual structure formation controller, which generates the acceleration references commanded to the aerial vehicles. The disturbances caused by the payload are treated as unmodeled disturbances, and a novel robust integral of the sign of the error (RISE) controller is proposed, guaranteeing the asymptotic convergence of the tracking errors. A model reference adaptive control is also incorporated into the RISE controller, combining the advantages of adaptive and robust control. The proposal is validated by numerous experiments using two quadrotors to transport a bar-shaped payload in adverse conditions. The results allow concluding that the proposed system is able to perform transportation and orientation tasks with the payload, subject to translational accelerations up to 3.5 m/s^2.

Supplementary material

Video of the experiments: https://youtu.be/KeZ5XcOn914

4.1 Introduction

In our society, for the flight of UAVs to be accepted in civil areas, the aerial vehicle should be able to stably fly under adverse environmental conditions, and track routes keeping safe distances from people and buildings. It is known that efficient collision-free trajectory tracking is harder when transporting payloads, once the additional payload dynamics increase the task complexity and impose additional performance and robustness needs. To guarantee the tracking under a broad range of applications, it is paramount to incorporate robust control algorithms to attenuate the effects of model uncertainties and disturbances.

Adaptive control is a powerful tool to address the parametric uncertainty present on models and to estimate unknown but constant parameters, thus improving tracking accuracy [1]. However, it may be unstable when facing large unmodeled disturbances, and offers limited (or no) help when the system is facing time-varying disturbances [2; 3]. On the other hand, robust techniques such as sliding mode control (SMC) excel in providing an easy-to-implement discontinuous control action that completely cancels any bounded modeling error or external

disturbance if the uncertainties/disturbances bounds are known [4; 5]. From a practical point-of-view, considerable drawbacks present in sliding mode controllers are the difficulty to find these bounds a priori and the chattering effect inherently present in these controllers due to the discontinuous control action. Regarding adaptive control and robust control, the integration of these fundamentally different control designs is still a pending demand in related research works.

In face of such a problem, the authors in [6] presented a continuous control strategy based on the **r**obust **i**ntegral of the **s**ign of the **e**rror (namely, RISE feedback control) which guarantees asymptotic convergence for systems subjected to sufficiently smooth bounded disturbances. After a careful examination of the control law of the RISE controller, one can note it resembles the second-order super-twisting sliding mode controller (see [7; 4]), and can be viewed in such a way as a continuous counterpart of the SMC. An interesting property of the RISE controller is that the control law learns the unknown disturbance, acting as a disturbance observer [6]. A major implementation issue in RISE feedback is that the disturbance derivative bounds, up to second-order derivative, must be known a priori. Similar to second-order sliding mode controllers, the RISE design requires the tuning of a control gain that needs to be higher than the disturbance derivative bounds. A common practice to deal with the unpredictable behavior of disturbances of different nature affecting the system is to overestimate the RISE control gain, guaranteeing asymptotic convergence but compromising the transient tracking performance.

A step in the direction of addressing this issue is given in this paper. Here, we propose a novel adaptive RISE controller, which iteratively searches for the minimal RISE gain that fulfills a given task. Here, no prior knowledge of the disturbance derivative bounds is needed. In order to integrate adaptive control and robust control techniques, also giving a step towards this demand, we integrate the adaptive RISE feedback with standard model reference adaptive control (MRAC), reducing the needed control efforts from the RISE due to parameter uncertainty, once those will be treated by the model reference adaptive control in closed-loop and will be feedforwarded by dynamic inversion.

To cover a broader range of transportation systems using quadrotors, individual and cooperative transportation are treated in this work. To manage the cooperative transportation, a framework similar to the one proposed in our previous work [8] is used here, where the two quadrotors used to transport a payload are treated as a virtual structure formation problem. Cooperative transportation brings advantages and difficulties related to individual transportation, such as the ability to carry heavier payloads, the ability to orientate the payload by managing the position of the quadrotors, but at a cost of increasing the algorithm complexity and dealing with a harder dynamics problem.

In such a context, the contributions of this work are the following: (i) a novel RISE feedback

controller that uses no prior knowledge of the disturbance derivative bounds and achieves asymptotic stability of the tracking errors for systems subjected to smooth disturbances; (ii) an improvement over the formation control paradigm proposed in [8], substituting the velocity mapping between the formation and quadrotor variables by an acceleration mapping; (iii) the proposition of a control framework that is readily applicable in commercial off-the-shelf quadrotors, such as the *Parrot Bebop 2* used in the experiments that validate this work; (iv) once the load swing motion during the transportation tasks is not suppressed, this proposal allows agile maneuvers; (v) numerous high performance experiments, demonstrating the stability and performance of the proposed controller in different scenarios, and (vi) the performance comparison against common used controllers to improve robustness, such as MRAC and industrial standard PID controller.

4.2 Methodology

4.2.1 Notation

Throughout this paper, we use lowercase letters for scalars, bold lowercase letters to represent vectors, and bold uppercase letters for matrices. Two coordinate systems are used in this paper: the inertial world frame, $\mathcal{I}$, defined by $\{\boldsymbol{x}^I, \boldsymbol{y}^I, \boldsymbol{z}^I\}$ with $\boldsymbol{z}^I$ pointing upward; and the body frame, $\mathcal{B}$, attached to the center of mass (CoM) of the quadrotor, defined by $\{\boldsymbol{x}^B, \boldsymbol{y}^B, \boldsymbol{z}^B\}$ with $\boldsymbol{x}^B$ pointing forward and $\boldsymbol{z}^B$ aligned with the collective thrust direction (See Figure 4.1). For the sake of readability, vectors without superscript are expressed in the inertial frame. We use subscript $[\cdot]_{des}$ and $[\cdot]_{ref}$ to describe, respectively, the desired states and the references sent to the quadrotor. The operator $\text{diag}(a_1, a_2, \ldots, a_n)$ denotes a diagonal matrix with scalars $(a_1, a_2, \ldots, a_n)$ as diagonal entries.

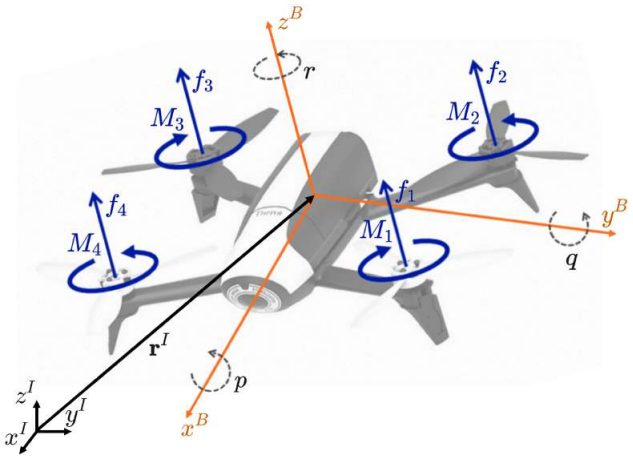

Figure 4.1 – The reference frames and the abstract control inputs $f_i, i = 1, \cdots, 4$, for a quadrotor.

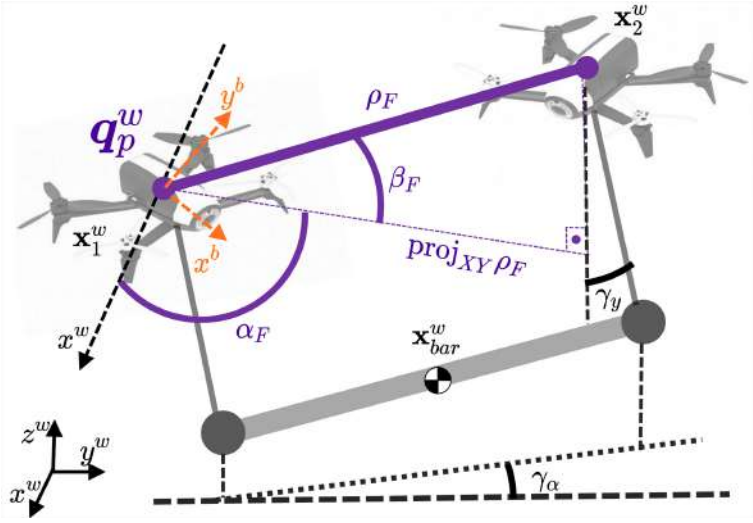

Figure 4.2 – Virtual structure formation for two UAVs carrying a payload. The virtual structure is depicted in purple.

4.2.2 Multiple robot formation

To cooperatively transport a bar-shaped payload using two quadrotors, instead of directly planning for the trajectories of each vehicle that synchronizes them during the task, we choose to formulate the cooperative transportation as a robot formation problem. The proposed formation framework is based on the virtual structure paradigm [9], where the virtual structure is given by a line in the 3D space, the line linking the two UAVs. Such a formation is characterized by the so-called formation variables $\boldsymbol{q}$ given as

$$\boldsymbol{q} = \begin{bmatrix} \boldsymbol{q}_p^\top & \boldsymbol{q}_c^\top \end{bmatrix}^\top \in \mathbb{R}^6 \tag{4.1}$$

where $\boldsymbol{q}_p = \begin{bmatrix} x_F & y_F & z_F \end{bmatrix}^\top \in \mathbb{R}^3$ represents the position coordinates of the virtual structure in the world frame, here given by the position of one of the UAVs in the formation extremities, whereas $\boldsymbol{q}_c = \begin{bmatrix} \alpha_F & \beta_F & \rho_F \end{bmatrix}^\top \in \mathbb{R}^3$ are the formation configuration, that also defines the other extremity, as it can be seen in Figures 4.2 and 4.3. As for the formation configuration components, α_F is the angle between the X-axis and the projection of the virtual structure on the XY-plane, β_F is the angle between the XY-plane and the virtual structure, and ρ_F is the length of the virtual structure (the distance between the two UAVs).

In summary, the position of a UAV with respect to the other is given by a set of spherical variables, and the cable-suspended payload is considered hanging in the vicinity of the virtual structure formation, at a distance limited by the length of the cables. The direct kinematics equation for the virtual-structure formation can be written in the form

$$\boldsymbol{q} = k(\boldsymbol{\xi}) \tag{4.2}$$

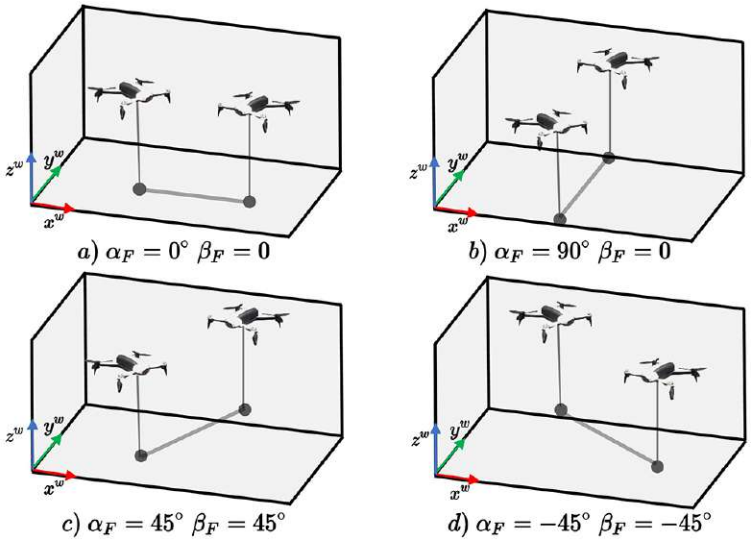

Figure 4.3 – Virtual structure formation at different configurations for two UAVs carrying a bar-shaped payload.

where $\boldsymbol{q} \in \mathbb{R}^6$ is the already defined vector of formation variables, $\boldsymbol{\xi} \in \mathbb{R}^6$ is the vector containing the position of quadrotors #1 and #2, i.e., $\boldsymbol{\xi} = \begin{bmatrix} \boldsymbol{x}_1^\top & \boldsymbol{x}_2^\top \end{bmatrix}^\top$, and $k(\cdot)$ is the nonlinear direct kinematics function. Thus, the differential kinematics equation can be obtained by differentiating (4.2) with respect to time, i.e., evaluating the analytical Jacobian [10], $\boldsymbol{J}_A = \partial \boldsymbol{q} / \partial \boldsymbol{\xi}$, leading to:

$$\dot{\boldsymbol{q}} = \boldsymbol{J}_A(\boldsymbol{\xi})\dot{\boldsymbol{\xi}} \tag{4.3}$$

The direct kinematics (4.2) and the differential kinematics (4.3) for the given formation are completely described in our previous work [8]. Here we move forward and improve the formation controller given in our previous work [8], which uses velocity references as the output of the formation controller. Since quadrotors use as common inputs attitude angles or body rates, and these are related to the second and third derivative of position [11], i.e., acceleration and jerk, respectively, the use of an acceleration mapping instead of a velocity mapping suits better to quadrotor applications. To obtain such acceleration mapping we proceed as follows.

Following the procedure presented in [12], and further differentiating (4.3), leads to

$$\ddot{\boldsymbol{q}} = \boldsymbol{J}_A(\boldsymbol{\xi})\ddot{\boldsymbol{\xi}} + \dot{\boldsymbol{J}}_A(\boldsymbol{\xi}, \dot{\boldsymbol{\xi}})\dot{\boldsymbol{\xi}} \tag{4.4}$$

Hereinafter, the dependency of $\boldsymbol{\xi}$ in $\boldsymbol{J}(\boldsymbol{\xi})$ is dropped for readability. As one can see in (4.4), given the desired references for the formation $\begin{bmatrix} \ddot{\boldsymbol{q}}_{des}^\top & \dot{\boldsymbol{q}}_{des}^\top & \boldsymbol{q}_{des}^\top \end{bmatrix}^\top$, the following second-order inverse kinematics controller can be constructed

$$\ddot{\boldsymbol{\xi}}_{ref} = \boldsymbol{J}_A^{-1}(\ddot{\boldsymbol{q}}_{des} + \boldsymbol{K}_D\dot{\tilde{\boldsymbol{q}}} + \boldsymbol{K}_P\tilde{\boldsymbol{q}} - \dot{\boldsymbol{J}}_A\dot{\boldsymbol{\xi}}) \tag{4.5}$$

where $\boldsymbol{K}_D$ and $\boldsymbol{K}_P$ are diagonal positive definite matrix gains.

Assuming that the aerial vehicles are able to follow the acceleration references given by the second-order kinematic controller (4.5), the controller stability can be straight-forwarded analyzed, once the substitution of (4.5) into (4.4) leads to the second-order exponentially stable linear system

$$\ddot{\tilde{\boldsymbol{q}}} + \boldsymbol{K}_D\dot{\tilde{\boldsymbol{q}}} + \boldsymbol{K}_P\tilde{\boldsymbol{q}} = \boldsymbol{0} \tag{4.6}$$

To deal with singular formation configurations, where the inversion of $\boldsymbol{J}_A^{-1}$ is ill-conditioned, we adopted the following damped-least-squares Jacobian, as in [12],

$$\boldsymbol{J}_A^{+} = \boldsymbol{J}_A^{\top}(\boldsymbol{J}_A\boldsymbol{J}_A^{\top} + \lambda^2\boldsymbol{I})^{-1} \tag{4.7}$$

where $\boldsymbol{I}$ is the identity matrix $\in \mathbb{R}^{6\times 6}$ and λ is the damping factor as described in [13; 14]. Substituting (4.7) into (4.5) yields

$$\ddot{\boldsymbol{\xi}}_{ref} = \boldsymbol{J}_A^{+}(\ddot{\boldsymbol{q}}_{des} + \boldsymbol{K}_D\dot{\tilde{\boldsymbol{q}}} + \boldsymbol{K}_P\tilde{\boldsymbol{q}} - \dot{\boldsymbol{J}}_A\dot{\boldsymbol{\xi}}) \tag{4.8}$$

The kinematic error behavior of introducing the damped-least-squares solution can be obtained by substituting (4.8) into (4.4), and after performing some algebraic manipulations,

$$\ddot{\tilde{\boldsymbol{q}}} + \boldsymbol{K}_D\dot{\tilde{\boldsymbol{q}}} + \boldsymbol{K}_P\tilde{\boldsymbol{q}} = \boldsymbol{\Delta}(\ddot{\boldsymbol{q}}_{des} + \boldsymbol{K}_D\dot{\tilde{\boldsymbol{q}}} + \boldsymbol{K}_P\tilde{\boldsymbol{q}} - \dot{\boldsymbol{J}}_A\dot{\boldsymbol{\xi}}) \tag{4.9}$$

where $\boldsymbol{\Delta} = (\boldsymbol{I} - \boldsymbol{J}_A\boldsymbol{J}_A^{+})$ represents the discrepancy of using the damped-least-squares Jacobian inverse versus the conventional Jacobian inverse. Further, this discrepancy is governed by the design of the damping factor λ; which for small values of λ deliver accurate solutions but with low robustness in the neighborhood of singular configurations, while large values of λ results in low tracking accuracy but guaranteed control feasibility (limited quadrotor acceleration references) [15]. In short, the damping factor λ is used to achieve a tradeoff between solution accuracy and feasibility, and can be suitably tuned by defining a singular region in the neighborhood of the singularity, and changing the values of λ in that region accordingly. The development of such λ estimate and the stability analysis of using the second-order kinematic controller with the damped-least-squares Jacobian (4.8) can be found in [12].

To accordingly control the two quadrotors by the given kinematic controller (4.8), the first three components of $\ddot{\boldsymbol{\xi}}_{ref}$ are the acceleration references to be sent to the quadrotor #1, and the last three components of $\ddot{\boldsymbol{\xi}}_{ref}$ are the references sent to quadrotor #2.

Lastly, in a real-world scenario, it is known that the tracking of acceleration references given by the kinematic controller (4.8) are hindered by model uncertainties and exogenous disturbances. Therefore, to deal with the uncertainties and disturbances we present in the following section a robust solution that guarantees asymptotic tracking of the references given by the proposed second-order kinematic controller.

4.2.3 System dynamics & baseline position control

In this work we opt to use a simplified dynamic model for the aerial vehicles, modeling only the effects caused by the inputs and the effects caused by the linear drag affecting the vehicles. Thus, we do not model any dynamic effects caused by the payload on the quadrotors or disturbances caused by the interaction between the two quadrotors. These disturbances are treated as unmodeled disturbances. In addition, we assumed that the disturbances with origin on the transported payload do not affect the attitude dynamics, i.e., the payload dynamics are decoupled from the attitude dynamics and do not affect the pitch and roll internal control loops. This assumption is made considering that the cable-suspended payload is attached to the quadrotor center-of-mass. Although being quite difficult to access the CoM in real quadrotors – it is likely to lie inside the vehicle body or components – we can adjust the attaching point at the base of the vehicle in such a way that any offset is just in the $\hat{\boldsymbol{z}}^b$ direction. The attachment assumption is reasonable and mild, in the sense that the resulting torque in the vehicle from the attachment offset is negligible, which can be seen in the results provided in [8], that uses a similar assumption, and in the results provided in Section 4.4 of this paper.

In such a manner, our analysis can be restricted only to the translational dynamics and we can treat each quadrotor controller individually. The translational mathematical model for a quadrotor is well covered in the literature [16], and can be given by

$$m\ddot{x} = (c_\psi s_\theta + s_\psi c_\theta s_\phi)u_1 - c_1\dot{x} - d_x, \tag{4.10a}$$

$$m\ddot{y} = (s_\psi s_\theta - c_\psi c_\theta s_\phi)u_1 - c_2\dot{y} - d_y, \tag{4.10b}$$

$$m\ddot{z} = (c_\phi c_\theta)u_1 - mg - c_3\dot{z} - d_z, \tag{4.10c}$$

where g is the gravity acceleration, m is the mass of the quadrotor, $\boldsymbol{c} = [c_1, c_2, c_3]^\top$ are the linear air drag coefficients, $\boldsymbol{d} = [d_x, d_y, d_z]^\top$ are the unmodeled disturbances, and u_1 is the vehicle thrust.

Considering (4.10), and exploiting the built-in low-level attitude controller present in off-the-shelf quadrotors, the desired translational accelerations can be obtained by high-level attitude inputs sent to the vehicles. In most off-the-shelf quadrotors, these commands are desired attitude or body rates. For either type of built-in low-level attitude controller, the control strategy proposed in this paper is valid, once these low-level controllers are related by

the following closed-loop attitude dynamics [17]:

$$\begin{aligned}\dot{\phi} &= \frac{1}{\tau_\phi}(k_\phi \phi_{ref} - \phi) \\ \dot{\theta} &= \frac{1}{\tau_\theta}(k_\theta \theta_{ref} - \theta) \\ \dot{\psi} &= \dot{\psi}_{ref}\end{aligned} \tag{4.11}$$

where $k_\phi,\ k_\theta$ and $\tau_\phi,\ \tau_\theta$ are the gains and time constants of the roll and pitch closed-loop dynamics, respectively, and ϕ_{ref}, θ_{ref} are the commanded reference for roll and pitch angles. Normally, for either type of low-level controller, the commanded signal for yaw is the yaw rate reference $\dot{\psi}_{ref}$.

In this work, we apply our controller to a Parrot Bebop 2 quadrotor, which uses desired attitude as inputs. These commands for translational control are the pitch command u_θ, the roll command u_ϕ, and the altitude rate command $u_{\dot{z}}$. These commands are grouped in the vector defined as $\boldsymbol{u} = \begin{bmatrix}\theta_{ref} & \phi_{ref} & u_{\dot{z}}\end{bmatrix}^\top = \begin{bmatrix}\hat{k}_\theta^{-1}\theta_{des} & \hat{k}_\phi^{-1}\phi_{des} & \hat{k}_{\dot{z}}^{-1}\dot{z}_{des}\end{bmatrix}^\top$, whose entries are all in the interval $[-1.0, +1.0]$, representing the normalized limits for the desired high-level commands, with $\boldsymbol{K}_u^{-1} = \text{diag}(\hat{k}_\theta^{-1},\ \hat{k}_\phi^{-1},\ \hat{k}_{\dot{z}}^{-1})$ being the diagonal matrix containing the estimate of the proportionality gains associating the normalized control commands to the embedded controller limit parameters. Due to flatness property, the yaw can be arbitrarily chosen [18], therefore, it is not considered in our analysis.

Aiming at safety and accuracy, normally the desired velocities and accelerations used to transport payloads are low or moderate. Thus, a linearization around a near-hover configuration can be applied to the quadrotor attitude in (4.10). Such a linearization results in the translational dynamics given by (4.12)

$$\begin{aligned}\ddot{x} &= \left(c_\psi \hat{k}_\theta \theta_{ref} + s_\psi \hat{k}_\phi \phi_{ref}\right) g - \frac{c_1}{m}\dot{x} - d_x, \\ \ddot{y} &= \left(s_\psi \hat{k}_\theta \theta_{ref} - c_\psi \hat{k}_\phi \phi_{ref}\right) g - \frac{c_2}{m}\dot{y} - d_y, \\ \ddot{z} &= \frac{1}{\tau_{\dot{z}}}\left(u_{\dot{z}} - \dot{z}\right) - \frac{c_3}{m}\dot{z} - d_z,\end{aligned} \tag{4.12}$$

where $s_\phi \approx \phi,\ c_\phi \approx 1$ (with similar linearization for θ), and $u_1 = mg$. To ensure validity of the near-hover linearization, limits are established for the desired pitch and roll θ_{des} and ϕ_{des} which are both $\leq 25°$. These limitation are equivalent to translational accelerations up to 4.0 m/s^2.

Considering $\boldsymbol{u} = \begin{bmatrix}\theta_{ref} & \phi_{ref} & u_{\dot{z}}\end{bmatrix}^\top$, it is straightforward to written the dynamics described in (4.12) in the linear form as

$$\boldsymbol{u} = R_\psi^{-1}(\boldsymbol{A}\ddot{\boldsymbol{x}} + \boldsymbol{B}\dot{\boldsymbol{x}} + \boldsymbol{d}) \tag{4.13}$$

where $\boldsymbol{A} = diag(a_1, a_2, a_3)$ and $\boldsymbol{B} = diag(b_1, b_2, b_3)$ are diagonal positive definite matrices containing the thrust-related dynamic parameters for the vehicle. The thrust-related dynamic parameters ($\hat{\boldsymbol{A}}$, $\hat{\boldsymbol{B}}$) can be estimated using a series of samples from experimental trials and least square identification, as in [19] and [20].

To develop the algorithms for the model reference adaptive control and adaptive RISE control, we need an error metric in the robot's space. Thus, a formation reference tracking error can be defined as $\boldsymbol{\nu} = \dot{\boldsymbol{x}}_{ref} - \dot{\boldsymbol{x}}$, where

$$\dot{\boldsymbol{x}}_{ref} = \boldsymbol{J}^{+}(\dot{\boldsymbol{q}}_{des} + \boldsymbol{K}_P\tilde{\boldsymbol{q}}). \tag{4.14}$$

Finally, one can steer the vehicles using the velocity and acceleration references given by the formation controller in (4.8), by implementing a feedback linearization control law in (4.13)

$$\boldsymbol{u} = R_{\psi}^{-1}(\hat{\boldsymbol{A}}\ddot{\boldsymbol{x}}_{ref} + \hat{\boldsymbol{B}}\dot{\boldsymbol{x}} + \boldsymbol{\kappa}_D\boldsymbol{\nu} + \boldsymbol{u}_{RISE}) \tag{4.15}$$

where $\boldsymbol{u}_{RISE}$ is the robust control action given by the adaptive RISE controller to be developed in the next section. The robust control action is responsible to counteract the effects of the disturbances $\boldsymbol{d}$ in closed-loop.

4.2.4 Model reference adaptive controller

To alleviate the control action $\boldsymbol{u}_{RISE}$, also guaranteeing faster convergence and less energy consumption, we follow the procedure described in [8] and online adapt the parameters ($\hat{\boldsymbol{A}}$, $\hat{\boldsymbol{B}}$) by implementing a model reference adaptive controller. This adaptation acts to improve our identified model, and can be computed by writing the translational control law (4.15) in compact form as

$$\boldsymbol{u} = \boldsymbol{G}(\ddot{\boldsymbol{x}}_{\boldsymbol{ref}}, \dot{\boldsymbol{x}})\hat{\boldsymbol{\Theta}} + \boldsymbol{\kappa}_D\boldsymbol{\nu}, \tag{4.16}$$

with

$$\begin{bmatrix} u_\theta \\ u_\phi \\ u_{\dot{z}} \end{bmatrix} = \begin{bmatrix} \ddot{x}_{ref} & \dot{x} & 0 & 0 & 0 & 0 \\ 0 & 0 & \ddot{y}_{ref} & \dot{y} & 0 & 0 \\ 0 & 0 & 0 & 0 & \ddot{z}_{ref} & \dot{z} \end{bmatrix} \begin{bmatrix} a_1 \\ b_1 \\ a_2 \\ b_2 \\ a_3 \\ b_3 \end{bmatrix}, \tag{4.17}$$

and thus the parameter update rule can be selected as

$$\dot{\hat{\boldsymbol{\Theta}}} = \boldsymbol{\kappa}_\Theta\boldsymbol{G}^{\top}\boldsymbol{\nu}, \tag{4.18}$$

where $\boldsymbol{\kappa}_\Theta \in \mathbb{R}^{3\times3}$ is a symmetric positive definite matrix, $\boldsymbol{G} \in \mathbb{R}^{3\times6}$ is a regression matrix which considers the velocities and accelerations, $\boldsymbol{\Theta} \in \mathbb{R}^6$ is a vector containing the constant or

slowly-varying model dynamic parameters, and $\hat{\boldsymbol{\Theta}}$ represents the vector of estimated dynamic parameters (characterized through $\tilde{\boldsymbol{\Theta}} = \hat{\boldsymbol{\Theta}} - \boldsymbol{\Theta}$).

Following the recommendations of [2; 21], a deadzone was considered in $\boldsymbol{\nu}$ to improve the adaptation performance.

4.2.5 Adaptive robust integral of the sign of the error controller

Regarding the disturbances, we assume that $\boldsymbol{d}(t)$ is sufficiently smooth and bounded, in the sense that

$$||\boldsymbol{d}(t)|| \leq \zeta_1, \quad ||\dot{\boldsymbol{d}}(t)|| \leq \zeta_2 \quad ||\ddot{\boldsymbol{d}}(t)|| \leq \zeta_3$$

where ζ_i are unknown bounding constants for $i = 1,\ 2,\ 3$. Considering that the main source of disturbances for the proposed system is the cable-suspended payload, this is a mild and reasonable assumption, as the disturbances caused by the payload have their origin in the translational accelerations of the vehicles [8]. By choosing desired accelerations that are smooth and bounded, the disturbances can be considered smooth and bounded as well. Lastly, note that due to the adaptive behavior of the here presented adaptive RISE controller, the disturbance bound ζ_1 is not necessary for the controller design, however, the bound ζ_1 is placed to guarantee that the system is controllable.

As firstly proposed in [6], the RISE control action is given by

$$\boldsymbol{u}_{RISE} = \int \boldsymbol{\beta}\text{sign}(\boldsymbol{\nu})\, dt + \boldsymbol{K}_r \int \boldsymbol{\nu}\, dt \tag{4.19}$$

where $\boldsymbol{\beta} = \text{diag}(\beta_x, \beta_y, \beta_z)$ and $\boldsymbol{K}_r$ are positive diagonal gain matrices, and $\text{sgn}(\cdot)$ is the signum function. As analyzed in [6], the proposed RISE feedback also has an interesting property that the control law learns the unknown disturbance asymptotically, i.e., $(\boldsymbol{u}_{RISE} - \boldsymbol{d}) \to 0$ as $t \to \infty$.

This asymptotic behavior only occurs if the RISE gain $\boldsymbol{\beta}$ is sufficiently large. In specific, if the gain $\boldsymbol{\beta}$ is selected to satisfy the following sufficient condition [22]:

$$\boldsymbol{\beta} > \zeta_{N_{des}} + \frac{1}{\boldsymbol{\kappa}_D}\zeta_{\dot{N}_{des}} \tag{4.20}$$

where the bounds $(\zeta_{N_{des}}, \zeta_{\dot{N}_{des}})$ in (4.20) are positive constants related to the following auxiliary function and its time derivative:

$$\boldsymbol{N}_{des} = \boldsymbol{A}\,\dddot{\boldsymbol{x}}_{des} + \boldsymbol{B}\ddot{\boldsymbol{x}}_{des} + \dot{\boldsymbol{d}} - \dot{\boldsymbol{G}}_{des}\hat{\boldsymbol{\Theta}} \tag{4.21}$$

$$\|\boldsymbol{N}_{des}\| \leq \zeta_{N_{des}} \qquad \|\dot{\boldsymbol{N}}_{des}\| \leq \zeta_{\dot{N}_{des}} \tag{4.22}$$

As already discussed, since the desired trajectories are smooth and bounded and consequently the disturbances caused by the payload are also smooth and bounded, the bounds

$(\zeta_{N_{des}}, \zeta_{\dot{N}_{des}})$ exist. However, these bounds are burdensome to evaluate, making the control action (4.19) difficult to be implemented. One implementation solution is to overestimate $(\zeta_{N_{des}}, \zeta_{\dot{N}_{des}})$, and, consequently, overestimating $\boldsymbol{\beta}$, guaranteeing robustness but at a cost of losing performance.

Inspired by the works that adapts the controller gain of sliding mode controllers, such as [23; 24; 25], we move forward to address the overestimation issue presenting a novel RISE controller which online adapts $\boldsymbol{\beta}$, guaranteeing robustness and reducing $\boldsymbol{u}_{RISE}$ control activity. The proposed adaptive control law for $\boldsymbol{\beta}$ can be described as

$$\dot{\beta}_i = \begin{cases} \beta_i |\nu_i| \text{sgn}(|\nu_i| - \epsilon_i) & \text{if } \beta_i > \mu_i \\ \mu_i & \text{if } \beta_i \leq \mu_i \end{cases} \tag{4.23}$$

where ϵ_i, μ_i are positive user-defined accuracy bounds. The parameter μ_i is introduced in order to get only positive values of β_i. These bounds are organized in vectors $\boldsymbol{\epsilon}, \boldsymbol{\mu} \in \mathbb{R}^3$, for $i = x, y, z$.

4.2.6 Stability considerations

In this paper, no formal proof for the stability of the novel adaptive RISE controller is provided. Although this will be the focus of future work, some stability-related aspects are briefly discussed here.

The structure of the proposed model reference adaptive controller is similar to the one proposed in [22], where the stability of combining the MRAC and RISE are proved. The intuition behind the proposed adaptive law for RISE (4.23) is the following: once $\boldsymbol{\beta}$ is adapted to be sufficiently large to match the variations in the uncertainties and disturbances, (4.20), the feedback controller given by (4.15) is able to guarantee asymptotic stability, and $\boldsymbol{\nu} \to 0$ as $t \to \infty$. In such a condition, the tracking error will eventually reach the region where $|\boldsymbol{\nu}| < \boldsymbol{\epsilon}$, which causes $\boldsymbol{\beta}$ to decline and adjust itself to avoid overestimation. As soon as $|\boldsymbol{\nu}|$ becomes greater than $\boldsymbol{\epsilon}$, we return to the case of $\boldsymbol{\beta}$ increasing and leading to a sufficient gain to achieve asymptotic stability. Therefore, the proposed adaptation law makes the tracking error to converge to a region given by the control design parameter $\boldsymbol{\epsilon}$.

Lastly, the verification of the stability of the proposed controller can be practical verified by the numerous flight experiments presented in the following section.

4.3 Experimental setup

To validate the proposed algorithms, extensive real-world experiments were run using two *Parrot Bebop 2* quadrotors to carry an aluminum bar measuring $L_{bar} = 1.45\,\text{m}$ and weighing

160 g. Each robot weighs 500 g, and the load is attached to the robots through flexible cables.

The algorithms run in an offboard station, at a rate of 50 Hz, acquiring the poses of the vehicles and the payload through an *OptiTrack* motion capture system configured with eight cameras, and computing the reference control signals that are sent to the robots via ROS.

The initial dynamic parameters for $\hat{\boldsymbol{A}}$ and $\hat{\boldsymbol{B}}$ were obtained according to the method presented in Section 4.2.3, considering a single quadrotor flying without a payload, and are given by $\boldsymbol{A} = diag(0.39,\ 0.4,\ 0.25)$ and $\boldsymbol{B} = diag(0.21,\ 0.20,\ 0.24)$. As for the gains adopted for the controller of each quadrotor in the experiments discussed ahead, they are the diagonal matrices $\boldsymbol{K}_P = diag(1.8, 1.8, 2.25, 2, 2, 2)$, $\boldsymbol{K}_D = diag(1.5, 1.5, 1.9, 1.2, 1.2, 1.5)$, $\boldsymbol{\kappa}_D = diag(2.7, 2.7, 4.5)$, $\boldsymbol{K}_r = 0.1\mathbf{I}$, where $\mathbf{I}$ is a 3×3 unit matrix, and $\boldsymbol{\kappa}_\Theta = 10^{-3}diag(1, 0.1, 1, 0.1, 2, 5)$.

4.4 Results and discussion

In this section, the results that validate our proposal are presented. Although we close the loop on the quadrotors, the following results also analyze the payload position, regarding its center of mass. The idea is that the desired movement of the payload is used to generate the references for the controllers of each quadrotor, so it can be considered that the payload is being controlled in open-loop. Considering a successful transportation one that is precise and safe, we consider a so-called *good tracking performance* those where the quadrotor tracking errors are around $15\,cm$ (or error norm around $\|\boldsymbol{x}\|_2 = 15\sqrt{3} \approx 26\,cm$) and the payload tracking errors are around $25\,cm$ (or error norm around $\|\boldsymbol{x}_{bar}\|_2 = 25\sqrt{3} \approx 44\,cm$), and payload orientation errors around 10°. For the payload error metrics, they are measured considering the center of mass of the transported bar. As our objective is to propose a robust but easy-to-implement controller for cooperative load transportation, simplicity and robustness were preferred over precision. Since the payload states are not fed back into the controllers, we used the *OptiTrack* system to measure the position of the payload center of mass, just to produce the graphics shown, not feedbacking such data.

In the following experiments, the desired references are constructed using the vector $\boldsymbol{q}_{des} = \begin{bmatrix}\boldsymbol{q}_{p,des}^\top & \boldsymbol{q}_{c,des}^\top\end{bmatrix}^\top$. To better understand the meaning for the desired $(\boldsymbol{q}_p, \boldsymbol{q}_c)$, note that the position of the quadrotor #1, $\boldsymbol{x}_1$, is equal to $\boldsymbol{q}_p$, and the position of the quadrotor #2, $\boldsymbol{x}_2$, is given by a relationship of the formation position $\boldsymbol{q}_p$ and configuration $\boldsymbol{q}_c$, i.e., related by inverting the kinematics (4.2) and as shown in Figure 4.2. Similarly, we can expect the payload to be hanging below the virtual structure formation, with no swing, at a distance $-\ell\hat{\boldsymbol{z}}^w$, defined by the length of the cables. This naive expected position for the payload is used here just to generate the graphics for the tracking error of the payload.

A video of the experimental results of this work can be found in https://youtu.be/KeZ5XcOn914

4.4.1 Individual transportation using the novel adaptive RISE controller

We begin our result analysis by presenting the robustness of the adaptive RISE controller, hereinafter referred to as ARISE controller, in an individual load transportation task. Thus, exceptionally in this first experiment, no formation is used. This trial intends to demonstrate the controller performance in a task simpler than cooperative transportation, but still a complex one due to the heavy payload and high accelerations. The load should be transported in a circular-shaped trajectory parameterized as

$$\boldsymbol{x}_{des} = \begin{bmatrix} r_x \cos\left(\frac{2\pi t}{T}\right) & r_y \sin\left(\frac{2\pi t}{T}\right) & z_0 \end{bmatrix}^\top, \tag{4.24}$$

where $r_x = r_y = 1$ m, $z_0 = 1.5\,m$, and T $= 3.35\,s$ which is equivalent to a translational acceleration up to 3.5 m/s^2. The transported payload weights $180\,g$, representing a payload-to-quadrotor weight ratio of 0.36. The tracking performance can be seen at Figure 4.4. For comparison, we matched the results obtained by the ARISE controller with the industrial standard PID controller. The position tracking root-mean-square-error for the ARISE and PID, considering that the effective transportation occurs between $5\,s$ and $45\,s$, are $0.09\,m$ and $0.13\,m$, respectively, which shows that the ARISE controller outperforms the PID in 30.7%. One can also infer in Figure 4.4, that this improvement is achieved without increasing the energy consumption, since the thrust profile for both controllers is similar. Another advantage of the ARISE controller is that the tracking improvement was achieved by using a time-continuous controller, just like the PID, instead of using a more aggressive solution for robustness, such as the discontinuous sliding mode controller.

4.4.2 Comparison ARISE vs. MRAC vs. PID in cooperative transportation

To further evaluate the performance of the ARISE controller against more conventional robust controllers, in this trial we compare the proposed ARISE controller, an MRAC controller (such as the one described in [8]) augmented by PID feedback, and a pure PID controller. Here, the transportation task consists of cooperatively transporting a bar-shaped payload with $1.45\,m$ of length and $160\,g$. We used as desired position for the formation, $\boldsymbol{q}_{p,des}$, a lemniscate-shaped trajectory parameterized such as (4.24), but with two times the frequency in y-direction to produce the lemniscate. The period was chosen as T $= 4.5\,s$ which is equivalent to accelerations up to 2 m/s^2. The desired configuration for the formation is given by $\boldsymbol{q}_{c,des} = \begin{bmatrix} -90^\circ & 0 & L_{bar} \end{bmatrix}^\top$. The payload-to-quadrotor weigh ratio is 0.16, or, 16% of the vehicles mass. The performance comparison is shown in Figure 4.5.

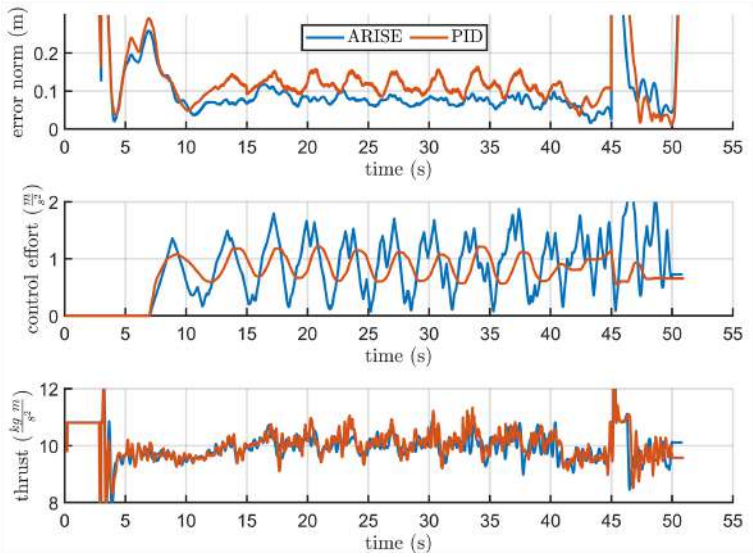

Figure 4.4 – Performance comparison between the novel adaptive RISE controller and the industrial standard PID controller.

	Controller				
	ARISE	**MRAC+PID**		**PID**	
	RMSE [m]	RMSE [m]	%↑	RMSE [m]	%↑
Comparison #1 ($\|\boldsymbol{x}\|$)	0.040	0.068	70.0	0.098	145.0
Comparison #1 ($\|\boldsymbol{x}_{bar}\|$)	0.192	0.235	22.4	0.319	66.1
Comparison #2 ($\|\boldsymbol{x}\|$)	0.055	0.076	38.1	crash	–
Comparison #2 ($\|\boldsymbol{x}_{bar}\|$)	0.209	0.224	07.1	crash	–

Table 4.1 – Tracking performance for each compared controller. %↑ columns represent the tracking error increase of a given controller when compared with to the proposed adaptive RISE controller.

Another comparison is made by repeating the task with the same controllers, but introducing a model uncertainty of 20% in the identified parameters ($\hat{\boldsymbol{A}}, \hat{\boldsymbol{B}}$). The results for this trial can be seen in Figure 4.6, where the tracking for PID controller is missing because it was not able to fulfill the task. The tracking RMSE for each controller compared in these two trials is presented in the Table 4.1, where the trials are called *comparison* #1 and *comparison* #2, respectively.

Analyzing Figures 4.5 and 4.6 and Table 4.1 it is clear the advantage of the ARISE controller, principally concerning the improvements on the reference tracking of the quadrotors. The MRAC+PID and the PID controllers showed an increase of 70% and 145% in the tracking error for the references given by the formation kinematic controller, respectively. These experiments also reinforced a known limitation of the PID controller, which is restricted, at best, to improve the robustness against slowly-varying time-varying states or disturbances,

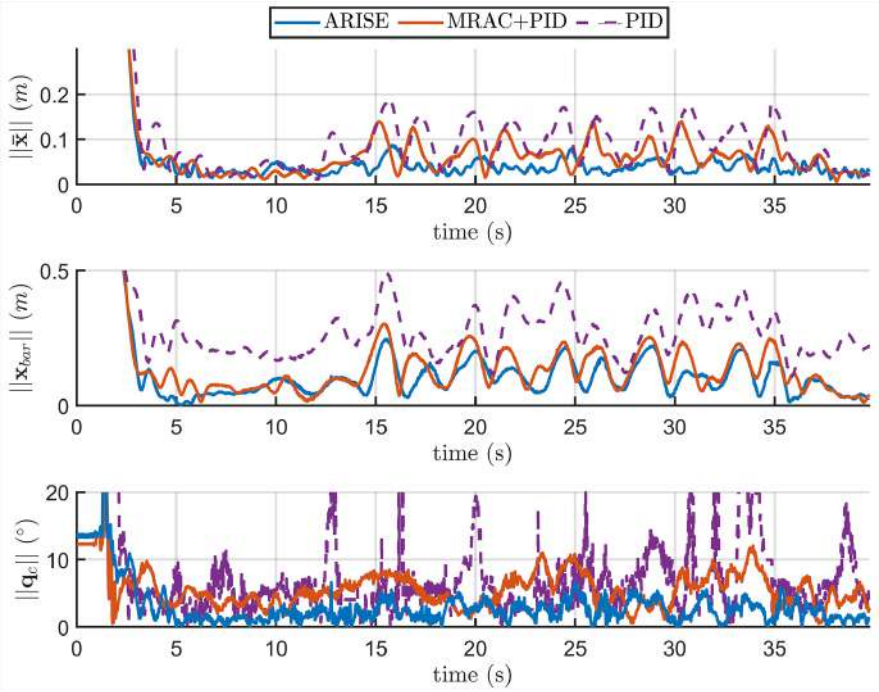

Figure 4.5 – Performance comparison between the novel adaptive RISE controller, a model reference adaptive controller plus integral feedback (MRAC+PID), and the industrial standard PID controller. The controllers were compared tracking a 2 m/s^2 trajectory while carrying a bar-shaped payload weighing 16% of the vehicles mass.

not being well-suited to address the errors caused by the misidentification of the parameters $\hat{\boldsymbol{A}}$ and $\hat{\boldsymbol{B}}$. This limitation becomes clear in *comparison* #2, where the PID controller was unable to fulfill the task and leads to a crash.

Concerning the payload transportation, every successful trial leads to good tracking for the payload, but once again the ARISE controller stands out when compared with the other methods.

4.4.3 Transportation at higher accelerations

Aiming to exploit the promising robustness characteristics of the ARISE controller, we further increased the desired transportation accelerations, which in turn increases the disturbance effects caused by the payload and by the quadrotors on each other. Thus, we transported the payload towards a lemniscate-shaped and a circular-shaped trajectory, once again parameterized as (4.24) and adjusted the frequency in y-direction for the lemniscate, but with lower period T, resulting in accelerations up to 3.5 m/s^2 in each trajectory. The desired configuration remains $\boldsymbol{q}_{c,des} = \begin{bmatrix} -90° & 0 & L_{bar} \end{bmatrix}^\top$.

For the sake of comparability, we tried to execute these transportations with the MRAC+PID

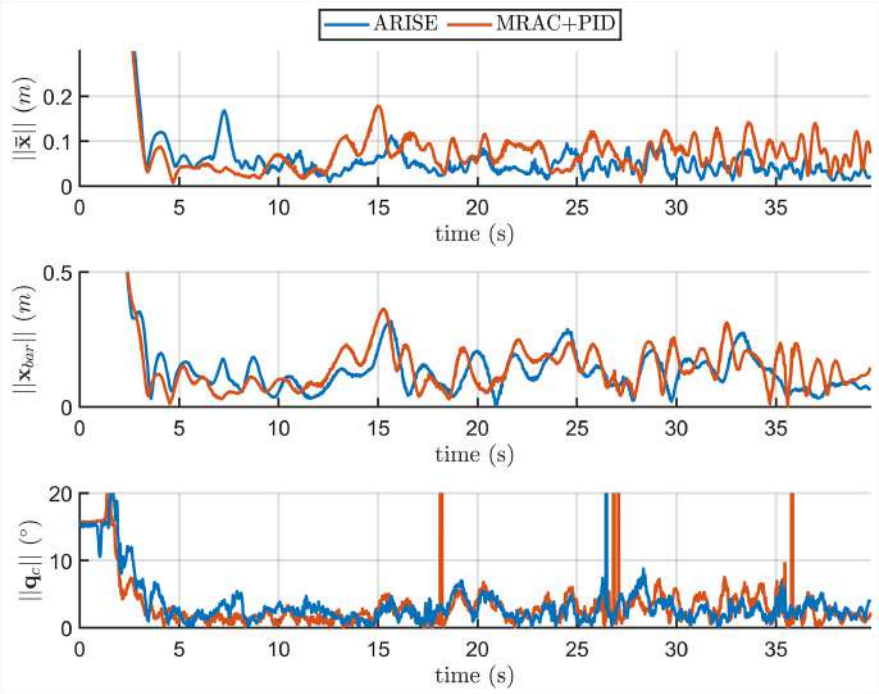

Figure 4.6 – In this test, we introduced a 20% error in the model parameters $(\hat{\boldsymbol{A}}, \hat{\boldsymbol{B}})$. The controllers were compared tracking a 2 m/s^2 trajectory while carrying a bar-shaped payload. The standard PID controller was not able to track the desired trajectory leading to a crash, thus, it was omitted in the plot.

and PID controllers, but both of these lead to crashes and, therefore, are not able to accomplish these tasks.

The results obtained for the lemniscate-shaped trajectory it is shown in Figure 4.7, exhibiting a 3D-view of the task and the tracking errors for the quadrotor, and payload position and orientation. The performance of the ARISE controller in tracking the circular-shaped trajectory can be seen in Figure 4.8.

As one can expect and see in the video of the experiments, these high-accelerations trials are very dynamic demanding, and the payload keeps swinging back-and-forth in the lemniscate-shaped trajectory, which has many points of acceleration and deceleration. For the circular trajectory, one can also perceive a centripetal behavior of the payload, that tries to escape the performed trajectory, pulling the quadrotors accordingly. In such a manner, these trials presented a higher tracking error for the payload position, as one can see in Figures 4.7 and 4.8. However, despite the intense disturbances caused by the payload and by one vehicle on each other, the tracking errors for the quadrotors in both lemniscate and circular trajectories are low and within the specifications to be considered a good tracking performance. In addition, one can see that the orientation tracking is also within the expected bounds, ensuring the good tracking of the references given by the formation controller.

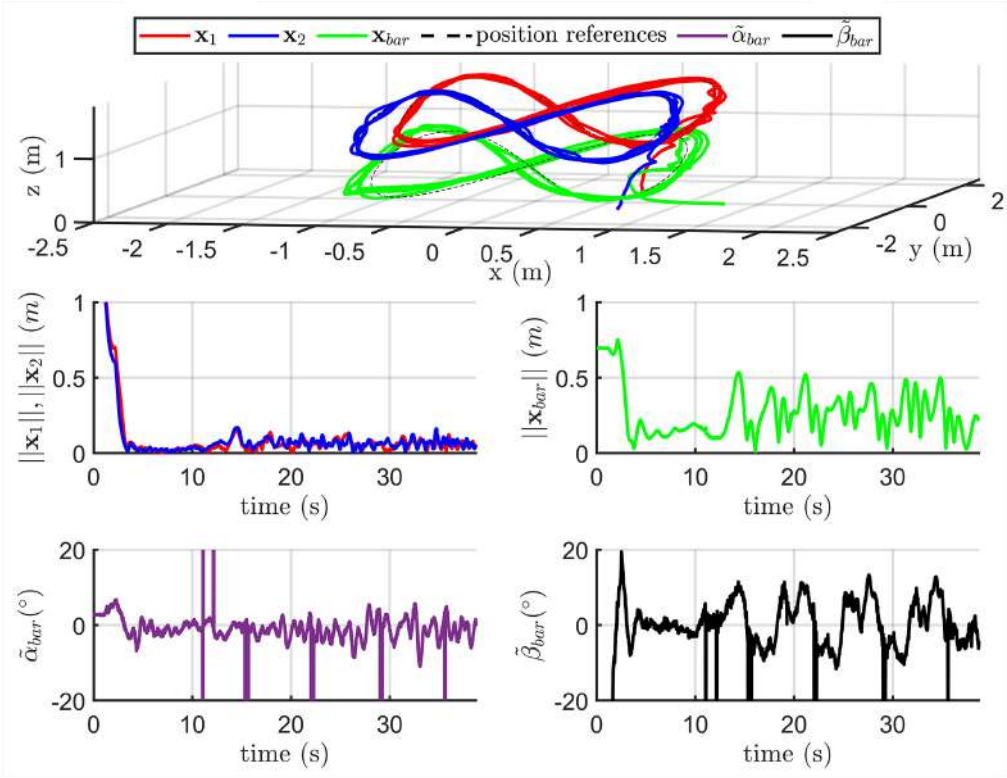

Figure 4.7 – Performance of the novel adaptive RISE controller in an aggressive transportation task. The payload position, orientation, and 3D-view is presented. The desired lemniscate-shaped trajectory have accelerations up to 3.5 m/s^2.

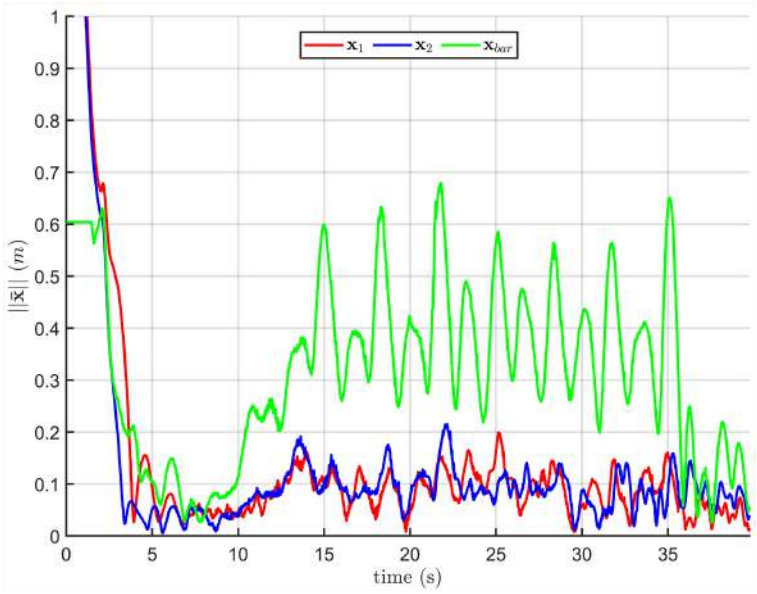

Figure 4.8 – Performance of the novel adaptive RISE controller in an aggressive transportation task. The desired circular-shaped trajectory have accelerations up to 3.5 m/s^2.

4.4.4 Payload orientation applications

The control framework proposed in this paper not only aims to guarantee a robust tracking by the ARISE controller, but is also interested in address the problem of orientating the transported payload during the transportation task. From a practical perspective, this problem is very relevant, since maneuvering the payload brings important features to the transportation, allowing, for instance, obstacle avoidance or transportation in narrow corridors and around corners.

This section presents three orientation experiments that highlight the task planning advantages of using the proposed formation framework for cooperative transportation.

In a first experiment, we emulate a teleoperation task, manipulating the desired formation configuration $\boldsymbol{q}_{c,des}$ directly by the use of a joystick. Since we can completely manipulate the quadrotor plus payload states by adjusting the formation variables $\boldsymbol{q}$, it becomes easy to assign these variables to a high-level command such as the ones sent by the joystick. The results of such experiment can be seen in Figure 4.9.

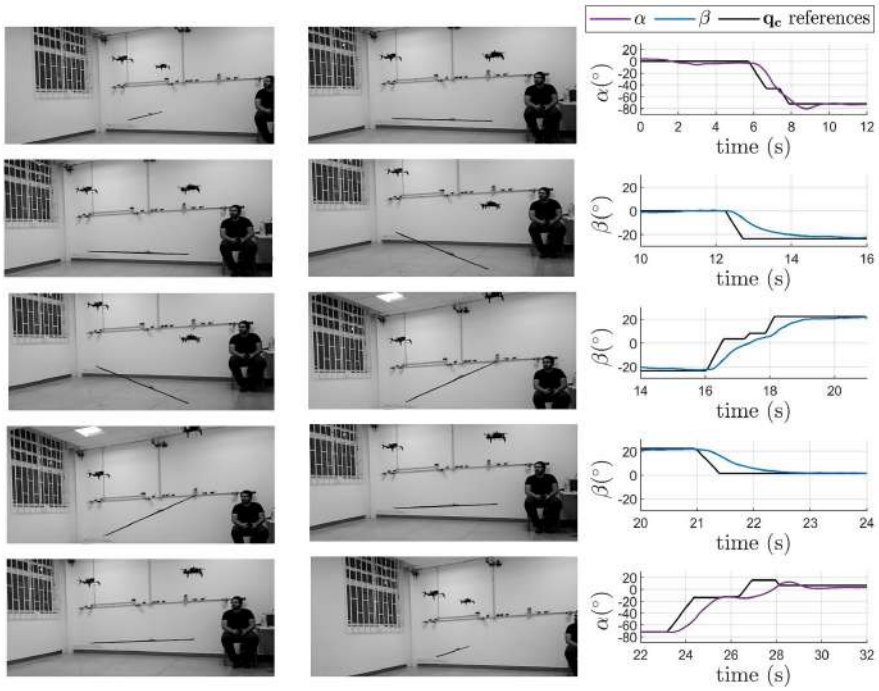

Figure 4.9 – A sequence of orientation references is given by a joystick, and a sequence of snapshots from the experiment is presented in this diagram. Each line of the diagram contains two snapshots, which contain an initial configuration and a final configuration, and the last cell of each line exhibits the orientation tracking for the respective formation variable.

In a second experiment, we maneuver the quadrotors and payload to navigate tangentially to a circular trajectory, emulating a maneuver typically used to pass through a narrow corridor

or around corners. Once again, we can easily tune the desired formation configuration to produce such results. To tangentially contour a circular trajectory, the formation desired orientation just needs to be adjusted to be equal to the tangent of the trajectory, i.e., $\alpha_{des} = \text{atan2}(\dot{y}_{F,des}, \dot{x}_{F,des})$. This same approach can be used to contour other types of trajectories.

To evaluate the system ability to maneuver the payload while transporting at high-speed, $\boldsymbol{q}_p$ was parameterized as (4.24), with T = 4.5 s, which is equivalent to horizontal accelerations up to 2 m/s^2. The complete desired configuration is given by $\boldsymbol{q}_c = \begin{bmatrix}\alpha_{des} - 180° & 0 & L_{bar}\end{bmatrix}^\top$, where -180° was added to the α reference to make the quadrotor #1 lead the formation. The obtained performance is presented in Figure 4.10, where one can see $\|\boldsymbol{x}_{bar}\|$ errors below 0.2 m, and orientation errors below 10° even for this highly dynamical maneuver.

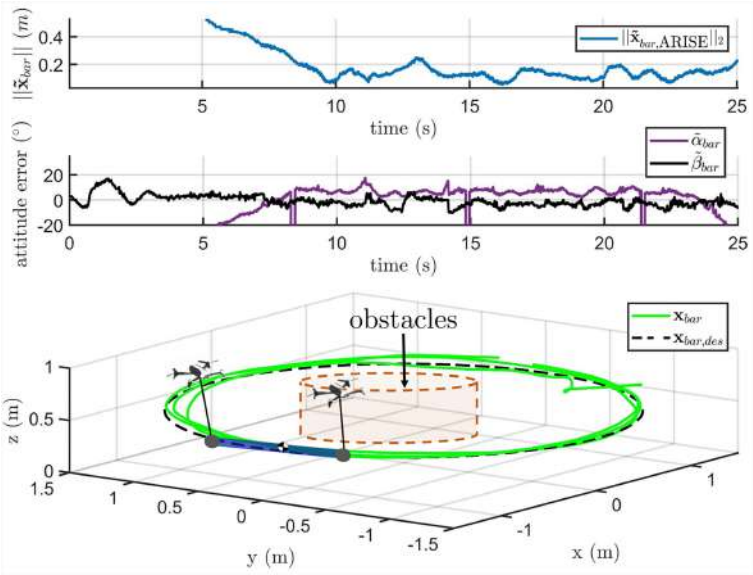

Figure 4.10 – Example where the payload is maneuvered tangentially to a circular trajectory to avoid obstacles or to pass around corners. The 3D view demonstrates the orientation application.

In a third and final payload orientation experiment, we go beyond maneuvering only α_F during the transportation and also maneuver β_F to avoid a series of obstacles. The graphics of this experiment is presented in Figure 4.11. Note that at timestamps around (12,14,17,22,24,27,36) seconds, a high error can be seen in the attitude. It occurs due to these being the moments where new desired values are given to the formation configuration $\boldsymbol{q}_c$ to perform the maneuvers. However, also note that a few seconds after these timestamps the attitude error converges to zero. Lastly, one can note that at exactly at these timestamps the error in $\|\boldsymbol{x}_{bar}\|$ also increases, and once again after a few seconds it reduces. These observations demonstrate that the proposed controller converges to the desired states.

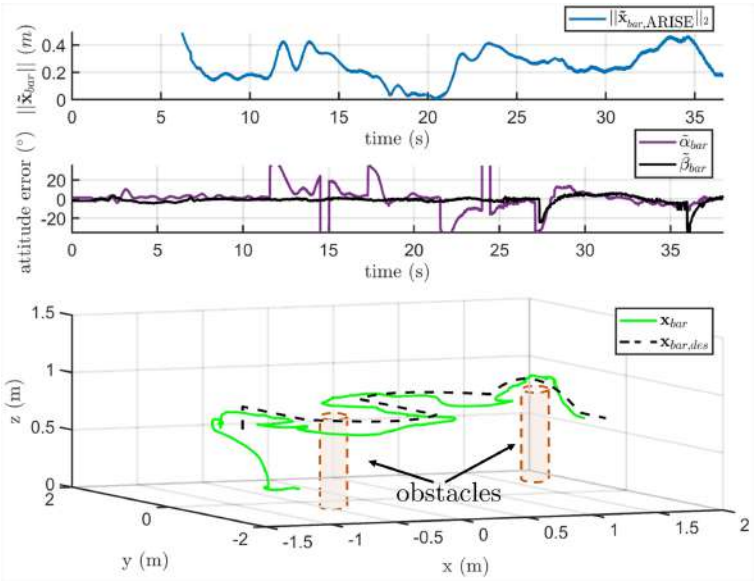

Figure 4.11 – In this task the load is maneuvered in α_F and β_F to avoid different kinds of obstacles. High attitude errors at timestamps around (12,14,17,22,24,27,36) seconds, can be seen due to new desired states for $\boldsymbol{q}_{c,des}$. The errors quickly vanish to zero due to the proposed control. A similar analysis can be made to $\|\boldsymbol{x}_{bar}\|$ at these timestamps.

We summarize the reference tracking for the desired formation configurations $\boldsymbol{q}_{c,des}$ for the three orientation experiments in Figure 4.12.

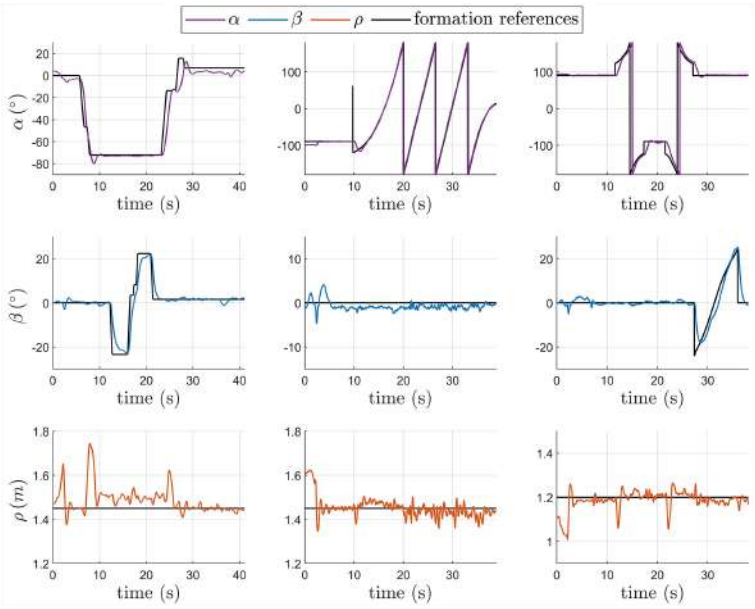

Figure 4.12 – Compilation of the formation configuration tracking for the three orientation experiments. The tracking for each experiment are given by the columns of this diagram, in the following order: teleoperation, maneuvering in α_F, and maneuvering in α_F and β_F.

4.5 Concluding remarks

The problem of transporting a payload using quadrotors was studied in this paper. The dynamic effects caused by the payload were counteracted by a robust adaptive controller. Experimental trials demonstrate that the proposed method can be used to perform agile load transportation either using one quadrotor or a team of two quadrotors. Also, an advantage of using a team of quadrotors is that the payload can be manipulated and orientated, as we also demonstrate in the experiments. Another advantage is the ability to carry heavier payloads.

As future works, aiming to move one step further to transport payloads using quadrotors in a real-world outdoor scenario, we plan to incorporate state estimation algorithms in this framework. The intention is to obtain comparable performance results without the use of a motion capture system.

4.6 References

[1] ÅSTRÖM, K. J.; WITTENMARK, B. *Adaptive control*. [S.l.]: Courier Corporation, 2013.

[2] LANDAU, I. D. et al. *Adaptive control: algorithms, analysis and applications*. [S.l.]: Springer Science & Business Media, 2011.

[3] IOANNOU, P. A.; SUN, J. *Robust Adaptive Control*. [S.l.]: Courier Corporation, 2012.

[4] SHTESSEL, Y. et al. *Sliding mode control and observation*. [S.l.]: Springer, 2014. v. 10.

[5] UTKIN, V. I. *Sliding modes in control and optimization*. [S.l.]: Springer Science & Business Media, 2013.

[6] XIAN, B. et al. A continuous asymptotic tracking control strategy for uncertain nonlinear systems. *IEEE Transactions on Automatic Control*, IEEE, v. 49, n. 7, p. 1206–1211, 2004.

[7] LEVANT, A. Sliding order and sliding accuracy in sliding mode control. *International journal of control*, Taylor & Francis, v. 58, n. 6, p. 1247–1263, 1993.

[8] VILLA, D. K. D. et al. Cooperative load transportation with two quadrotors using adaptive control. *IEEE Access*, IEEE, v. 9, p. 129148–129160, 2021.

[9] LEWIS, M. A.; TAN, K.-H. High precision formation control of mobile robots using virtual structures. *Autonomous robots*, Springer, v. 4, n. 4, p. 387–403, 1997.

[10] SCIAVICCO, L.; SICILIANO, B. *Modelling and control of robot manipulators*. [S.l.]: Springer Science & Business Media, 2001.

[11] MAHONY, R.; KUMAR, V.; CORKE, P. Multirotor aerial vehicles: Modeling, estimation, and control of quadrotor. *IEEE Robotics and Automation magazine*, Institute of Electrical and Electronics Engineers Inc., v. 19, n. 3, p. 20–32, 2012.

[12] CACCAVALE, F.; CHIAVERINI, S.; SICILIANO, B. Second-order kinematic control of robot manipulators with jacobian damped least-squares inverse: Theory and experiments. *IEEE/ASME Transactions on Mechatronics*, IEEE, v. 2, n. 3, p. 188–194, 1997.

[13] NAKAMURA, Y.; HANAFUSA, H. Inverse kinematic solutions with singularity robustness for robot manipulator control. 1986.

[14] WAMPLER, C. W. Manipulator inverse kinematic solutions based on vector formulations and damped least-squares methods. *IEEE Transactions on Systems, Man, and Cybernetics*, IEEE, v. 16, n. 1, p. 93–101, 1986.

[15] WIT, C. C. de; SICILIANO, B.; BASTIN, G. *Theory of robot control*. [S.l.]: Springer Science & Business Media, 2012.

[16] MUÑOZ, F. et al. Robust trajectory tracking for unmanned aircraft systems using a nonsingular terminal modified super-twisting sliding mode controller. *Journal of Intelligent & Robotic Systems*, Springer, v. 93, n. 1, p. 55–72, 2019.

[17] NGUYEN, H. et al. Model predictive control for micro aerial vehicles: A survey. In: IEEE. *2021 European Control Conference (ECC)*. [S.l.], 2021. p. 1556–1563.

[18] MELLINGER, D.; KUMAR, V. Minimum snap trajectory generation and control for quadrotors. In: IEEE. *2011 IEEE international conference on robotics and automation*. [S.l.], 2011. p. 2520–2525.

[19] Santos, M. C. P. et al. A novel null-space-based uav trajectory tracking controller with collision avoidance. *IEEE/ASME Transactions on Mechatronics*, v. 22, n. 6, p. 2543–2553, December 2017.

[20] PINTO, A. O. et al. High-level modeling and control of the bebop 2 micro aerial vehicle. In: IEEE. *2020 International Conference on Unmanned Aircraft Systems (ICUAS)*. [S.l.], 2020. p. 939–947.

[21] SLOTINE, J.-J. E.; LI, W. et al. *Applied nonlinear control*. [S.l.]: Prentice hall Englewood Cliffs, NJ, 1991. v. 199.

[22] PATRE, P. M. et al. Asymptotic tracking for systems with structured and unstructured uncertainties. In: IEEE. *Proceedings of the 45th IEEE Conference on Decision and Control*. [S.l.], 2006. p. 441–446.

[23] PLESTAN, F. et al. New methodologies for adaptive sliding mode control. *International journal of control*, Taylor & Francis, v. 83, n. 9, p. 1907–1919, 2010.

[24] UTKIN, V. I.; POZNYAK, A. S. Adaptive sliding mode control with application to super-twist algorithm: Equivalent control method. *Automatica*, Elsevier, v. 49, n. 1, p. 39–47, 2013.

[25] EDWARDS, C.; SHTESSEL, Y. B. Adaptive continuous higher order sliding mode control. *Automatica*, Elsevier, v. 65, p. 183–190, 2016.

5 [P4] - Adaptive sliding mode control applied to quadrotors - a practical comparative study

This chapter presents a comparative study, evaluating the advantages and disadvantages of the three most common methods to implement adaptive sliding mode controllers (ASMC). Aiming at testing the compared methods in realistic and harsh conditions, the three controllers are tested far from quasi-static motion and under severe disturbances. The quadrotor was subjected to disturbances such as stabilization under intermittent wind, landing precisely subject to wind-gusts, high-speed trajectory tracking while carrying an unmodeled suspended payload with a center-of-mass offset, and trajectory tracking with a damaged propeller. The performance of the analyzed adaptive sliding mode controllers was also compared to the industrial standard PID controller. Our experimental analysis demonstrates that, in face of such disturbances, one of the analyzed adaptive sliding mode controllers excels when compared to the others, and every ASMC excels when compared to the PID.

Supplementary material

A video of the experiments can be found at: https://youtu.be/miWOr7rsHBg

5.1 Introduction

Quadrotors are light, non-expensive, and agile flying robots that can be used in several practical applications, such as load transportation, surveillance, and emergency response, for instance [1; 2; 3; 4]. To integrate these robots into our society, they should be able to fly safely under challenging and diverse environmental conditions, i.e., they should be able to fly under disturbances.

Sliding mode control (SMC) is a simple and efficient tool to counteract disturbances acting over quadrotors [5; 6]. In its conventional design, the classical first-order sliding mode controller (FOSMC), this robust controller guarantees almost perfect tracking, in finite-time, if the gain of its discontinuous control action is greater than the upper bounds of the disturbances [7; 8]. Since an aerial vehicle can be subjected to disturbances of different kinds during real-world missions, from a practical standpoint, it is difficult to find the required disturbance bounds. A straightforward approach to contour this problem is to use rather large gains to guarantee robustness. However, the FOSMC discontinuous control action causes an undesirable effect

named *chattering*, which is proportional to the gain of this discontinuous control [9; 10]. Diversely, continuous sliding mode controllers (CSMC), such as the super twisting sliding mode controller (STSMC) [11], hides the discontinuous control action under an integral, replacing the discontinuous input by a continuous one, aiming at attenuating the chattering phenomenon while retaining some robustness properties and finite-time stabilization [12; 13]. However, as explained in [14], the STSMC exhibits very large control action for trajectories near the sliding manifold, which induces chattering with a higher magnitude than the FOSMC.

Understanding the chattering as a still open problem among sliding mode applications [15], many authors proposed solutions trying to mitigate this undesirable effect while maintaining robustness. The most common approach for chattering reduction is the use of a boundary layer, which smooths the discontinuous control action using sigmoid or saturation function with a trade-off between tracking precision and chattering elimination [16]. Another efficient tool to suppress chattering is the use of state observers [17], but a precise system model is necessary, to allow designing the observer. Higher-order sliding mode controllers (HOSMC) can offer chattering mitigation by artificially increasing the input-output relative degree. However, the main challenge of HOSMC is that higher-order derivatives of the sliding variable are needed, which are difficult to obtain due to noise. In addition, all these approaches contain signum structures multiplied by some uncertainty bound. Therefore, the problem of conservative uncertainty estimation and chattering is mitigated but not eliminated [18].

The problem of discontinuous control gain minimization and disturbance upper bound estimation can be attacked simultaneously by using an adaptive sliding mode controller. These algorithms attempt to estimate the minimum gain to guarantee that the sliding motion is achieved and maintained, i.e., the minimum gain necessary to counteract a given disturbance [19]. In short, we can divide the ASMC gain adaptation into three families: (i) those with monotonically increasing gains [20]; (ii) with increasing-and-decreasing gains [21; 22]; and (iii) those using equivalent control [23; 17]. In the first approach, the adaptive gain is increased until the sliding mode is achieved. However, the adaptive gain cannot be reduced to adapt to varying disturbances and uncertainties, and, therefore, the gain can be overestimated. The second and third approaches were proposed to overcome this problem, allowing gain reduction. Moreover, the equivalent control approach has an additional benefit of being able to estimate the disturbance after the sliding motion is established. However, a low-pass filter is used in the process which may induce a delay in the adaptation process.

In such a context, in this work we compare the performance of three first-order adaptive sliding mode controllers applied to a quadrotor subject to disturbances. Aiming to compare the most common methods used for gain adaptation in ASMC, we compare two controllers from the increasing-and-decreasing family – the one presented in the seminal work from Plestan et al. [21], and the one presented by Roy et al. [24], that uses a common approach for

lowering unnecessary large gains, which is to add leakage terms in the control law [22; 25; 26] – plus one controller from the equivalent control family, the one presented in the well-cited work of Edwards et al. [18], that follows the scheme first demonstrated by Utkin et al. [23; 17].

We opt to compare only first-order sliding mode controllers for two main reasons: the nature of disturbances that a small aerial vehicle can be subjected, and chattering attenuation. According to sliding mode control theory, FOSMC rejects bounded disturbances, including discontinuous disturbances, while the CSMC compensates Lipschitz disturbances, including not bounded disturbances [27]. Knowing that the available thrust for disturbance compensation in quadrotors is bounded, and that the nature of environmental disturbances is unknown but possibly high-switching and non-Lipschitz continuous, we believe that the characteristics of FOSMC fit better for aerial vehicles than those from CSMC. As for chattering attenuation, following the already discussed results presented in [14], we are also convinced towards the use of FOSMC.

Despite the opportunities and compelling demand for the integration of small aerial vehicles into our society [1; 28; 29], most of the existing literature focuses on navigation with quasi-static motion, using conservative maneuvers, and flying in a well-behaved environment, without disturbances. Just a few works effectively test their systems to track agile trajectories in the presence of model uncertainties and external disturbances. Therefore, aiming to explore and analyze more realistic and harsh conditions to which such aerial systems can be subjected, the main contributions of this comparative work can be given as: (i) experimental implementation of the most common approaches for first-order adaptive sliding mode control in quadrotors; (ii) evaluation of the robust behavior and performance of these controllers in adverse situations and strong disturbances – such as stabilization under intermittent wind, landing precisely subject to wind-gusts, high-speed trajectory tracking while carrying an unmodeled suspended payload with a CoM offset, and trajectory tracking with a damaged propeller –; and (iii) the presentation of an experimental survey comparing the main features of each adaptive sliding mode control scheme when applied to quadrotors, also comparing these controllers to the industrial standard PID controller.

5.2 Methodology

5.2.1 Notation

Throughout this paper, we use lowercase letters for scalars, bold lowercase letters to represent vectors, and bold uppercase letters for matrices. Two coordinate systems are used in this chapter: the inertial world frame, $\mathcal{I}$, defined by $\{\boldsymbol{x}^I, \boldsymbol{y}^I, \boldsymbol{z}^I\}$ with $\boldsymbol{z}^I$ pointing upward; and the body frame, $\mathcal{B}$, attached to the center of mass (CoM) of the quadrotor, defined by

$\{\boldsymbol{x}^B, \boldsymbol{y}^B, \boldsymbol{z}^B\}$ with $\boldsymbol{x}^B$ pointing forward and $\boldsymbol{z}^B$ aligned with the collective thrust direction (See Figure 5.1). For the sake of readability, vectors without superscript are expressed in the inertial frame. To represent orientations, we use unit quaternions $\boldsymbol{q} = [q^0, q^1, q^2, q^3]^\top \in \mathbb{S}^3$. To denote the multiplication of two quaternions $\boldsymbol{q}_1$ and $\boldsymbol{q}_2$ we write $\boldsymbol{q}_1 \otimes \boldsymbol{q}_2$, and to denote the rotation of a vector $\boldsymbol{v} \in \mathbb{R}^3$ by a quaternion $\boldsymbol{q}$ we write $\boldsymbol{q} \odot \boldsymbol{v}$, which stands for $\boldsymbol{q} \otimes [0\ \boldsymbol{v}^\top]^\top \otimes \boldsymbol{q}^*$, where $\boldsymbol{q}^*$ is the quaternion conjugate. We use subscript $[\cdot]_{des}$ and $[\cdot]_{ref}$ to describe, respectively, the desired states and the references sent to the quadrotor. The operator $\text{diag}(a_1, a_2, \ldots, a_n)$ denotes a diagonal matrix with scalars $(a_1, a_2, \ldots, a_n)$ as diagonal entries.

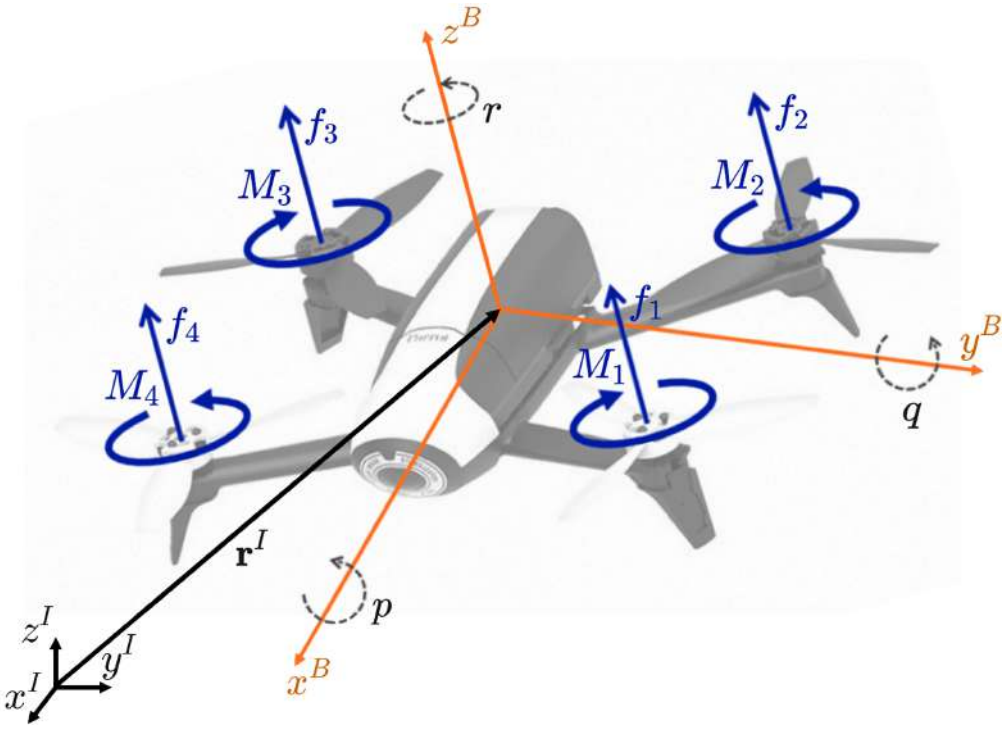

Figure 5.1 – The reference frames and the abstract control inputs $f_i, i = 1, \cdots, 4$, for a quadrotor.

5.2.2 Modeling

In this work we opt to use a simplified dynamic model for the aerial vehicle, without any modeling for well-known effects that a quadrotor are subjected to (e.g, rotor drag), nor for any external disturbances. Therefore, to counteract an eventual disturbance present in the following real-world experiments, our control algorithm only relies on the adaptive sliding mode controller. As for the mathematical model of a quadrotor, this topic has been extensively covered in the literature, and because of this just a brief description is presented here.

The equations of motion of a quadrotor based in Newton-Euler rigid body dynamics can

be written as

$$\ddot{\boldsymbol{r}}^I = \frac{1}{m}\boldsymbol{q} \odot \boldsymbol{F}^B - \boldsymbol{g}^I + \boldsymbol{d}^I \tag{5.1}$$

$$\dot{\boldsymbol{\omega}}^B = \boldsymbol{J}^{-1}\left(\boldsymbol{\tau}^B - \boldsymbol{\omega}^B \times \boldsymbol{J}\boldsymbol{\omega}^B + \boldsymbol{d}_{\omega}^B\right) \tag{5.2}$$

$$\dot{\boldsymbol{q}} = \frac{1}{2}\boldsymbol{q} \otimes \begin{bmatrix} 0 \\ \boldsymbol{\omega}^B \end{bmatrix} \tag{5.3}$$

where $\boldsymbol{r}^I$ is the position of the quadrotor, $\boldsymbol{F}^B = \begin{bmatrix} 0 & 0 & F_\Sigma \end{bmatrix}^\top$ with F_Σ being the collective thrust, m is the mass of the quadrotor, $\boldsymbol{g}^I = \begin{bmatrix} 0 & 0 & g \end{bmatrix}^\top$ is the gravity acceleration, $\boldsymbol{d}$ and $\boldsymbol{d}_{\boldsymbol{\omega}}$ are unmodeled disturbances, $\boldsymbol{\omega} = \begin{bmatrix} p & q & r \end{bmatrix}^\top$ are the angular body rates, $\boldsymbol{J} = \text{diag}(J_{xx},\ J_{yy},\ J_{zz})$ is the vehicle's matrix of moments of inertia, and $\boldsymbol{\tau}^B$ are the body torques.

The collective thrust F_Σ and the body-frame torque vector $\boldsymbol{\tau}^B$ are related to the motor forces by

$$\begin{bmatrix} F_\Sigma \\ \boldsymbol{\tau}^B \end{bmatrix} = \begin{bmatrix} F_\Sigma \\ \tau_p \\ \tau_q \\ \tau_r \end{bmatrix} = \begin{bmatrix} 1 & 1 & 1 & 1 \\ \frac{\sqrt{2}}{2}(+l & +l & -l & -l) \\ \frac{\sqrt{2}}{2}(-l & +l & +l & -l) \\ -c & +c & -c & +c \end{bmatrix} \begin{bmatrix} f_1 \\ f_2 \\ f_3 \\ f_4 \end{bmatrix}, \tag{5.4}$$

where l is the distance from the propellers to the quadrotor CoM, c is the rotor drag constant, and f_i and $M_i = cf_i$ are, respectively, the individual motor forces and moments produced.

5.2.3 Baseline position and attitude controllers

A common low-level controller found in off-the-shelf quadrotors uses feedback linearization on the attitude dynamics (5.2), computing the required body torque from the body rate references $\boldsymbol{\omega}_{ref}^B$ and the body rate measurements $\boldsymbol{\omega}^B$, which are obtained by rate gyros. This inner-loop controller operates at high frequency, commonly ten times faster than the outer-loop controller, and can be given as

$$\boldsymbol{\tau}^B = \boldsymbol{J}\left(\boldsymbol{K}_{\boldsymbol{p},\boldsymbol{\tau}}(\boldsymbol{\omega}_{ref}^B - \boldsymbol{\omega}^B) + \boldsymbol{K}_{\boldsymbol{i},\boldsymbol{\tau}}\int(\boldsymbol{\omega}_{ref}^B - \boldsymbol{\omega}^B)\,dt\right) + \boldsymbol{\omega}^B \times \boldsymbol{J}\boldsymbol{\omega}^B, \tag{5.5}$$

where $\boldsymbol{K}_{\boldsymbol{p},\boldsymbol{\tau}}$ and $\boldsymbol{K}_{\boldsymbol{i},\boldsymbol{\tau}}$ are gain matrices, and integral feedback was used to account for constant or slowly-varying disturbances $\boldsymbol{d}_{\boldsymbol{\omega}}$.

Considering a quadrotor that uses as user's inputs collective thrust and body-rates, these control signals can be obtained as follows.

1) Collective thrust reference: To track a reference trajectory, a baseline position controller with PD feedback and feed-forward terms for the desired acceleration and gravity can be given as

$$\ddot{\boldsymbol{r}}_{ref}^I = \ddot{\boldsymbol{r}}_{des}^I + \boldsymbol{K}_{\boldsymbol{d}}(\dot{\boldsymbol{r}}_{des}^I - \dot{\boldsymbol{r}}^I) + \boldsymbol{K}_{\boldsymbol{p}}(\boldsymbol{r}_{des}^I - \boldsymbol{r}^I) + \boldsymbol{g}^I \tag{5.6}$$

where, $\boldsymbol{K_p}$ and $\boldsymbol{K_d}$ are positive definite gain matrices. The collective thrust reference F_Σ is directly obtained from (5.6):

$$F_\Sigma = ||\boldsymbol{F}^I_{ref}|| = m||\ddot{\boldsymbol{r}}^I_{ref}|| \tag{5.7}$$

2) Body rate references: As one can see in (5.1), a quadrotor can only accelerate in $\boldsymbol{F}^B$ direction, and, to follow a desired trajectory $\boldsymbol{r}^I_{ref}$, the vehicle must align the body-frame force vector $\boldsymbol{F}^B$ with the inertial-frame reference force vector $\boldsymbol{F}^I_{ref}$. This is accomplished by generating body torques to rotate $\boldsymbol{F}^B$ with the desired attitude $\boldsymbol{q}_{des}$. Following the procedure presented in [30], the minimal rotation to align the current and the desired body axis is given by

$$\boldsymbol{q}_{des} = \begin{bmatrix} \cos(\frac{\alpha}{2}) \\ \sin(\frac{\alpha}{2}) \left(\frac{\hat{\boldsymbol{F}}^B \times \hat{\boldsymbol{F}}^I_{ref}}{||\hat{\boldsymbol{F}}^B \times \hat{\boldsymbol{F}}^I_{ref}||} \right) \end{bmatrix}, \tag{5.8}$$

where α is the angle between the current thrust direction and the desired thrust direction,

$$\alpha = \arccos(\hat{\boldsymbol{F}}^B \cdot \hat{\boldsymbol{F}}^I_{ref}). \tag{5.9}$$

Note that to align the collective thrust with $\boldsymbol{F}^I_{ref}$, only tilting the quadrotor is needed, i.e., a pitch and roll maneuver. Further, note that the rotation axis in (5.8) is perpendicular to $\boldsymbol{F}^B$, and, therefore, no $\hat{\boldsymbol{z}}^B$ rotation is induced by $\boldsymbol{q}_{des}$. Due to flatness property, the commanded yaw can be arbitrarily chosen [31]. The full vehicle desired attitude is shown in (5.10) where ψ_{des} is the desired yaw angle.

$$\boldsymbol{q}_{des,full} = \boldsymbol{q}_{des} \otimes \begin{bmatrix} \cos(\frac{\psi_{des}}{2}) & 0 & 0 & \sin(\frac{\psi_{des}}{2}) \end{bmatrix}^\top \tag{5.10}$$

The body rate references can be obtained by proportional-derivative feedback using the attitude error and desired body rate as in [30]

$$\boldsymbol{\omega}^B_{ref} = \boldsymbol{\omega}^B_{des} + \boldsymbol{K_q} \mathrm{sgn}(q^0_e) \boldsymbol{q}^{\mathbf{1:3}}_{\boldsymbol{e}} \qquad \mathrm{sgn}(q^0_e) = \begin{cases} 1, & q^0_e \geq 0 \\ -1, & q^0_e < 0 \end{cases} \tag{5.11}$$

where $\boldsymbol{q}_e = \boldsymbol{q}^* \otimes \boldsymbol{q}_{des}$ is the error quaternion, that can be computed using the composition property of quaternions [32]. Due to the cascaded control structure, the output of the low-level inner-loop attitude controller, $\boldsymbol{q}$, can be used as one of the inputs of the outer-loop position controller. The desired angular body rate $\boldsymbol{\omega}^B_{des}$ is proportional to the jerk of the trajectory, and its formulation can be obtained by differentiating (5.1), as in [33],

$$\begin{bmatrix} 0 \\ -q_{des} \\ p_{des} \\ 0 \end{bmatrix} = \boldsymbol{q}_{des} \odot \dot{\hat{\boldsymbol{F}}}^I_{ref} = \boldsymbol{q}_{des} \odot \left(\frac{\dot{\boldsymbol{F}}^I}{||\boldsymbol{F}^I||} - \frac{\boldsymbol{F}^I \boldsymbol{F}^{I\top} \dot{\boldsymbol{F}}^I}{||\boldsymbol{F}^I||^3} \right)_{ref} \tag{5.12}$$

For conservative maneuvers, the use of desired angular rate $\boldsymbol{\omega}_{des}$ in (5.11) can be skipped. Lastly, note that the formulations described in this section are also valid for a quadrotor that uses attitude angles as inputs. The references for these kind of vehicles can be implemented directly from (5.8).

5.2.4 Disturbance compensation

In this work, we are assuming that the proportional-integrative controller (5.5) that runs at the low-level is sufficient to counteract the torque-related disturbances $\boldsymbol{d}_{\boldsymbol{\omega}}$ in the majority of the real-world scenarios. We understand that the PI controller is rather simple and can only account for constant or slowly varying disturbances, but due to the high frequency that it is running – between 500-1000 Hz in most cases –, this drawback is mitigated, allowing the PI controller to provide excellent attitude tracking even under time-varying disturbances. This assumption is confirmed by our experiments, as one can see in the Section 5.3.3 and 5.3.4, where good attitude tracking was achieved while carrying a payload hanging from one of the quadrotor arms and while flying with a damaged propeller – which in both cases directly generate torque-related disturbances.

Under the assumption of $\boldsymbol{d}_{\boldsymbol{\omega}}$ being already addressed by PI feedback, we are only concerned with translational disturbances $\boldsymbol{d}$. Thus, adaptive sliding mode controllers were implemented only as position controllers. We augmented (5.6) with adaptive sliding mode compensation:

$$\ddot{\boldsymbol{r}}^I_{ref} = \ddot{\boldsymbol{r}}^I_{ff} + \ddot{\boldsymbol{r}}^I_{fb} + \ddot{\boldsymbol{r}}^I_{smc} \tag{5.13}$$

where $\ddot{\boldsymbol{r}}^I_{ff}$ and $\ddot{\boldsymbol{r}}^I_{fb}$ refers, respectively, to the feedfoward and feedback signals in (5.6), and $\ddot{\boldsymbol{r}}^I_{smc}$ refers to the SMC disturbance compensation.

To compensate the translational disturbances, the performance of the most common approaches for first-order adaptive sliding mode controllers were compared. In the following, we provide the formulation for $\ddot{\boldsymbol{r}}^I_{smc}$ on each tested SMC controller.

5.2.5 Adaptive sliding mode controller 1 – ASMC1

The intuition behind sliding mode control is to drive the system state trajectory to a pre-specified linear manifold $\mathcal{S}$ and to maintain the state trajectory on this manifold. Thus, the design of the sliding control law consists in (i) the proposal of a sliding manifold with a desirable behavior for the system's states while sliding, and (ii) the proposal of a switching control law to guarantee that the system's states reaches the manifold in finite time, and stay there.

Consider the sliding manifold $\mathcal{S}$ defined by $\boldsymbol{s} = \mathbf{0} \in \mathbb{R}^3$ and

$$\boldsymbol{s} = \dot{\boldsymbol{e}} + \boldsymbol{\Lambda}\boldsymbol{e} \tag{5.14}$$

where $\dot{\boldsymbol{e}}$ and $\boldsymbol{e}$ are the tracking errors defined as $\dot{\boldsymbol{e}} = \dot{\boldsymbol{r}}_{ref} - \dot{\boldsymbol{r}}$ and $\boldsymbol{e} = \boldsymbol{r}_{ref} - \boldsymbol{r}$, and $\boldsymbol{\Lambda}$ is a positive definite gain matrix.

The first-order sliding mode controller designed to force the sliding variable $\boldsymbol{s}$ to the sliding surface ($\boldsymbol{s} = \boldsymbol{0}$), can be given as [16]:

$$\ddot{\boldsymbol{r}}^{I}_{smc} = \boldsymbol{K}\text{sgn}(\boldsymbol{s}) \tag{5.15}$$

where $\boldsymbol{K} = \text{diag}\,(k_x, k_y, k_z)$ is the SMC positive definite gain matrix and its k_i terms are determined by the magnitude of the model uncertainty and disturbances. Once the system states reaches the manifold $\mathcal{S}$, this control law guarantees that the tracking error converges to zero exponentially, with dynamics given by (5.14).

In the context of adaptive sliding mode controllers, the SMC gain matrix $\boldsymbol{K}$ is tuned in real-time to estimate the minimum gain to guarantee that the sliding motion is achieved and maintained, resulting in minimization of the chattering effect. The most acknowledged first-order adaptive sliding mode controller was presented in the seminal work [21] of Plestan et al. Here, we choose this controller as one of our candidates for performance comparison. We denote the controller proposed by Plestan et al. as *adaptive sliding mode controller 1* – also referred as *ASMC1*. The formulation for this controller is given as follows.

Considering the sliding mode control signal (5.15), the adaptation of the sliding mode control gain k_i for each term of $\boldsymbol{K} = \text{diag}(k_x, k_y, k_z)$ is defined as ([21])

$$\dot{k}_i = \begin{cases} k_i|s_i|\text{sgn}(|s_i| - \epsilon_i) & \text{if } k_i > \mu_i \\ \mu_i & \text{if } k_i \leq \mu_i \end{cases} \tag{5.16}$$

where ϵ_i, μ_i are positive user-defined bounds. The parameter μ_i is introduced in order to get only positive values of k_i. These bounds are organized in vectors $\boldsymbol{\epsilon}, \boldsymbol{\mu} \in \mathbb{R}^3$, defined as $\boldsymbol{\epsilon} = \begin{bmatrix} \epsilon_x & \epsilon_y & \epsilon_z \end{bmatrix}^\top$ and $\boldsymbol{\mu} = \begin{bmatrix} \mu_x & \mu_y & \mu_z \end{bmatrix}^\top$.

Intuition: Consider the disturbance $\boldsymbol{d}$ in (5.1) to be unknown but bounded. The position controller (5.13) with SMC signal (5.15) and adaptation law (5.16) increases the gain $\boldsymbol{K}$ up to a value large enough to counteract the bounded uncertainty $\boldsymbol{d}$ so that the sliding manifold can be reached, and sliding mode starts. Once sliding mode with respect to $\boldsymbol{s}$ is established ($\boldsymbol{s} \approx \boldsymbol{0}$), the proposed gain adaptation law (5.16) allows the gain $\boldsymbol{K}$ to decline while $|\boldsymbol{s}| < \boldsymbol{\epsilon}$. As soon as $|\boldsymbol{s}|$ becomes greater the $\boldsymbol{\epsilon}$, the control law once again increase $\boldsymbol{K}$, repeating this analysis back-and-forth. Thus, the adaptation gain (5.16) tries to maintain the gain $\boldsymbol{K}$ at the smallest level that allows a given accuracy of $\boldsymbol{s}$-stabilization. In other words, the system states will converge to the domain $|\boldsymbol{s}| \leq \boldsymbol{\epsilon}$ in finite time.

5.2.6 Adaptive sliding mode controller 2 – ASMC2

The second candidate for performance comparison is the ASMC proposed by Edwards et al. in [18], which follows a design similar to the one proposed by Utkin et al. in [23]. Following the framework provided in the previous section for the *ASMC1*, the *adaptive sliding mode controller 2* (*ASMC2*) differs only in the adaptation law of $\boldsymbol{K}$.

The design proposed by Edwards et al. uses the notion of *equivalent control*. Namely, during the sliding motion ($\boldsymbol{s} = 0$) the so-called equivalent control $\bar{\boldsymbol{u}}_{eq}$ represents the switching control average required to maintain the sliding, i.e., to exactly cancel the unknown disturbance/uncertainty, $|\bar{\boldsymbol{u}}_{eq}| = |\boldsymbol{d}|$. Although the equivalent control needed for perfect sliding being considered an abstraction, it can be approximated in real-time by low-pass filtering the switching control signal $\ddot{\boldsymbol{r}}_{smc}$.

Once we are looking for a minimal adaptation gain $\boldsymbol{K}$ that rejects a given disturbance $\boldsymbol{d}$, an error variable $\boldsymbol{\delta} \in \mathbb{R}^3$ relating the equivalent control $\bar{\boldsymbol{u}}_{eq}$, obtained by low-pass filtering $\ddot{\boldsymbol{r}}_{smc}$, and $\boldsymbol{K}$ can be defined as

$$\delta_i = k_i - \frac{1}{\alpha_i}|\bar{u}_{eq,i}| - \epsilon_i \tag{5.17}$$

where $0 < \alpha_i < 1$ and $\epsilon_i > 0$ are design scalars and ϵ_i is small. In this controller, the objective of maintaining sliding is transposed to one of forcing $\delta_i \to 0$. In this sense, the gain k_i should tend to $\frac{1}{\alpha_i}|\bar{u}_{eq,i}|$. Note that if $\delta_i = 0$, or at least sufficiently close to zero, then $k_i = \frac{1}{\alpha_i}|\bar{u}_{eq,i}| + \epsilon > |\bar{u}_{eq,i}| = |d_i|$, which guarantees $k_i > |d_i|$. Also, note that $\alpha_i \in (0, 1)$ acts as a safety margin to guarantee that $k_i > |\bar{u}_{eq,i}|$. To reduce chattering, α_i should be chosen close to 1.

The design proposed by Edwards et al. is also known as dual-layer adaptation, where the first layer adapts the magnitude $\boldsymbol{K}$ of the sliding control, and the second layer adapts the rate of change of the adaptation law parameter $\dot{\boldsymbol{K}}$. The formulation of the dual-layer adaptation laws is given as follows.

In the first layer, the adaptation of the sliding mode control gain k_i for each term of $\boldsymbol{K} = \text{diag}(k_x, k_y, k_z)$ is proposed as (aiming at $\delta_i \to 0$)

$$\dot{k}_i = -\rho_i \text{sgn}(\delta_i) \tag{5.18}$$

where $\rho_i > 0$ is a scalar adapted in the second layer of the proposed adaptation algorithm:

$$\dot{\rho}_i = r_{0,i} + r_i \tag{5.19}$$

$$\dot{r_i} = \begin{cases} \gamma_i|\delta_i| & \text{if } |\delta_i| > \delta_{0,i} \\ 0 & \text{otherwise} \end{cases} \tag{5.20}$$

with $r_{0,i}$ being a small positive scalar, $\gamma_i > 0$, and $\delta_{0,i} > 0$ is an adaptation accuracy parameter representing a small boundary around $\delta_i = 0$.

Intuition: The ASMC proposed by Edwards et al. assume that the disturbance $\boldsymbol{d}$ and its derivative $\dot{\boldsymbol{d}}$ are bounded but unknown. This is a big departure from previous adaptation laws – as the ones proposed in Prestan et al. [21] and Utkin et al. [23], for instance –, where the parameters of the adaptation law should be hand-tuned to dominate the rate of change of the disturbance, $\dot{\boldsymbol{d}}$. In Edwards et al., the second layer adapts the adaptation parameter of the first layer $\boldsymbol{\rho}$, thus, ensuring that $\boldsymbol{\rho} > |\dot{\boldsymbol{d}}|$.

5.2.7 Adaptive sliding mode controller 3 – ASMC3

The third candidate for performance comparison is the ASMC proposed by Roy et al. in [24]; here identified as *adaptive sliding mode 3*. The design proposed by Roy et al. does not require any a priori knowledge of the system dynamic parameters or disturbances. To prove bounded stability, the ASMC3 uses a leakage-based adaptive law [34].

This candidate also follows the framework provided for the *ASMC1*, differing in the adaptation law for $\boldsymbol{K}$. The formulation for the k_i terms of $\boldsymbol{K} = \text{diag}(k_x, k_y, k_z)$ is given as follows.

$$k_i = h_{0,i} + h_{1,i}||\boldsymbol{\xi}_i|| + h_{2,i}||\boldsymbol{\xi}_i||^2 \tag{5.21}$$

where $\boldsymbol{\xi}_i = \begin{bmatrix} e_i & \dot{e}_i \end{bmatrix}^\top$. The gains $h_{j,i}$ are adapted via

$$\dot{h}_{j,i} = ||\boldsymbol{\xi}_i||^j |s_i| - \alpha_{j,i} h_{j,i} \qquad j = 0, 1, 2 \tag{5.22}$$

with $h_{j,i}(0) > 0$; and $\alpha_{j,i} > 0$ are user-defined leakage terms.

Intuition: Most previous works assume that uncertainties and disturbances are bounded by a constant a priori, i.e., before the controller is implemented. However, the parameter's uncertainties are always coupled with a system state. Therefore, such an assumption requires the system states to be bounded a priori, before designing the controller, which is unreasonable. The controller proposed by Roy et al. relaxes this assumption and does not require any prior knowledge of the state-dependent uncertainties as well as of external disturbances.

5.2.8 Experimental setup

The proposed algorithms were validated experimentally using a *Parrot Bebop 2* quadrotor. This quadrotor weights 500 g and has a thrust-to-weight ratio of about 1.7. The algorithms run in an offboard station at 50 Hz. An *OptiTrack* motion capture system, configured with eight cameras, provides the position and orientation of the vehicle. The communication between the

quadrotor, motion capture system, and offboard station was established using ROS (Robot Operation System).

In the following experiments, we benchmark the three adaptive sliding mode controllers (ASMC1, ASMC2, ASMC3) with a industrial standard PID controller. Every controller use the same attitude and position controllers, described by (5.5) and (5.13), respectively. The reference inputs for body rate and thrust are given by (5.11) and (5.7). The compared ASMC's differs from each other on the gain $\boldsymbol{K}$ of $\ddot{\boldsymbol{r}}_{smc}$ (see (5.15)). The PID controller differs from the others by assuming $\ddot{\boldsymbol{r}}_{smc} = \boldsymbol{0}$ and by augmenting $\ddot{\boldsymbol{r}}_{fb}$ in (5.13) with the integral feedback gain $\boldsymbol{K}_i \int \boldsymbol{e}\, dt$. For a fair comparison, the PD feedback gains used in all controllers are the same; and the gains used in the adaptation law of each adaptive sliding mode controller was the best gain we could find for trajectory tracking missions. We opt to tune the gains for trajectory tracking by consider it the most common navigation task in quadrotor applications.

5.3 Results and discussion

In this section, we present the results of our experiments. The comparison between the adaptive sliding mode controllers examine the following research questions: (i) Given the unpredictable nature of external disturbances, how *quick* and *accurate* these controllers react to disturbance variations and disturbances of different nature; (ii) how these controllers avoid the main issue of SMCs, the chattering; (iii) how these robust controllers improve over the industrial standard PID controller.

A video of the experimental results of this work can be found in https://youtu.be/miWOr7rsHBg

5.3.1 Test #1: Stabilization under intermittent wind

We begin our comparative tests by commanding the quadrotor to hold a position under one of the most common disturbances that an aerial system can be subject to: wind. For the test #1, the quadrotor desired position is given by $\boldsymbol{r}_{des} = [0.0,\ -1.0,\ 1.0]^\top$m, and an industrial fan was positioned at $\boldsymbol{r}_{\text{fan}} = [0.0,\ -2.2,\ 1.0]^\top$m, producing a wind frontal to the vehicle. The quadrotor is oriented towards $-\boldsymbol{y}^I$ direction, i.e., $\psi_{des} = -90°$. To further increase the wind disturbance effects, a foam plate of $(25 \times 25)\,\text{cm}^2$ was attached to the vehicle, increasing its frontal area and, therefore, the drag effects. The foam plate weighs 40 g (or 8% the vehicle's mass), also acting as a payload disturbance. To investigate how quick the ASMCs can adapt to sudden changes in the disturbances, the fan is turned off at 20 s of the running experiment,

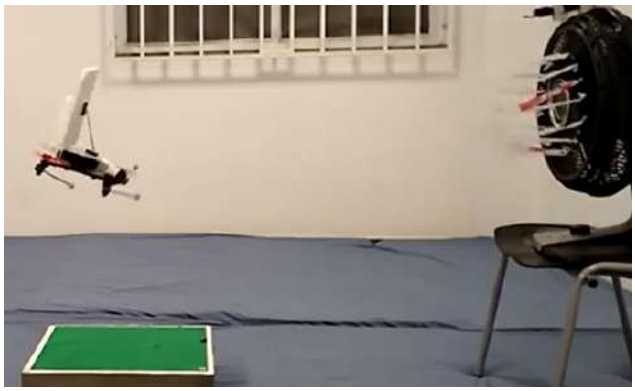

Figure 5.2 – Experimental setup for test #1.

turned on at 40 s, and turned off again at 58 s. The experimental setup for test #1 can be seen in Figure 5.2

Figure 5.3 shows the norm of the tracking error and the sliding gain adaptation during the test #1. As one can see, the four compared controllers (the three ASMCs and PID) can stabilize the UAV when it is subjected to strong wind disturbances. As expected, the PID controller presents a larger transitory, easily observed at the disturbance transitions around 20 s, 40 s, and 58 s, moments where the fan is turned off and on. Regarding the sliding controllers, comparable transitory and tracking can be seen.

To aid in our analysis, Table 5.1 exhibits the root-mean-square-error (RMSE) of the position tracking for each compared controller at tests #1, #3, and #4. Test #2 is not included in the table because each controller takes a different time to fulfill the test #2. Looking at the results referred to task #1, the ASMC2 performs better when compared to the other ASMCs, with 27.7% of RMSE decrease vs. PID. Note that, the lesser the RMSE, the closer the aerial vehicle is from fulfilling the positioning objective, therefore, the closer the UAV is from the fan and the higher is the magnitude of the wind disturbance. In this sense, the ASMC2 obtained better tracking at higher disturbances.

As for the analysis of the sliding gain, also presented in Figure 5.3, we can observe, by the regions in grey and white, that the three ASMCs are capable of increasing and decreasing the sliding gain accordingly to the disturbance presence. One can see comparable control agility by the ASMCs in building up the sliding gain to counteract the disturbances when the fan is turned on. Notably, the ASMC2 could more quickly adapt to decreasing disturbance variations (fan turning off).

A careful examination of the adaptive law of each ASMC clarifies this behavior. For the ASMC1, with adaptation law given by (5.16), the sliding gain k_i is decreased when $|s_i| < \epsilon_i$, however, the adaptation speed is given by the product $k_i|s_i|$, which is small when $|s_i| < \epsilon_i$. Therefore, it is expected for the ASMC1 an aggressive adaptation when k_i is increasing and a

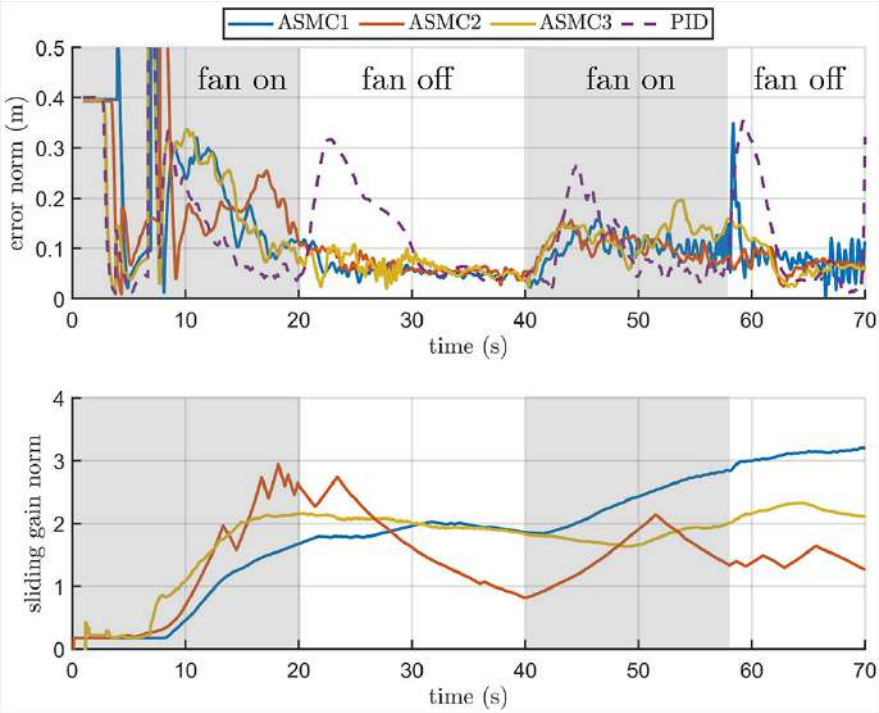

Figure 5.3 – Norm of the error for the ASMC and PID controllers during the disturbance rejection test #1; and sliding gain norm for each compared adaptive sliding mode controller. Regions in grey represent that the fan is turned on.

	Controller						
	PID	**ASMC1**		**ASMC2**		**ASMC3**	
	RMSE [m]	RMSE [m]	%↓	RMSE [m]	%↓	RMSE [m]	%↓
Test #1	0.148	0.118	20.27	0.107	**27.70**	0.124	16.22
Test #3	crash	**0.080**	—	0.085	—	0.111	—
Test #4	0.204	0.201	1.47	0.146	**28.43**	0.157	23.04

Table 5.1 – Tracking performance for each compared controller at each test. %↓ columns represent the tracking error decrease of a given controller when compared with the PID controller. Values in bold on each row represent the best controller for each test.

mild adaptation when k_i is decreasing. Moreover, chattering can be seen at the end of test #1 for the ASMC1, after the fan is turned off at 58 s. This undesirable behavior manifests because at this point of the experiment the sliding gain is high, accumulated by adaptation to counteract the wind disturbance, and suddenly the fan is turned off and the disturbance is removed. The high sliding gain in the absence of disturbances leads to tracking overshoot, or, in this context, chattering. As discussed, the sliding gain for ASMC1 is decreased only

when the UAV is near the desired position ($|s_i| < \epsilon_i$), thus, the sliding gain is increased when overshooting and chattering. This behavior can be completely understood in Figure 5.3, where the sliding gain k_i increases while chattering. Regarding the ASMC3, although in this test it also presented a slower gain decrease when compared to ASMC2, it does not present the same flaw as ASMC1. Observing the adaptation law of ASMC3 (5.21), as the leakage terms $\alpha_{j,i}h_{j,i}$ are responsible for decreasing the sliding gain continuously with a leakage proportional to the sliding gain, the unbounded gain increase while chattering does not occur as in ASMC1. In fact, the leakage terms of ASMC3 guarantee bounded sliding gain. The slower sliding gain decrease in test #1 of ASMC3 compared to ASMC2 was occasioned by the low leakage gain used in the experiment.

Sliding gain decrease for ASMC1 and ASMC3 can be improved by gain tuning. By increasing ϵ_i in ASMC1, and increasing the leakage terms $\alpha_{j,i}$ in the ASMC3, one can decrease k_i quicker and reduce chattering. However, as ϵ_i and $\alpha_{j,i}$ increase, it is straightforward to note that the performance of these controllers decreases. This tradeoff between chattering reduction and tracking performance renders both ASMC1 and ASMC3 to be difficult to tune.

Constructed in a cleaver way, the adaptation law of ASMC2 does not suffer from the above-discussed issues. Since the gain k_i in ASMC2 decreases when the system is in sliding mode ($\boldsymbol{s} \approx 0$), as soon as the system presents the chattering behavior, k_i decreases and the chattering decreases. Moreover, the difficulty in finding suitable ϵ_i and $\alpha_{j,i}$ for ASMC1 and ASMC3, respectively, is attenuated by the dual-layer adaptation present in ASMC2, where the second-layer adapts the adaptation gain of the first-layer.

5.3.2 Test #2: Landing subjected to wind

At this second test, we command the UAV in a positioning task once again in front of an industrial fan, as depicted in Figure 5.2. At test #2, instead of just hold position, we command the UAV to track a landing trajectory if the horizontal errors in x and y are within 10 cm. The descent trajectory is parameterized as

$$z_{des} = z_0 + \frac{t}{T_{land}}(z_{land} - z_0) \tag{5.23}$$

where $z_0 = 1\,\text{m}$ represent the initial altitude, $z_{land} = 0.25$ the final altitude where the UAV motors are turned off, and $T_{land} = 5\,\text{s}$ is the desired time of the controlled landing maneuver. If during the descent the UAV escapes the horizontal error margin of 10 cm, the landing try is aborted and it is resumed as soon as the UAV returns to the horizontal error margin.

Note that during the landing maneuver, the disturbance produced by the fan on the quadrotor is continuously changing, once the area that is hit by the wind gust, in the quadrotor and the foam plate attached, is changing during the descent. In such a manner, the

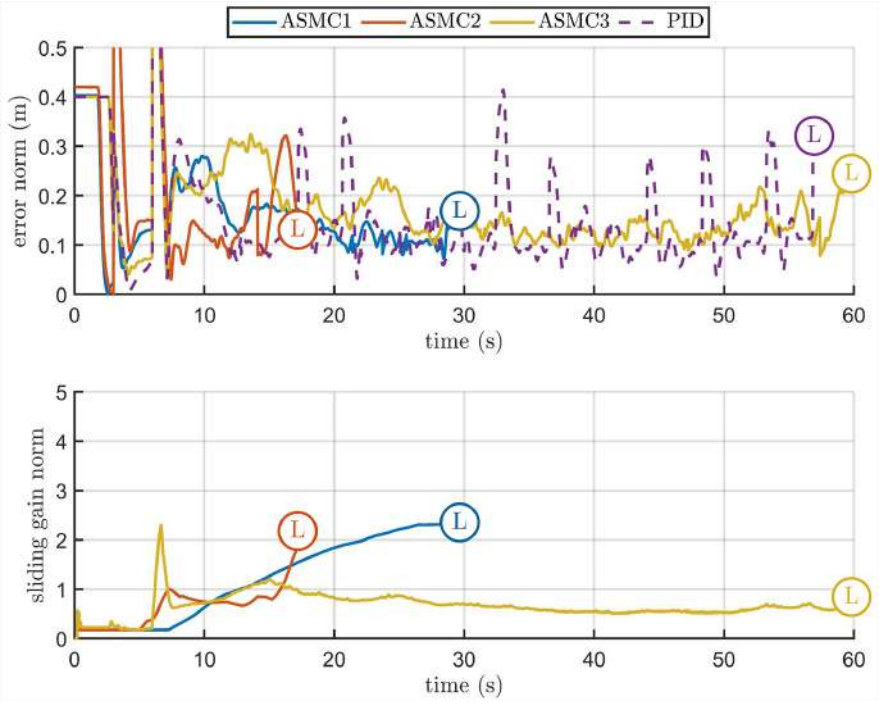

Figure 5.4 – Tracking performance for the ASMC and PID controllers during the disturbance rejection test #2; and sliding gain norm for each compared adaptive sliding mode controller. The timestamps marked by the letter 'L' represent a successful landing.

addition of the foam plate in the quadrotors makes this maneuver particularly difficult, thus, making this a good robustness test for the discussed control methods.

Figure 5.4 exhibits the tracking performance for test #2, as well as the sliding gain norm and the time that each compared controller achieves the landing task, represented by the letter 'L' in the graph.

Notably, the ASMC2 stands out, being the first to successfully land, after two failed attempts at timestamps around 12 s and 15 s. By just observing the Figure 5.4 it is difficult to figure out the landing attempts, and we recommend watching the video of the experiments for this purpose. A few seconds later, the ASMC1 controlled UAV lands. A good adaptation behavior can be seen for ASMC1 in this test, where k_i is gradually increasing by adaptation, making the tracking error gradually reduces until the vehicle is inside the horizontal error margin and successfully land. Since no quick decrease in the adaptive gain was needed in test #2, the main flaw of ASMC1 does not appear. Conversely, the behavior of ASMC3 was not satisfactory, rendering it to be unable to fulfill the landing task. Large leakage terms caused ASMC3 to be unable to land since, for small errors, k_i builds up slowly and it matches or it is dominated by the leakage terms. A possible solution is to decrease the leakage terms, however, as already discussed, this may lead to chattering. Although unable to land, ASMC3

keeps the system stable while subject to strong disturbances, with bounded convergence to the desired position. Regarding the PID controller, expected behavior can be seen in Figure 5.4, where the integral gain builds up, allowing landing attempts, but failing to land because the disturbance profile varies as the UAV descent. Since the PID controller can not manage time-varying disturbances, it tries to land, the disturbance change, and it overshoot, leaving the horizontal landing margin.

5.3.3 Test #3: Load transportation with a payload suspended from an offset of the CoM

To compare the robustness provided by the controllers, in test #3 the UAV should perform a trajectory tracking task at high-speed, while transporting a cable-suspended payload attached to one of the quadrotor arms. The payload dynamics are not modeled and act as a disturbance. The payload weighs 100 g, which is equivalent to 20% the vehicle's mass. The desired trajectory is circular-shaped, parameterized as follows

$$\boldsymbol{r}_{des} = \begin{bmatrix} R_x \cos\left(\frac{2\pi t}{T}\right) & R_y \sin\left(\frac{2\pi t}{T}\right) & z_0 \end{bmatrix}^\top, \tag{5.24}$$

where $R_x = R_y = 1$ m, and $z_0 = 1\,\text{m}$. The period T was chosen to be $T = 6.3\,\text{s}$ for t between $t = 0\,\text{s}$ and $t = 10\,\text{s}$ (equivalent to accelerations up to 1.0 m/s^2); and $T = 3.15\,\text{s}$ for t between $t = 10\,\text{s}$ and $t = 25\,\text{s}$ (equivalent to accelerations up to 4.0 m/s^2). At $t = 25\,\text{s}$, the trajectory tracking is halted, and the UAV should perform a positioning task at origin with $z_{des} = 1\,\text{m}$. The sudden change in the trajectory acceleration, and the sudden transition between a high-speed trajectory to a positioning task, was intended to excite the nonlinear dynamics of the system, induce large oscillations on the transported payload, stressing the system, thus allowing the analysis of the robust controllers. Moreover, a special difficulty arises when carrying a payload suspended from an offset of the center-of-mass. Under this condition, the payload exerts a torque-related disturbance on the UAV, which is readily addressed by the low-level PI controller as described in (5.5). However, as the exogenous torque compensation is obtained by increasing the speed of one or more rotors, under torque-related disturbances, the system is more prone to issues related to actuator saturation. The relationship between actuator saturation and loss of translational tracking performance is evident.

Figure 5.5 presents the tracking performance for each controller at test #3, where the PID controller was omitted because it could not track the desired trajectory, leading to a crash. The failure of the PID controller in this test was expected since the disturbances generated by the hanging payload are time-varying and can not be addressed by integral feedback.

To further analyze the impact of the leakage terms, continuing the discussion started in previous sections, in this trial we choose to reduce the leakage terms of ASMC3 in order to

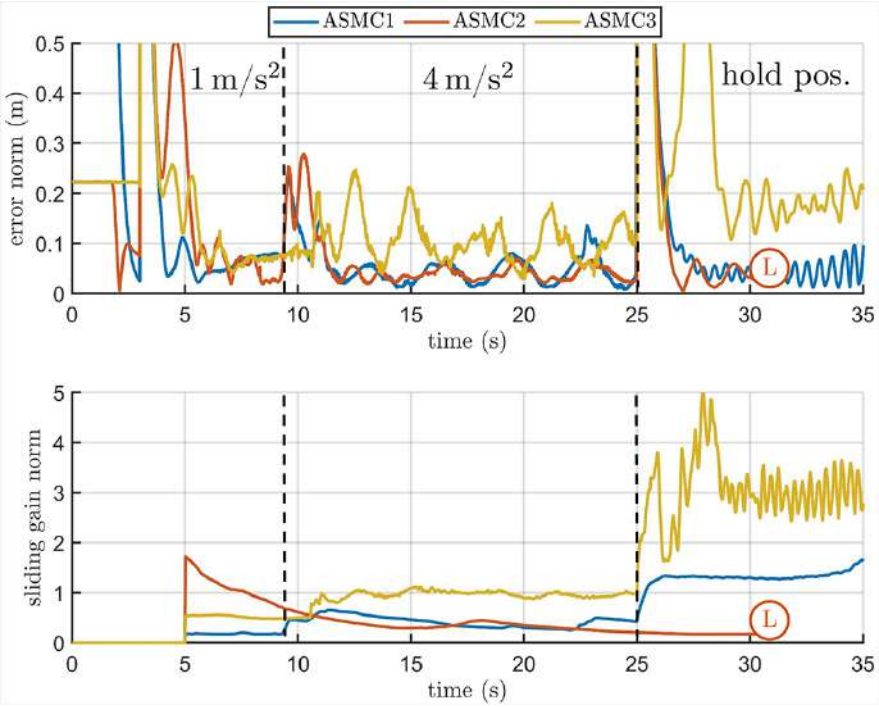

Figure 5.5 – Norm of the error for the compared controllers during the disturbance rejection test #3. PID control was not able to track the desired trajectory and leads to crash, thus, it was omitted in the plot.

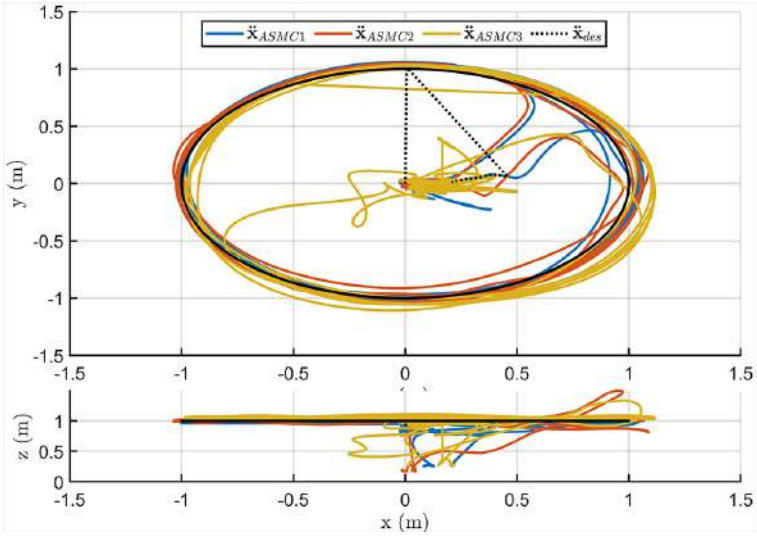

Figure 5.6 – 3D view of the tracking performance for the ASMCs during the disturbance rejection test #3.

perform a more aggressive control, aiming at better performance. The tracking RMSE for each controller can be seen in Table 5.1. Note that the RMSE was evaluated between $t = 5\,\text{s}$ and $t = 25\,\text{s}$, referring only to the trajectory tracking. As one can see, the ASMCs presented comparable RMSE, with ASMC1 being the most accurate.

Figure 5.7 – A bebop 2 quadrotor with a damaged propeller.

Although the ASMCs successfully performed this highly dynamical disturbance rejection test, an interesting behavior can be seen at the positioning task starting at $t = 25$s. Note that an abrupt increase in the adaptive gain of the ASMC1 and ASMC3 occurs at $t = 25$s, caused by the change in the desired position. Since both ASMC1 and ASMC3 use the tracking error $|s_i|$ to increase or decrease the sliding gain, the large initial errors for a new given desired position may lead to this sudden gain increase. Being the task after $t = 25$s a positioning task, the payload swing angles become mild, and the horizontal disturbances drastically reduce. Since ASMC1 and ASMC3 sliding gains are high due to the sudden change in the desired state, these controllers suffer from the same problem that the ASMC1 suffered in test #1, i.e., high sliding gain in the absence of disturbances, leading to chattering. Regarding the ASMC1, as already discussed, the chattering will lead to an unbounded increase of the sliding gain, leading to instability, as one can see in Figure 5.6, where the sliding gain and chattering in increasing right before the experiment was interrupted. Regarding the ASMC3, since we reduced the leakage terms in this test for better performance, more accentuated chattering is seen in relationship with test #1. However, the increase in the sliding gain caused by the chattering halts at some point, where the increasing k_i gain is matched or is dominated by the leakage terms.

Lastly, analyzing the test #1, #2 and #3 as a whole, one can realize that ASMC1 and ASMC3 have strong limitations in precision, once decreasing ϵ_i or $\alpha_{j,i}$ most probably will lead the system to strong chattering, actuators saturation, or, for the case of ASMC1, even instability.

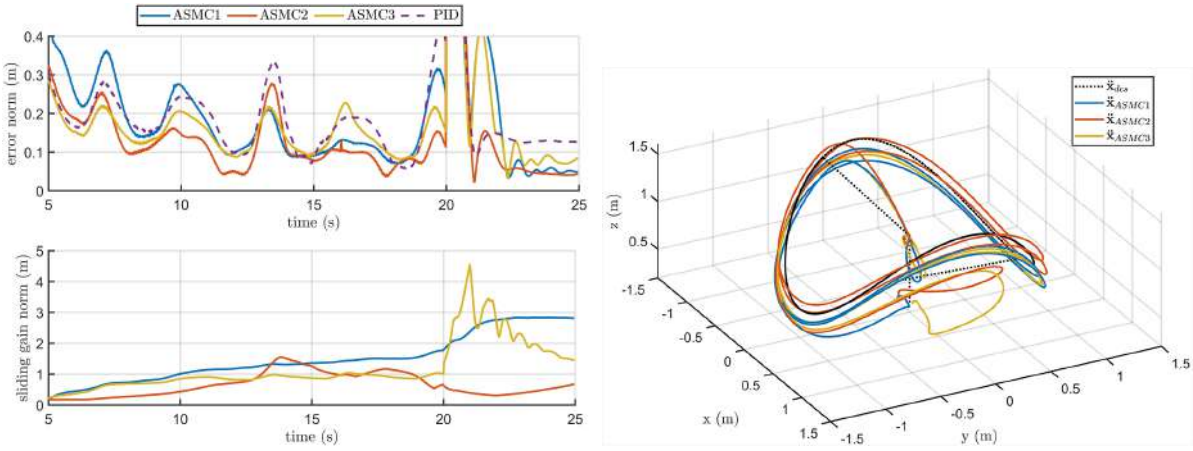

(a) Tracking error and ASMC gain (b) experiment 3D-view

Figure 5.8 – **a)** Norm of the error for the ASMC and PID controllers during the disturbance rejection test #4. Control effort for the ASMC and PID controllers during the disturbance rejection test #4. **b)** The 3D tracking performance for the compared controllers during the disturbance rejection test #4.

5.3.4 Test #4: Trajectory tracking with a damaged propeller

In this final test, we emulated a faulty rotor condition for the quadrotor by reducing the diameter of the right front rotor disk by 3.5 cm, as shown in Figure 5.7. Under this condition, the quadrotor has diminished thrust to deal with uncertainties and disturbances. Moreover, a faulty rotor acts as a torque-related disturbance by unbalancing the control allocation in the low-level motor controllers. As discussed in Section 5.3.3, torque-related disturbances decrease the system capability of tracking trajectories, and here we compare the behavior of the proposed ASMC controllers in dealing with these kinds of disturbances.

The test #4 consists of a trajectory tracking under a damaged propeller condition. The desired trajectory has the shape of a hyperbolic paraboloid, parameterized as

$$\boldsymbol{r}_{des} = \left[R_x \sin\left(\frac{2\pi t}{T}\right) \quad R_y \cos\left(\frac{2\pi t}{T}\right) \quad z_0 - R_z \cos\left(\frac{4\pi t}{T}\right)\right]^\top \tag{5.25}$$

where $R_x = R_y = 1.0\,\text{m}$, $R_z = 0.5\,\text{m}$, $z_0 = 1.0\,\text{m}$, and the period $T = 4.4\,\text{s}$ (which is equivalent to accelerations up to 2 m/s^2). In $t = 20\,\text{s}$ the trajectory tracking comes to a halt, and the quadrotor is commanded to perform a positioning task to the origin with $z_{des} = 1.0\,\text{m}$.

Figure 5.8 presents the tracking performance for the compared controllers, and the 3D view of the experiments run. Furthermore, Table 5.1 contains the tracking RMSE for each compared controller.

The same behavior can be found in test #4 as already discussed in test #3, as the ASMCs, despite the strong disturbances, are able to stabilize the aerial vehicle and track the trajectory with good performance, with emphasis on the 28.48% error decrease for the ASMC2 vs. PID,

and 23.04% error decrease for the ASMC3 vs. PID. Once again, for ASMC1 and ASMC3, a sliding gain increase is observed after the quadrotor halts the trajectory tracking and perform the positioning to the origin. However, regarding the ASMC3, since in this test we returned the leakage terms to the optimal values previously found, the sliding gain is reduced by leakage as one can see in Figure 5.8.

5.4 Concluding remarks

This work compares three of the most common types of adaptive sliding mode controllers. Extensive real-world experiments were made to evaluate the controllers performance, aiming at quick adaptation, tracking precision, and chattering reduction. In comparing the adaptive sliding mode controllers with the industrial standard PID controller, we reported several advantages in use those robust methods.

Accordingly to the obtained experimental results, the so-called *ASMC2* demonstrated to us the most beneficial features among the adaptive sliding mode controller compared.

5.5 References

[1] LOIANNO, G.; SCARAMUZZA, D. Special issue on future challenges and opportunities in vision-based drone navigation. *Journal of Field Robotics*, John Wiley and Sons Inc., v. 37, n. 4, p. 495–496, 2020.

[2] TANG, S.; KUMAR, V. Autonomous flight. *Annual Review of Control, Robotics, and Autonomous Systems*, Annual Reviews, v. 1, p. 29–52, 2018.

[3] VILLA, D. K. D. et al. Cooperative load transportation with two quadrotors using adaptive control. *IEEE Access*, IEEE, 2021.

[4] VILLA, D. K.; BRANDÃO, A. S.; SARCINELLI-FILHO, M. Outdoor navigation using two quadrotors and adaptive sliding mode control. In: IEEE. *2020 International Conference on Unmanned Aircraft Systems (ICUAS)*. [S.l.], 2020. p. 716–721.

[5] BESNARD, L.; SHTESSEL, Y. B.; LANDRUM, B. Quadrotor vehicle control via sliding mode controller driven by sliding mode disturbance observer. *Journal of the Franklin Institute*, Elsevier, v. 349, n. 2, p. 658–684, 2012.

[6] DERAFA, L.; BENALLEGUE, A.; FRIDMAN, L. Super twisting control algorithm for the attitude tracking of a four rotors uav. *Journal of the Franklin Institute*, Elsevier, v. 349, n. 2, p. 685–699, 2012.

[7] SHTESSEL, Y. et al. *Sliding mode control and observation*. [S.l.]: Springer, 2014. v. 10.

[8] UTKIN, V. Variable structure systems with sliding modes. *IEEE Transactions on Automatic control*, IEEE, v. 22, n. 2, p. 212–222, 1977.

[9] SWIKIR, A.; UTKIN, V. Chattering analysis of conventional and super twisting sliding mode control algorithm. In: IEEE. *2016 14th international workshop on variable structure systems (VSS)*. [S.l.], 2016. p. 98–102.

[10] VENTURA, U. P.; FRIDMAN, L. Chattering measurement in smc and hosmc. In: IEEE. *2016 14th international workshop on variable structure systems (VSS)*. [S.l.], 2016. p. 108–113.

[11] LEVANT, A. Principles of 2-sliding mode design. *automatica*, Elsevier, v. 43, n. 4, p. 576–586, 2007.

[12] BOIKO, I.; FRIDMAN, L. Analysis of chattering in continuous sliding-mode controllers. *IEEE transactions on automatic control*, IEEE, v. 50, n. 9, p. 1442–1446, 2005.

[13] CASTILLO, I.; FRIDMAN, L.; MORENO, J. A. Super-twisting algorithm in presence of time and state dependent perturbations. *International Journal of Control*, Taylor & Francis, v. 91, n. 11, p. 2535–2548, 2018.

[14] UTKIN, V. Discussion aspects of high-order sliding mode control. *IEEE Transactions on Automatic Control*, IEEE, v. 61, n. 3, p. 829–833, 2015.

[15] PÉREZ-VENTURA, U.; FRIDMAN, L. Chattering comparison between continuous and discontinuous sliding-mode controllers. In: *Variable-Structure Systems and Sliding-Mode Control*. [S.l.]: Springer, 2020. p. 197–211.

[16] SLOTINE, J.-J. E.; LI, W. et al. *Applied nonlinear control*. [S.l.]: Prentice hall Englewood Cliffs, NJ, 1991. v. 199.

[17] LEE, H.; UTKIN, V. I. Chattering suppression methods in sliding mode control systems. *Annual reviews in control*, Elsevier, v. 31, n. 2, p. 179–188, 2007.

[18] EDWARDS, C.; SHTESSEL, Y. B. Adaptive continuous higher order sliding mode control. *Automatica*, Elsevier, v. 65, p. 183–190, 2016.

[19] EDWARDS, C.; SHTESSEL, Y. Enhanced continuous higher order sliding mode control with adaptation. *Journal of the Franklin Institute*, Elsevier, v. 356, n. 9, p. 4773–4784, 2019.

[20] HUANG, Y.-J.; KUO, T.-C.; CHANG, S.-H. Adaptive sliding-mode control for nonlinear-arsystems with uncertain parameters. *IEEE Transactions on Systems, Man, and Cybernetics, Part B (Cybernetics)*, IEEE, v. 38, n. 2, p. 534–539, 2008.

[21] PLESTAN, F. et al. New methodologies for adaptive sliding mode control. *International journal of control*, Taylor & Francis, v. 83, n. 9, p. 1907–1919, 2010.

[22] SHAO, K. et al. Adaptive sliding mode control for uncertain euler–lagrange systems with input saturation. *Journal of the Franklin Institute*, Elsevier, v. 358, n. 16, p. 8356–8376, 2021.

[23] UTKIN, V. I.; POZNYAK, A. S. Adaptive sliding mode control with application to super-twist algorithm: Equivalent control method. *Automatica*, Elsevier, v. 49, n. 1, p. 39–47, 2013.

[24] ROY, S.; BALDI, S.; FRIDMAN, L. M. On adaptive sliding mode control without a priori bounded uncertainty. *Automatica*, Elsevier, v. 111, p. 108650, 2020.

[25] CHEN, Y.-H.; ZHANG, X. Adaptive robust approximate constraint-following control for mechanical systems. *Journal of the Franklin Institute*, Elsevier, v. 347, n. 1, p. 69–86, 2010.

[26] SHAO, K. et al. Leakage-type adaptive state and disturbance observers for uncertain nonlinear systems. *Nonlinear Dynamics*, Springer, v. 105, n. 3, p. 2299–2311, 2021.

[27] PÉREZ-VENTURA, U.; FRIDMAN, L. When is it reasonable to implement the discontinuous sliding-mode controllers instead of the continuous ones? Frequency domain criteria. *International Journal of Robust and Nonlinear Control*, Wiley Online Library, v. 29, n. 3, p. 810–828, 2019.

[28] D'ANDREA, R. Human–robot collaboration: The future of smart warehousing. In: *Disrupting Logistics*. [S.l.]: Springer, 2021. p. 149–162.

[29] USA Federal Aviation Administration. *UAS by the Numbers*. 2021. https://www.faa.gov/uas/resources/by_the_numbers/. [Online; accessed 14-October-2021].

[30] BRESCIANINI, D.; HEHN, M.; D'ANDREA, R. *Nonlinear quadrocopter attitude control: Technical report*. [S.l.], 2013.

[31] MELLINGER, D.; KUMAR, V. Minimum snap trajectory generation and control for quadrotors. In: IEEE. *2011 IEEE international conference on robotics and automation*. [S.l.], 2011. p. 2520–2525.

[32] KUIPERS, J. B. *Quaternions and rotation sequences: a primer with applications to orbits, aerospace, and virtual reality*. [S.l.]: Princeton university press, 1999.

[33] HEHN, M.; D'ANDREA, R. Quadrocopter trajectory generation and control. *IFAC proceedings Volumes*, Elsevier, v. 44, n. 1, p. 1485–1491, 2011.

[34] IOANNOU, P. A.; SUN, J. *Robust adaptive control*. [S.l.]: Courier Corporation, 2012.

6 [P5] - Outdoor load transportation using two quadrotors and adaptive sliding mode control

In this chapter, a solution to the problem of transporting a cable-suspended payload in outdoors using quadrotors is presented. The unmanned aerial vehicles (UAVs) navigate under the leader-follower formation, where the pose of the leader is estimated using its onboard sensors, and the pose of the follower by position-based visual servoing. The payload is carried using flexible cables, and to handle the outdoor environment perturbations and dynamic disturbances caused by the wind and payload, a robust sliding mode controller is used. The proposal is experimentally validated using two *Parrot Bebop 2* quadrotors carrying an aluminum bar in an outdoor scenario. Tracking errors of around 20 cm demonstrate the capability of the proposed system to fulfill the outdoor transportation task.

Supplementary material

Video of the experimental results of this work https://youtu.be/Fta30Kr9r70

6.1 Introduction

The enthusiasm that our society sees in UAVs applications has been motivating great efforts by the industry and scientific community to the development of UAV algorithms for a great range of applications. In specific, quadrotors can hover, carry and manipulate payloads [1; 2; 3], and have fascinating agility and maneuverability [4; 5]. Besides, they are also low-cost vehicles able to navigate using only onboard sensing and processing capabilities [6; 7].

The cooperation between a group of quadrotors, the so-called multi-robot formations [8], exploits the applicability of the vehicle, since flying as a team may improve mission efficiency, provide solutions that a single agent cannot attend (e.g., transport a load heavier than the payload capacity of a single vehicle [9]), and offer increased autonomy against agent failure. As a team, even if one agent fails, the remaining agents may be able to continue cooperating till accomplishing the mission [10].

As discussed in these surveys [11; 12], remarkable progress has been achieved in the design of control algorithms applied to quadrotors carrying payloads. There are works using quadrotors to grasp, manipulate, and transport payloads [13; 14; 15], performing aggressive maneuvers [16], transporting in cluttered scenarios [17], and so on. Although impressive, most

Figure 6.1 – The *Parrot Bebop 2* quadrotors carrying the aluminum bar in outdoors using only onboard sensors and visual servoing.

of these results rely on motion capture systems to estimate the team pose. In this paper, we overcame this indoor-only and pricey method presenting an outdoor cooperative strategy based on the leader-follower approach. Only onboard sensors and a built-in monocular camera were used for the UAVs pose estimation. The vehicles perform a trajectory tracking mission carrying a cable-suspended rod-shaped payload (see Figure 6.1).

6.1.1 Related Work

The literature on cooperative transport of payloads via quadrotors is extensive and is plenty of impressive experimental results [11; 18]. The design of model-based controllers to manage the dynamic effects caused by a hanging load proved to be challenging, as it is difficult to estimate the load pose and the torque wrenches generated by it. Moreover, due to the quadrotor-with-payload system being underactuated, the design of stable controllers that actively control the vehicle and payload states during aggressive maneuvers is difficult to obtain. Thus, early works rely on counterbalancing the load movement, aiming for swing-free transport [19], or attaching the load to the UAV body [20], hence, in both cases, sacrificing agility for simplicity.

On the subject of navigation in real-world outdoors environments, usually, a combination of one or more cameras with an IMU is used for state estimation; being the camera images used to obtain the position and velocity information, while the IMU delivers the rotational velocity and linear acceleration. Many surveys, such as [21; 22; 23; 12], compare the visual-inertial odometry methods, also presenting experimental results.

Another complication regarding real-world UAV navigation is the presence of parameter uncertainties and disturbances. Conventional PID controllers based on dynamic-inversion/feedback-linearization may perform poorly under these circumstances, so that solutions with adaptive or robust control are preferred. The adaptive controllers are easy to

implement and efficient against non-varying disturbances and uncertainties. For instance, in [24] a model-predictive adaptive controller is implemented, addressing changes in the moment of inertia and drag forces by adaptation. A similar result was observed in [25]. On the other hand, robust controllers perform better when submitted to time-varying disturbances [26], as its stability is guaranteed if the disturbances behave within the controller-designed bounds.

An additional approach for robustness is the use of sliding mode controllers (SMCs), since they have a fast dynamical response, strong robustness against disturbances, while being simple to implement [27]. One known drawback of these controllers is the high switching actuator activity, causing chattering and high energy consumption. Enhanced versions of traditional SMC try to attenuate the chatter either by changing the switching action [28], or through combination with adaptive feedback or disturbance observers [29], limiting the switching just to the necessary to counteract the unmodeled dynamics.

6.1.2 Contributions

The main goal of this research work is to present a solution to the problem of transporting a cable-suspended payload in outdoors using two quadrotors. For getting robustness against the disturbances frequently present in outdoor scenarios, an adaptive sliding mode controller is used, and the performance evaluation of combining visual-servoing with adaptive sliding mode controller is the main contribution of this chapter. Additionally, as we use visual-servoing to close the loop of the formation controller, our proposal is not subjected to formation collapsing due to state estimation errors or drifts. Moreover, the approach here proposed does not rely on: (i) an expensive motion capture (e.g., VICON) or high-precision global position system (e.g., RTK-GPS) to fulfill the mission, (ii) mathematical model or knowledge about the time-behavior of the disturbances (just the actuators feasibility should be addressed), and (iii) communication links between the aerial vehicles.

To validate our approach, real-world experiments were conducted using two *Parrot Bebop 2* quadrotors navigating as a leader-follower formation, transporting an aluminum bar under environmental disturbances, such as wind, and payload disturbances. As aforementioned, the position of the leader quadrotor is estimated using only its internal sensors, whereas the position of the follower one with respect to the leader one is estimated through computer vision techniques, with the leader carrying a target visible by the frontal camera onboard the follower quadrotor.

To discuss the topics related to this application, this chapter is organized as follows. In the beginning, an overview of the control strategy used in our approach is presented in Section 6.2. In the sequel, Section 6.3 describes the model for the vehicles, and Section 6.4 presents the robust dynamic compensator used for the real-world transportation experiments. Following,

in Section 6.5, it is discussed the leader and follower pose estimations, whereas in Section 6.6, the experimental setup adopted for running the validating experiments is presented. Next, Section 6.7 shows and discusses the results obtained, and, finally, Section 6.8 highlights the main conclusions of the work.

6.2 System design

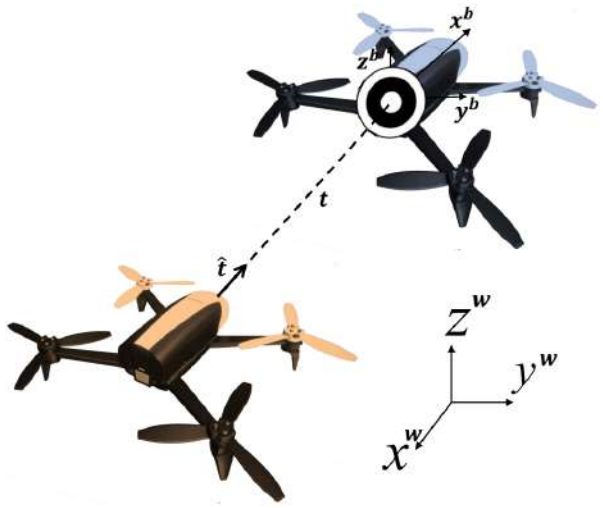

Figure 6.2 – The leader-follower formation. The instantaneous distance between the agents, $\boldsymbol{t}$, is estimated through visual servoing.

The vehicles cooperate by working as a leader-follower formation, as shown in Figure 6.2, where the leader agent tracks the reference trajectories inserted by the operator in the trajectory planner. The leader estimates its pose using only onboard sensors, and acts as if it was navigating alone, what is proper of the leader-follower formation [30]. In turn, the follower agent uses its onboard sensors for stabilization and navigation, maintaining its 3D distance $\boldsymbol{t}$ to the leader using a position-based visual servoing. The desired distance from the leader to the follower is also specified by the trajectory planner, since the agents do not change any information via communication links.

6.3 Modeling

The mathematical model for quadrotors has been extensively covered in the literature [31]. Thus, just a brief description is presented here. The coordinates of the quadrotor in the 3D space are $\boldsymbol{\xi} = \begin{bmatrix} x & y & z \end{bmatrix}^\top$ indicating the longitudinal, lateral and normal displacements with respect to the world referential system $\langle w \rangle$. By its turn, $\boldsymbol{\eta} = \begin{bmatrix} \phi & \theta & \psi \end{bmatrix}^\top$ is a vector that

contains the roll, pitch and yaw angles correspondent to the vehicle, also in $\langle w \rangle$. In other words, $\boldsymbol{\xi}$ and $\boldsymbol{\eta}$ represent, respectively, the translational and attitude variables associated to the UAV. Figure 6.3 shows the UAV pose variables, the input signals, and the reference systems.

As seen in Figure 6.3, the sum of the forces f_i, $i = 1, ..., 4$, generated by the propellers is given by

$$u_1 = \sum_{i=1}^{4} f_i.$$

The result of applying such a propulsion force to the aerial vehicle is the vector of generalized forces $\boldsymbol{F}_\xi = {}^w\boldsymbol{R}_b[0 \quad 0 \quad u_1]^\top$, being

$${}^w\boldsymbol{R}_b = \begin{bmatrix} c_\psi c_\theta - s_\psi s_\phi s_\theta & -s_\psi c_\phi & c_\psi s_\theta + s_\psi c_\theta s_\phi \\ s_\psi c_\theta + c_\psi s_\phi s_\theta & c_\psi c_\phi & s_\psi s_\theta - c_\psi c_\theta s_\phi \\ -c_\phi s_\theta & s_\phi & c_\phi c_\theta \end{bmatrix}$$

where $s(\cdot)$ and $c(\cdot)$ represents $sin(\cdot)$ and $cos(\cdot)$, respectively.

As for the vector of generalized torques, it is given by

$$\boldsymbol{\tau} = \begin{bmatrix} \tau_\phi \\ \tau_\theta \\ \tau_\psi \end{bmatrix} = \begin{bmatrix} u_{2,\phi} \\ u_{2,\theta} \\ u_{2,\psi} \end{bmatrix} = \begin{bmatrix} a[(f_2 + f_3) - (f_1 + f_4)] \\ a[(f_3 + f_4) - (f_1 + f_2)] \\ M_1 - M_2 + M_3 - M_4 \end{bmatrix},$$

where a is the distance from the propellers to the center of mass of the quadrotor, and $u_{2,\phi}$, $u_{2,\theta}$ and $u_{2,\psi}$ are the commands generated by the low-level controllers responsible to stabilize the attitude of the vehicle (autopilot), not addressed in this work.

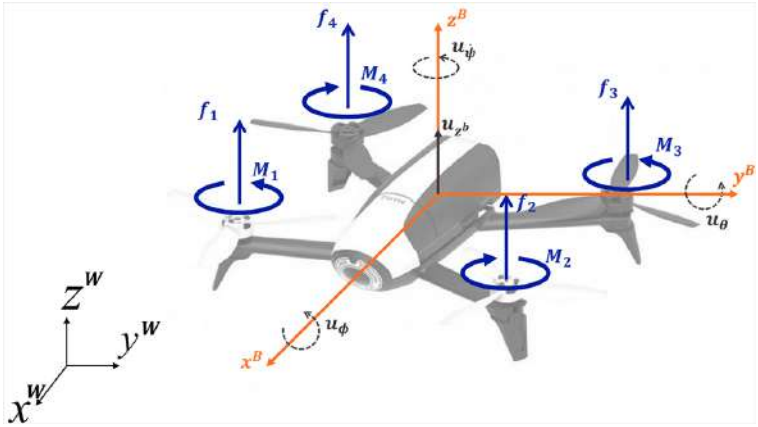

Figure 6.3 – The reference frames and the abstract control inputs $f_i, i = 1, \cdots, 4$, for a quadrotor.

Using Newton-Euler formulation as in [32], one can write

$$\begin{aligned} m\ddot{\boldsymbol{\xi}} &= \boldsymbol{F}_{\xi} - \begin{bmatrix} 0 \\ 0 \\ mg \end{bmatrix} \\ \boldsymbol{I}\dot{\boldsymbol{\Omega}} &= \boldsymbol{\tau} - \boldsymbol{\Omega} \times \boldsymbol{I}\boldsymbol{\Omega} \end{aligned} \tag{6.1}$$

where g is the gravity acceleration, m is the mass of the quadrotor, $\boldsymbol{I} \approx \text{diag}(I_{xx}, I_{yy}, I_{zz})$ is a diagonal matrix containing the moments of inertia, and

$$\boldsymbol{\Omega} = \begin{bmatrix} c_\theta & 0 & -c_\phi s_\theta \\ 0 & 1 & s_\phi \\ s_\theta & 0 & c_\phi c_\theta \end{bmatrix} \dot{\boldsymbol{\eta}}.$$

Thus, the dynamics of a quadrotor can be written as

$$\begin{aligned} m\ddot{x} &= (c_\psi s_\theta + s_\psi c_\theta s_\phi)u_1 - c_1\dot{x} - d_x \\ m\ddot{y} &= (s_\psi s_\theta - c_\psi c_\theta s_\phi)u_1 - c_2\dot{y} - d_y \\ m\ddot{z} &= (c_\phi c_\theta)u_1 - mg - c_3\dot{z} - d_z \\ I_{xx}\ddot{\phi} &= u_{2,\phi} + (I_{zz} - I_{yy})\dot{\theta}\dot{\psi} - c_4\dot{\phi} - d_\phi \\ I_{yy}\ddot{\theta} &= u_{2,\theta} + (I_{xx} - I_{zz})\dot{\phi}\dot{\psi} - c_5\dot{\theta} - d_\theta \\ I_{zz}\ddot{\psi} &= u_{2,\psi} + (I_{yy} - I_{xx})\dot{\phi}\dot{\theta} - c_6\dot{\psi} - d_\psi \end{aligned} \tag{6.2}$$

with $\boldsymbol{c} = [c_1, ..., c_6]^\top$ representing drag coefficients and $\boldsymbol{d} = [d_x, d_y, d_z]^\top$ representing the translational unmodeled disturbances, and $\boldsymbol{d}_w = [d_\phi, d_\theta, d_\psi]^\top$ representing the rotational unmodeled disturbances.

6.4 Control

As explained in [33], aerial vehicles with embedded autopilots use (6.2) to stabilize and achieve attitude control, and accepts high-level translational command signals. These high-level commands are desired roll angle u_ϕ, desired pitch angle u_θ, desired altitude rate $u_{\dot{z}}$, and desired yaw rate $u_{\dot{\psi}}$, grouped in a vector defined as $\boldsymbol{u}_{aug} = \begin{bmatrix} u_\theta & u_\phi & u_{\dot{z}} & u_{\dot{\psi}} \end{bmatrix}^\top$, whose entries are all in the interval $[-1.0, +1.0]$. Therefore, it is possible to exploit the embedded autopilots leaving the stabilization action to be responsibility of the firmware of the vehicle, modeling the UAV translational dynamics just as a function of high-level control signals, here defined as $\boldsymbol{u} = \begin{bmatrix} u_\theta & u_\phi & u_{\dot{z}} \end{bmatrix}^\top$.

Therefore, exploiting the embedded autopilots and considering moderate flight speeds, a near-hover linearization can be applied to translational dynamics in (6.2), i.e., $\text{sen}(\theta) \approx$

θ, $\text{sen}(\phi) \approx \phi$, $\cos(\theta) \approx \cos(\phi) \approx 1$, and $u_1 \approx mg$. Under this consideration, and assuming an internal loop to transform the altitude velocity references $u_{\dot{z}}$ in accelerations, the translational dynamics in (6.2) can be written as

$$\begin{aligned}
\ddot{x} &= (c_\psi K_\theta u_\theta + s_\psi K_\phi u_\phi)g - \frac{c_1}{m}\dot{x} - d_x \\
\ddot{y} &= (s_\psi K_\theta u_\theta - c_\psi K_\phi u_\phi)g - \frac{c_2}{m}\dot{y} - d_y \\
\ddot{z} &= \frac{1}{\tau_{\dot{z}}}(u_{\dot{z}} - \dot{z}) - \frac{c_3}{m}\dot{z} - d_z
\end{aligned} \tag{6.3}$$

Thus, a near-hover model for the quadrotor can be written in the linear form

$$\ddot{\boldsymbol{x}} = \boldsymbol{F}\boldsymbol{K}_u\boldsymbol{u} - \boldsymbol{K}_{\dot{x}}\dot{\boldsymbol{x}} - \boldsymbol{d}, \tag{6.4}$$

where $\boldsymbol{F}$ is a rotation matrix relating $\langle w \rangle$ to $\langle b \rangle$ only dependent of ψ, $\boldsymbol{x} = \begin{bmatrix} x & y & z \end{bmatrix}^\top$ are the translational displacements, and $\boldsymbol{u} = \begin{bmatrix} u_\theta & u_\phi & u_{\dot{z}} \end{bmatrix}^\top$ is a vector of UAV high-level autopilot commands. The matrices $\boldsymbol{K}_u$ and $\boldsymbol{K}_{\dot{x}}$ are diagonal matrices containing, respectively, the dynamic and drag parameters for the model.

Due to the flatness property of quadrotors [34], the yaw can be commanded independently, with dynamics described as

$$\ddot{\psi} = \frac{1}{\tau_{\dot{\psi}}}(k_{\dot{\psi}}\dot{\psi}_{ref} - \dot{\psi}) \tag{6.5}$$

where $k_{\dot{\psi}}$ and $\tau_{\dot{\psi}}$ are, respectively, the gain to convert the yaw rate $\dot{\psi}_{ref}$ into values between $[-1, +1]$ and the time constant in closed-loop. Further, by following the near-hover linearization, we considered the product $\dot{\phi}\dot{\theta} \approx 0$ and that the yaw drag effects and disturbances are negligible.

An important step in this work is to provide a controller with a fast response and robust enough to support environmental and payload disturbances, which are grouped in the vector $\boldsymbol{d}$. To fulfill this goal, we propose an adaptive sliding mode controller (ASMC), similar to the one proposed in [35]. A pure discontinuous sliding mode control law, ($\boldsymbol{u} = \boldsymbol{u}_{ASMC}$), is sufficient to track trajectories in quadrotor applications. However, we decided to combine $\boldsymbol{u}_{ASMC}$ with continuous model-based feedback control, aiming to cancel the dynamics of the vehicle by dynamic inversion technique (DI), letting only the model uncertainties effects and disturbances be compensated by the ASMC. By constructing the control law in such a way it is possible to reduce the SMC control gain.

Therefore, the proposed control signal is given by

$$\boldsymbol{u} = \boldsymbol{u}_{DI} + \boldsymbol{u}_{ASMC}. \tag{6.6}$$

Inverting the dynamics (6.4), a model-based PD control can be given as

$$\boldsymbol{u}_{DI} = (\boldsymbol{F}\boldsymbol{K}_u)^{-1}(\ddot{\boldsymbol{x}}_{des} + \boldsymbol{K}_d\dot{\tilde{\boldsymbol{x}}} + \boldsymbol{K}_p\tilde{\boldsymbol{x}} + \boldsymbol{K}_{\dot{x}}\dot{\boldsymbol{x}}), \tag{6.7}$$

where $\tilde{\boldsymbol{x}} = \boldsymbol{x}_{des} - \boldsymbol{x}$, with $\boldsymbol{K}_d$ and $\boldsymbol{K}_p$ being positive definite gain matrices.

To complete (6.6), $\boldsymbol{u}_{ASMC}$ is proposed as discussed in the sequel. Assuming in (6.4) that $\boldsymbol{d}$ represents unmodeled dynamics and disturbances, and that $|\boldsymbol{d}| \leq \boldsymbol{L}$, where $\boldsymbol{L} \in \mathbb{R}^3$ is a vector composed of positive disturbance bounds, the control law descried in (6.7) can only achieve bounded asymptotic convergence. In order to achieve asymptotic convergence of the tracking errors to zero, an error state $\boldsymbol{\sigma}$ is proposed, with dynamics described by the sliding surface

$$\boldsymbol{\sigma} = \dot{\tilde{\boldsymbol{x}}} + \boldsymbol{K}_\sigma \tilde{\boldsymbol{x}} \tag{6.8}$$

Aiming to make $(\dot{\tilde{\boldsymbol{x}}}, \tilde{\boldsymbol{x}}) \to \boldsymbol{0}$ in the presence of bounded disturbances, $\boldsymbol{d}$, a control law that drives $\boldsymbol{\sigma} \to \boldsymbol{0}$ should be provided. As described in [36], such a robust control law can take the form

$$\boldsymbol{u}_{ASMC} = \boldsymbol{\rho}(t)\text{sign}(\boldsymbol{\sigma}) \tag{6.9}$$

with $\boldsymbol{\rho}(t)$ being a diagonal matrix containing the strictly positive adaptive sliding mode control gains. According to the sliding mode control theory [36; 26], a sufficient condition to $(\dot{\tilde{\boldsymbol{x}}}, \tilde{\boldsymbol{x}}) \to \boldsymbol{0}$ is that the sliding mode gain $\rho_i > L_i$ for $i = x, y, z$.

Thus, to obtain $\boldsymbol{\rho}(t)$ sufficiently large to fulfill this robustness requirement, an adaptive law for the sliding mode gain can be given as in [35]

$$\dot{\rho}_i(t) = \begin{cases} \rho_i(t)|\sigma_i|\text{sign}(|\sigma_i| - \epsilon_i) & \text{if } \rho_i(t) > \mu_i \\ \mu_i & \text{if } \rho_i(t) \leq \mu_i \end{cases} \tag{6.10}$$

for $i = x, y, z$, and $\boldsymbol{\mu} = [\mu_x \quad \mu_y \quad \mu_z]^\top$ being positive user-defined accuracy bounds, and $\boldsymbol{\mu}(t)$ being responsible to guarantee that $\boldsymbol{\rho}$ is strictly positive.

The control strategy given by (6.6) is applied to both quadrotors used in the cooperative transportation proposed by this work. Regarding the leader-follower control structure, it can be seen in Figure 6.4. As shown, the trajectory planner is responsible for delivering the desired states for the leader (e.g., a position, a trajectory), and the desired distance, $\boldsymbol{t}_{des}$, between the leader and the follower. Assuming that the controller (6.6) is able to track the vehicles' desired states under the disturbances caused by the environment and the payload, the system can fulfill transportation missions in formation.

6.5 Pose estimation

As onboard sensors, the *Parrot Bebop 2* quadrotors have a built-in Inertial Measurement Unit (IMU), a downward-facing camera, for estimating the velocities in the axes x^b and y^b through optical flow calculation, GPS, and a pressure and ultrasound sensors for altitude

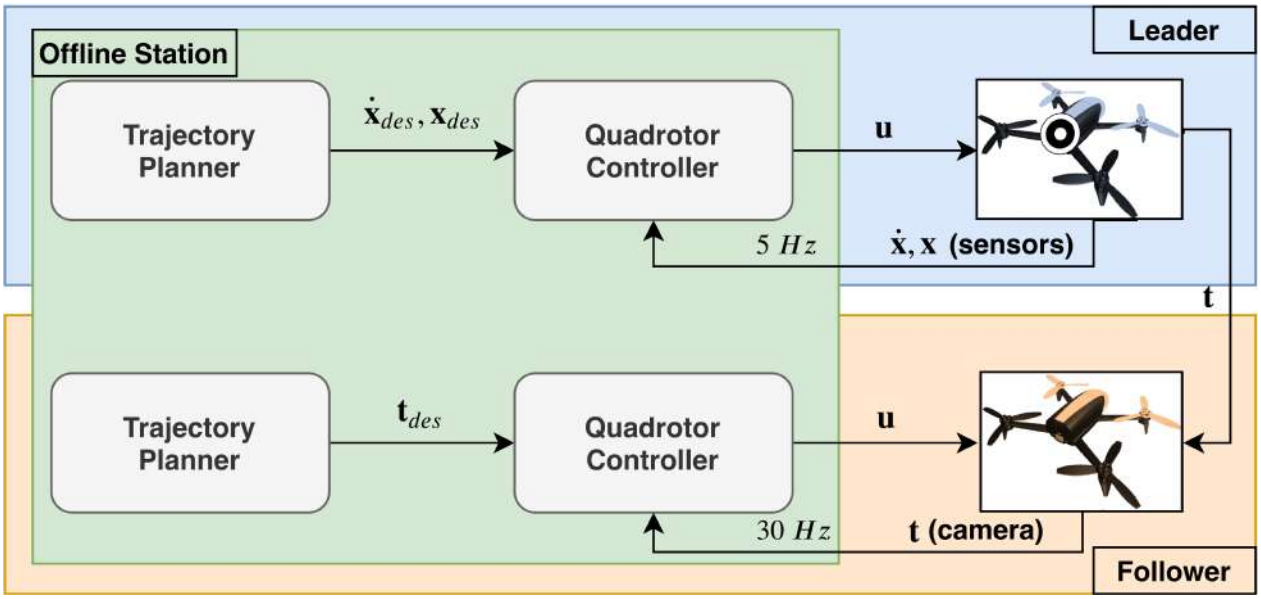

Figure 6.4 – Leader-follower control strategy for the quadrotor formation.

estimation. These sensors are combined by sensor fusion and used to deliver the pose estimation of the leader, in this application.

For the follower, a position-based visual servoing provides the estimations of $\boldsymbol{\xi}_{follower}$ in frame $\langle b \rangle$, given by $\boldsymbol{\xi}_{follower} = \boldsymbol{\xi}_{\boldsymbol{leader}} - \boldsymbol{t}$. To obtain $\boldsymbol{t}$, the visual solution uses a black and white circular pattern tag, as seen in Figure 6.5, which is detected by the frontal camera of the follower UAV and recognized by an open-source detector [37]. This system is robust to variable lighting conditions and requires very little processing time.

To illustrate the follower quadrotor actions, a video available at `https://youtu.be/RgTXic6CFsw` exhibits the follower UAV keeping a desired distance from a visual marker handled by a human operator. In this example, a payload weighing 180 g is attached to the quadrotor using flexible cables. To track the visual marker references a positioning task following the control law (6.6) was applied, serving as an example of the robustness of the proposed controller.

6.6 Experimental setup

The proposed algorithms were validated experimentally using two *Parrot Bebop 2* quadrotors performing trajectory tracking while transporting a bar-shaped payload in an outdoor scenario. The payload is 1.45 m long and weighs 160 g, corresponding to 16% of the quadrotors' mass. The algorithms run in an offboard station at 30 Hz. As the *Bebop 2* firmware delivers the odometry data only at a rate of 5 Hz, the leader control was downsampled to this frequency. The communication between the agents and the offboard station was established

Figure 6.5 – Black and white pattern attached to the leader to be used by the follower to keep the desired distance $\boldsymbol{t}_{des}$.

using ROS[1] (Robot Operating System).

To control the *Bebop 2* quadrotors, the parameters for the model described in (6.4) are obtained by an identification method similar to the one adopted in [33; 38]. The obtained parameters are $\boldsymbol{K}_u = diag(0.8417, 0.8354, 3.966)$ and $\boldsymbol{K}_{\dot{x}} = diag(0.18227, 0.17095, 4.001$.

6.7 Experimental results

A video of the experimental results of this work can be found in https://youtu.be/Fta30Kr9r70

The desired trajectory for the leader has the shape of a hyperbolic paraboloid, parameterized as

$$\boldsymbol{x}_{des} = \left[r_x \sin\left(\frac{2\pi t}{T}\right) \quad r_y \cos\left(\frac{2\pi t}{T}\right) \quad z_0 - r_z \cos\left(\frac{4\pi t}{T}\right)\right]^\top,$$

where $r_x = r_y = 1.5\ m$, $r_z = 0.5\ m$, $z_0 = 2.5\ m$, and $T = 60\ s$. For the follower, $\boldsymbol{t}_{des} = [-1.35 \quad 0 \quad 0]^\top\ m$, which means that the follower should stay $1.35\ m$ behind the leader, at the same altitude. To verify the robustness and adaptive behavior of the controller described in (6.6), we keep the same gains used for the follower UAV demonstration presented in Section 6.5.

The tracking performance for the proposed system in this task can be seen in Figure6.6, which shows the desired and effective positions of the leader and the follower (in this case

[1] See https://www.ros.org/

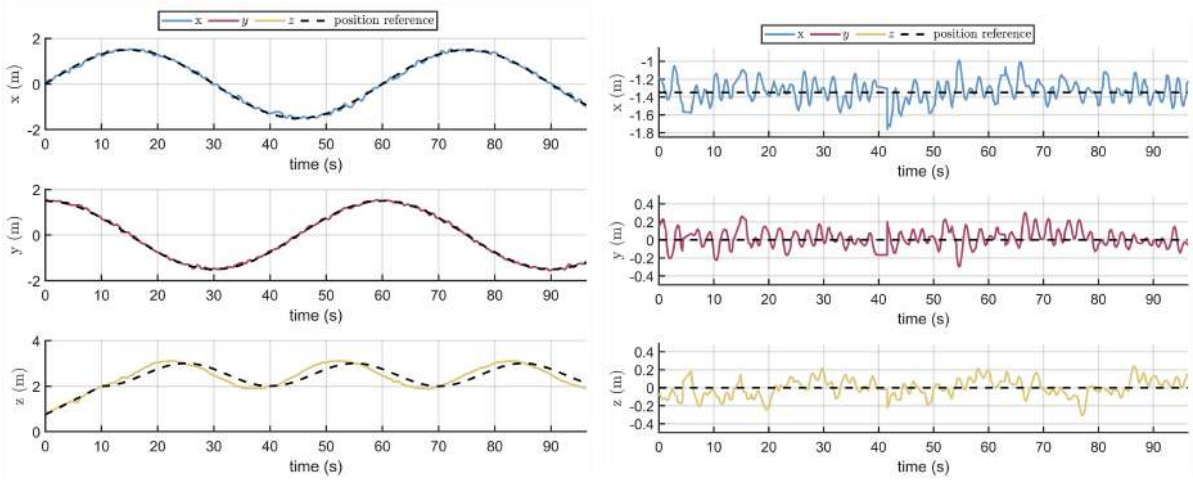

(a) Quadrotor 1 (b) Quadrotor 2

Figure 6.6 – Performance of the two quadrotors for the transportation task. The current and desired positions, as well as the tracking error are shown.

with respect to the position of the leader). Complementing the analysis, Figure 6.7 shows a 2D and a 3D views of the tracking performed by the leader.

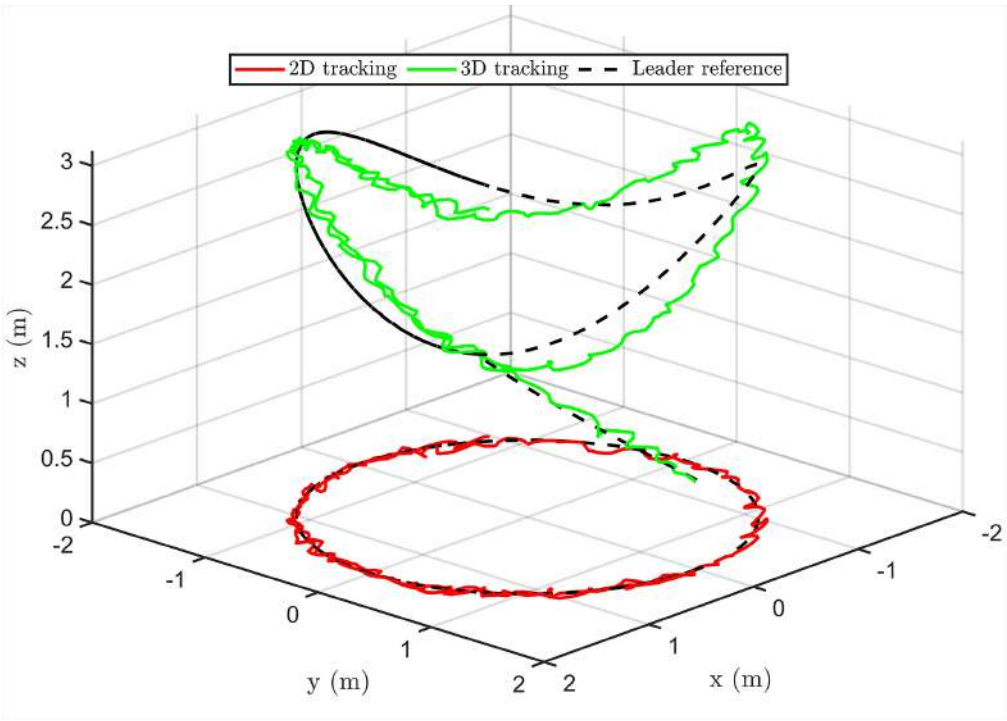

Figure 6.7 – 2D and 3D view of the trajectory tracking performed by the leader agent.

As one can see, the tracking errors are around 10 cm for the leader and around 20 cm for the follower, which we consider a good tracking for outdoor transportation. Since the transportation occurs outdoors, no ground-truth error metric can be produced to certificate

that the tracked trajectory coincides with the real desired trajectory. In other words, the quadrotor estimates that it is in a given position but no ground-truth can be used to guarantee that the estimated position is the real one. However, since the quadrotors' positions are satisfactorily converging to the trajectory, the proposed control system can be used for transportation in outdoor environments, with precision limited by the localization system and state estimation algorithms of the leader UAV.

As a minor observation, one can see in Figure 6.6 a tracking delay in the z-direction, for the leader UAV. Debugging our algorithms, we found an implementation mistake in the leader control signal $\boldsymbol{u}_{DI}$, delivering to it only position feedback, and not position and velocity feedback. The absence of velocity feedback lead to the tracking delay, and this misconduct caused the higher tracking error in z-direction when compared to xy-direction.

Lastly, it is important to reinforce that the follower UAV uses visual-servoing to follow the leader. Thus, although estimation algorithms and localization systems, such as GPS, are subject to errors and drift, the formation controller is not affected by these estimation errors. Therefore, despite the ground-truth position errors, the formation will not collapse.

6.8 Concluding remarks

In this work, we presented a solution to the problem of transporting a cable-suspended payload in outdoors using two quadrotors. With the proposed method, good performance in tracking was obtained, limited only by the leader UAV ground-truth capabilities, i.e., the leader's localization system and state estimation algorithms. As a natural next step, our future work is directed toward improvements in the leader state estimation algorithms, with the intention to obtain accurate ground-truth transportation.

6.9 References

[1] ORSAG, M. et al. Lyapunov based model reference adaptive control for aerial manipulation. In: IEEE. *2013 International Conference on Unmanned Aircraft Systems (ICUAS)*. [S.l.], 2013. p. 966–973.

[2] KIM, S.; CHOI, S.; KIM, H. J. Aerial manipulation using a quadrotor with a two dof robotic arm. In: IEEE. *2013 IEEE/RSJ International Conference on Intelligent Robots and Systems*. [S.l.], 2013. p. 4990–4995.

[3] ZHANG, G. et al. Grasp a moving target from the air: System & control of an aerial manipulator. In: IEEE. *2018 IEEE International Conference on Robotics and Automation (ICRA)*. [S.l.], 2018. p. 1681–1687.

[4] CASTILLO, A. et al. Disturbance observer-based quadrotor attitude tracking control for aggressive maneuvers. *Control Engineering Practice*, Elsevier, v. 82, p. 14–23, 2019.

[5] MELLINGER, D.; MICHAEL, N.; KUMAR, V. Trajectory generation and control for precise aggressive maneuvers with quadrotors. *The International Journal of Robotics Research*, SAGE Publications Sage UK: London, England, v. 31, n. 5, p. 664–674, 2012.

[6] SA, I.; CORKE, P. Close-quarters quadrotor flying for a pole inspection with position based visual servoing and high-speed vision. In: IEEE. *2014 International Conference on Unmanned Aircraft Systems (ICUAS)*. [S.l.], 2014. p. 623–631.

[7] GASSNER, M.; CIESLEWSKI, T.; SCARAMUZZA, D. Dynamic collaboration without communication: Vision-based cable-suspended load transport with two quadrotors. In: IEEE. *2017 IEEE International Conference on Robotics and Automation (ICRA)*. [S.l.], 2017. p. 5196–5202.

[8] DONG, X. et al. Theory and experiment on formation-containment control of multiple multirotor unmanned aerial vehicle systems. *IEEE Transactions on Automation Science and Engineering*, v. 16, n. 1, p. 229–240, January 2019. ISSN 1558-3783.

[9] Pizetta, I. H. B.; Brandão, A. S.; Sarcinelli-Filho, M. Cooperative load transportation using three quadrotors. In: *2019 International Conference on Unmanned Aircraft Systems (ICUAS)*. Atlanta, GA, USA: [s.n.], 2019. p. 644–650. ISSN 2373-6720.

[10] Novák, D.; Čermák, P. Advantages of using multi-agent principles in fail - safe uav system design. In: *2011 16th International Conference on Methods & Models in Automation & Robotics*. Miedzyzdroje, Poland: [s.n.], 2011. p. 162–167. ISSN null.

[11] VILLA, D. K.; BRANDAO, A. S.; SARCINELLI-FILHO, M. A survey on load transportation using multirotor uavs. *Journal of Intelligent & Robotic Systems*, Springer, v. 98, n. 2, p. 267–296, 2020.

[12] TANG, S.; KUMAR, V. Autonomous flight. *Annual Review of Control, Robotics, and Autonomous Systems*, Annual Reviews, v. 1, p. 29–52, 2018.

[13] ABAUNZA, H. et al. Dual quaternion modeling and control of a quad-rotor aerial manipulator. *Journal of Intelligent & Robotic Systems*, Springer, v. 88, n. 2, p. 267–283, 2017.

[14] VILLA, D. K. D. et al. Cooperative load transportation with two quadrotors using adaptive control. *IEEE Access*, IEEE, v. 9, p. 129148–129160, 2021.

[15] OLLERO, A. et al. Past, present, and future of aerial robotic manipulators. *IEEE Transactions on Robotics*, IEEE, 2021.

[16] TANG, S.; WÜEST, V.; KUMAR, V. Aggressive flight with suspended payloads using vision-based control. *IEEE Robotics and Automation Letters*, IEEE, v. 3, n. 2, p. 1152–1159, 2018.

[17] SON, C. Y. et al. Real-time optimal trajectory generation and control of a multi-rotor with a suspended load for obstacle avoidance. *IEEE Robotics and Automation Letters*, IEEE, v. 5, n. 2, p. 1915–1922, 2020.

[18] VILLA, D. K.; BRANDÃO, A. S.; SARCINELLI-FILHO, M. A survey on load transportation using multirotor uavs. *Journal of Intelligent & Robotic Systems*, Springer, v. 98, p. 267–296, 2020.

[19] GUERRERO-SÁNCHEZ, M. E. et al. Swing-attenuation for a quadrotor transporting a cable-suspended payload. *ISA transactions*, Elsevier, v. 68, p. 433–449, 2017.

[20] MELLINGER, D. et al. Cooperative grasping and transport using multiple quadrotors. In: *Distributed autonomous robotic systems*. [S.l.]: Springer, 2013. p. 545–558.

[21] LI, A. Q. et al. Experimental comparison of open source vision-based state estimation algorithms. In: SPRINGER. *International Symposium on Experimental Robotics*. [S.l.], 2016. p. 775–786.

[22] KANELLAKIS, C.; NIKOLAKOPOULOS, G. Survey on computer vision for uavs: Current developments and trends. *Journal of Intelligent & Robotic Systems*, Springer, v. 87, n. 1, p. 141–168, 2017.

[23] MÁTHÉ, K.; BUŞONIU, L. Vision and control for uavs: A survey of general methods and of inexpensive platforms for infrastructure inspection. *Sensors*, Multidisciplinary Digital Publishing Institute, v. 15, n. 7, p. 14887–14916, 2015.

[24] BEUL, M. et al. Team nimbro at mbzirc 2017: Fast landing on a moving target and treasure hunting with a team of micro aerial vehicles. *Journal of Field Robotics*, Wiley Online Library, v. 36, n. 1, p. 204–229, 2019.

[25] SANTOS, M. C. P. et al. An adaptive dynamic controller for quadrotor to perform trajectory tracking tasks. *Journal of Intelligent & Robotic Systems*, Springer, v. 93, n. 1-2, p. 5–16, 2019.

[26] SLOTINE, J.-J. E.; LI, W. et al. *Applied nonlinear control*. [S.l.]: Prentice hall Englewood Cliffs, NJ, 1991. v. 199.

[27] ZHAO, Z. et al. Output feedback continuous terminal sliding mode guidance law for missile-target interception with autopilot dynamics. *Aerospace Science and Technology*, Elsevier, v. 86, p. 256–267, 2019.

[28] GONZÁLEZ, I.; SALAZAR, S.; LOZANO, R. Chattering-free sliding mode altitude control for a quad-rotor aircraft: Real-time application. *Journal of Intelligent & Robotic Systems*, Springer, v. 73, n. 1-4, p. 137–155, 2014.

[29] RAJAPPA, S. et al. Adaptive super twisting controller for a quadrotor uav. In: IEEE. *2016 IEEE International Conference on Robotics and Automation (ICRA)*. [S.l.], 2016. p. 2971–2977.

[30] Santana, L. V.; Brandão, A. S.; Sarcinelli-Filho, M. Heterogeneous leader-follower formation based on kinematic models. In: *2016 International Conference on Unmanned Aircraft Systems (ICUAS)*. Arlington, VA, USA: [s.n.], 2016. p. 342–346. ISSN null.

[31] MUÑOZ, F. et al. Robust trajectory tracking for unmanned aircraft systems using a nonsingular terminal modified super-twisting sliding mode controller. *Journal of Intelligent & Robotic Systems*, Springer, v. 93, n. 1-2, p. 55–72, 2019.

[32] LOIANNO, G. et al. Estimation, control, and planning for aggressive flight with a small quadrotor with a single camera and imu. *IEEE Robotics and Automation Letters*, IEEE, v. 2, n. 2, p. 404–411, 2016.

[33] SANTANA, L. V.; BRANDÃO, A. S.; SARCINELLI-FILHO, M. Navigation and cooperative control using the ar.drone quadrotor. *Journal of Intelligent & Robotic Systems*, v. 84, n. 1, p. 327–350, December 2016. ISSN 1573-0409.

[34] MELLINGER, D.; KUMAR, V. Minimum snap trajectory generation and control for quadrotors. In: IEEE. *2011 IEEE international conference on robotics and automation*. [S.l.], 2011. p. 2520–2525.

[35] PLESTAN, F. et al. New methodologies for adaptive sliding mode control. *International journal of control*, Taylor & Francis, v. 83, n. 9, p. 1907–1919, 2010.

[36] SHTESSEL, Y. et al. *Sliding mode control and observation*. [S.l.]: Springer, 2014.

[37] KRAJNÍK, T. et al. A practical multirobot localization system. *Journal of Intelligent & Robotic Systems*, Springer, v. 76, n. 3-4, p. 539–562, 2014.

[38] Santos, M. C. P. et al. A novel null-space-based uav trajectory tracking controller with collision avoidance. *IEEE/ASME Transactions on Mechatronics*, v. 22, n. 6, p. 2543–2553, December 2017. ISSN 1941-014X.

7 Concluding Remarks and Future Works

In this doctoral thesis, we presented a practical study on the topic of load transportation using quadrotors. Safe and agile transportation is one of the main focuses of this thesis, as well as the proposal of robust control algorithms that are easy-to-implement and that are readily enabled for use on commercial off-the-shelf quadrotors. In the works presented in this thesis, the transported payload was treated as an unmodeled disturbance, and transportation solutions were provided considering individual and cooperative transportation. We validate the proposed algorithms in harsh conditions, where the disturbances have a heavy influence over the vehicle dynamics; and we also demonstrated the use of our algorithms in high-speed transportation, far from quasi-static motion.

As future works, here we provide a list containing the suggestions for the next steps that we judge necessary to fully test the proposed algorithms in real-world outdoors transportation:

- The implementation of state observers to be used by the adaptation algorithms, enabling the use of the proposed controllers without the dependency of the motion capture system.
- In this thesis, only one of the proposed algorithms was tested in outdoors. Note that the final destination of any transportation strategy is to develop algorithms that enable the use of quadrotors to deliver payload in the real-world. Therefore, we recommend the execution of more trials in outdoors, also comparing the other control strategies presented in this thesis.
- Regarding the trials in outdoors, due to the absence of a reliable system to estimate the states such as the motion capture systems in indoors, more elaborate algorithms for state estimation should be pursued, such as sensor fusion by Kalman filtering and visual-servoing.
- In this thesis we do not specifically treat the pick-and-place problem involved in any transportation task. Algorithms in this direction are recommended. Nevertheless, we strongly believe that the algorithms here presented will readily attend the pick-and-place stabilization criteria.
- Lastly, we recommend new experiments testing the algorithms here developed with different families of off-the-shelf quadrotors. In our trials, we only used Parrot Bebop 2 quadrotors, thus, further experimental verification is needed to certify the applicability

of the algorithms in a broad sense, mainly with bigger quadrotors, which are capable of carrying heavier payloads.